Structural Engineering Report, No. 38

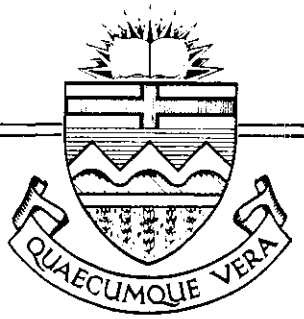

TIME DEPENDENT DEFLECTIONS OF REINFORCED CONCRETE SLABS

By
A. Scanlon

December, 1971

Structural Engineering Report No. 38

TIME DEPENDENT DEFLECTIONS OF REINFORCED CONCRETE SLABS

by

A. SCANLON

Faculty Investigator: D. W. Murray

Produced with the support of the
National Research Council of Canada
Operating Grant: NRC-A5307

Department of Civil Engineering
University of Alberta
Edmonton, Canada

December, 1971

ABSTRACT

A finite element approach to the analysis of reinforced concrete slabs, which includes the effects of cracking and time dependent effects, is presented.

Constitutive relations for reinforced concrete are developed which account for the reduced stiffness due to cracking. Time dependent strains in concrete are accounted for by considering concrete to behave as an ageing linear visco-elastic material which exhibits shrinkage. Classical small deflection plate bending theory is modified for these constitutive relations and a method of analysis is developed using a rectangular plate bending element. Numerical results are obtained and compared with available classical solutions and experimental results.

A study of factors affecting slab deflections is carried out and simplified procedures for computing slab deflections are examined.

TABLE OF CONTENTS

Table of Contents (cont'd)

Table of Contents (cont'd)

Table of Contents (cont'd)

Table of Contents (cont'd)

LIST OF FIGURES

List of Figures (cont'd)

List of Figures (cont'd)

LIST OF TABLES

LIST OF SYMBOLS

< >	row vector
{ }	column vector
[ ]	matrix

Subscripts

B	out of plane quantity
c	concrete or compression
cr	cracked
o	reference quantity
P	in plane quantity
s	steel
t	tension
uc	uncracked

Superscripts

σ	quantities dependent on stress
E	elastic
I	inelastic
s	shrinkage
T	total

Variables

a,k,α,p,q	constants in compliance function
a,b	lengths of sides of rectangular element
A	area
A_s,A'_s	areas of tensile and compressive steel respectively
A_i,B_i,D	functions in specific compliance kernel

b,Q,A,R,c	functions used in element stiffness matrix formulation
$[B]$	matrix relating curvatures and twist to element degrees of freedom
c	width of column
$[C]$	constitutive matrix
$C(t,\tau)$	specific compliance function
$C_j(t,\tau)$	computed value of compliance at t for loading at τ
$\bar{C}_j(t,\tau)$	observed value of compliance at t for loading at τ
d	slab depth
d_{nx},d_{ny},d_{nxy}	depths to reference points in plate element
D	plate flexural rigidity
$[D]$	plate stiffness matrix
D_{ij},B_i	functions defined in Equation (B.7)
e_j	square of difference of two quantities in least squares procedure
E	sum of e_j for all j, also Young's Modulus
$\bar{E}$	pseudo instantaneous elastic modulus
$[E]$	plane stress constitutive matrix
f_r	modulus of rupture
f'_c	compressive strength of concrete
G	shear modulus
$H_{ij}^{(1)}$	Hermitian interpolation function
I	operator $\int_0^t C(t,\tau)\frac{\partial}{\partial\tau}\cdot d\tau$
I_{cr}	moment of inertia of cracked transformed section
I_{eff}	effective moment of inertia of a cracked section
I_g	moment of inertia of gross section neglecting steel
I_{ST}	moment of inertia of gross section including steel

u,v,w	displacements in x,y,z directions
V_{xi},V_{yi},V_{xyi}	functions used in numerical integration procedure
$w(t,\tau)$	specific shear compliance
W	potential of external forces
$Y(t,\tau)$	function used in least squares analysis
α	factor for reduction of Young's modulus in tension and Poisson's ratio for a cracked layer
β	angle defining orientation of local coordinate system
δ	memory function for cracking analysis
Δ	deflection at a point in a slab
Δt	increment in time
ε	strain
ε_c	C.E.B. shrinkage parameter
Σ	strain energy
$\kappa_x,\kappa_y,\kappa_{xy}$	plate curvatures and twist
$\{\phi_D\}$	vector of linear interpolation functions
$\{\phi\}$	vector of interpolation functions relating vertical displacement w to element degrees of freedom
ϕ_t	C.E.B. creep parameter
σ	stress
σ_1,σ_2	principal stresses
σ_{Ti}	limiting stress in branch i of stepped stress strain diagram
Π	total potential
τ	variable of integration, also time of loading
ξ,η	non dimensionalized coordinates

CHAPTER 1

INTRODUCTION

1.1 Introductory Remarks

The design of reinforced concrete structures requires the satisfaction of two main criteria, namely strength and serviceability. Strength refers to the ability of the structure to carry the loads for which it is designed and is therefore the primary consideration. Since reinforced concrete structures are generally designed to produce a ductile failure requiring yielding of the reinforcement before failure of the concrete, the strength of a member or structure may be considered to be mainly a function of the steel reinforcement. The properties of steel are generally well defined so that the strength may be determined with reasonable accuracy.

Serviceability in reinforced concrete generally refers to behaviour at working load levels with particular reference to cracking and deflections. Both cracking and deflections are primarily dependent on the behaviour of concrete and are consequently much more difficult to predict than strength since the properties of concrete are highly variable and are dependent on a large number of factors.

When structures were designed on the basis of allowable stresses and straight line theory, the relatively low stresses resulted in stiff sections which rarely produced concern for deflections. However, with the advent of ultimate strength design, higher concrete stresses and higher steel yield stresses, shallower more highly reinforced sections could be used, and this in turn resulted in more concern for serviceability requirements. This concern is reflected in

the development of deflection requirements in the A.C.I. Building Code. Before A.C.I. 318-63[2] there were no specific requirements for control of deflections of beams and one-way slabs, although limiting thicknesses were specified for flat slabs and two-way construction. In A.C.I. 318-63, deflection requirements were introduced to cover both one-way and two-way construction, particularly with respect to ultimate strength design.

These requirements have been expanded in A.C.I. 318-71[3] to cover lightweight concrete, composite construction, pre-stressed concrete and varying yield strengths. Methods are indicated for computing both short and long time deflections. These procedures, however, do not take into account variations in creep and shrinkage properties which may have a considerable effect on deflections. The need to consider the effects of deflections of reinforced concrete structures, particularly floor slabs, is indicated by the results of a survey of damage to concrete structures carried out in Germany by Mayer and Rusch[36]. By far the most common cause of damage was excessive slab deflection leading to partition wall damage, and damage to plaster and finishes. Among the causes cited for damage were use of the uncracked section for deflection calculations and insufficient consideration of creep and shrinkage deformations.

Several procedures have been developed for the analysis of reinforced concrete floor slabs assuming the material to be linear elastic. These include plate bending theory, plate analogue, finite difference solutions, and grillage solutions, all of which are discussed in reference (18). It was not until the development of finite element techniques that more realistic non-linear material properties

could be used for solutions of problems of reasonable complexity. King[30] applied the theory of linear viscoelasticity to the solution of two dimensional stress problems using the finite element approach while Selna[46] developed a solution for planar reinforced concrete structures which included cracking and time-dependent effects, also using linear visco-elasticity. Manuel and McGregor[35] used a rate of creep approach in the study of the effects of sustained loads on reinforced concrete columns in frames.

1.2 Object and Scope

The objectives of this investigation are

1. To develop constitutive relations for reinforced concrete which account for the effects of cracking and time dependent behaviour.
2. To apply these non-linear constitutive relations to a finite element analysis of reinforced concrete floor slabs.
3. To study the effects of several parameters on slab deflections using the analysis procedure developed.

In addition, the results of the parameter study are used in a preliminary assessment of available simplified procedures for evaluation of slab deflections.

1.3 Outline of Contents

The plane stress constitutive relations used in this dissertation are developed in Chapter 2. In the general case, the instantaneous elastic relationships are developed for a layer of unit thickness consisting of reinforcement placed at arbitrary angles to the coordinate

system and a set of orthogonal cracks in the concrete also oriented in an arbitrary fashion. The relationships obtained are generally anisotropic. Assumptions are then made concerning the behaviour of the layer which allow the relationships to be specialized to the case of orthotropy with respect to the global coordinate system. Time dependent effects are introduced by treating the concrete as an ageing linear visco-elastic material exhibiting shrinkage. A numerical integration technique with respect to time, developed by Selna[46] for the uniaxial stress case is generalized for plane stress.

In Chapter 3, the general method of analysis is described. An iterative procedure is developed to account for cracking and an attempt is made to account for the tensile stiffening effect of concrete between cracks. An incremental procedure with respect to time is used to trace the time-dependent behaviour.

An attempt to verify the analytical model is made in Chapter 4. Elastic plate bending, cracking and time dependent solutions are compared with available classical and experimental results.

Chapter 5 describes the results of a study in which the analysis was applied to a number of flat plate floor slabs to determine the effects of varying certain parameters.

A brief examination of available simplified procedures for computing short and long time deflections is made in Chapter 6 using the results of the study carried out in Chapter 5. A short summary and recommendations for further studies are presented in Chapter 7.

CHAPTER 2

MATERIAL PROPERTIES AND CONSTITUTIVE RELATIONS

2.1 Introduction

This chapter deals with the constitutive relations to be used in the analysis of reinforced concrete floor slabs. These relations require knowledge of the properties of the constituent materials, steel and concrete, and of the behaviour of the two combined as a composite material. A precise point-wise evaluation of stress and strain in the composite material is not attempted. Instead it is assumed that sufficiently accurate information can be obtained from a structural engineering point of view by considering stress and strain measured over a relatively long gauge length.

The properties of reinforcing steel are generally well defined and steel may be considered to behave as a linear elastic material. (This study is concerned with the behaviour at working load levels and it is therefore assumed that the steel stress remains in the elastic range.)

The properties of concrete are known to depend on a large number of factors including mix proportions, environmental conditions, load level, size and shape of member, age at loading and duration of load. In addition the properties will generally vary throughout the structure so that the assigned material properties can only be considered to represent the average conditions in the body.

The analysis of reinforced concrete slabs may be treated as a problem of plate bending under transverse loading. The stress in the direction of the normal to the surface of the plate may be neglected

so that any point in the plate may be considered to be in a state of plane stress under load[47]. The constitutive relations in this chapter are therefore developed for plane stress.

The constitutive relations are first developed in general terms for a layer of unit thickness containing reinforcement oriented arbitrarily with respect to the global coordinates and a set of orthogonal cracks also at an arbitrary angle. A simple cracking criterion is then established which allows these relations to be specialized to the case of orthotropy with respect to the global coordinate system. This is accomplished by replacing the cracked concrete layer by a material orthotropic with respect to the global system and which is assumed to have a reduced tensile modulus of elasticity.

Time dependent constitutive relations for a layer of concrete under plane stress are then developed and a numerical integration technique is described for the evaluation of the strain history for an applied stress which varies with time. Finally, evaluation of creep and shrinkage properties for different concretes is discussed.

2.2 Constitutive Relations for a Layer of Reinforced Concrete under Plane Stress (Instantaneous - Elastic)

In order to formulate the constitutive relations for a layer of reinforced concrete which may have reinforcing steel at an arbitrary angle to the global coordinate system and which may be uncracked or cracked in an arbitrary direction the following assumptions are made.

1. Under an arbitrary infinitesimal strain field the reinforcing bars carry uniaxial stress only.

2. Reinforcing steel is expressed in terms of the ratio of

steel area to total area per unit of length measured perpendicular to the direction of the reinforcement. The actual size and spacing of reinforcing bars within a layer is considered to have no effect on the analysis.

3. The stiffnesses for steel and concrete may be formulated separately and the results superimposed to obtain the stiffness for the layer.

4. The volume of concrete displaced by the steel may be ignored.

5. In the case of a cracked layer, the tensile stiffening effect of concrete between cracks may be accounted for by replacing the concrete with a continuous material having a reduced modulus in tension perpendicular to the cracks and a reduced Poisson's ratio.

6. The shear modulus of a layer whether cracked or uncracked is assumed to be that of an uncracked plane concrete layer. This assumption is intended to account for the effects of dowel action and aggregate interlock on the shear stiffness of a cracked layer. Small percentages of reinforcing steel are assumed to have an insignificant effect on the shear stiffness or twisting stiffness of the plate before cracking.

7. Cracking at more than one orientation may be represented by a system of orthogonal cracks.

8. Complete strain compatibility between steel and concrete is maintained.

9. Linear elastic behaviour is assumed for steel and for instantaneous response of the concrete.

2.2.1 Steel

Figure 2.1(a) shows an element taken from a layer of reinforced concrete of unit thickness containing one set of reinforcing bars and one set of cracks each at an arbitrary angle to the global x,y axes. The steel and concrete are shown separately in Figure 2.1(b) and Figure 2.1(c) respectively.

The local coordinate system x',y' for the steel is orientated at an angle β' to the global x-axis and the steel runs parallel with the x'-axis. For an arbitrary strain field, the resulting stress field is expressed as,

$$\begin{Bmatrix} \sigma_{sx'} \\ \sigma_{sy'} \\ \tau_{sx'y'} \end{Bmatrix} = \begin{bmatrix} p_{x'}E_s & \cdot & \cdot \\ \cdot & \cdot & \cdot \\ \cdot & \cdot & \cdot \end{bmatrix} \begin{Bmatrix} \varepsilon_{sx'} \\ \varepsilon_{sy'} \\ \gamma_{sx'y'} \end{Bmatrix}$$

where $p_{x'}$ is the area of steel per unit of length in the y' direction and E_s is Young's modulus for steel.

Symbolically,

$$\{\sigma_s'\} = [C_s'][\varepsilon_s'\} \tag{2.1}$$

Stresses and strains are related to the global axes by the second order tensor transformation,

$$\{\sigma_s'\} = [T]\{\sigma_s\} \tag{2.2}$$

$$\{\varepsilon_s'\} = [T]\{\varepsilon_s\} \tag{2.3}$$

where,

$$[T] = \begin{bmatrix} c^2 & s^2 & 2sc \\ s^2 & c^2 & -2sc \\ -sc & sc & c^2-s^2 \end{bmatrix} \tag{2.4}$$

and $c = \cos\beta'$, $s = \sin\beta'$

The constitutive relation referred to the global system becomes,

$$\{\sigma_s\} = [T]^{-1}[C_s'][T]\{\varepsilon_s\} = [C_s]\{\varepsilon_s\} \tag{2.5}$$

For n sets of reinforcing steel in the same layer,

$$\{\sigma_s\} = [\sum_{i=1}^{n}[C_{si}]]\{\varepsilon_s\} \tag{2.6}$$

2.2.2 Concrete

Figure 2.1(c) shows the local coordinate system x",y" for the layer of concrete with cracks running parallel with the y"-axis. The layer is seen to be orthotropic with respect to the local system. Orthotropy is maintained if an additional set of cracks is formed parallel with the x" axis.

The plane stress constitutive relation referred to the local system may be expressed as,

$$\begin{Bmatrix} \sigma_{cx"} \\ \sigma_{cy"} \\ \tau_{cx"y"} \end{Bmatrix} = \begin{bmatrix} \frac{E_{cx"}}{(1-\nu_{cx"}\nu_{cy"})} & \frac{\nu_{cx"}E_{cy"}}{(1-\nu_{cx"}\nu_{cy"})} & . \\ \frac{\nu_{cy"}E_{cx"}}{(1-\nu_{cx"}\nu_{cy"})} & \frac{E_{cy"}}{(1-\nu_{cx"}\nu_{cy"})} & . \\ . & . & G_{x"y"} \end{bmatrix} \begin{Bmatrix} \varepsilon_{cx"} \\ \varepsilon_{cy"} \\ \gamma_{cx"y"} \end{Bmatrix}$$

or $\{\sigma_c"\} = [C_c"]\{\varepsilon_c"\}$ (2.7)

where

$E_{cx"}$, $\nu_{cx"}$ are Young's modulus and Poisson's ratio for the x" direction

$E_{cy"}$, $\nu_{cy"}$ are Young's modulus and Poisson's ratio for the y" direction

and $G_{x"y"}$ is the shear modulus.

Referred to the global system the above expression becomes,

$$\{\sigma_c\} = [T]^{-1}[C_c"][T]\{\varepsilon_c\} = [C_c]\{\varepsilon_c\} \qquad (2.8)$$

where $\beta"$ replaces β' in [T].

Before cracking takes place, the elastic constants take the values for plane concrete and the material may be considered to be isotropic. However, after cracking the overall stiffness is reduced because of the inability of the concrete to transfer tensile stresses across a crack. In this case the elastic constants must be reduced. The definition of elastic constants in a cracked layer is postponed until section 2.3.

2.2.3 Combined Steel and Concrete

For compatibility of strain between steel and concrete,

$$\{\varepsilon\} = \{\varepsilon_s\} = \{\varepsilon_c\} \qquad (2.9)$$

The total stress in the composite layer is expressed by,

$$\{\sigma\} = \{\sigma_c\} + \{\sigma_s\}$$

$$= [[C_c] + \sum_{i=1}^{n} [C_{si}]]\{\varepsilon\}$$

or, $$\{\sigma\} = [C]\{\varepsilon\} \qquad (2.10)$$

These constitutive relations have been developed for the general case of arbitrary reinforcement layouts and a system of orthogonal cracks oriented at an arbitrary angle to the global coordinate system.

The present investigation will be restricted to slabs in which reinforcement is placed in an orthogonal pattern coinciding with the global coordinate system. In the next section a cracking criterion will be established which allows the above relationships to be specialized to the case of orthotropy in the global coordinate system in which case the transformation matrix [T] is not required.

2.3 Cracking Criterion

In order to include the effect of cracking in the analysis a cracking criterion must be established. The cracking criterion should define

a) the conditions under which cracking occurs

and b) the general direction of crack propagation.

Consideration should also be given to the tensile stiffening effect of concrete between cracks and to the effects of reinforcing steel dowel action and aggregate interlock on the twisting stiffness after cracking.

2.3.1 Plain Concrete

Experimental work on the failure criteria for plain concrete under biaxial stress[31] indicates that the failure envelope in terms of principal stresses is of the form shown in Figure 2.2. The shaded area indicates the stress levels to be expected under working load conditions. The direction of cracking is determined by the direction of the maximum principal tensile stress. It can be seen that little

error will be introduced by assuming that cracking occurs when either of the principal tensile stresses exceeds the uniaxial tensile strength, particularly in the working load range.

Figure 2.3 shows a typical stress strain diagram for plain concrete in tension. At approximately 80% of the ultimate stress, micro-cracking begins to occur at the aggregate-paste inter-face, and the stress strain diagram becomes non-linear[20]. At the ultimate tensile stress cracking propagates throughout the specimen and the stress drops to zero.

2.3.2 Reinforced Concrete

Cracking in reinforced concrete is complicated by the presence of the reinforcing bars which act both as crack arrestors and crack instigators[19].

Figure 2.4(a) shows a reinforced concrete element under uniaxial stress. When the concrete stress reaches the ultimate tensile strength, primary cracks form at intervals along the length[22]. The total load is transferred across these cracks by the reinforcement but the concrete between cracks is still capable of carrying stress because of the bond between steel and concrete. As the load increases, intermediate cracks form and the proportion of the load carried by the concrete gradually diminishes. In terms of average stress over a relatively long gauge length, the concrete average stress vs strain diagram may be considered to have an unloading portion. In this analysis it is assumed that the tensile response of concrete in a reinforced concrete slab may be represented in terms of a series of discrete steps as shown in Figure 2.4(b). The tensile stress is assumed to increase

linearly until the ultimate tensile stress is reached at which point the modulus of elasticity drops to the next lower step on the diagram. The stress in the softened material is allowed to increase to the limiting value corresponding to this branch of the diagram. This process continues until the modulus for concrete drops to zero. By gradually reducing the concrete modulus relative to the steel modulus, the proportion of load carried by the steel gradually increases until finally all of the load is assumed to be carried by the steel. This process will under-estimate the maximum stress in the steel at all stages between first cracking and no stress carried by the concrete since at first cracking the total load will be carried by the steel across the primary cracks, while the steel between cracks will be stressed at a lower level.

The application of the above concept to the analysis of reinforced concrete slabs is described in section 3.4 and the choice of reduced moduli and corresponding limiting stresses is discussed in section 4.3.

The direction of crack propagation in a two dimensional system is also affected by the reinforcement. Morley[40], in tests carried out to investigate the behaviour of reinforcement placed at an angle to the direction of maximum applied tensile stress, has observed the tendency of cracks to propagate along the reinforcement and perpendicular to it as shown in Figure 2.5(a).

In tests carried out to investigate the cracking behaviour of concrete slabs reinforced with welded wire fabric, Nawy[41] has observed that the direction of crack propagation may be determined by the size and spacing of the reinforcement rather than the direction of

maximum principal tensile stress. For closely spaced wires (of the order of 4" to 8" apart) placed orthogonally, the cracks tended to propagate in an orthogonal pattern coinciding with the reinforcement layout (see Figure 2.5(b)). In the case of more widely spaced wires, cracks tended to follow the general direction of the maximum principal tensile stress, thus tending towards plain concrete behaviour.

Cracking in reinforced concrete slabs therefore appears to be influenced to a large extend by local stress concentrations, caused in particular by the presence of reinforcing steel. In practical situations, cracking at service load will occur in regions of high moment where the reinforcement percentage is greatest and the spacing will generally be such as to encourage the orthogonal cracking patterns observed by Nawy. This would certainly be desirable from the point of view of control of crack spacing and crack width.

In view of the above observations it is apparent that the direction of crack propagation may not easily be predicted in all cases and therefore a very simple cracking criterion has been established. It is assumed that reinforcement is placed parallel with the sides of the slab. The stress strain diagram for concrete in tension is assumed to be in the form of a stepped function, as shown in Figure 2.4, and after cracking a concrete layer is considered to consist of an orthotropic material with a different modulus of elasticity in tension and compression, the moduli being defined in the global coordinate system. By defining orthotropic elastic constants in the global coordinate system it is implicitly assumed that cracks propagate parallel and perpendicular to the reinforcement. While this will not always be the case, the approximation is considered to be a satisfactory means of

determining the overall reduction in flexural stiffness due to cracking and in view of the variability of the material and the number of factors which affect cracking in concrete, a more sophisticated criterion would appear to be unwarranted at present. The evaluation of the constants E_x, E_y, ν_x and ν_y in the analysis is discussed in more detail in section 3.4.

An orthotropic material under plane stress requires four elastic constants to be defined in the principal directions[47]. To maintain symmetry of the constitutive matrix,

$$\frac{\nu_x}{E_x} = \frac{\nu_y}{E_y}$$

For the purpose of the analysis, if the elastic modulus is reduced for tension, the corresponding Poisson's ratio is reduced in the same proportion. It now remains to establish a value for the shear modulus of a layer. Sandhu[45] presents an expression for a bimodular isotropic material in which the modulus in tension is different from that in compression, but each modulus is invariant with orientation of the coordinate system. The shear modulus may be expressed as

$$G = \frac{1}{\frac{1}{E_c} + \frac{1}{E_t} + \frac{2\nu}{E_c}} \qquad (2.11)$$

where E_c = modulus of elasticity in compression

E_t = modulus of elasticity in tension

$\nu = \nu_c$ = Poisson's ratio for compression

$\nu_t = \frac{E_t \nu_c}{E_c}$ = Poisson's ratio for tension

For a generally orthotropic material, G cannot be related to

the elastic constants E_x, E_y, ν_x and ν_y and must be defined separately. For an uncracked slab, the small percentages of reinforcement will have a negligible effect on the twisting stiffness and the shear modulus may be considered to be constant throughout the depth of the slab and equal to the value for uncracked concrete. After cracking, the situation becomes more complex and although the shear stiffness is undoubtedly reduced by cracking, the effects of dowel action in the steel, and aggregate interlock tend to minimize the reduction. Rather than attempt to develop a theoretical expression for shear stiffness which takes these factors into account the uncracked shear modulus value was used both before and after cracking for the model developed in this work.

The constitutive relations represented by Equation 2.10 may now be written for the orthotropic case,

$$\begin{Bmatrix} \sigma_x \\ \sigma_y \\ \tau_{xy} \end{Bmatrix} = \begin{bmatrix} & & \\ & [C_c] + [C_s] & \\ & & \end{bmatrix} \begin{Bmatrix} \varepsilon_x \\ \varepsilon_y \\ \gamma_{xy} \end{Bmatrix} \qquad (2.12)$$

where

$$[C_c] = \begin{bmatrix} \dfrac{E_x}{(1-\nu_x\nu_y)} & \dfrac{\nu_x E_y}{(1-\nu_x\nu_y)} & . \\ \dfrac{\nu_y E_x}{(1-\nu_x\nu_y)} & \dfrac{E_y}{(1-\nu_x\nu_y)} & . \\ . & . & G_{xy} \end{bmatrix}$$

and

$$[C_s] = \begin{bmatrix} p_x E_s & . & . \\ . & p_y E_s & . \\ . & . & . \end{bmatrix}$$

E_x, E_y, ν_x, ν_y and G_{xy} are elastic constants for concrete in the global coordinate system and are defined as follows

$$E_x = \alpha_x E_c \qquad \nu_x = \alpha_x \nu_c \qquad G_{xy} = G_c$$

$$E_y = \alpha_y E_c \qquad \nu_y = \alpha_y \nu_c$$

and E_c = Young's modulus for uncracked concrete

ν_c = Poisson's ratio for uncracked concrete

G_c = Shear modulus for uncracked concrete

The "cracking coefficients" α_x and α_y equal unity for the uncracked state and are reduced for tensile stresses after cracking takes place. The evaluation of these coefficients is discussed further in section 3.4.

2.4 Time Dependent Constitutive Relations

The instantaneous elastic constitutive relations for reinforced concrete have been developed above. These are now extended to include the time dependent effects of creep and shrinkage. Creep is defined as the time dependent strain due to stress, and shrinkage is defined as the time dependent strain in a stress free specimen, or the volume change with time under zero applied stress. From a mathematical standpoint it is convenient to consider the creep and shrinkage effects as independent phenomena, although the physical mechanisms involved in creep and shrinkage and their interdependence are as yet incompletely

understood.

The literature on time dependent behaviour of concrete is extensive. A review of analytical and experimental work is given by Selna[46] while Ali & Kesler[1] have surveyed the work done on the development of rheological models and related topics.

2.4.1 Uniaxial Stress

The stress-strain-time relation is developed for the uniaxial case and then generalized to the two-dimensional stress state. The following assumptions are made.

1. The Boltzman principal of superposition[37] of creep strains is valid.

2. Concrete is assumed to be an ageing linear visco-elastic material.

3. The time dependent response is the same in tension and compression for uncracked concrete.

4. Temperature effects are not included.

These assumptions have been discussed by several authors including McHenry[37], Arutyunyan[7] and Selna[46] and on the basis of available experimental data are generally accepted to be satisfactory for concrete up to approximately one half of the ultimate stress. Although tensile stresses will exceed one half of the ultimate tensile stress under working load conditions, it is assumed that the assumptions are valid over the complete range of tensile stress.

Under a given stress history $\sigma(\tau)$, the principal of superposition of creep strains allows the total stress-produced strain at time t, $\varepsilon^{\sigma}(t)$ to be written in terms of a superposition integral

$$\varepsilon^{\sigma}(t) = \int_0^t C(t,\tau)\frac{\partial\sigma(\tau)}{\partial\tau} \cdot d\tau \qquad (2.13)$$

where $C(t,\tau)$ is the specific compliance, defined as the total strain at time t due to a unit sustained stress applied at time τ.

The general form of the compliance function is shown in Figure 2.6 and may be written in the form

$$C(t,\tau) = \frac{1}{E(\tau)} + f(t-\tau,\tau) \qquad (2.14)$$

where $E(\tau)$ is the instantaneous elastic modulus at time τ and $f(t-\tau,\tau)$ is the "apparent" creep as defined by McHenry[37]. The "true" creep, also defined by McHenry is obtained from

$$\varepsilon_{CT}(t) = C(t,\tau) - \frac{1}{E(t)} \qquad (2.15)$$

Several functions have been proposed in the literature to represent the compliance. A function developed by Selna[46] and based on forms suggested by McHenry[37] and Arutyunyan[7] is used in this investigation. This function is of the general form

$$C(t,\tau) = \frac{1}{E(\tau)} + \sum_{i=1}^{m} a_i(\tau)(1-e^{-k_i(t-\tau)})$$

which may be written as

$$C(t,\tau) = (\frac{p}{\tau}+q) + (a_1+\frac{a_2}{\tau_{0.1}}+\frac{a_3}{\tau_{0.2}}+\frac{a_4}{\tau_{0.3}})[\alpha_1(1-e^{-k_1(t-\tau)})+\alpha_2(1-e^{-k_2(t-\tau)}) + \alpha_3(1-e^{-k_3(t-\tau)})] \qquad (2.16a)$$

where a value of m = 3 is used.

Separating the variables t, τ and collecting terms the compliance function may be written in the general form,

$$C(t,\tau) = A_i(\tau)\, B_i(t) + D(\tau) \quad \text{(summation convention)}$$

where

$$A_i(\tau) = -a_i(\tau)e^{k_i\tau} \quad \text{(no sum)}$$

$$B_i(t) = e^{-k_i t}$$

$$D(\tau) = \sum a_i(\tau) + \frac{1}{E(\tau)}$$

The instantaneous compliance $1/E(\tau)$ decreases hyperbolically with time, tending to a value q at infinite time. The terms $a_i(\tau)$ are the functions which account for the reduced response with increasing age at loading. For a unit stress applied at time τ this form of compliance function implies that the strain tends to a finite value at infinite time. Alternative forms of the compliance function[25] suggest that creep strains increase indefinitely. From a practical point of view, creep strains beyond a few years are not generally required and the difference between the two types of function may be made negligibly small in this time range[30].

The twelve constants, p, q, a_1, a_2, a_3, a_4, α_1, α_2, α_3, k_1, k_2, and k_3 may be obtained from standard creep test data using a least squares curve fitting technique, the details of which are given in Appendix B.

2.4.2 Plane Stress

A generalization of the time dependent constitutive relation to two dimensions requires a knowledge of Poisson's ratio for creep. In this investigation it is assumed that Poisson's ratio applied to

total stress produced strains is constant with time. Available experimental data[15,21] would suggest that this is not an unreasonable assumption.

The creep shear compliance $w(t,\tau)$ is related to the uniaxial compliance by[7]

$$w(t,\tau) = 2(1 + \nu_c)\, C(t,\tau) \tag{2.17}$$

The two dimensional constitutive relation may therefore be expressed as

$$\begin{Bmatrix} \varepsilon_x^{\sigma}(t) \\ \varepsilon_y^{\sigma}(t) \\ \gamma_{xy}^{\sigma}(t) \end{Bmatrix} = \begin{bmatrix} I & -\nu_c I & . \\ -\nu_c I & I & . \\ . & . & 2(1+\nu_c)I \end{bmatrix} \begin{Bmatrix} \sigma_x(\tau) \\ \sigma_y(\tau) \\ \tau_{xy}(\tau) \end{Bmatrix} \tag{2.18}$$

where I represents the operator $\int_0^t C(t,\tau)\frac{\partial}{\partial\tau}\,.\,d\tau$.

Adding shrinkage strains $\{\varepsilon^s(t)\}$ to stress-produced strains, the total strain at time t may be written in the form,

$$\begin{Bmatrix} \varepsilon_x^{T}(t) \\ \varepsilon_y^{T}(t) \\ \gamma_{xy}^{T}(t) \end{Bmatrix} = \begin{Bmatrix} \varepsilon_x^{\sigma}(t) \\ \varepsilon_y^{\sigma}(t) \\ \gamma_{xy}^{\sigma}(t) \end{Bmatrix} + \begin{Bmatrix} \varepsilon^{s}(t) \\ \varepsilon^{s}(t) \\ 0 \end{Bmatrix}$$

or, $\{\varepsilon^T(t)\} = \{\varepsilon^{\sigma}(t)\} + \{\varepsilon^s(t)\}$ (2.19)

2.4.3 Numerical Integration Procedure

In general, although the loading history for a structure may be specified, the corresponding stress history will be unknown because of the gradual transfer of stress from concrete to steel. To evaluate the stress and strain histories under a given applied loading, a numerical integration technique developed by Selna[46] for the uniaxial stress condition has been extended to two dimensions for the plane stress case.

The derivation of the method is given in Appendix A where it is shown that the total strain vector at time $t + \Delta t$ may be written in the form

$$\{\varepsilon^T(t+\Delta t)\} = \{\varepsilon^E(t+\Delta t)\} + \{\varepsilon^I(t+\Delta t)\} \qquad (2.20)$$

where $\varepsilon^E(t+\Delta t)$ represents the instantaneous elastic strains and $\varepsilon^I(t+\Delta t)$ represents the inelastic strains which include creep and shrinkage strains developed up to time $t + \Delta t$. The detailed expressions for $\{\varepsilon^I(t+\Delta t)\}$ are given in Equations A13, A14 and A15.

The main advantage of the numerical integration technique used is that the vector $\varepsilon^I(t+\Delta t)$ may be determined from quantities stored from the two previous time steps t and $t - \Delta t$. This is possible because the variables t and τ may be separated in the compliance function. For a more general form of the compliance function it is necessary to store the complete stress history from the first application of load since the compliance function contains the upper limit of integration in the superposition integral. In terms of the uniaxial stress condition and a series of stepwise stress increments the total stress-produced strain at time t_m may be evaluated from

$$\varepsilon^{\sigma}(t_m) = \sum_j C(t_m,t_j)\ \Delta\sigma_j \qquad (2.21)$$

It is apparent that for each time t_m, each stress increment $\Delta\sigma_j$ must be multiplied by the specific compliance corresponding to t_m. It is thus necessary to store $\Delta\sigma_j$ for all j. A numerical scheme in which it is necessary to store the complete stress history is presented by Ghali, Dilger and Neville[19].

2.4.4 Shrinkage

Shrinkage strains are known to vary throughout the thickness of a concrete member. A mathematical model of diffusion has been developed by Bresler, Helmich and Ramakrishna[12] to include the effect of a non-uniform shrinkage distribution on the behaviour of reinforced concrete columns.

In the present analysis where the slab is divided into a set of layers it would be possible to arbitrarily specify the value of shrinkage strain from layer to layer. However, for simplicity, shrinkage strains are assumed to be uniformly distributed throughout the slab. Since shrinkage tends to occur more rapidly at the surface of a concrete member this assumption neglects the restraining effect of the interior concrete on the relative movement at the exterior surface. However, this effect is less marked for thin members such as slabs than for massive concrete structures and the assumption of uniform shrinkage is considered to be a reasonable first approximation to the actual distribution of shrinkage strains in a slab.

2.5 Evaluation of Creep and Shrinkage Properties

The standard procedure for obtaining creep data for a

particular concrete is to measure the strain variation with time on an axially loaded cylinder under constant stress. Shrinkage strains are obtained from measurements in a companion cylinder with no applied stress. The creep strains due to stress are obtained by subtracting these shrinkage strains from the total strain obtained in the creep test.

Several experimental investigations (eg. Troxell, et al.[48]) have been reported in the literature describing the effects of different parameters on creep and shrinkage of concrete.

In Europe, the Comité Européen du Béton (C.E.B.) has presented expressions based on available experimental data for the evaluation of creep and shrinkage strains[43]. These expressions have been used to evaluate creep and shrinkage curves for use in the present investigation and are discussed below.

2.5.1 Creep Coefficients

Creep strains are obtained from the following expression,

$$\varepsilon^c(t) = \frac{\sigma}{E(28)} \cdot \phi_t \qquad (2.22)$$

where $\phi_t = k_c\, k_d\, k_b\, k_e\, k_t$

$E(28)$ = Modulus of elasticity at 28 days

and σ = constant applied stress

The coefficients from which ϕ_t is obtained are presented graphically in reference (43) and represent the effects of various parameters on the creep characteristics. These parameters are

k_c = f(relative humidity)

k_d = f(age at loading)

k_b = f(water/cement ratio $\frac{w}{c}$)

k_e = f(theoretical thickness)

k_t = f(duration of load)

The modulus of elasticity at j days is expressed in terms of the compressive strength by,

$$E(j) = 66{,}000 \sqrt{f'_c(j)} \tag{2.23}$$

where E and f'_c are expressed in p.s.i.

The theoretical thickness is defined as the area of the cross section divided by the semi-perimeter and for slabs may be taken equal to the actual thickness. To obtain the total strain at time t, the instantaneous strain on application of load is added to the creep strain computed above.

It is thus possible to construct a series of creep curves for a sustained load applied at different times. For the purpose of this investigation creep curves for three different concretes were constructed and designated C1, C2, and C3. The parameters k_c, k_b and k_e applicable to each of the curves are presented in Table 2.1. C1 and C2 were used for the parameter study described in Chapter 5 where C1 is intended to represent conditions under which creep strains will be considerably greater than for average conditions which are considered to be represented by C2. Curve C3 was obtained for use in chapter 4 where the analytical model is applied to examples of reinforced concrete beams for which experimental results are available.

The first step in evaluating the constants in the compliance function (Equation 2.16) is to evaluate the instantaneous elastic modulus defined in Equation 2.16 by

$$\frac{1}{E(\tau)} = \frac{p}{\tau} + q \qquad (2.24)$$

For each concrete $E(\tau)$ was computed for two values of τ and inserted in Equation 2.24. The resulting equations were then solved for p and q.

In the case of C1 and C2 the two values of $E(\tau)$ were obtained from Equation 2.23 in which f'_c was related to the w/c ratio as a function of time from curves given by McIntosh[38]. For C3 the instantaneous modulus was obtained from the published experimental results for two different times. Table 2.2 presents the two values used in each case and the resulting values for p and q.

For each concrete, three loading times were used, 7 days, 28 days and 90 days. The instantaneous elastic strain per unit stress for each loading time was computed from

$$\varepsilon^E(\tau) = 1/E(\tau)$$

and the creep strains corresponding to each loading time were computed from Equation 2.22. Adding the two strains together, three creep curves were obtained for each concrete. Using the least squares curve fitting technique described in Appendix B, the remaining 10 constants in Equation 2.16 were obtained. Table 2.3 presents the 12 constants required in the compliance function for each concrete and the compliance curves are shown in Figures 2.7 and 2.8.

2.5.2 Shrinkage Coefficients

Shrinkage strains are obtained from the expression

$$\varepsilon_s(t) = \varepsilon_c \, k_b \, k_c \, k_p \, k_t \qquad (2.25)$$

where k_b, k_c, k_t are the same as for the creep expression

k_p = f(longitudinal reinforcement) = 1.0 for plane concrete

ε_c = f(relative humidity)

Shrinkage curves for the three concretes C1, C2 and C3 are given in Figure 2.9 as well as an experimental shrinkage curve given by Troxell[48].

2.6 Summary

The constitutive relations for a layer of reinforced concrete under plane stress have been developed to include the effects of cracking and time dependent strains. To represent the behaviour after cracking concrete is treated as a bimodular material for which the modulus of elasticity in tension may be different from that in compression. With respect to time dependent behaviour, concrete is considered to be an ageing linear visco-elastic material which exhibits shrinkage. A numerical integration procedure is described which allows the strain history to be evaluated for an applied stress history, and creep and shrinkage characteristics for three different concretes have been evaluated for use in this investigation.

Concrete	R.H.%	k_c	w/c	k_b	k_e
C1	50	2.85	0.60	1.18	1.0
C2	70	2.30	0.45	0.8	1.0
C3	70	2.30	0.60	1.18	1.0

TABLE 2.1 PARAMETERS FOR EVALUATION OF CREEP STRAINS

Concrete	Young's Modulus-P.S.I.x10^6			Coeffs-Eq. 2.24-1/(P.S.I.x10^6)	
	E(14)	E(28)	E(91)	p	q
C1	-	3.84	4.34	0.77	0.1843
C2	-	4.72	5.18	1.20	0.2172
C3	2.675	2.945	-	0.95972	0.30528

TABLE 2.2 VALUES OF INSTANTANEOUS MODULUS

Concrete	k_1	k_2	k_3	α_1	α_2	α_3	a_1	a_2	a_3	a_4	p	q
C1	0.2	0.04	0.002	0.39105	0.37638	1.0	$-.17189 \times 10^{-5}$	0.45416×10^{-5}	-0.13153×10^{-5}	$-.75942 \times 10^{-7}$	1.20×10^{-6}	0.2172×10^{-6}
C2	0.2	0.03	0.002	0.49568	0.46588	1.0	$.15095 \times 10^{-5}$	$-.65104 \times 10^{-5}$	$.96410 \times 10^{-5}$	$-.40182 \times 10^{-5}$	0.77×10^{-6}	0.1843×10^{-6}
C3	0.2	0.02	0.002	1.0968	1.83811	1.0	$-.8742 \times 10^{-7}$	$-.5802 \times 10^{-6}$	0.2437×10^{-5}	$-.1221 \times 10^{-5}$	0.9597×10^{-6}	0.3053×10^{-6}

TABLE 2.3 CONSTANTS FOR COMPLIANCE FUNCTION

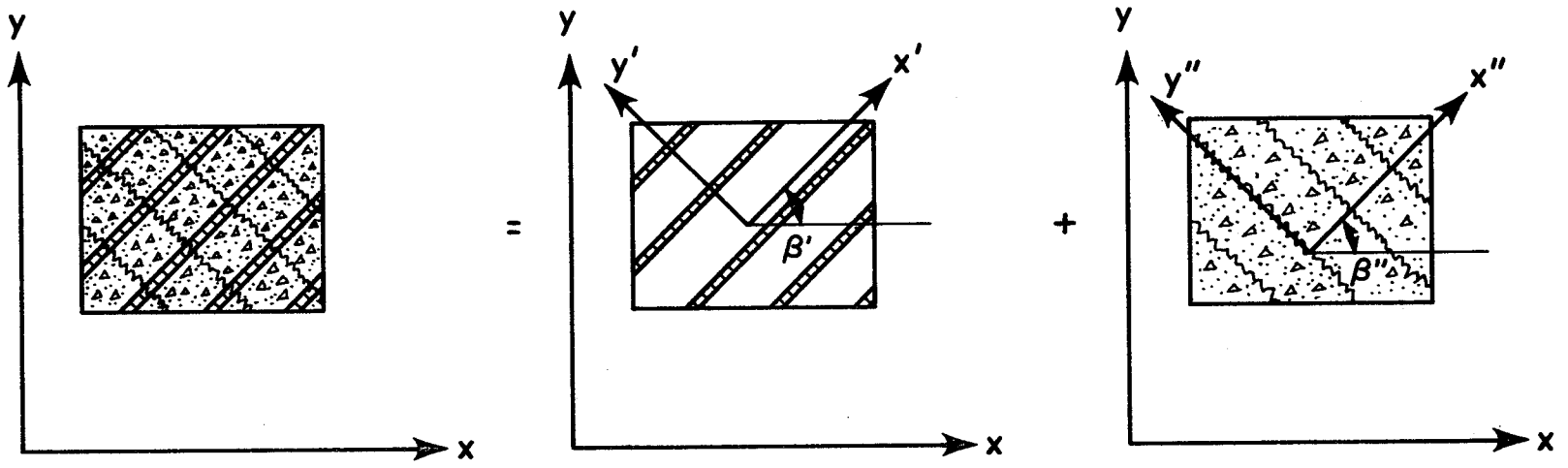

FIGURE 2.1 ELEMENT FROM REINFORCED CONCRETE LAYER CONTAINING CRACKS

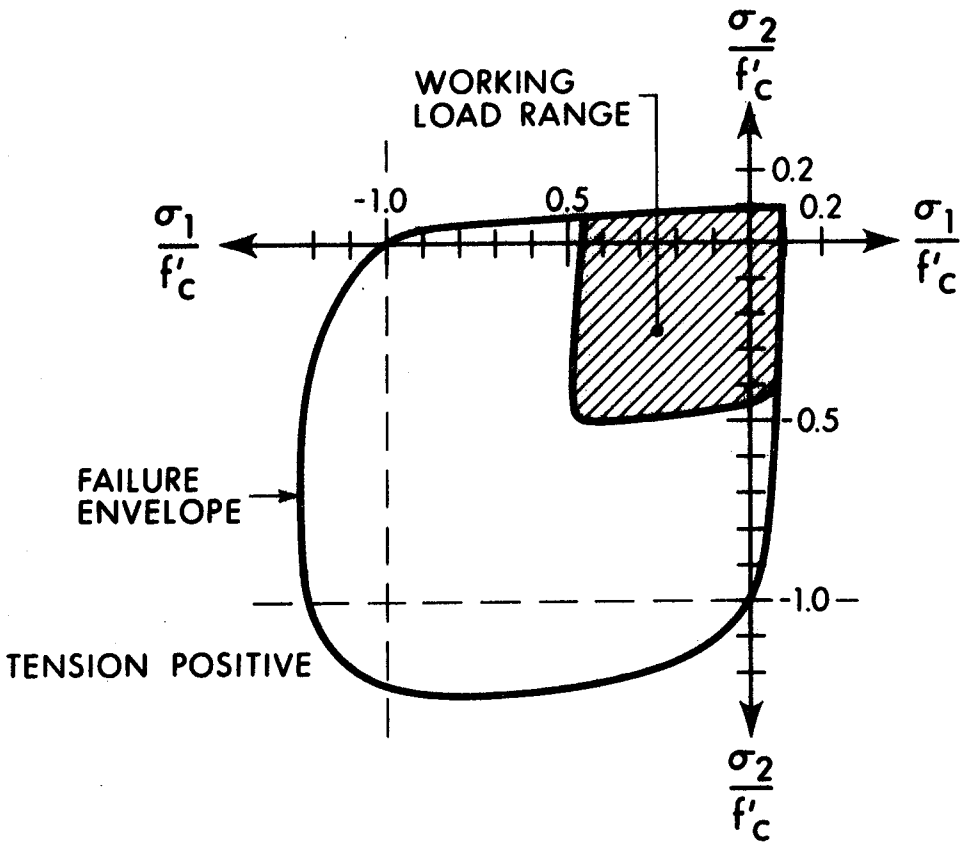

FIGURE 2.2 BIAXIAL STRENGTH OF CONCRETE

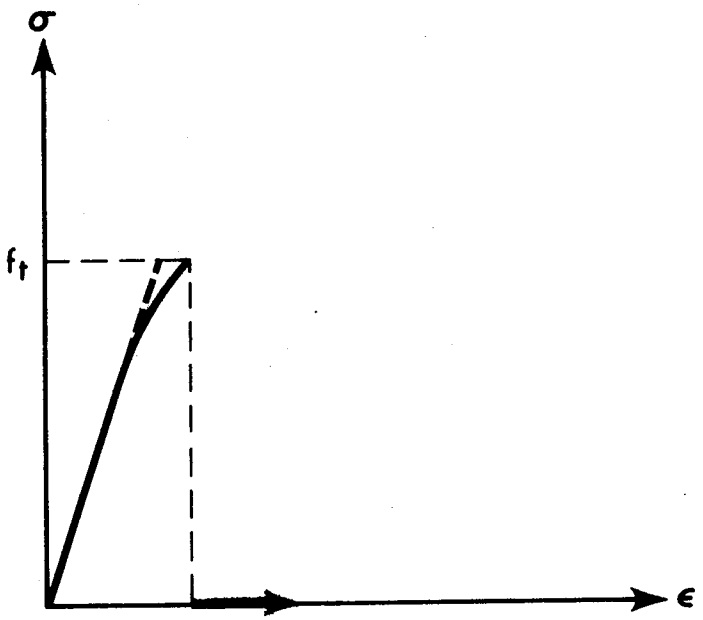

FIGURE 2.3 STRESS STRAIN DIAGRAM FOR PLANE CONCRETE IN TENSION

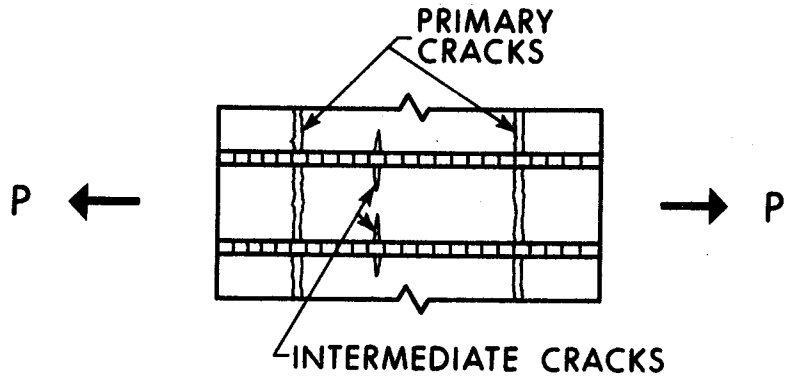

(a) CRACKING IN MEMBER UNDER UNIAXIAL TENSION

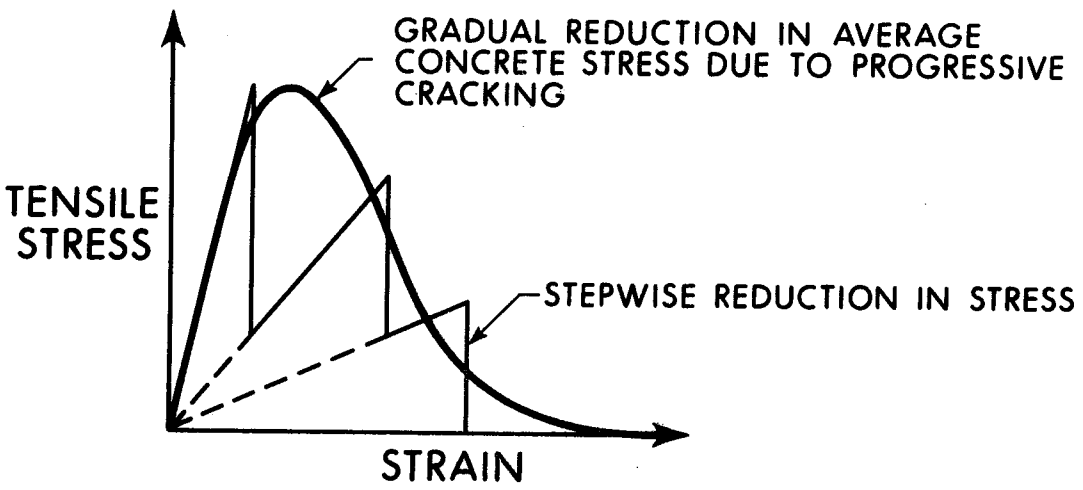

FIGURE 2.4 TENSILE STRESS IN REINFORCED CONCRETE

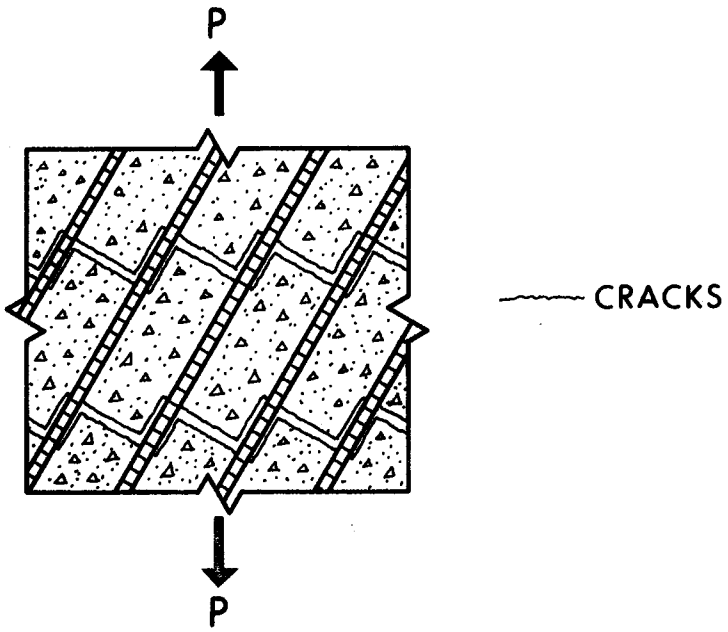

(a) CRACKING BEHAVIOUR OBSERVED BY MORLEY (ref. 40)

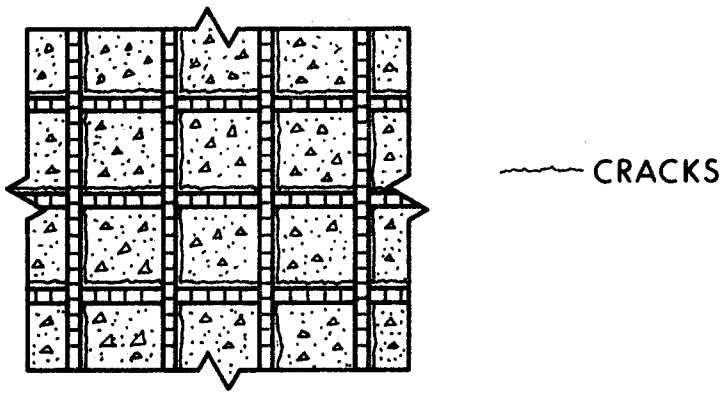

(b) CRACKING PATTERNS OBSERVED BY NAWY (ref. 41)

FIGURE 2.5 CRACKING IN REINFORCED CONCRETE

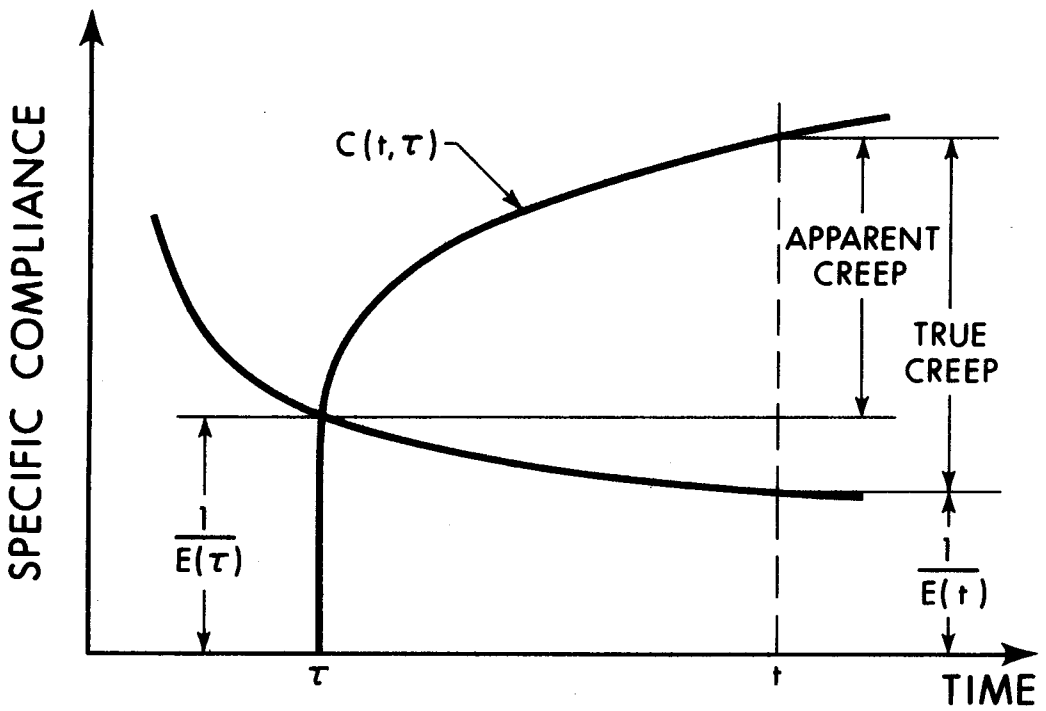

FIGURE 2.6 COMPLIANCE CURVE FOR AGEING CONCRETE

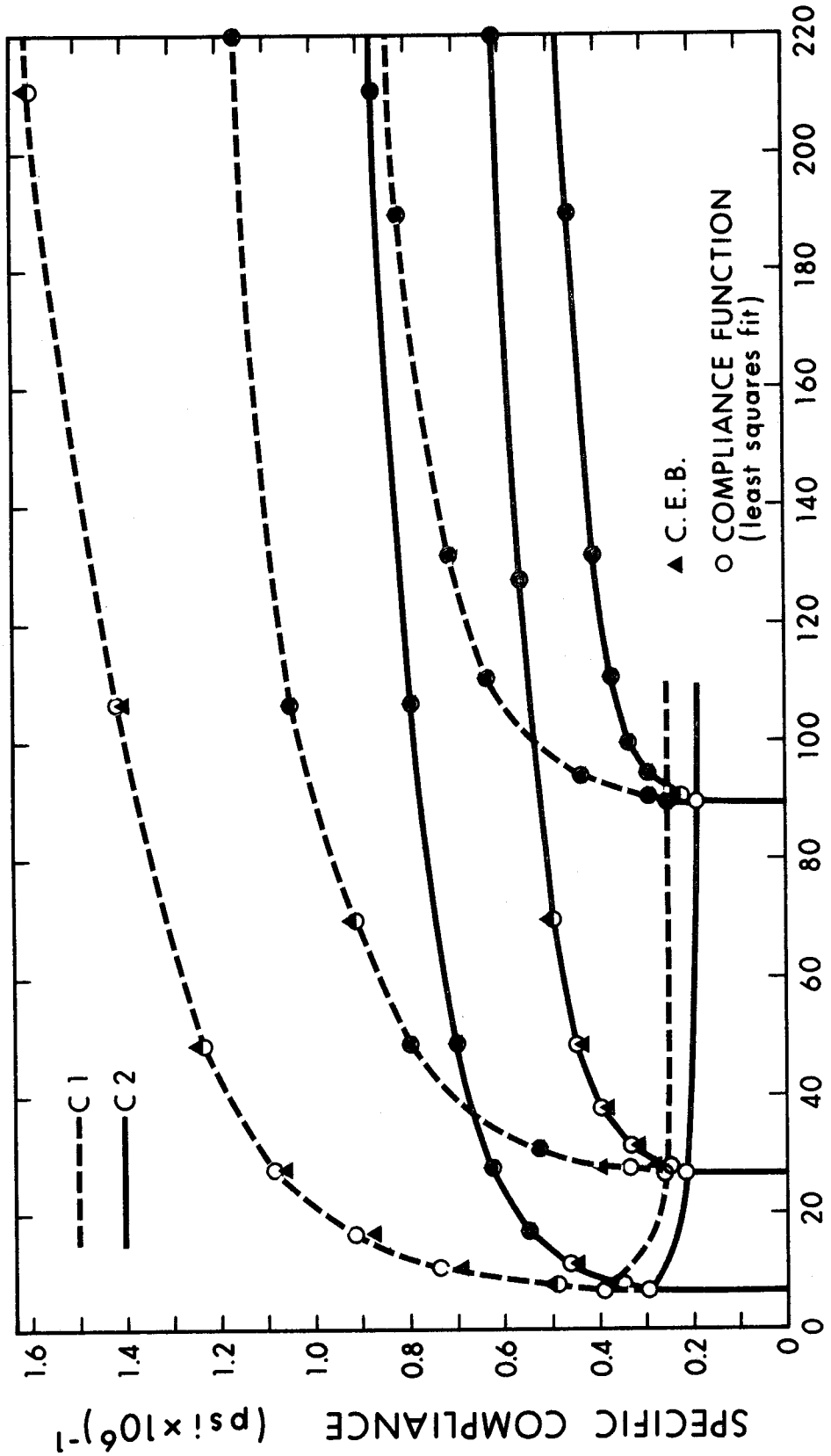

FIGURE 2.7 COMPLIANCE CURVES FOR C1 and C2

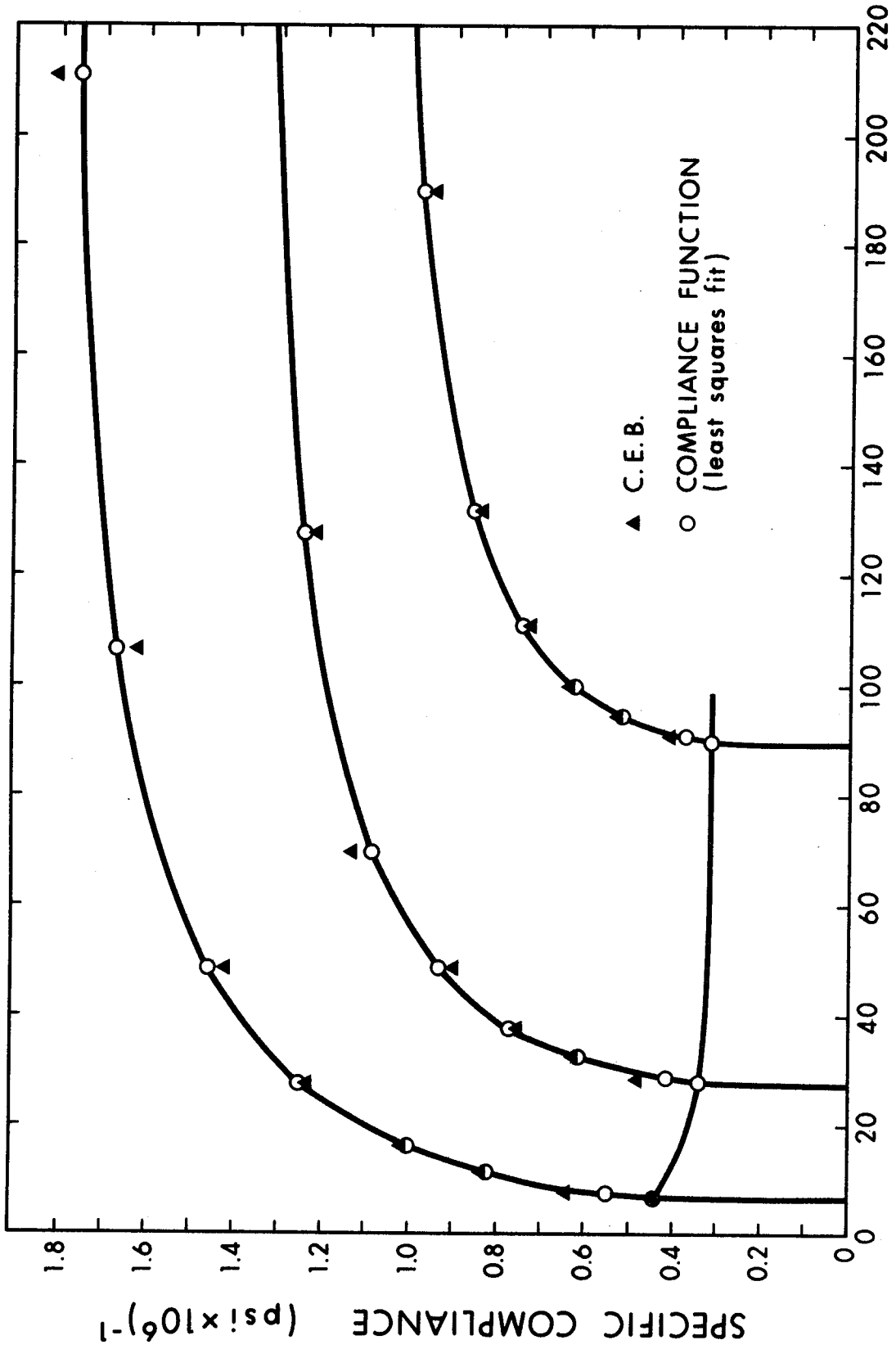

FIGURE 2.8 COMPLIANCE CURVES FOR C3

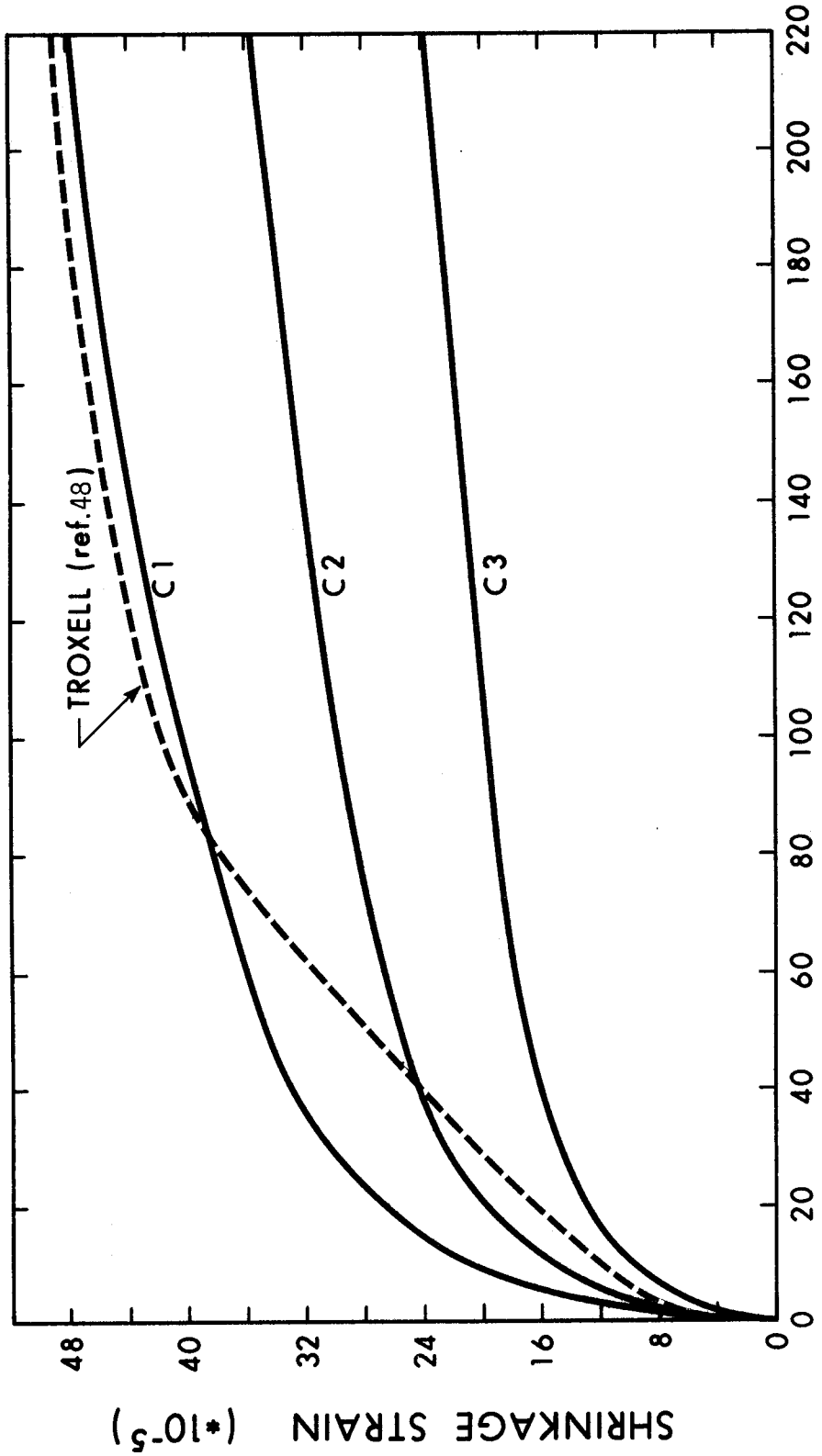

FIGURE 2.9 SHRINKAGE CURVES

CHAPTER 3

METHOD OF ANALYSIS

3.1 Introduction

In order to perform a structural analysis it is necessary to define a mathematical model which simulates as accurately as is required, the actual behaviour of the structure. Such a model generally requires assumptions regarding the geometry of the structure, boundary conditions, and load deformation response or constitutive relations. Once the model has been defined the conditions of equilibrium and compatibility of deformations must be satisfied.

Reinforced concrete slabs have generally been analyzed[18] on the basis of classical small deflection plate bending theory[47] assuming the material to be linear elastic, homogeneous and isotropic, thereby neglecting the effects of cracking, reinforcement and time dependent behaviour. The assumptions used in this thesis concerning material properties have been described in Chapter 2. On the basis of these constitutive relations, the general method of analysis is described in this chapter. The analysis is based on the finite element method applied to plate bending. A major advantage of this approach over other methods is that material properties may be varied from element to element. The analysis is therefore able to take into account variations in reinforcement in the slab as well as the effects of cracking in the highly stressed regions. The initial strain method[6,26,34] is used for time-dependent behaviour.

3.2 Plate Bending Theory Applied to Slabs

Classical small deflection plate bending theory[47] assumes

that the material is linear elastic,homogeneous and isotropic and that the strain developed at the mid-surface may be neglected for transverse loading so that the net force developed in the plane of the plate is zero. The corresponding theory of anisotropic plates developed by Lekhnitskii[32] assumes that material properties are symmetrical with respect to the mid-surface in which case the strains in the mid-surface may be neglected and the net force in the plane of the plate is again zero.

Reinforced concrete slabs do not in general have such a "neutral" mid-surface due to the presence of cracking and unsymmetrical reinforcement layouts. The assumptions used in formulating the problem must therefore be modified. The Kirchhoff assumption that normals to a surface remain normal after deformation is retained and the constitutive relations are considered to represent an orthotropic material but may vary throughout the plate. Appendix E describes the general formulation for coupling between in-plane and out-of-plane behaviour for small deflections. For the purposes of the analysis developed in this work, it is assumed that the net in-plane force on any cross section is zero. This assumption implies that restraint to shrinkage is supplied only by the reinforcement and that in-plane restraints applied at the boundary and by adjacent slab segments may be neglected.

Figure 3.1(a) shows the coordinate system defining the undeformed configuration of the plate. The x and y axes lie on the top surface. Figure 3.1(b) shows the elevation of a small element of the plate in the x,z plane before and after deformation where the points A and B take up the positions A' and B'. From the Kirchoff assumption the displacements of the line AB may be defined in terms of the

displacement of any point on AB and the slope of the reference surface,

$$u = u(x,y,z) = u_o(x,y) + (d_{nx}(x,y)-z)\frac{\partial w}{\partial x}$$

$$v = v(x,y,z) = v_o(x,y) + (d_{ny}(x,y)-z)\frac{\partial w}{\partial y} \qquad (3.1)$$

$$w = w(x,y,z) = w(x,y)$$

where d_{nx} and d_{ny} represent the depths corresponding to u_o and v_o respectively and are not necessarily the same. The strain displacement relations may be written as,

$$\varepsilon_x = \frac{\partial u}{\partial x} = \frac{\partial u_o}{\partial x} + (d_{nx}-z)\frac{\partial^2 w}{\partial x^2} = \varepsilon_{ox}+(d_{nx}-z)\frac{\partial^2 w}{\partial x^2}$$

$$\varepsilon_y = \frac{\partial v}{\partial y} = \frac{\partial v_o}{\partial y} + (d_{ny}-z)\frac{\partial^2 w}{\partial y^2} = \varepsilon_{oy}+(d_{ny}-z)\frac{\partial^2 w}{\partial y^2}$$

$$\gamma_{xy} = \frac{\partial u}{\partial y} + \frac{\partial v}{\partial x} = \frac{\partial u_o}{\partial y} + \frac{\partial v_o}{\partial x} + (\frac{d_{nx}+d_{ny}}{2} - z)\cdot 2\frac{\partial^2 w}{\partial x \partial y} = \bar{\gamma}_{oxy}+(\frac{d_{nx}+d_{ny}}{2} - z)\cdot 2\frac{\partial^2 w}{\partial x \partial y}$$

Although u_o and v_o represent displacements which may be at different depths, d_{nx} and d_{ny} respectively, the expression for γ_{xy} is linear with respect to the depth and may therefore be re-written in the form

$$\gamma_{xy} = \gamma_{oxy} + (d_{nxy} - z)\cdot 2\frac{\partial^2 w}{\partial x \partial y}$$

where γ_{oxy} represents the shear strain at an arbitrary depth d_{nxy}.

These equations for strain may be written as a single matrix equation

$$\{\varepsilon\} = \{\varepsilon_o\} + [N]\{\kappa\} \qquad (3.2)$$

where

$$\{\varepsilon\} = \langle \varepsilon_x, \varepsilon_y, \gamma_{xy} \rangle^T$$

$$\{\varepsilon_o\} = \langle \varepsilon_{ox}, \varepsilon_{oy}, \gamma_{oxy} \rangle^T$$

$$\{\kappa\} = \langle \kappa_x, \kappa_y, \kappa_{xy} \rangle^T$$

$$= \langle \frac{\partial^2 w}{\partial x^2}, \frac{\partial^2 w}{\partial y^2}, 2\frac{\partial^2 w}{\partial x \partial y} \rangle^T$$

and

$$[N] = \begin{bmatrix} d_{nx}-z & . & . \\ . & d_{ny}-z & . \\ . & . & d_{nxy}-z \end{bmatrix}$$

Defining d_{nx}, d_{ny} and d_{nxy} such that $\varepsilon_{ox} = \varepsilon_{oy} = \gamma_{oxy} = 0$, Equation (3.2) becomes

$$\{\varepsilon\} = [N]\{\kappa\} \tag{3.3}$$

The plane stress constitutive relations for an orthotropic material may be written as (Equation 2.12),

$$\begin{Bmatrix} \sigma_x \\ \sigma_y \\ \tau_{xy} \end{Bmatrix} = \begin{bmatrix} E_x/(1-\nu_x\nu_y) & \nu_x E_y/(1-\nu_x\nu_y) & . \\ \nu_y E_x/(1-\nu_x\nu_y) & E_y/(1-\nu_x\nu_y) & . \\ . & . & G_{xy} \end{bmatrix} \begin{Bmatrix} \varepsilon_x \\ \varepsilon_y \\ \gamma_{xy} \end{Bmatrix}$$

or in matrix form

$$\{\sigma\} = [C]\{\varepsilon\} = [C][N]\{\kappa\} \tag{3.4}$$

The assumption that no in-plane forces are developed in the plane of the plate requires that,

$$\int_0^d \sigma_x dz = \int_0^d \frac{E_x}{(1-\nu_x\nu_y)} (d_{nx}-z)\kappa_x dz + \int_0^d \frac{\nu_x E_y}{(1-\nu_x\nu_y)} (d_{ny}-z)\kappa_y dz = 0$$

$$\int_0^d \sigma_y dz = \int_0^d \frac{\nu_y E_x}{(1-\nu_x\nu_y)} (d_{nx}-z)\kappa_x dz + \int_0^d \frac{E_y}{(1-\nu_x\nu_y)} (d_{ny}-z)\kappa_y dz = 0$$

$$\int_0^d \tau_{xy} dz = \int_0^d G_{xy} (d_{nxy}-z) \cdot 2\kappa_{xy}\, dz = 0$$

i.e.

$$\int_0^d [C][N]dz \{\kappa\} = 0 \qquad (3.5)$$

To allow for a variation in elastic constants with depth the slab is considered as a series of layers. The constitutive matrix may vary from layer to layer but is considered to be constant within the layer. Figure 3.2 shows an element of a reinforced concrete slab represented as a layered plate. Layers of concrete are numbered consecutively from top to bottom and the constitutive matrix for layer i is represented by $[C]_i$,

$$[C]_i = \begin{bmatrix} \frac{E_{xi}}{(1-\nu_{xi}\nu_{yi})} & \frac{\nu_{xi} E_{yi}}{(1-\nu_{xi}\nu_{yi})} & . \\ \frac{\nu_{yi}E_{xi}}{(1-\nu_{xi}\nu_{yi})} & \frac{E_{yi}}{(1-\nu_{xi}\nu_{yi})} & . \\ . & . & G_{xyi} \end{bmatrix} \qquad (3.6)$$

Making the simplifying assumption that G_{xy} is constant over

the depth (see Section 2.3) it is apparent that Equation (3.5) requires that $d_{nxy} = \frac{d}{2}$.

For complete symmetry of elastic constants with respect to the mid surface, d_{nx} and d_{ny} are also defined by $d_{nx} = d_{ny} = d/2$. However, for the general case of unsymmetrical elastic constants, it can be seen from Equation (3.5) that d_{nx} and d_{ny} are coupled with the curvatures κ_x and κ_y. This coupling is due to the Poisson's ratio terms. In reinforced concrete slabs, the amount of reinforcement is usually small so that for uncracked sections even if the reinforcement is placed unsymetrically with respect to the mid surface, the Poisson's ratio effect on d_{nx} and d_{ny} will be small. For a cracked section Poisson's ratio, which for uncracked concrete lies in the range 0.1 to 0.2 drops to a value approaching zero over a large part of the depth. The coupling terms therefore have a reduced effect. Since curvatures are unknown at the beginning of the analysis, an iterative procedure would be required to evaluate d_{nx} and d_{ny} exactly. However, since the coupling due to the Poisson's ratio effect will be weak, for the purposes of this analysis d_{nx} and d_{ny} are computed assuming Poisson's ratio equal to zero. In this case d_{nx} and d_{ny} simply define the centroid of transformed area on the x and y faces respectively and are computed as follows,

$$d_{nx} = \left(\sum_{i=1}^{n} \alpha_{xi}(z_{i+1} - z_i)\left(\frac{z_{i+1}+z_i}{2}\right) + A_{tx}\frac{E_s}{E_c}d_{tx} + A_{bx}\frac{E_s}{E_c}d_{bx}\right)/A_x$$

$$d_{ny} = \left(\sum_{i=1}^{n} \alpha_{yi}(z_{i+1} - z_i)\left(\frac{z_{i+1}+z_i}{2}\right) + A_{ty}\frac{E_s}{E_c}d_{ty} + A_{by}\frac{E_s}{E_c}d_{by}\right)/A_y \qquad (3.7)$$

where A_x and A_y represent transformed cross-sectional areas per unit length in the x and y directions respectively and are obtained from,

$$A_x = \sum_{i=1}^{n} \alpha_{xi}(z_{i+1} - z_i) + (A_{tx} + A_{bx}) \frac{E_s}{E_c}$$

$$A_y = \sum_{i=1}^{n} \alpha_{yi}(z_{i+1} - z_i) + (A_{ty} + A_{by}) \frac{E_s}{E_c}$$

If d_{nx} and d_{ny} are evaluated as above, Equation (3.5) is approximately satisfied and in subsequent development it is assumed that,

$$\int_o^d [C]\,[N]\,dz = 0 \tag{3.8}$$

Moments and twist per unit length may now be evaluated from,

$$M_x = \int_o^d \sigma_x(d_{nx} - z)\,dz$$

$$M_y = \int_o^d \sigma_y(d_{ny} - z)\,dz$$

$$M_{xy} = \int_o^d \tau_{xy}(d_{nxy} - z)\,dz$$

which may be expressed in matrix form as

$$\{M\} = \int_o^d [N]^T[C][N]dz\ \{\kappa\}$$

$$= [D]\ \{\kappa\} \tag{3.9}$$

where

$$[D] = \begin{bmatrix} D_{11} & D_{12} & \cdot \\ D_{21} & D_{22} & \cdot \\ \cdot & \cdot & D_{33} \end{bmatrix}$$

The elements of [D] may be obtained by layer integration from the following expressions,

$$D_{11} = \sum_{i=1}^{n} \frac{E_{xi}}{(1-\nu_{xi}\nu_{yi})} \left(d_{nx} - \frac{(z_{i+1}+z_i)}{2}\right)^2 (z_{i+1}-z_i) + A_{tx}E_s(d_{nx}-d_{tx})^2 + A_{bx}E_s(d_{nx}-d_{bx})^2$$

$$D_{22} = \sum_{i=1}^{n} \frac{E_{yi}}{(1-\nu_{xi}\nu_{yi})} \left(d_{ny} - \frac{(z_{i+1}+z_i)}{2}\right)^2 (z_{i+1}-z_i) + A_{ty}E_s(d_{ny}-d_{ty})^2 + A_{by}E_s(d_{ny}-d_{by})^2 \qquad (3.10)$$

$$D_{12} = \sum_{i=1}^{n} \frac{\nu_{xi}E_{yi}}{(1-\nu_{xi}\nu_{yi})} \left(d_{nx} - \frac{(z_{i+1}+z_i)}{2}\right)\left(d_{ny} - \frac{(z_{i+1}+z_i)}{2}\right)(z_{i+1}-z_i)$$

$$D_{21} = D_{12}$$

$$D_{33} = \frac{Gd^3}{12}$$

where $E_{xi} = \alpha_{xi} E_c$, $E_{yi} = \alpha_{yi} E_c$

$\nu_{xi} = \alpha_{xi} \nu_c$, $\nu_{yi} = \alpha_{yi} \nu_c$

The governing equation for bending of an orthotropic plate is given by[47]

$$D_{11} \frac{\partial^4 w}{\partial x^4} + 2(D_{12}+2D_{33}) \frac{\partial^4 w}{\partial x^2 \partial y^2} + D_{22} \frac{\partial^4 w}{\partial y^4} = q \qquad (3.11)$$

For the case in which the elements of [D] vary with x and y, a closed form solution of Equation (2.11) becomes difficult if not

impossible. In addition cracked regions will not in general be known at the beginning of the analysis so that an iterative solution is required for the evaluation of [D].

The finite element approach is ideally suited to this type of problem since material properties may be easily varied from element to element and if required, within each element. An iterative procedure for cracking may also be programmed for the computer.

3.3 Plate Bending Element-Elastic Response

In terms of the displacement method of analysis the finite element method[53] may be considered as a means of expressing the unknown continuous displacement function approximately in terms of a linear combination of assumed shape functions. The multiplying parameters are the displacement degrees of freedom at the nodes. The problem may then be formulated in terms of a set of algebraic equations rather than differential equations. The accuracy of the solution compared with the "exact" solution generally depends on how closely the assumed displacement function can represent the actual function.

The finite element method has been applied extensively to the problem of plate bending and much effort has been expended on the development of plate bending elements and evaluation of convergence criteria. A survey of work done in this field is given by Gallagher [17]. The element used in this analysis is the sixteen degrees of freedom rectangular element developed by Bogner, Fox and Schmit[10]. This element was chosen because of its excellent convergence

characteristics and because only slabs which are rectangular in plan are considered. The general method of analysis however is independent of the particular element used.

The transverse displacement function w(x,y) within each element is represented by a combination of Hermitian interpolation functions which express w(x,y) in terms of four nodal degrees of freedom at each corner of the element. Satisfaction of compatibility requirements at each node ensures complete inter-element kinematic compatibility along the edges of all elements. In addition, all constant strain states (curvature and twist) are represented.

Figure 3.3 shows a rectangular element with sides of length 'a' in the x direction and 'b' in the y direction. The degrees of freedom at each node ij are,

transverse displacement	w_{ij}
slope in the x-direction	$(\frac{\partial w}{\partial x})_{ij}$
slope in the y-direction	$(\frac{\partial w}{\partial y})_{ij}$
twist	$(\frac{\partial^2 w}{\partial x \partial y})_{ij}$

In terms of the non-dimensionalized coordinates $\xi = \frac{x}{a}$ and $\eta = \frac{y}{b}$ the displacement function may be written as,

$$w(\xi,\eta) = \sum_{i=1}^{2} \sum_{j=1}^{2} [H_{oi}^{(1)}(\xi)\, H_{oj}^{(1)}(\eta) \cdot w_{ij} + H_{1i}^{(1)}(\xi)\, H_{oj}^{(1)}(\eta) \cdot a \cdot w_{,xij}$$

$$+ H_{oi}^{(1)}(\xi)\, H_{1j}^{(1)}(\eta) \cdot b\, w_{,yij} + H_{1i}^{(1)}(\xi)\, H_{1j}^{(1)}\, a\, b\, w_{,xyij}] \quad (3.12)$$

where $H_{01}^{(1)}(s) = 2s^3 - 3s^2 + 1$

$$H_{02}^{(1)}(s) = -2s^3 + 3s^2 \qquad (3.13)$$

$$H_{11}^{(1)}(s) = s^3 - 2s^2 + s$$

$$H_{12}^{(1)}(s) = s^3 - s^2$$

The form of each function in Equation (3.13) is shown in Figure 3.3.

Writing the set of nodal degrees of freedom as a column vector $\{r\}$ given by

$$\{r\}^T = \langle w_{11}\ w_{,x11}\ w_{,y11}\ w_{,xy11}\ w_{12}\ w_{,x12}\ w_{,y12}\ w_{,xy12}$$
$$w_{22}\ w_{,x22}\ w_{,y22}\ w_{,xy22}\ w_{21}\ w_{,x21}\ w_{,y21}\ w_{,xy21} \rangle$$

and the combinations of interpolation functions as a row vector $\langle\phi\rangle$, in which the components are functions of ξ and η, results in,

$$w(\xi,\eta) = \langle\phi\rangle \{r\} \qquad (3.14)$$

By differentiation, curvatures and twist are obtained,

$$\{\kappa\} = [B] \{r\} \qquad (3.15)$$

and the strain distribution through the thickness may be written from Equation (3.3) as

$$\{\varepsilon\} = [N] \{\kappa\} = [N][B] \{r\} \qquad (3.16)$$

The principle of minimum potential energy requires that the total potential be a minimum for an equilibrium configuration. The

total potential, Π, is given by,

$$\Pi = \Sigma + W \tag{3.17}$$

where Σ represents the strain energy and W the potential of the applied forces. The strain energy may be written as,

$$\Sigma = \frac{1}{2}\int_V \{\sigma\}^T \{\varepsilon\}\, dV \tag{3.18}$$

Substituting for $\{\varepsilon\}$ and $\{\sigma\}$ using Equations (3.4), (3.9) and (3.16),

$$\Sigma = \frac{1}{2}\int_A \{r\}^T[B]^T[D][B]dA\{r\} \tag{3.19}$$

The potential of the external forces may be obtained from,

$$W = -\int_A q(\xi,\eta) \cdot w(\xi,\eta)\, dA$$

Substituting from Equation (3.14),

$$W = -\int_A q(\xi,\eta)\{r\}^T \{\phi\}\, dA$$

$$= -\{r\}^T \{R\} \tag{3.20}$$

where $$\{R\} = \int_A q(\xi,\eta)\{\phi\}\, dA \tag{3.21}$$

and may be considered to represent the vector of work-equivalent generalized forces corresponding to the vector $\{r\}$.

To minimize Π,

$$\frac{\partial \Pi}{\partial \{r\}^T} = 0 \tag{3.22}$$

which yields

$$\int_A [B]^T[D][B]\, dA \cdot \{r\} = \{R\} \tag{3.23}$$

or,

$$[k]\,\{r\} = \{R\} \tag{3.24}$$

where $[k] = \int_A [B]^T[D][B]\, dA$ represents the element stiffness matrix. Explicit expressions for [k] are given in reference (10) for a linear elastic, homogeneous and isotropic plate element and reference (26) presents expressions for an anisotropic plate element (all elements of [D] non-zero in general). For the purposes of this investigation a subroutine was written to generate the elements of the stiffness matrix for an orthotropic plate element. The input required for this subroutine consists of the matrix [D], the lengths of the sides of the element and the coefficients of the functions represented by the matrix [B]. Details of the subroutine are presented in Appendix C along with expressions for the load vector {R}.

The standard procedures of matrix structural analysis[42] are now followed in assembling the structure stiffness matrix and load vector, for the complete structure treated as a free body, to form the equations

$$[K']\,\{\Delta'\} = \{P'\} \tag{3.25}$$

In order to obtain a solution, the equations must be modified for the prescribed boundary conditions to form the equations,

$$[K]\,\{\Delta\} = \{P\} \tag{3.26}$$

where $\{\Delta\}$ represents the set of unknown degrees of freedom. The equations are solved by a Gauss elimination procedure utilizing the banded

symmetric form of [K].

3.4 Computation of Elastic Constants for a Layer

In Section 2.3.2, the use of a stepped stress-strain diagram to account for the tensile stiffening effect of concrete between cracks was discussed. The application of this concept to the iterative analysis for cracking is now described.

For each layer it is necessary to record the current branch of the stress strain diagram defining the tensile elastic constants in the layer. This is accomplished by means of a "memory function" δ, which is assigned a different value for each branch of the diagram. The procedure for specifying the elastic constants in a layer for each cycle of the iteration procedure is illustrated by the flow chart in Figure 3.4(b) which is written for a stress strain diagram with N branches. A stress strain diagram with 4 branches is shown in Figure 3.4(a).

At the beginning of the analysis, all layers are assumed to be uncracked, in which case, $\delta = \alpha_x = \alpha_y = \alpha_1 = 1$. At a subsequent stage in the iterative procedure the principal stresses σ_1 and σ_2 are computed for the layer using elastic constants associated with the δ established in the previous cycle. The principal stresses are compared with the limiting tensile stress σ_{Ti} corresponding to $\delta = i$. If the limiting stress is exceeded by either σ_1 or σ_2 the tensile elastic constants are modified to correspond to the next lower branch on the diagram. The elastic constants for either the x or y direction are modified only if the corresponding normal stress is tensile.

The variable REPEAT which is set equal to zero at the beginning of each cycle is set equal to 1 which signifies that another

iteration cycle will be required for the new elastic constants. For each iteration cycle, the elastic constants are examined in each layer at each corner of each element. The correct cracked configuration is attained when no further modification of elastic constants takes place.

3.5 Analysis for Cracking

Equation (3.10) presents the expressions for the evaluation of the plate bending stiffness coefficients D_{ij} at a point x,y in the plate. The evaluation of the elastic constants throughout the depth is accomplished by the method described in Section 3.4. It now remains to evaluate [D] = [D(x,y)] for use in Equation (3.19) which is written for an arbitrary variation of [D] over the area of the element.

Several methods might be envisaged for evaluating [D]. The simplest means would be to evaluate the stress conditions at the centre of the element, modify the elastic constants if necessary and compute the resulting [D] matrix. The values thus obtained could be considered to be constant over the area.

Alternatively, [D] could be evaluated at the corner of the element from the stress conditions at these points. The choice then remains as to how the variation is to be assumed over the area. By the use of interpolation functions[16], a linear variation may be assumed with each term in the matrix written in the form

$$D_{ij}(x,y) = < \phi_D > \begin{Bmatrix} D_{ij}^{(1)} \\ D_{ij}^{(2)} \\ D_{ij}^{(3)} \\ D_{ij}^{(4)} \end{Bmatrix}$$

where $<\phi_D>$ represents a set of linear interpolation functions and $D_{ij}^{(k)}$ represents D_{ij} evaluated at node k. An alternative, simpler procedure and the one chosen for this analysis is to take the average of the nodal values,

$$D_{ij} = \frac{1}{4} \sum_{k=1}^{4} D_{ij}^{(k)} \tag{3.27}$$

and insert the resulting [D] matrix in Equation (3.22). Since the assumed displacement function is cubic in x and y, the strain distribution over an element will be linear and the maximum stress values will occur at the corners. It is therefore possible that cracking detected at the corner of an element may not be detected for stress conditions evaluated only at the centre.

The steps required in the iterative procedure for cracking may be summarized as follows:

1. Divide the slab into a number of rectangular finite elements. The location of the element is defined by the x and y coordinates of the four corners (Figure 3.3).

2. At the corner of each element, divide the slab into a number of layers (Figure 3.2). The number of layers may vary from corner to corner but will usually be the same throughout the slab.

3. For each layer at the corner of each element, set the cracking coefficients equal to unity (i.e. assume the slab to be uncracked).

4. Compute d_{nx} and d_{ny} at the corner of each element (Equation 3.7).

5. Evaluate [D] at the corner of each element (Equation 3.10).

6. Evaluate the average [D] for each element (Equation 3.27).

7. Evaluate the element stiffness matrix (Equation 3.24) for each element and assemble the structure stiffness matrix.

8. Compute the contribution of each element to the applied load vector (Equation 3.21) and assemble the load vector for the structure.

9. Modify the assembled equations (Equation 3.25) for the given boundary conditions and solve the resulting set (Equation 3.26) for the unknown displacements.

10. At the corner of each element, compute curvatures and twist (Equation 3.15) and the strain distribution throughout the depth (Equation 3.16).

11. Check the stress conditions in each layer for further cracking by the procedure described in Section 3.4.

12. If α_x or α_y require modification in any layer, repeat steps 4-11 (inclusive) with the revised values of the cracking coefficients.

13. If no further modification is necessary, the correct approximate solution has been obtained for the load level considered.

The iterative procedure is shown schematically in Figure 3.5. In Figure 3.5(a), a load P greater than the load P_c required to produce cracking is applied to the structure producing a deflection δ_u assuming no cracking. The iterative procedure gradually reduces the overall stiffness to a value K_c at which no further cracking is detected. The resulting deflection is δ_c. Figure 3.5(b) shows the procedure applied to incremental loading to produce a load-deflection curve for increasing load (unloading always takes place along a line through the origin). The iterative procedure is carried out at each load level.

3.6 Time-Dependent Strains

The major difference between the analysis for cracking described above and the analysis for time-dependent effects is that for the latter, the relationship between total stress and total strain is a non-linear function of time. The time-dependent constitutive relations have been described in Sections 2.4.1 and 2.4.2 along with a numerical integration technique (Section 2.4.4) which allows the total strain at time $t + \Delta t$, $\varepsilon^T(t+\Delta t)$, to be written as the sum of the instantaneous elastic strain $\varepsilon^E(t+\Delta t)$ and the inelastic strain $\varepsilon^I(t+\Delta t)$ consisting of creep and shrinkage strains up to time $t + \Delta t$.

$$\{\varepsilon^T(t+\Delta t)\} = \{\varepsilon^E(t+\Delta t)\} + \{\varepsilon^I(t+\Delta t)\} \qquad (3.28)$$

From Equation (A.18), stress is related to elastic strain by the instantaneous elastic constitutive relation for time $t + \Delta t$,

$$\{\sigma(t+\Delta t)\} = [C(t+\Delta t)]\,\{\varepsilon^E(t+\Delta t)\}$$

$$= [C(t+\Delta t)]\,\{\{\varepsilon^T(t+\Delta t)\} - \{\varepsilon^I(t+\Delta t)\}\} \qquad (3.29)$$

3.6.1 Initial Strain Method

Any material or structure for which the relationship between stress and total strain is non-linear may be analyzed by the initial strain method[34]. Figure 3.6 shows three cases for which initial stress may arise in the material. Figure 3.6(a) represents a linear elastic material in which the initial strains are independent of stress; eg. thermal, shrinkage or "lack-of'fit" strains. In Figure 3.6(b) the initial strains are due to a non-linear stress strain diagram.

Figure 3.5(c) represents initial strains due to creep, where a constant stress is applied at time τ_0. The initial strains are obtained by projecting on to the strain axis using the elastic modulus at time τ_1 which will be different from that at time τ_0 for an ageing material.

If the distribution of initial strains is known, a solution may be obtained by:

(a) Determining restraining forces, to prevent all deformations which would arise from inelastic strains, using current values of the linear elastic constitutive matrix.

(b) Determining the displacements of the structure by a linear elastic analysis in which the applied loads are augmented by the negative of the restraining forces in (a).

(c) Evaluating stresses by subtracting the initial strains from total strains for use with the current linear elastic constitutive matrix.

If the initial strains are not known at the beginning of the analysis, either an iterative procedure or an incremental procedure is required to evaluate the correct set of initial strains. In the present case, an incremental procedure with respect to time is used since the creep strains are a function of the total stress history of the material. The formulation of the procedure may be carried out from potential energy considerations.

Since the instantaneous modulus of elasticity for concrete is assumed to be a function of time while the elastic modulus for steel is assumed to be constant, the values of d_{nx} and d_{ny} as computed by Equation (3.7) vary with time. In addition, because the total strain consists of two components, elastic and inelastic, the total strains

ε^T_{ox} and ε^T_{oy} at depths d_{nx} and d_{ny} respectively will not in general be zero if the constitutive relations are unsymmetrical with respect to the mid-surface. The mid-surface shear strain in the coordinate directions will however remain zero since the shear modulus is assumed constant with depth. The total strains at depth z may therefore be written as follows, for time $t + \Delta t$,

$$\varepsilon^T_x = \varepsilon^T_{ox} + (d_{nx} - z)\,\kappa_x$$

$$\varepsilon^T_y = \varepsilon^T_{oy} + (d_{ny} - z)\,\kappa_y$$

$$\gamma^T_{xy} = 0 + (d/2 - z)\,2\kappa_{xy}$$

or, in matrix form

$$\{\varepsilon^T\} = \{\varepsilon^T_o\} + [N]\,\{\kappa\} \tag{3.30}$$

Instantaneous elastic strains may be expressed as,

$$\varepsilon^E_x = \varepsilon^T_x - \varepsilon^I_x = \varepsilon^T_{ox} + (d_{nx} - z)\kappa_x - \varepsilon^I_x$$

$$\varepsilon^E_y = \varepsilon^T_y - \varepsilon^I_y = \varepsilon^T_{oy} + (d_{ny} - z)\kappa_y - \varepsilon^I_y$$

$$\gamma^E_{xy} = \gamma^T_{xy} - \gamma^I_{xy} = 0 + (d/2 - z)\,2\kappa_{xy} - \gamma^I_{xy}$$

or, in matrix form,

$$\{\varepsilon^E\} = \{\varepsilon^T_o\} + [N]\,\{\kappa\} - \{\varepsilon^I\} \tag{3.31}$$

The strain energy Σ may be written as,

$$\Sigma = \frac{1}{2}\int_V \{\sigma\}^T\,\{\varepsilon^E\}\,dV$$

$$= \frac{1}{2}\int_V \{\varepsilon^E\}^T\,[C]\,\{\varepsilon^E\}\,dV \tag{3.32}$$

Substituting from Equation (3.29)

$$\Sigma = \frac{1}{2}\int_V \{\{\varepsilon_o^T\} + [N]\{\kappa\} - \{\varepsilon^I\}\}^T[C]\{\{\varepsilon_o^T\} + [N]\{\kappa\} - \{\varepsilon^I\}\}dV$$

Expanding this expression and substituting from Equation (3.15),

$$\Sigma = \int_V [\frac{1}{2}\{\varepsilon_o^T\}^T[C]\{\varepsilon_o^T\} + \{\varepsilon_o^T\}^T[C][N][B]\{r\} - \{\varepsilon_o^T\}[C]\{\varepsilon^I\}$$

$$+ \frac{1}{2}\{r\}^T[B]^T[N]^T[C][N][B]\{r\} - \{\varepsilon^I\}^T[C][N][B]\{r\}$$

$$+ \frac{1}{2}\{\varepsilon^I\}^T[C]\{\varepsilon^I\}]\ dV$$

The potential of the external forces is obtained from Equation (3.16) as,

$$W = -\{r\}^T\{R\}$$

Minimizing the total potential, $\Pi = \Sigma + W$, yields

$$\int_A [B]^T[D][B]\ dA\ \{r\} + \int_V \{\varepsilon_o^T\}^T[C][N][B]\ dV - \int_V [B]^T[N]^T[C]\{\varepsilon^I\}dV = \{R\} \tag{3.33}$$

From Equation (3.5), $\int_d [N]^T[C]\ dz = 0$ and Equation (3.33) may therefore be written as,

$$\int_V [B]^T[D][B]\ dV\ \{r\} = \int_V [B]^T[N]^T[C]\{\varepsilon^I\}\ dV + \{R\}$$

or

$$[k]\{r\} = \{Q\} + \{R\} \tag{3.34}$$

where [k] represents the element stiffness matrix evaluated at time

$t + \Delta t$ and $\{Q\}$ represents a set of equivalent loads corresponding to the initial strains $\{\varepsilon^I\}$ which exist at time $t + \Delta t$ and which may be evaluated by Equation A.18. The matrix [D] may be evaluated from the expressions in Equation (3.10) using the cross-section and elastic material properties corresponding to time $t + \Delta t$.

For each time t, the structure stiffness matrix and load vector are assembled as in the elastic analysis except that in this case, the load vector contains the set of equivalent loads corresponding to the initial strain distribution. Solution of the resulting equations,

$$[K(t+\Delta t)]\ \{\Delta(t+\Delta t)\} = \{P(t+\Delta t)\} \qquad (3.35)$$

produces the total displacements at time $t + \Delta t$.

3.6.2 Evaluation of Total Strains

The total displacements $\{\Delta\}$ obtained from Equation (3.35) are used to compute curvatures and twist by Equation (3.15). To evaluate total strains the curvatures and twist are substituted in Equation (3.30). However, since the location of zero normal strain on each cross-section varies with time it is necessary to establish the values of the reference strains ε^T_{ox}, ε^T_{oy} in Equation (3.30). This is accomplished by ensuring that no net force is developed on the cross-section. The quantities d_{nx} and d_{ny} are computed at each time step from Equation (3.7) using the current pseudo instantaneous elastic constants. For zero normal stress resultants at time $t + \Delta t$,

$$\int_o^d \sigma_x(t+\Delta t)\, dz = 0$$

$$\int_o^d \sigma_y(t+\Delta t)\, dz = 0 \tag{3.36}$$

Substituting for concrete stresses from Equation (3.29) and using the linear elastic relations for steel, Equation (3.36) becomes,

$$\begin{aligned}
&\int_o^d \frac{\bar{E}_x}{(1-\nu_x\nu_y)} \{\varepsilon_{ox}^T + (d_{nx}-z)\kappa_x - \varepsilon_x^I\}\, dz + \\
&\int_o^d \frac{\nu_x\bar{E}_y}{(1-\nu_x\nu_y)} \{\varepsilon_{oy}^T + (d_{ny}-z)\kappa_y - \varepsilon_y^I\}\, dz + \sum_{s=1}^{nx} F_{sx} = 0 \\
&\int_o^d \frac{\bar{E}_y}{(1-\nu_x\nu_y)} \{\varepsilon_{oy}^T + (d_{ny}-z)\kappa_y - \varepsilon_y^I\}\, dz + \\
&\int_o^d \frac{\nu_y\bar{E}_x}{(1-\nu_x\nu_y)} \{\varepsilon_{ox}^T + (d_{nx}-z)\kappa_y - \varepsilon_x^I\}\, dz + \sum_{s=1}^{ny} F_{sy} = 0
\end{aligned} \tag{3.37}$$

where nx, ny represent the number of layers of steel in the x and y directions respectively and F_{sx} and F_{sy} represent the contributions of steel layers to the net stress resultant on each face

$$F_{sx} = A_{sx}\, E_s \{\varepsilon_{ox}^T + (d_{nx}-d_{sx})\, \kappa_x\}$$

$$F_{sy} = A_{sy}\, E_s \{\varepsilon_{oy}^T + (d_{ny}-d_{sy})\, \kappa_y\}$$

Solving Equation (3.37) for ε_{ox}^T and ε_{oy}^T the total strain distribution at a point in the plane of the slab may be determined from Equation (3.30). Knowing the total strains ε^T as well as the inelastic strains ε^I the elastic strains may be obtained by subtraction (Equation 3.28) and consequently concrete stresses may be

computed from Equation (3.29). Steel stresses are computed using the total normal strain at the level of the steel.

Bending and twisting moments {M} are obtained from Equation (3.9) by substituting the computed stresses for steel and concrete in each layer and integrating over the depth.

3.6.3 Computation of Equivalent Load Vector

The computation of the vector {Q} of Equation (3.34) may be carried out in several ways using either averaging or interpolation procedures. The method chosen is similar to that used in computing [D]. The distribution of initial strains $\{\varepsilon^I\}$ is computed at each corner of an element and layer integration over the thickness used to obtain the quantity

$$\{m^I\} = \int_d [N]^T[C]\{\varepsilon^I\}\, dz \tag{3.38}$$

The components of $\{m^I\}$ are computed as follows

$$\begin{aligned}
m_x^I &= \sum_{i=1}^{n} \frac{\bar{E}_{xi}}{(1-\nu_{xi}\nu_{yi})}\left(d_{nx} - \frac{(z_{i+1}+z_i)}{2}\right)(z_{i+1}-z_i)\,\varepsilon_{xi}^I \\
&\quad + \sum_{i=1}^{n} \frac{\nu_{xi}\bar{E}_{yi}}{(1-\nu_{xi}\nu_{yi})}\left(d_{nx} - \frac{(z_{i+1}+z_i)}{2}\right)(z_{i+1}-z_i)\,\varepsilon_{yi}^I \\
m_y^I &= \sum_{i=1}^{n} \frac{\nu_{yi}\bar{E}_{xi}}{(1-\nu_{xi}\nu_{yi})}\left(d_{ny} - \frac{(z_{i+1}+z_i)}{2}\right)(z_{i+1}-z_i)\,\varepsilon_{xi}^I \\
&\quad + \sum_{i=1}^{n} \frac{\bar{E}_{yi}}{(1-\nu_{xi}\nu_{yi})}\left(d_{ny} - \frac{(z_{i+1}+z_i)}{2}\right)(z_{i+1}-z_i)\,\varepsilon_{yi}^I \\
m_{xy}^I &= \sum_{i=1}^{n} G_{xyi}\left(d_{nxy} - \frac{(z_{i+1}+z_i)}{2}\right)(z_{i+1}-z_i)\,\gamma_{xyi}^I
\end{aligned} \tag{3.39}$$

where n equals the number of layers.

The average of the four corner values,

$$\{M^I\} = \frac{1}{4} \sum_{k=1}^{4} \{m^I\} \tag{3.40}$$

is used in Equation (3.34) to compute

$$\{Q\} = \int_A [B]^T \{M^I\} \, dA \tag{3.41}$$

which represents the contribution of the element to the equivalent load vector for the structure. The elements of $\{Q\}$ are given in Appendix C.

3.7 Analysis Procedure for Cracking and Time-Dependent Effects

The analysis developed herein for cracking and time-dependent effects in reinforced concrete slabs involves an iterative procedure at a particular time and loading to determine cracking, and an incremental procedure with respect to time for the evaluation of the stress and strain history for a given load history. An algorithm for the iterative procedure for cracking has already been given in Section 3.6 and this will now be extended to include the steps required for the time dependent analysis.

It is assumed that the analysis has been completed for time t and that the analysis is now to be carried out for an increment in time Δt to time $t + \Delta t$.

1. Compute pseudo instantaneous modulus for time $t + \Delta t$, $\bar{E}(t+\Delta t)$ (Equation A.11).

2. Compute the inelastic strains at $t + \Delta t$ for each corner of each element (Equations A.13, A.14, A.15).

3. Compute $\{Q(t+\Delta t)\}$ at each corner of each element (Equation 3.41).

4. Using the elastic constants for time t + Δt compute [D] for each element (Equations 3.10 and 3.27).

5. Evaluate element stiffness matrices [k] (Equation 3.24).

6. Evaluate the applied load vector {R} at time t + Δt for each element.

7. Assemble the structure stiffness matrix [K(t+Δt)] and load vector P(t+Δt) and solve the resulting equations for total displacements at time t + Δt (Equation 3.35).

8. From the total displacements compute curvatures and twist (Equation 3.15).

9. Evaluate total strains at reference surface to ensure zero net in-plane force at each corner of each element (Equation 3.37).

10. Evaluate concrete stresses (Equation 3.29).

11. Check for further cracking and modify the cracking coefficients α_x and α_y and memory function δ if necessary.

12. If further cracking occurs repeat the procedure (steps 2 to 12); if not, go on to the next time step.

The analysis procedure is illustrated schematically in Figures 3.7 and 3.8 in terms of a structure with a load parameter P and deflection parameter Δ.

The applied loading history is shown in Figure 3.7(a). At time τ_0, a load P_0 is applied and remains constant until time τ_2 at which time an additional load P_{2a} is applied. The total load remains constant thereafter. Figures 3.7(b) and (c) show the resulting deflection-time and load-deflection responses.

The uncracked structure at time τ_0 has an overall stiffness K_0' (Figure 3.8). The load P_0 produces a corresponding deflection Δ_0'

and examination of the resulting stress distribution indicates cracking. The iterative procedure described in Section 3.6 is carried out producing a final stiffness K_o and corresponding deflection Δ_o.

The numerical integration procedure for time increment τ_o to τ_1 produces a set of initial strains at time τ_1 which are converted to a set of equivalent loads represented by Q_1 which are added to the applied load P_1 (= P_o). The overall stiffness K_1 is computed using the elastic constants evaluated for the current time step. The resulting displacements represented by Δ_1 along with the known initial strains are used to evaluate the stress distribution and a check is again made for cracking. (In this example it will be assumed that no further cracking occurs after τ_o).

The analysis procedure is then carried out for time increment τ_1 to τ_2 yielding equivalent loads Q_2 and total deflection Δ_2. At time τ_2 the additional load P_{2a} is applied to the structure and a second analysis is required at time τ_2 with the equivalent loads Q_{2a} equal to Q_2. This may be considered as a time increment of zero length. The resulting deflection Δ_{2a} is obtained. Although Figure 3.8 shows the same stiffness K_2 for the two analyses carried out at time τ_2, the stiffness will in fact be different. The stiffness K_2 for the time increment τ_1 to τ_2 reflects the variation in material properties in the increment. As can be seen from the evaluation of the pseudo instantaneous compliance by Equation A.11,

$$\frac{1}{\bar{E}(\tau_2)} = (C(\tau_2,\tau_1) + C(\tau_2,\tau_2))/2.0$$

The corresponding expression for time τ_{2a} is

$$\frac{1}{\bar{E}(\tau_{2a})} = (C(\tau_{2a},\tau_2) + C(\tau_{2a},\tau_{2a}))/2.0$$

$$= (C(\tau_2,\tau_2) + C(\tau_2,\tau_2))/2.0$$

$$= \frac{1}{E(\tau_2)}$$

where $E(\tau_2)$ is the actual instantaneous modulus at time τ_2.

Figure 3.8 shows the analysis extended to τ_3 and τ_4.

3.8 Summary

The formulation described in this chapter is based on the displacement method of analysis in which the primary variables are displacement quantities. Classical small deflection plate theory is modified for a non-homogeneous, orthotropic material and the finite element method is used to obtain an approximate solution for the sole primary variable, the transverse displacement. The effect of cracking is included by considering the slab to consist of a set of layers in which constitutive relations throughout the plate are defined. The reduction in stiffness due to cracking is defined by the stress-strain diagram for concrete in tension described in Chapter 2 and an iterative procedure is employed to define the extent of cracking. The initial strain method is used to evaluate the effects of time-dependent-strains in the concrete.

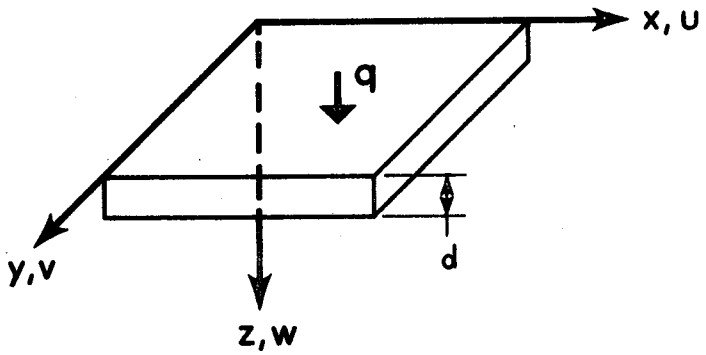

(a) PLATE COORDINATE SYSTEM

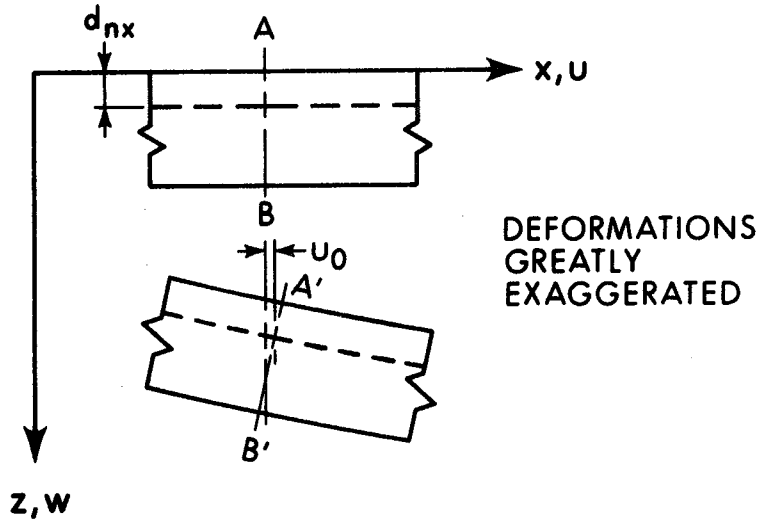

(b) DEFORMATION IN x-z PLANE

FIGURE 3.1 PLATE DEFORMATION

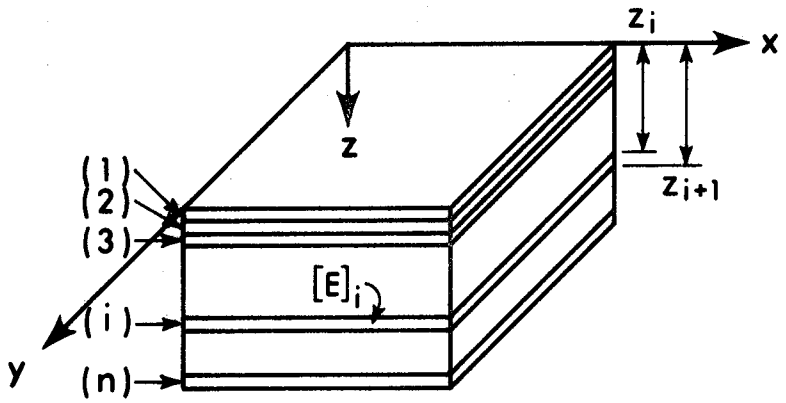

(a) CONCRETE LAYERS

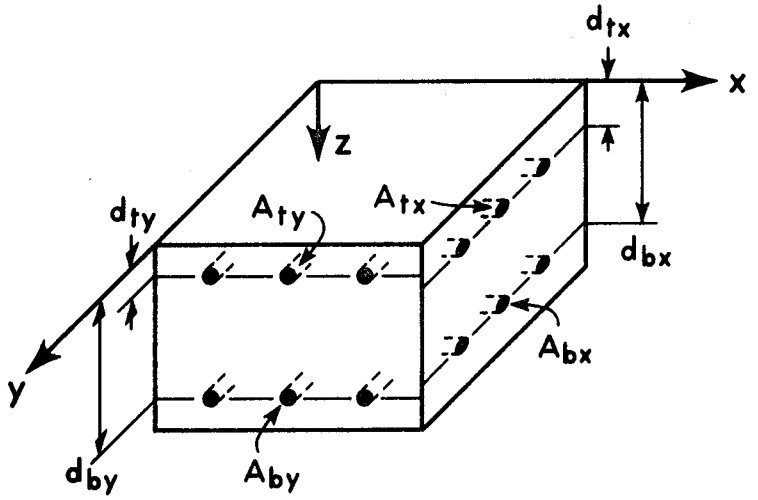

(b) REINFORCEMENT LAYERS

FIGURE 3.2 REPRESENTATION OF LAYERED PLATE

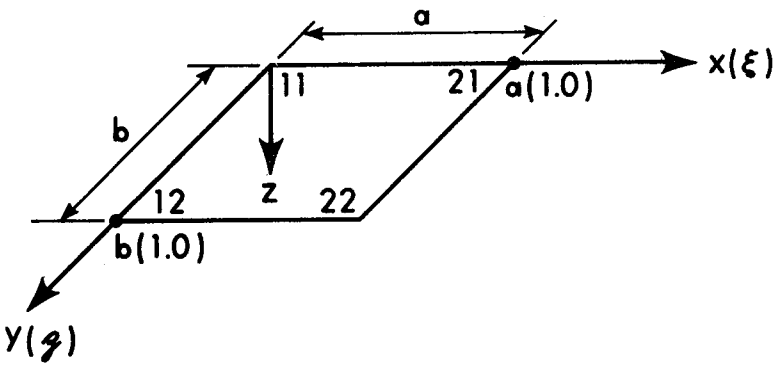

(a) ELEMENT CONFIGURATION

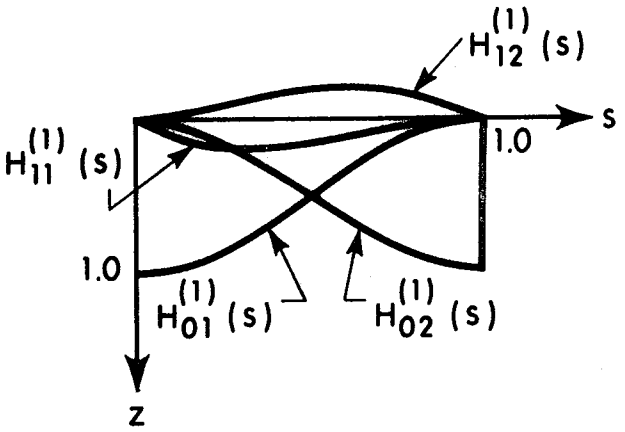

(b) HERMITIAN INTERPOLATION FUNCTIONS

FIGURE 3.3 PLATE BENDING ELEMENT

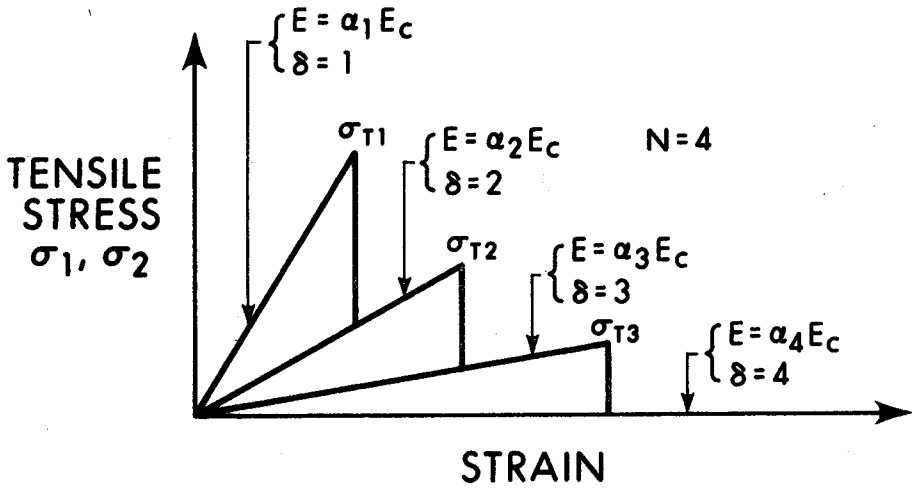

(a) STEPPED STRESS STRAIN DIAGRAM IN TENSION

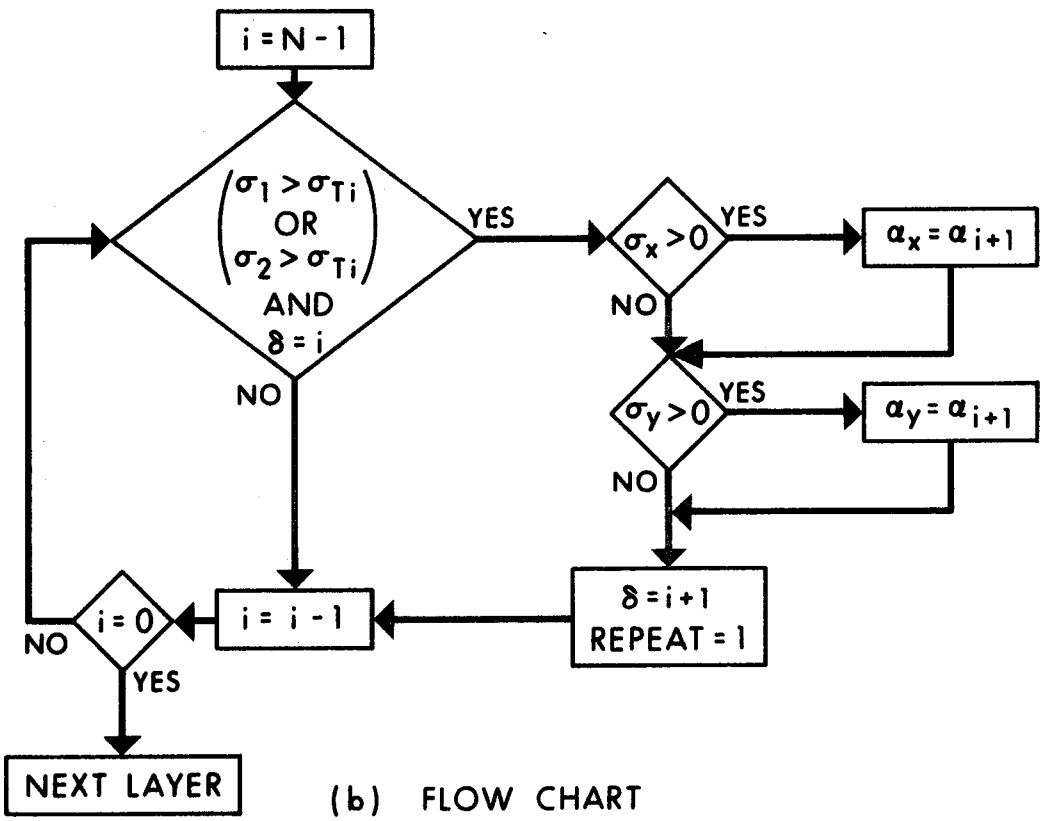

(b) FLOW CHART

FIGURE 3.4 COMPUTATION OF ELASTIC CONSTANTS FOR A LAYER

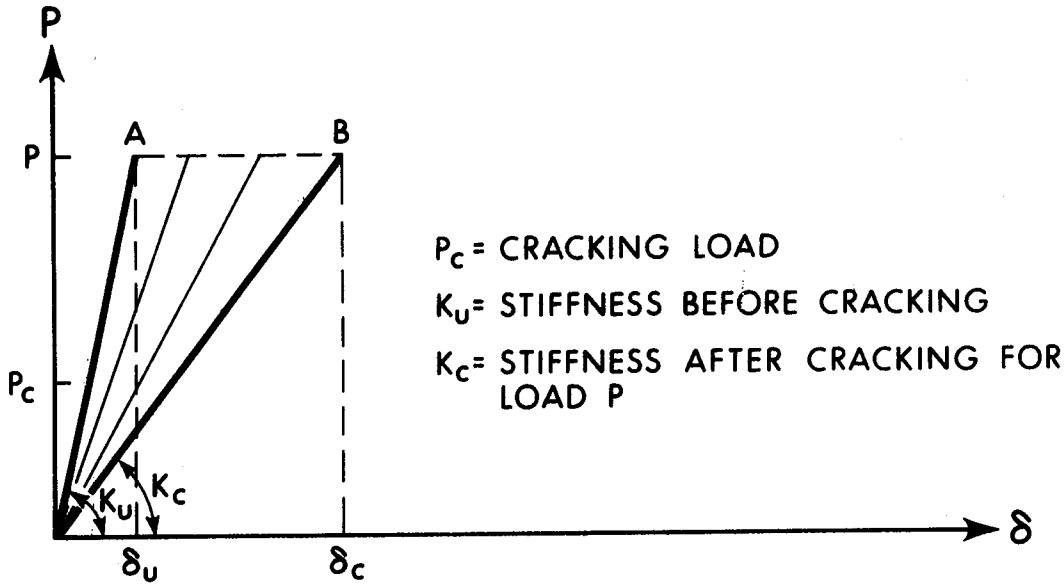

(a) ITERATIVE PROCEDURE FOR APPLICATION OF $P > P_c$

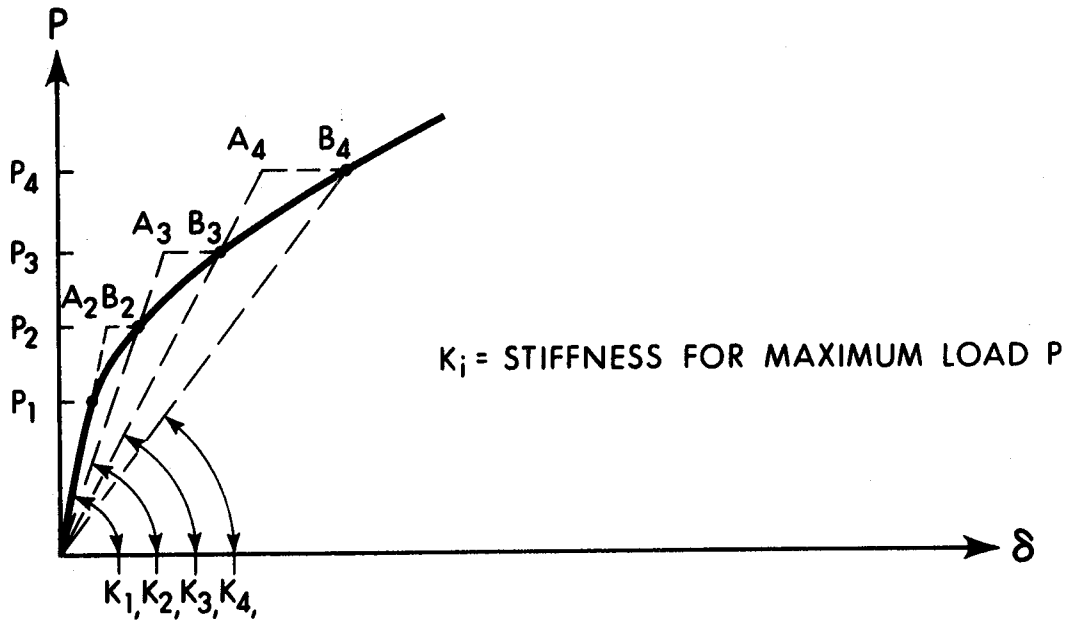

(b) ITERATIVE PROCEDURE FOR INCREMENTAL LOADING

FIGURE 3.5 ITERATIVE PROCEDURE FOR CRACKING

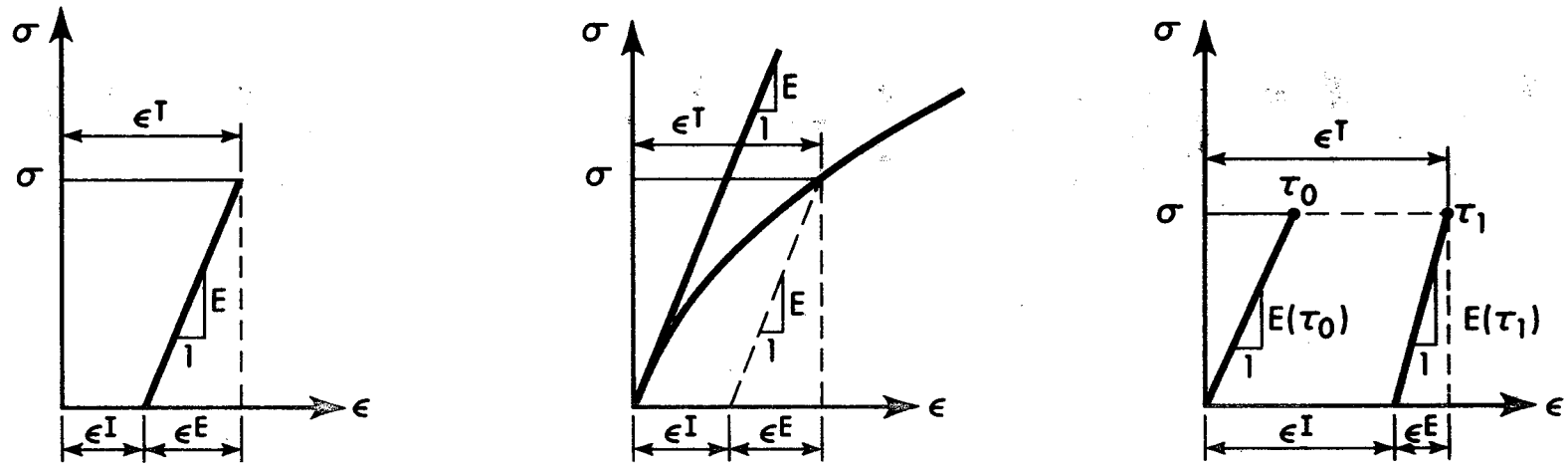

(a) NON STRESS PRODUCED INITIAL STRAINS

(b) NON LINEAR STRESS STRAIN DIAGRAM

(c) TIME DEPENDENT STRAINS

FIGURE 3.6 NON LINEAR STRESS STRAIN RELATIONSHIPS

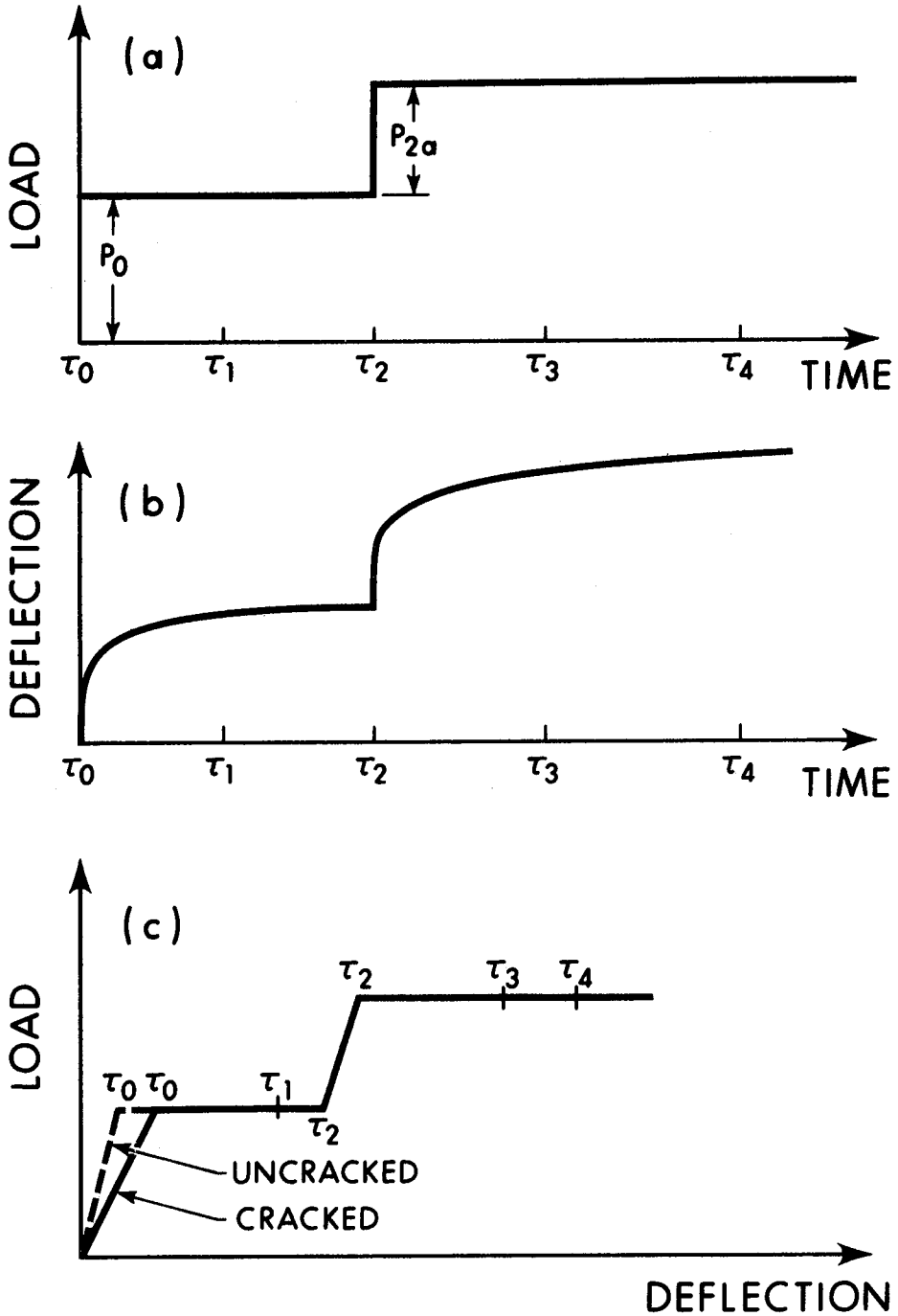

FIGURE 3.7 LOAD-DEFLECTION-TIME RELATIONSHIPS

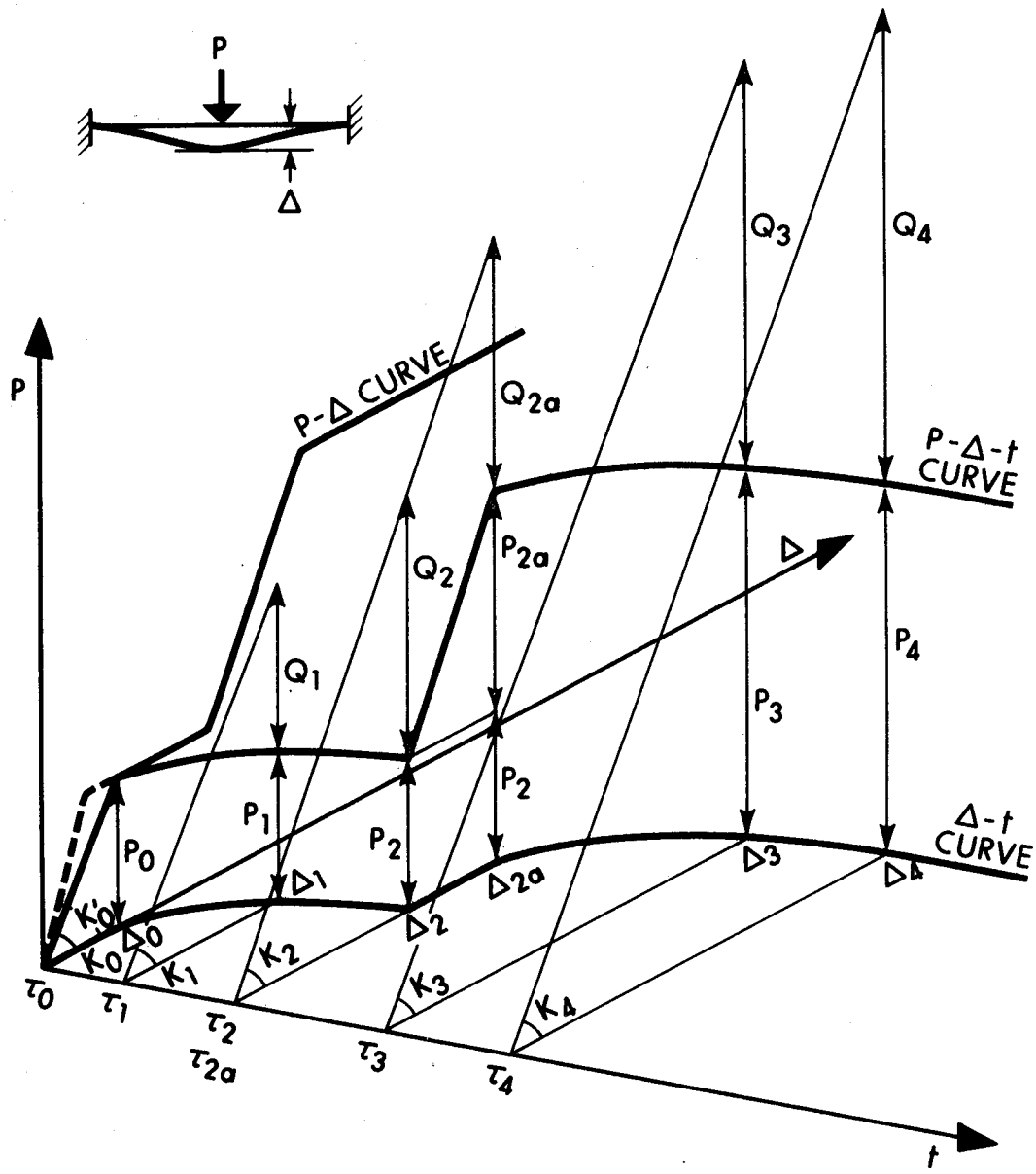

FIGURE 3.8 SCHEMATIC ILLUSTRATION OF TIME DEPENDENT ANALYSIS PROCEDURE

CHAPTER 4

VERIFICATION OF MODEL

4.1 Introduction

A common method of assessing the accuracy of a finite element formulation is to compare the solution obtained with available closed form or 'exact' solutions. In the case of elastic, isotropic and homogeneous material properties, closed form solutions are available for most classes of problems. However, for non-linear material properties, there may be no available closed form solution for the particular problem under study and recourse must be made to comparison with results obtained from experimental studies.

In this Chapter, the method of analysis described in Chapter 3 is applied to several problems for which either closed form solutions or experimental results are available in an attempt to assess the ability of the mathematical model to simulate the behaviour of actual structural systems. Firstly the elastic plate bending element is applied to problems where the classical solution contains singularities, to determine the effect of such singularities on the accuracy of the finite element solution. The method used to simulate the effect of cracking or the load deflection behaviour is then applied to a slab for which experimental results are available, and the creep model is applied to a set of beams tested under sustained load. Finally a brief study is made of the effect of mesh layout and time step variation on the results obtained for a slab subjected to cracking and time-dependent deformation.

4.2 Elastic Plate Bending Solutions

The plate bending element described in Section 3.3 was applied

by Bogner, Fox and Schmit[10] to the problem of bending of a square clamped plate under uniform load to illustrate the element's convergence characteristics. A more severe test of the element, however, is the case of a uniformly loaded continuous plate supported either by point supports or rectangular columns. In each case the classical elastic solution involves singularities in the form of infinite moments per unit length at the point supports[47] and at the corners of the rectangular columns[52].

The application of a triangular plate bending element to these problems is discussed by Cheung, King and Zienciewicz[14] and similar results obtained using the rectangular element are presented here as a check on the formulation and to illustrate the trends to be expected in the application of the method to problems involving non-linear material properties.

4.2.1 Continuous Plate on Point Supports

Figure 4.1 shows the geometric configuration of a portion of a continuous plate on point supports and the mesh layout considered in the study. Only one quadrant of a panel is required for the analysis because of symmetry.

The moment M_x and the deflection w evaluated at mid-panel (c) are given in Table 4.1 for each mesh. The rapid convergence of the computed deflection towards the correct value is clearly seen where the coarse mesh #1 produces an error of 2.36% compared with .21% for the more refined mesh #5. Although refinement of the mesh size in the region of high stress gradient produces a significant effect on the deflection at mid-panel the effect on the moment computation at

mid-panel is less marked. The computation of moments appears to be more directly related to the mesh layout in the immediate vicinity of the point considered. This may be attributed to the fact that the moment is computed as a linear function of the degrees of freedom of the element concerned and is therefore less sensitive to variations in the mesh size at some distance from the element than the deflection which depends on an accumulation of curvature effects. The closer the actual moment variation in the element is to a linear function, the more accurate will be the moment computation. This point is further illustrated in Figure 4.2 and Figure 4.3. The moments M_x and M_y along the column line AD are plotted for mesh #1 and #5 and compared with the classical solution obtained using forty terms in the series solution given by Timoshenko and Woinowsky Krieger[47]. The actual variation in each element is plotted rather than average nodal values which accounts for the discontinuities in the finite element solutions. Where only one point is plotted, the moments in adjacent elements are essentially the same. The largest discontinuities occur for each mesh at the node adjacent to the point support, due to the fact that in the element adjacent to the point support a theoretically infinite stress (moment) gradient is being approximated by a linear function.

4.2.2 Continuous Plate on Square Columns

This case is more closely related to the practical situation. However, as pointed out by Woinowsky - Krieger the elastic solution (obtained by the method of complex variables and assuming rigid columns) produces theoretically infinite moments at the corners of the square (or rectangular) columns. An alternative solution by Timoshenko and Woinowsky - Krieger assumes the reaction to be uniformly distributed

over the area of the column and produces finite moment values at the column. The true behaviour in the practical situation lies somewhere between the two assumptions. The former assumption of rigid columns is considered to be more applicable and is used in the present context.

Figure 4.4 shows a quadrant of an infinite plate supported by square columns. The variation of M_y along the column line AB is shown for c/L = 0.2 and c/L = 0.1. The classical solution due to Woinowsky - Krieger is also given for c/L = 0.2. Of particular interest is the fact that the maximum hogging moment occurs a small distance from the face of the column and this is reflected in the finite element solution. It should be noted however that the finite element solution will not reflect this behaviour unless there is a nodal point in the vicinity of the actual maximum moment, due to the assumed linear moment variation.

The manner in which the finite element solution attempts to approximate the theoretically infinite moments at the corner of the column is shown in Figure 4.5, the behaviour being similar to that for point supports. Some care however is required in interpreting the moments computed at point E where three elements are represented at the nodal point, each with its moment value computed at E(E_1,E_2 and E_3). The values plotted at E are E_1 and the average of E_2 and E_3 (E_{23}). The difference between E_{23} and E_1 represents a discontinuity in the moment M_y at E.

The values of M_x along AB and DF are compared in Figure 4.6 again indicating the high moment concentration at the corner of the column compared with the moment at the mid-point of the column face.

The above examples indicate that, for elastic material

properties, the finite element formulation used herein produces excellent deflection evaluations even in cases where singularities arise, and that the computed moments while being somewhat less accurate than deflections are certainly acceptable for most engineering applications. For the cases of non-linear material response where the non-linearity is a function of stress level, it will be important to obtain reasonably accurate values for moments and stresses. The application of the model to non-linear response due to cracking and creep is discussed below.

4.3 Reinforced Concrete Slab Subject to Cracking

In this section, the mathematical model developed in Chapter 3 is applied to a reinforced concrete slab for which the experimental load-deflection response and an alternative finite element solution are available. A square slab supported at the corners was tested by McNeice[39] and analyzed by Jofriet and McNeice[27] using a finite element formulation rather different from the present analysis. They used a tangent stiffness approach based on empirical bi-linear moment-curvature relationships, one of which was proposed by Beeby[9] and the other of which was based on an expression by Branson[11] for the effective moment of inertia of a cracked cross-section. In addition they attempted to include the effects of crack orientation by assuming that cracks form perpendicular to the direction of maximum principal tensile stress. The cracking directions obtained in this manner were considered to represent principal directions of orthotropy. Where the cracks formed at an angle to the reinforcement, the reinforcing bars were replaced by a fictitious set of bars running parallel

and perpendicular to the crack directions. The areas of steel required for the fictitious reinforcing bars were obtained from expressions presented by Lenschow and Sozen[33]. The orthotropic plate bending stiffness matrix [P] was then transformed to the global coordinate system. No attempt was made to evaluate the stress distribution over the thickness so that an extension of this approach to the creep problem might be rather difficult.

4.3.1 One-Dimensional Moment Curvature Relationships

Figure 4.7 shows a set of moment curvature relationships for a doubly reinforced cross-section based on stepped stress-strain curves for concrete in tension as discussed in Section 3.4.

Three stress-strain diagrams for average tensile stress in the concrete are shown in Figure 4.7. The first diagram shows the case where the concrete carries no tension after cracking. In the second curve the concrete is assumed to crack at a stress of 525 p.s.i. at which point the tensile modulus of elasticity reduces to 10% of its initial value and remains at this level for all stress levels thereafter, implying that the tensile stress may exceed the original limiting value. The third curve shows three successively lower limiting values of 525 p.s.i., 315 p.s.i. and 205 p.s.i.

The empirical expression for the effective moment of inertia of a section after cracking, given by Branson[11], is

$$I_{eff} = \left(\frac{M_c}{M}\right)^4 I_g + \left(1 - \left(\frac{M_c}{M}\right)^4\right) I_{cr}$$

where M_c = cracking moment

M = applied moment

I_g = moment of inertia of gross concrete section

I_{cr} = moment of inertia of cracked transformed section

This type of expression simply represents a transition from I_g to I_{cr} which will be necessary for stiffness computations involving sections with low reinforcement ratios.

The moment curvature relationship based on the above expression for the doubly reinforced section considered is shown in Figure 4.7 along with the curves corresponding to the stress strain diagrams described above. The latter curves were obtained by an iterative procedure similar to that used in the proposed analysis procedure for deflection computations involving cracking. Details of the procedure for evaluation of the moment curvature relationship are presented in Appendix F.

The jagged nature of the curves is due to the fact that the slab is divided into layers. The difference between the initial linear portion of the Branson curve and the computed curves is due to the fact that the Branson curve does not include the steel area in the gross moment of inertia. Examination of Figure 4.7 indicates that curve #3 most closely resembles the Branson curve. It is apparent that by a suitable choice of tensile stress-strain curve the Branson curve could be approximated to any required degree.

4.3.2 Application to the Two-Dimensional Case (Plane Stress)

In applying the concept of the stepped stress-strain diagram to the two dimensional case, the plane stress constitutive relation may be written as follows,

$$\begin{Bmatrix} \sigma_x \\ \sigma_y \\ \tau_{xy} \end{Bmatrix} = \begin{bmatrix} E_x/(1-\nu_x\nu_y) & \nu_x E_y/(1-\nu_x\nu_y) & . \\ \nu_y E_x/(1-\nu_x\nu_y) & E_y/(1-\nu_x\nu_y) & . \\ . & . & G_{xy} \end{bmatrix} \begin{Bmatrix} \varepsilon_x \\ \varepsilon_y \\ \gamma_{xy} \end{Bmatrix}$$

and $E_x = \alpha_x E_c$, $E_y = \alpha_y E_c$, $\nu_x = \alpha_x \nu$, $\nu_y = \alpha_y \nu$, where α_x and α_y are factors representing the current branch of the stress strain diagram for stresses in the x and y directions respectively. The constitutive matrix thus remains symmetric at all times.

4.3.3 Comparison with Experimental Results

Details of the slab tested by McNeice are presented in Figure 4.8 along with the mesh layout used for the present analysis. The computed load-deflection relationships for various constitutive assumptions are compared with the experimental results and the results of Jofriet's analysis in Figure 4.9.

Initially the assumption was made that a concrete layer takes no tension after cracking, i.e. $\alpha_x = \alpha_y = 0$ (Figure 4.7(b) - #1). In order to obtain an initial cracking load equal to that indicated by Jofriet's analysis, a modulus of rupture of 770 p.s.i. was used. It can be seen that neglecting the tension stiffening effect of the concrete between cracks in this case greatly overestimates deflections after cracking. Curves of the form of Figure 4.7(b) - #2 were then applied in an attempt to simulate tension stiffening using reduced moduli after cracking of 5%, 10% and 20% of the initial value. Of these, a value of 10% closely follows the experimental curve in the

early stages of loading, but gradually stiffens relative to the experimental curve. Finally a stepped stress strain curve of the form of Figure 4.7(b) - #3 was applied. This curve shows reasonable correlation with the experimental curve over the total loading range given.

The effect of cracking on the distribution of moments in the slab can be seen in Figure 4.10 which shows the variation of M_x/P along AC for various load levels. The maximum error in the computed total moment was 4.7%.

In the uncracked state (P = 800#) a high peak in moment occurs at the centre due to the point load. Initial cracking takes place in this high moment region which reduces the stiffness significantly in relation to the surrounding portions of the slab so that at P = 1600# the moment at the centre drops significantly and the total moment is more evenly distributed over the width of the slab.

As the loading is increased, cracking extends into regions away from the centre tending to equalize the stiffness distribution over the slab and thereby attracting a higher proportion of the moment back into the centre.

4.4 Simply Supported Beams Under Sustained Load

The creep representation described in Chapter 2 is based on the formulation by Selna who compared his technique with results obtained by Ross[44] for an axially loaded prism under various forms of block type stress histories. Although satisfactory agreement was obtained, no attempt was made to verify the application of the model to reinforced concrete flexural elements with or without cracking.

To the author's knowledge no experimental data is available

on creep deflections of reinforced concrete slabs under two-way action. However, a series of tests was carried out by Washa and Fluck[51] to study the behaviour of reinforced concrete beams under sustained load. In this section, the present method of analysis is compared with the results of series C of the Washa and Fluck tests, this series consisting of beams 5 inches deep by 12 inches wide with varying amounts of compression reinforcement. Details of the beams are given in Figure 4.11 and Table 4.2.

The creep function used in the analysis was based on the C.E.B. creep parameters, as discussed in Section 2.5. The shrinkage curve was based on an experimental curve obtained by Troxell, Raphael and Davis[48] under conditions similar to those of the beam tests and is shown in Figure 2.9. The modulus of rupture was taken as 500 p.s.i.

4.4.1 Deflections

The analysis was carried out for the sustained load acting for 240 days after which time the experimental results indicate that the increase in deflection occurred at a very much reduced rate.

Each beam was analyzed for two conditions,

a) No tension in a layer after cracking,

b) Stepped stress strain diagram in tension.

The stepped stress strain diagram was of the form shown in Figure 4.7 (#3) with the initial modulus of rupture at 500 p.s.i. and the two lower values reduced proportionately. Displacement-time curves are presented in Figure 4.12.

The no-tension assumption produces an initial elastic deflection greater than the actual deflection as would be expected while the

stepped stress-strain diagram produces an instantaneous deflection slightly lower than the actual value. However, the rate of increase of creep deflections for the initial portion of the loading history is greater for the stepped stress strain diagram which may be explained by the fact that the tensile concrete is assumed to be exhibiting creep, thereby gradually transferring stress to the steel whereas in the no-tension case, all the tensile stress in the cracked layer is immediately transferred to the steel. The final computed deflection after 240 days is in each case very close to the actual deflection and the rates of increase of deflection are also similar at this stage.

4.4.2 Cracking Envelopes

Figure 4.13 shows the cracking envelopes obtained for each of the beams analyzed. Although Washa and Fluck did not present cracking patterns in their results, they did observe that cracking occurred in all beams shortly after application of the load. The cracking envelopes are seen to extend to a greater depth in the case of the no-tension assumption compared with the stepped stress-strain diagram.

4.4.3 Steel Stresses

The computed steel stresses using the no-tension assumption for the beams containing compression steel are shown in Figure 4.14. In the period immediately after loading there is a rapid transfer of stress to the compression steel, the rate of increase gradually decreasing with time. It is evident that for very small percentages of compression steel, yielding is likely to occur. The tensile steel stress on the other hand after a small initial rise remains more or

less constant at a value a little over 20,000 p.s.i.

4.5 Effects of Mesh Layout and Timestep on Creep Deflections

4.5.1 Mesh Layout

The effect of mesh size on elastic plate solutions was discussed in Section 4.2. To determine the effects of mesh layout on deflections where cracking and creep occur, a brief study was carried out on the interior panel of a flat plate supported on square columns. The dimensions and reinforcement of the slab analyzed were as follows,

Depth = 8 inches

Span = 20 ft (centre to centre of columns)

Column Width = 2 ft

Reinforcement = 0.036 sq. in. per in. top and bottom in each direction

The mesh layouts used in the study are shown in Figure 4.15. The creep and shrinkage curves used were those designated as C.E.B. curves C1 in Section 2.5 and no tension was assumed in a layer after cracking. The loading history consisted of a total uniform load of 144 p.s.f. applied at 14 days and held constant thereafter.

A measure of the plate stiffness immediately after cracking on first application of the load is also given in Figure 4.15 where relative values of D_{11} are presented for elements in which cracking has occurred. Cracking is seen to occur only in the region surrounding the column, and the more refined mesh layouts in this region predict the higher degree of cracking. This trend is reflected in the instantaneous values obtained in each case in Figure 4.16. Mesh #1 and #2 which have the same mesh layout around the column produce the

same stiffness reduction due to cracking and the same instantaneous deflection at mid-panel. Mesh #3 produces a deflection 10% higher than #1 and #2 and for mesh #4 the difference is 15.5%.

The same trend indicated by the instantaneous deflection is reflected in the longtime deflections where the maximum difference for the mesh layouts used is of the order of 10%.

4.5.2 Time Step Variation

To determine the influence of the numerical integration technique on the solution, two very different time step variations designated T_A and T_B were applied to the slab example described above, using mesh #1 with the initial load applied at 30 days. Table 4.3 gives the time step variations used with the corresponding mid-panel displacements and maximum concrete compressive stresses. The results are presented graphically in Figures 4.17 and 4.18.

Variation T_A was chosen to produce approximately equal deflection increments in each time interval while T_B is based on equal time increments. The former variation produces a much smoother change in both deflections and stresses with time. However, the discrepancy tends to be minimal after the initial rapid change has taken place. The rapid drop in compressive stress may be attributed to the presence of reinforcing steel in the compressive zone.

The choice of time step variation therefore does not appear to be critical in terms of computation of longtime deflections although a variation of the type T_A is to be preferred.

4.6 Effect of Mesh Layout on Computed Moments

In Section 4.2 it was pointed out that the present finite

element formulation based on a displacement model, when applied to elastic plate bending problems produces good deflection values but somewhat less accurate stress quantities. To investigate the computed moments in the time dependent analysis, a typical interior panel was analyzed for three mesh layouts. The dimensions and reinforcement for the slab are the same as for slab S10 in Table 5.1. The three mesh layouts numbered 5, 6 and 7 consisting of 15, 24 and 35 elements respectively are shown in Figure 4.19. The slab was analyzed for the loading history L2 in Figure 5.7 using the compliance and shrinkage curves representing concrete C1 (Section 2.5).

Figure 4.20 shows the negative moment $M_x^{(-)}$ on the line of the column face and the positive moment $M_x^{(+)}$ on the centre line of the panel. The sum of these two quantities is equal to one half of the total static moment for the panel on the clear span between the column faces. The moment variation along these two lines for each mesh is shown in Figure 4.21, 4.22 and 4.23 for 9 days, 300 days and 800 days (with the exception of mesh #7 for which no values are given at 800 days). Moments were computed at the corner of each element and the average for the node was used in computing the total moment. The total moment was computed by numerical integration assuming a linear variation in moment along the side of each element. Figure 4.24 shows the variation in the computed total negative moment and total positive moment with time for each mesh. For each case the error in the total static moment is shown in Figure 4.25 as a function of time. The values plotted show a rather wide variation from mesh to mesh. However, from Figure 4.25 is is apparent that the accuracy of the moment computation is improved by increasing the number of elements. There appears

to be little redistribution of moments with time although the total negative moment shows a tendency to increase slightly with a corresponding decrease in positive moment.

The deflection vs. time curves shown in Figure 4.26 indicate that although the computed moments vary widely from mesh to mesh the computed deflections are remarkably similar. Therefore, in the study of slab deflections a relatively course mesh may be used whereas for accurate moment values, the number of elements must be increased.

4.7 Summary

In this Chapter the analytical model developed in Chapter 3 was applied to cases involving elastic plate bending, cracking of a square reinforced concrete slab supported at the corners and creep deflections of simply supported reinforced concrete beams. In addition a brief assessment was made of the effects of mesh layout and time step variation on the solution. On the basis of the results obtained, the following conclusions may be stated.

1. The plate bending element used adequately predicts deflections and stresses in an elastic plate even if singularities are present. The accuracy depends primarily on the mesh layout used in the region adjacent to such singularities.

2. Neglecting the tension stiffening effect of concrete between cracks grossly over-estimates deflections, particularly for sections with low reinforcement ratios.

3. The concept of a stepped stress strain diagram for concrete in tension is an approximate method of including tension stiffening which produces satisfactory results.

4. The creep formulation using functions based on the C.E.B. creep parameters produces good correlation with one-dimensional flexural behaviour which provides some confidence in applying the method to the two-dimensional slab problem.

5. The computation of slab deflections subject to cracking and time-dependent strains is fairly sensitive to the mesh layout used, and a relatively fine mesh should be used in areas of high stress gradients.

6. The choice of time step to be used is less critical. A series of time increments producing approximately equal deflection increments is recommended.

MESH#	Nr.°F	M_x(in.lb)	Error	w(in)	Error	Exact(Ref. 47, p 249)
1	36	1522.7	13.7%	.90768	2.36%	M_x = 1339.1
2	64	1525.6	13.9%	.92256	.76%	w = .9296
3	100	1382.5	3.32%	.92296	.71%	
4	144	1382.45	3.32%	.92671	.31%	
5	196	1382.41	3.32%	.92765	.21%	

TABLE 4.1 MOMENT AND DEFLECTION AT MID-PANEL

Beam No	Width (in)	Total Depth (in)	Span (ft)	L/D	Tension Steel Area (sq in)	Compression Steel Area (sq in)	Total Uniform Load (lb/ft)
C1,C4	12	5	20.8	50	0.80	0.80	82
C2,C5	12	5	20.8	50	0.80	0.40	82
C3,C6	12	5	20.8	50	0.80	0.0	82

TABLE 4.2 BEAM DETAILS(WASHA & FLUCK)

T_A			T_B		
TIME(days)	Δ(in)	σ_{max}(p.s.i.)	TIME(days)	Δ(in)	σ_{max}(p.s.i.)
30	.0796	145	30	.0796	145
31	.0973	141	60	.2098	109
32	.1105	139	90	.2159	112
34	.1315	133	120	.2226	108
38	.1570	125	150	.2276	108
46	.1801	119	180	.2322	106
62	.1990	114	210	.2364	105
94	.2159	110	240	.2405	104
158	.2313	106	270	.2443	102
286	.2516	101	300	.2478	101
542	.2780	93			
800	.2897	91			

TABLE 4.3 MID-PANEL DEFLECTIONS AND STRESSES FOR DIFFERENT TIME STEP VARIATIONS

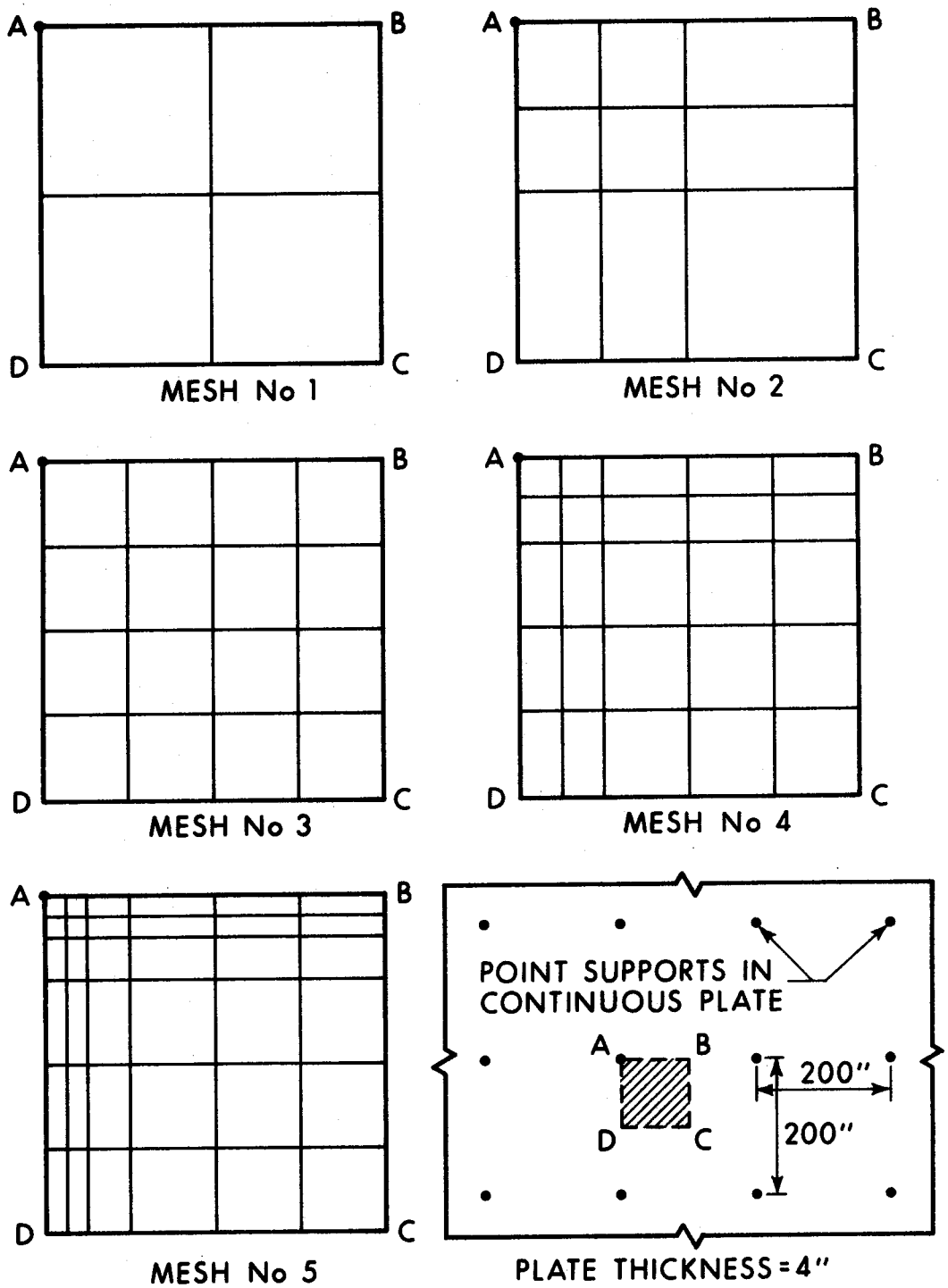

FIGURE 4.1 MESH CONFIGURATIONS FOR CONTINUOUS PLATE ON POINT SUPPORTS

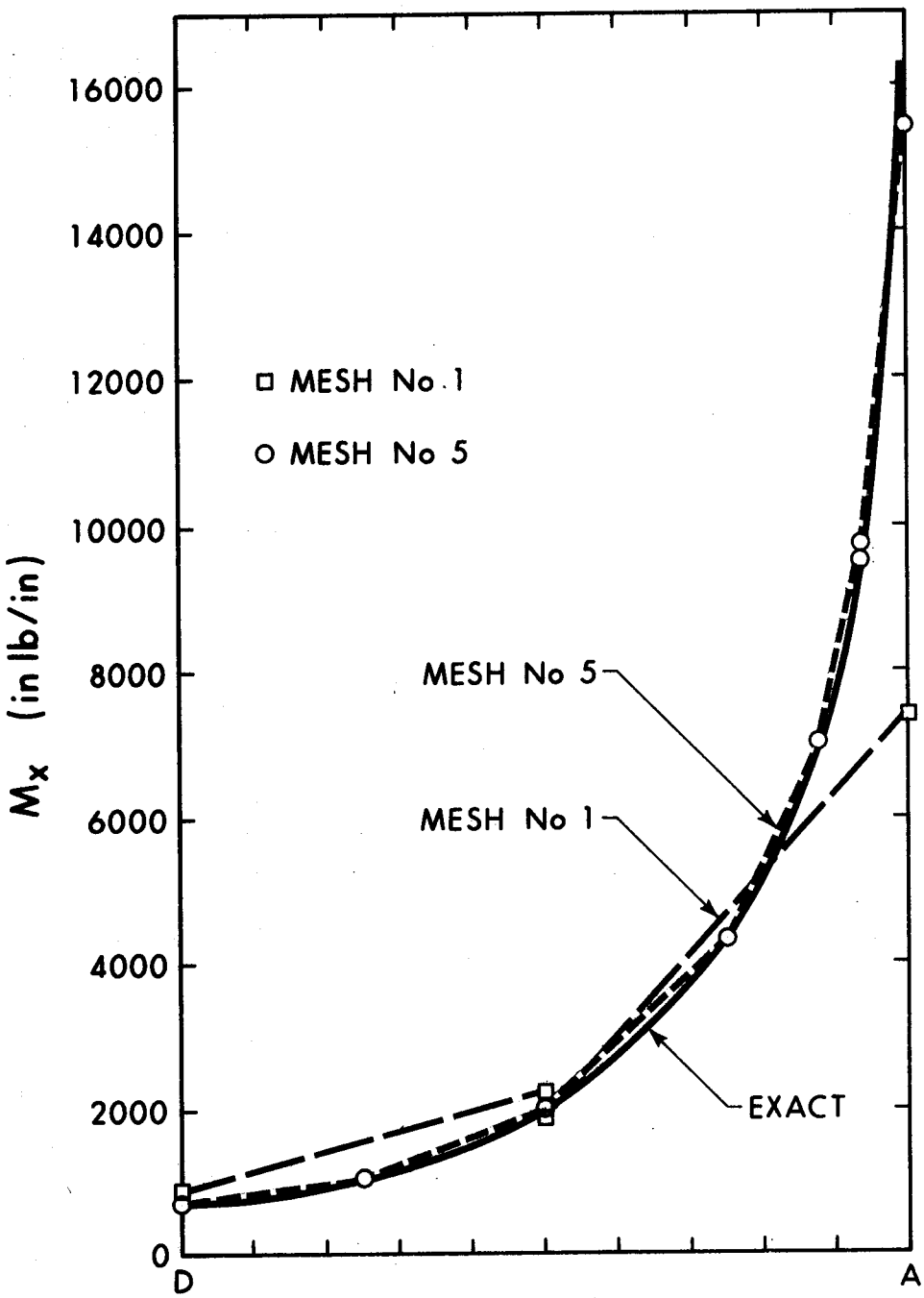

FIGURE 4.2 M_x ALONG AD-POINT SUPPORTS

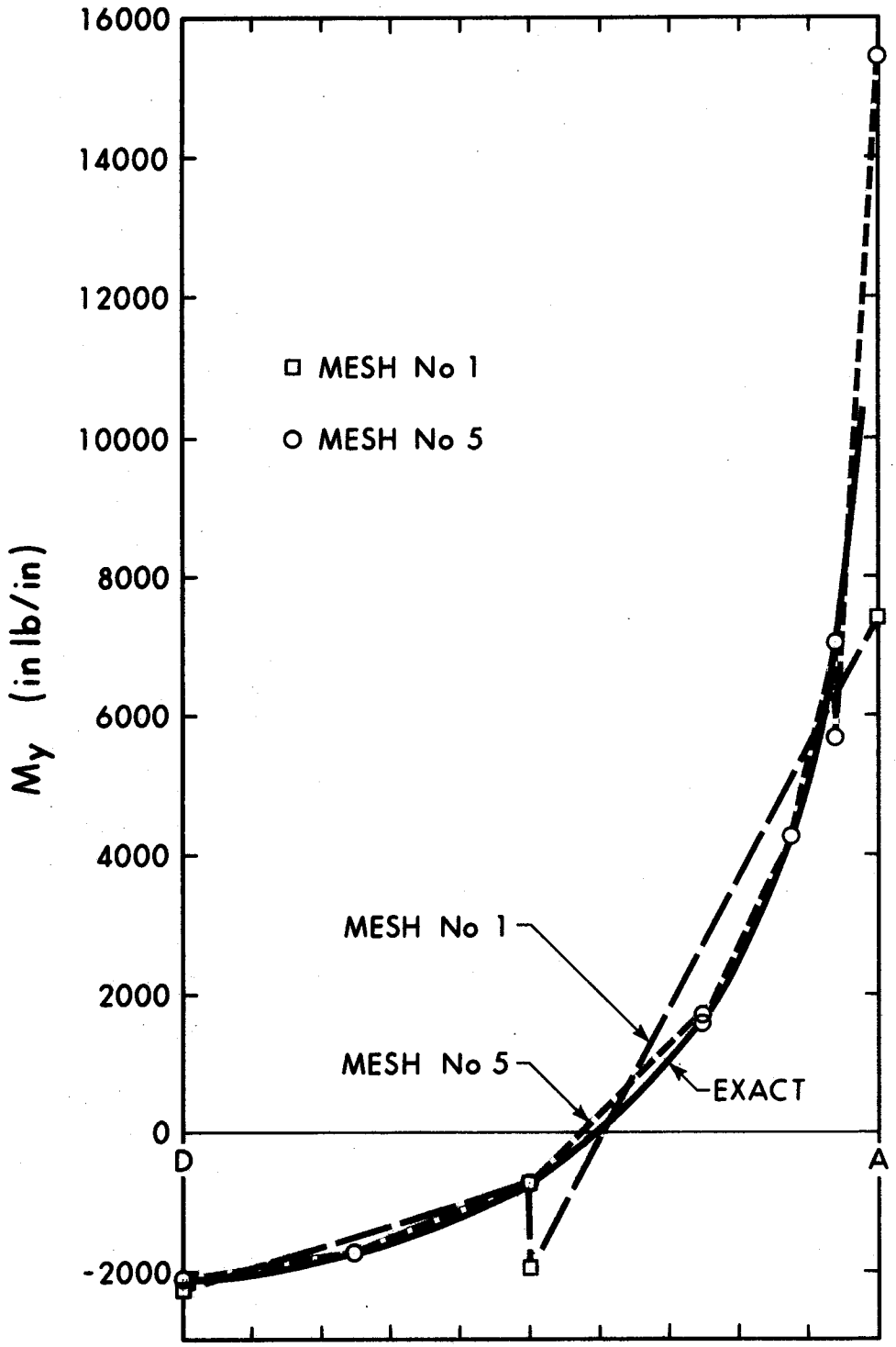

FIGURE 4.3 M_y ALONG AD-POINT SUPPORTS

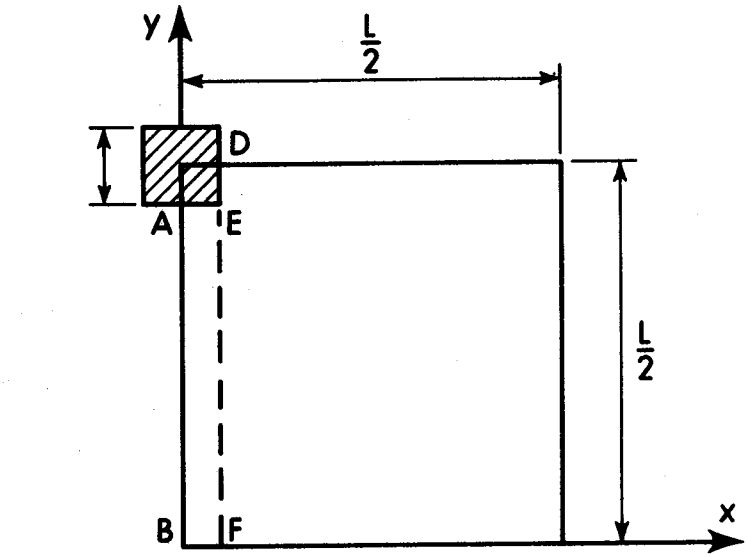

QUADRANT OF PANEL WITH SQUARE COLUMN

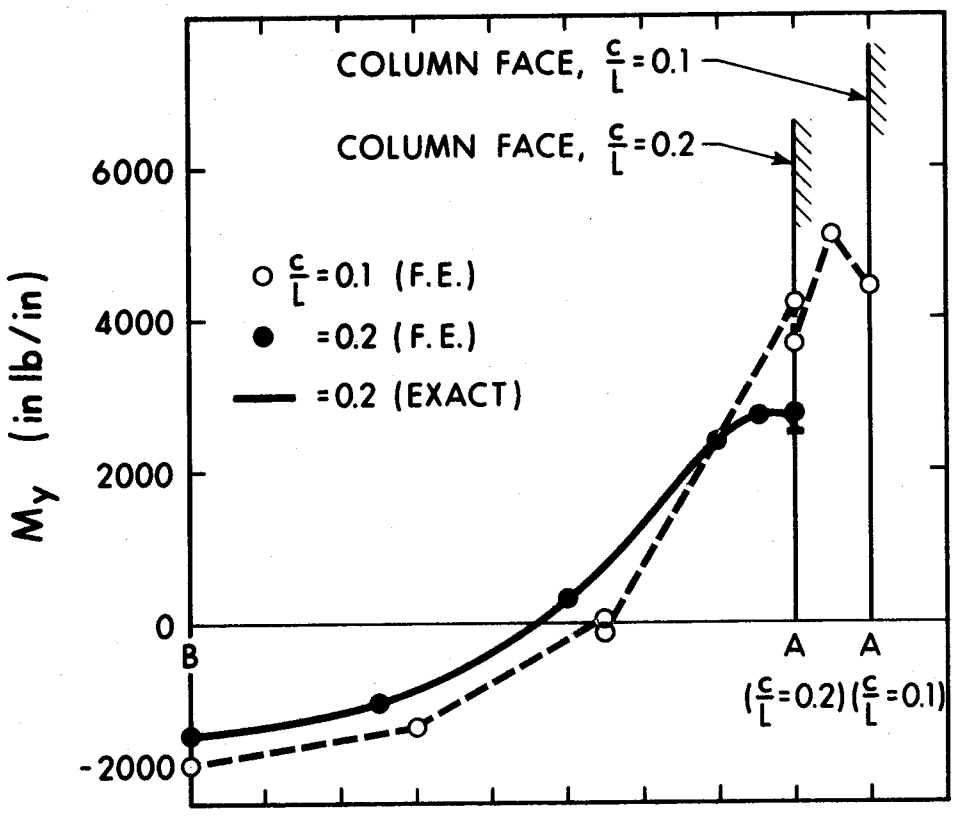

FIGURE 4.4 M_y ALONG AB-SQUARE COLUMNS

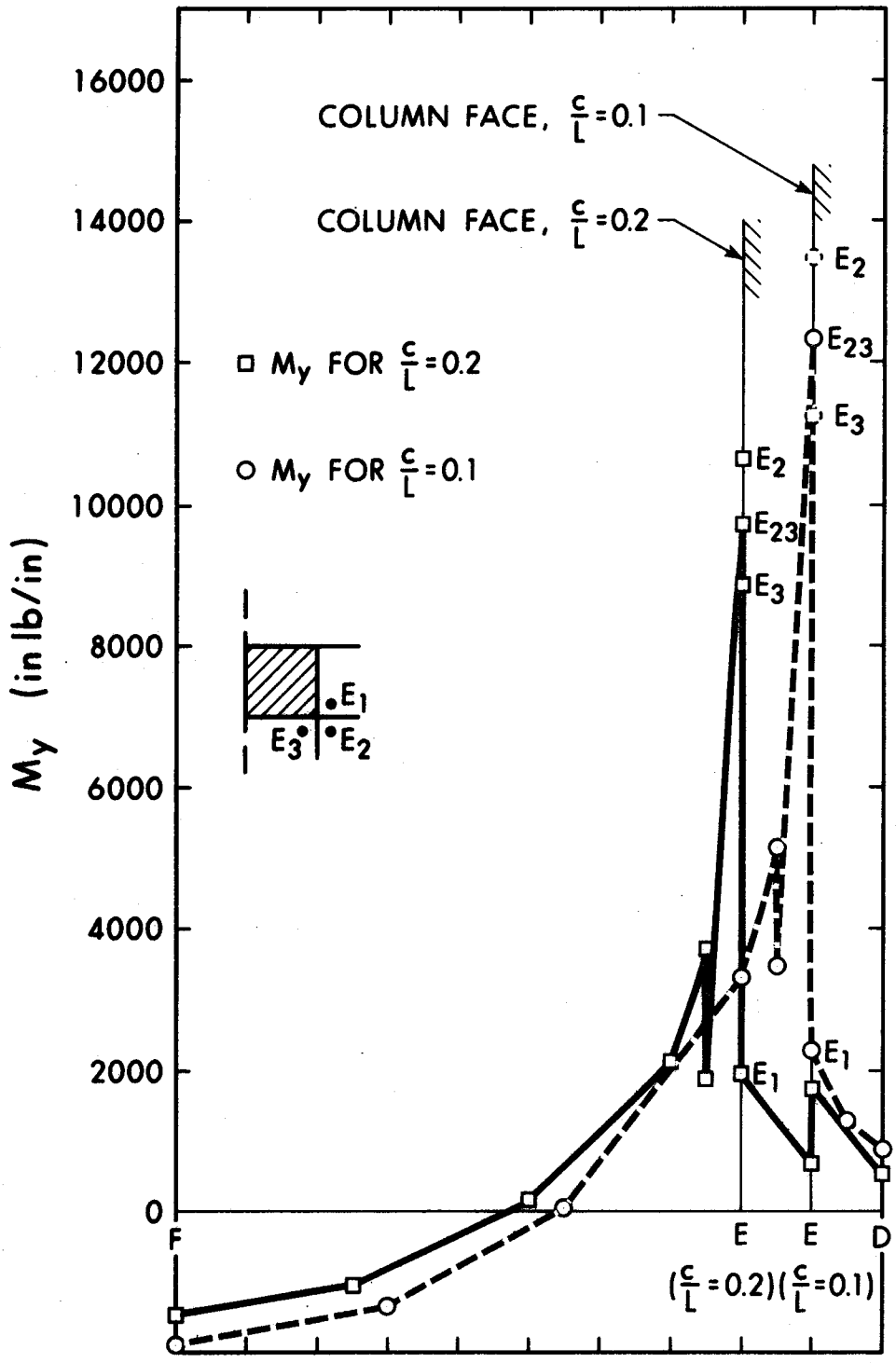

FIGURE 4.5 M_y ALONG DF-SQUARE COLUMNS

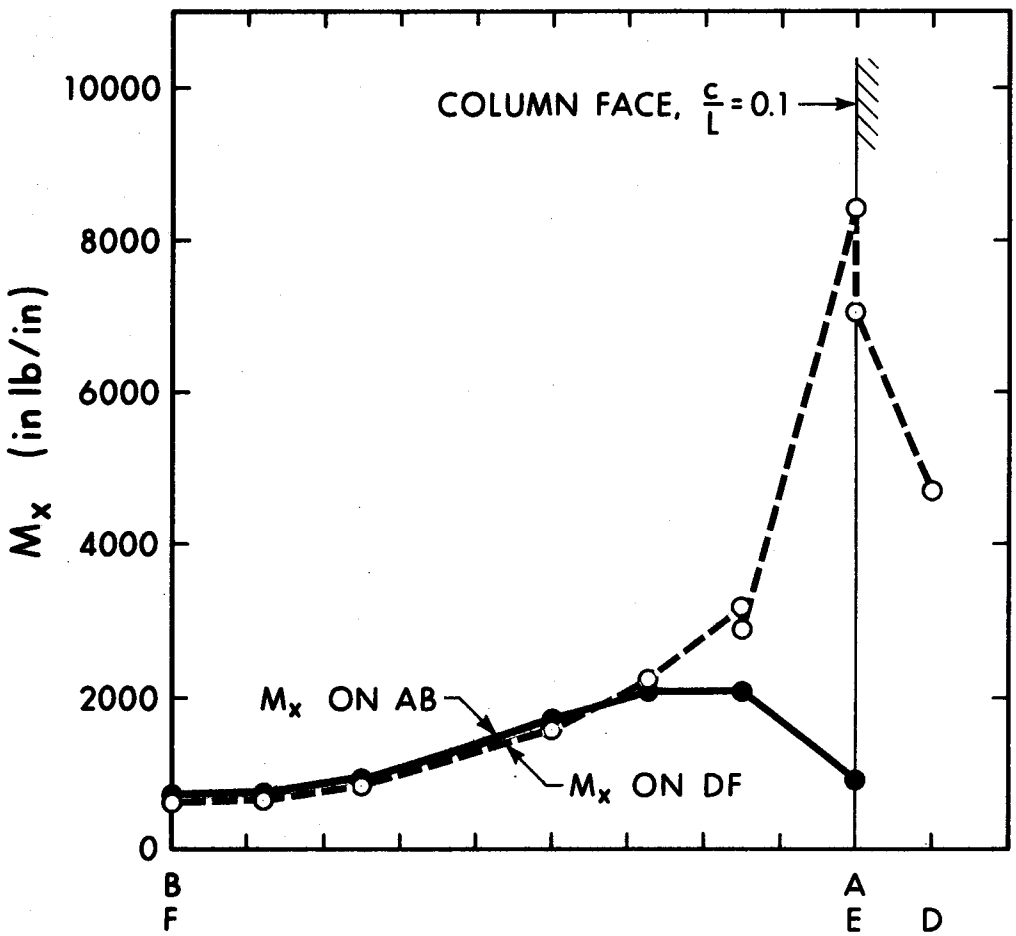

FIGURE 4.6 M_x ALONG AB AND DF - SQUARE COLUMNS

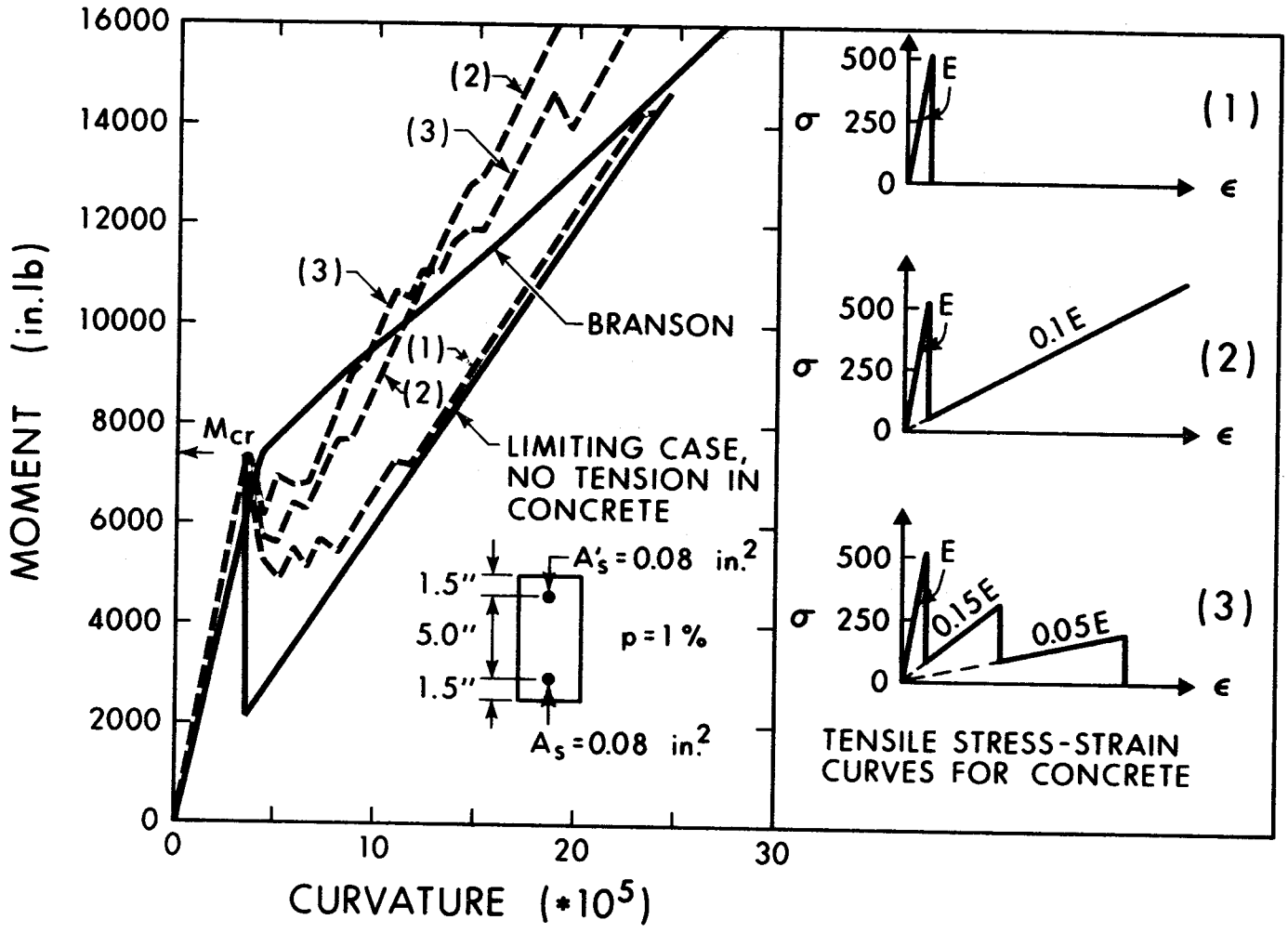

FIGURE 4.7 MOMENT CURVATURE RELATIONSHIPS

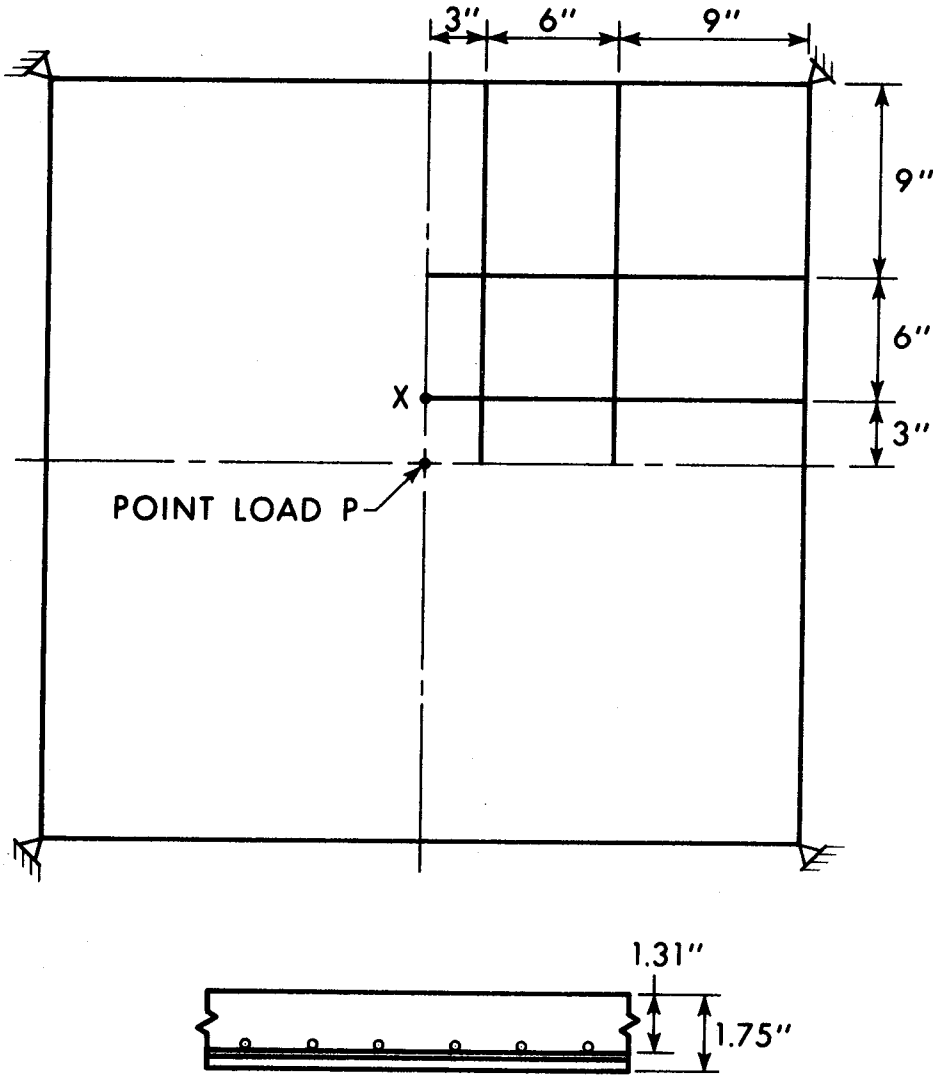

E_c = 4.15 x 10^6 p.s.i.
E_s = 29 x 10^6 p.s.i.
ν = 0.15
p = .85%
f'_c = 5500 p.s.i.

FIGURE 4.8 SLAB TESTED BY McNEICE

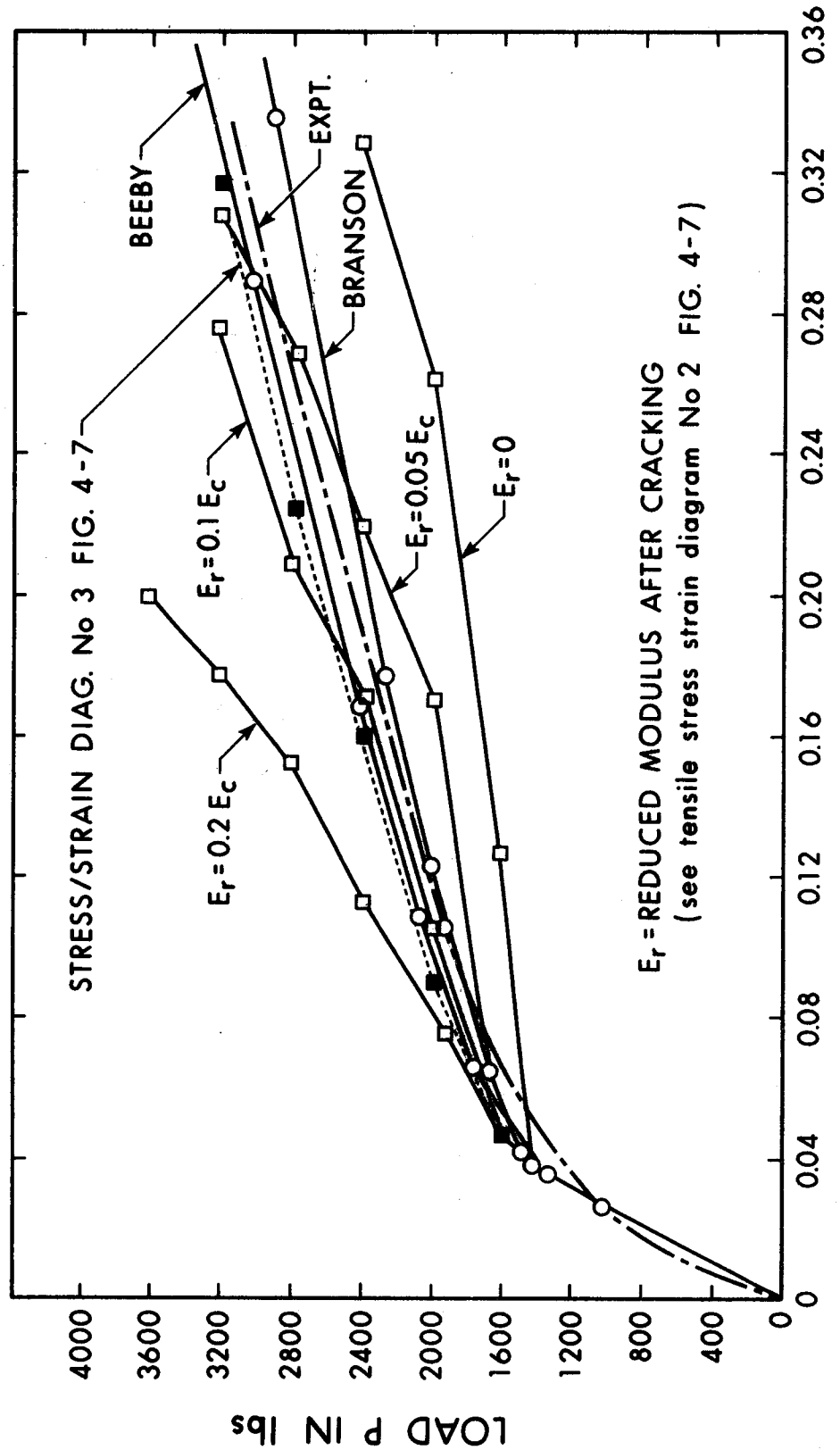

FIGURE 4.9 LOAD DEFLECTION CURVE FOR VARIOUS TENSILE STRESS STRAIN CURVES

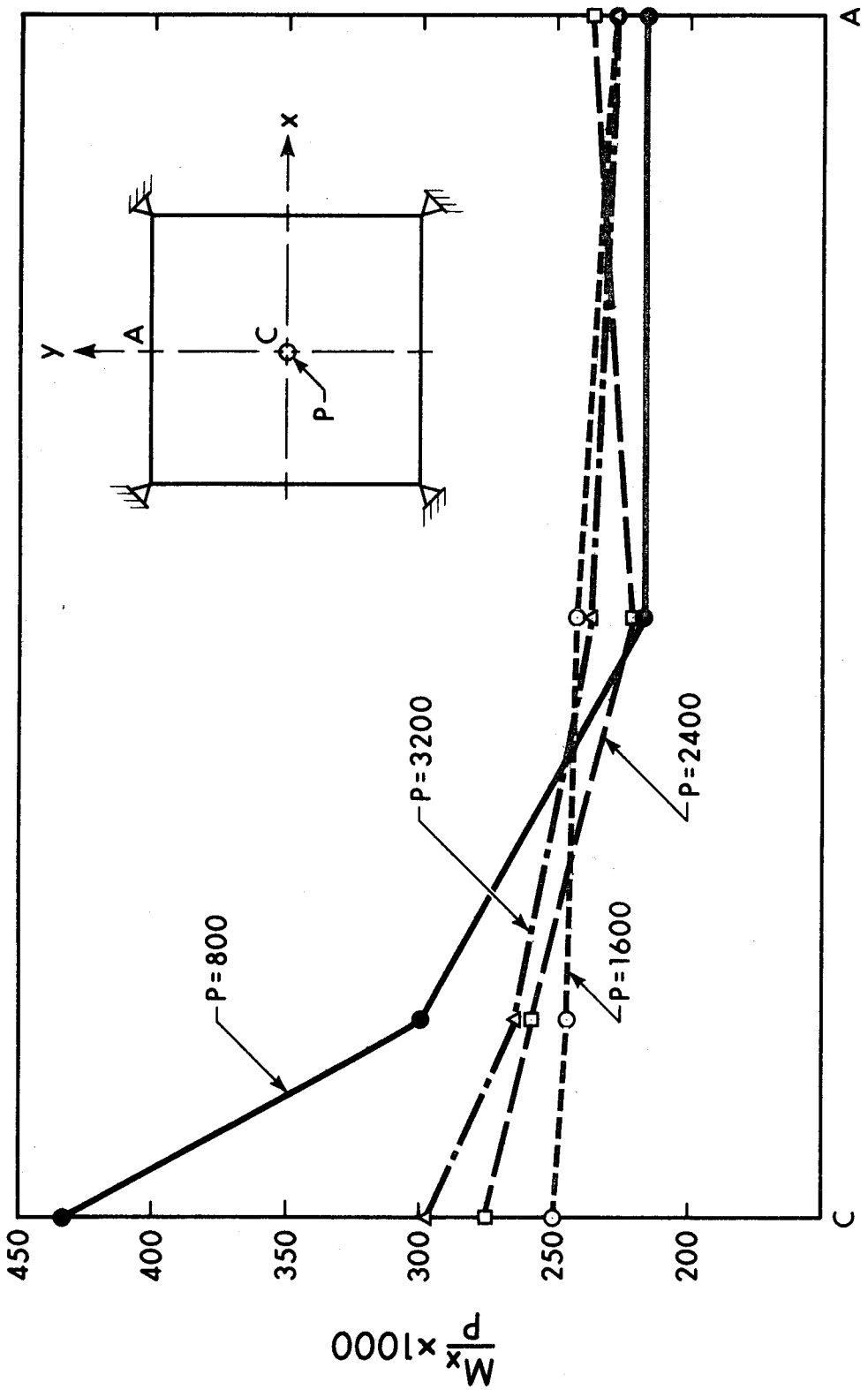

FIGURE 4.10 VARIATION OF M_x ON AC FOR INCREASING P

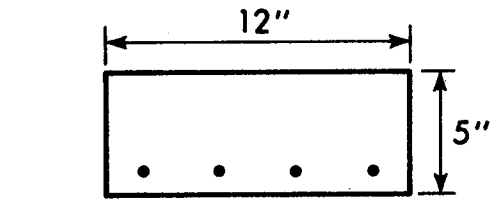

$A_s' = 0.$

$A_s = 0.8$ sq·in

C3, C6

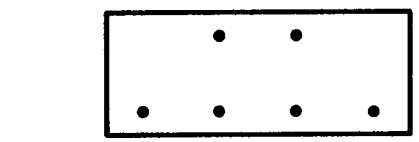

$A_s' = 0.4$ sq·in

$A_s = 0.8$ sq·in

C2, C5

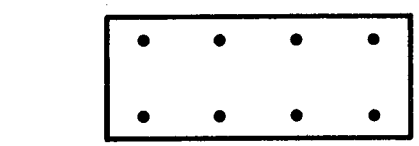

$A_s' = 0.8$ sq·in

$A_s = 0.8$ sq·in

C1, C4

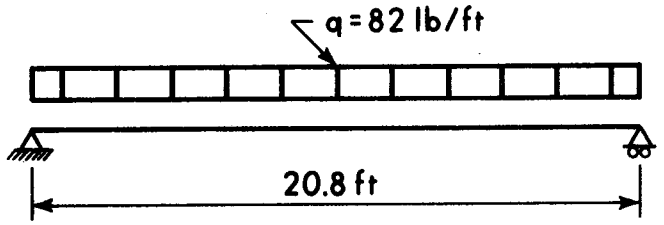

FIGURE 4.11 WASHA & FLUCK TEST BEAMS

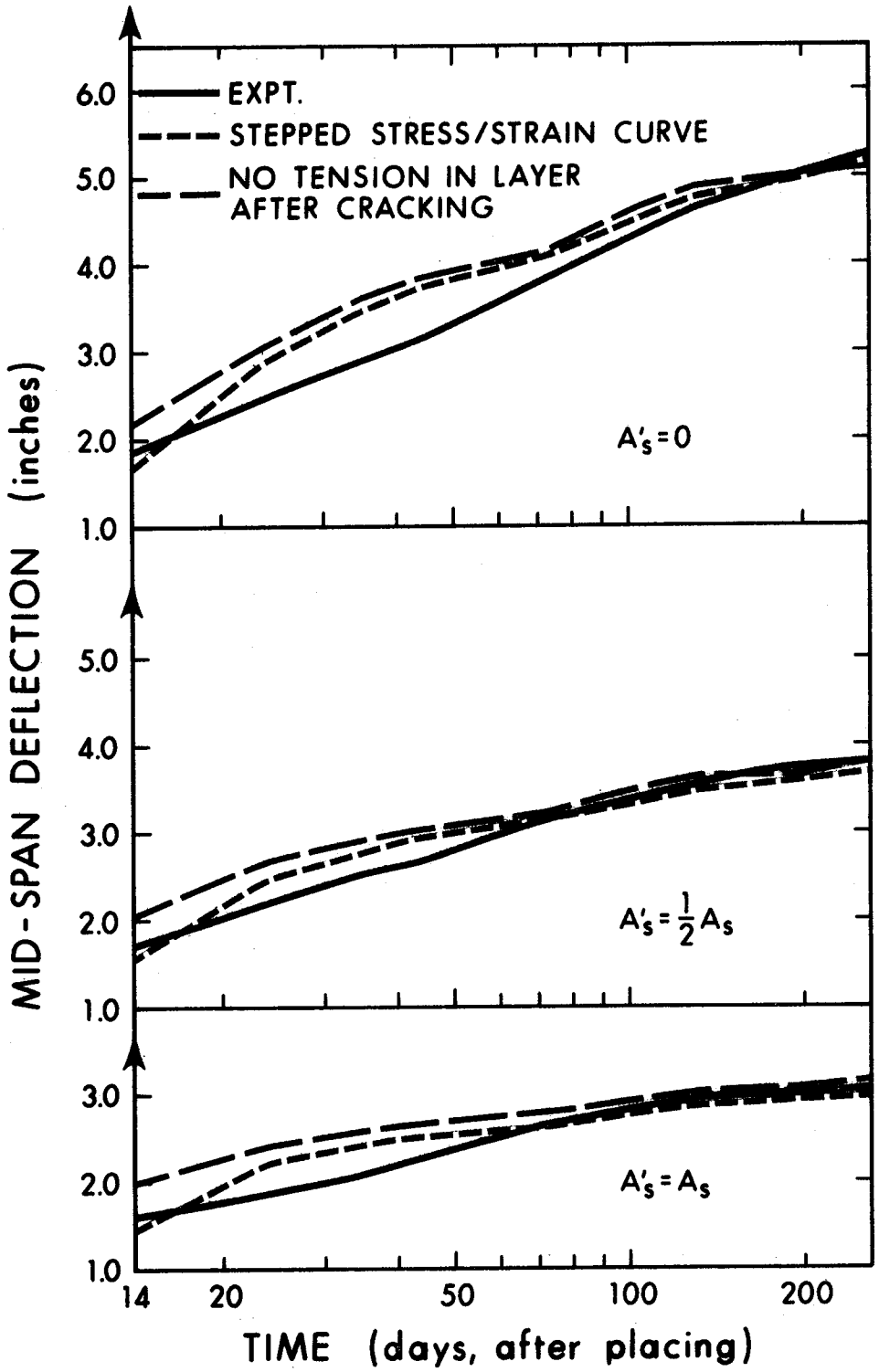

FIGURE 4.12 DEFLECTION-TIME CURVES WASHA & FLUCK BEAMS

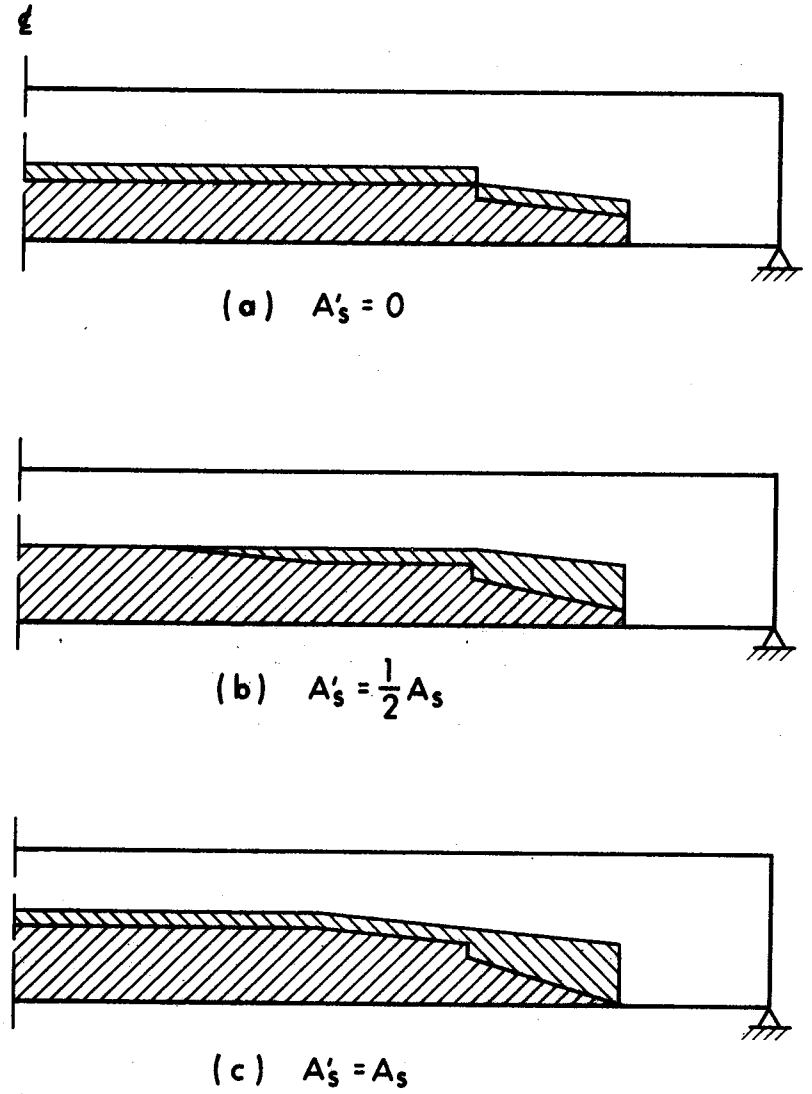

FIGURE 4.13 CRACKING ENVELOPES WASHA & FLUCK BEAMS

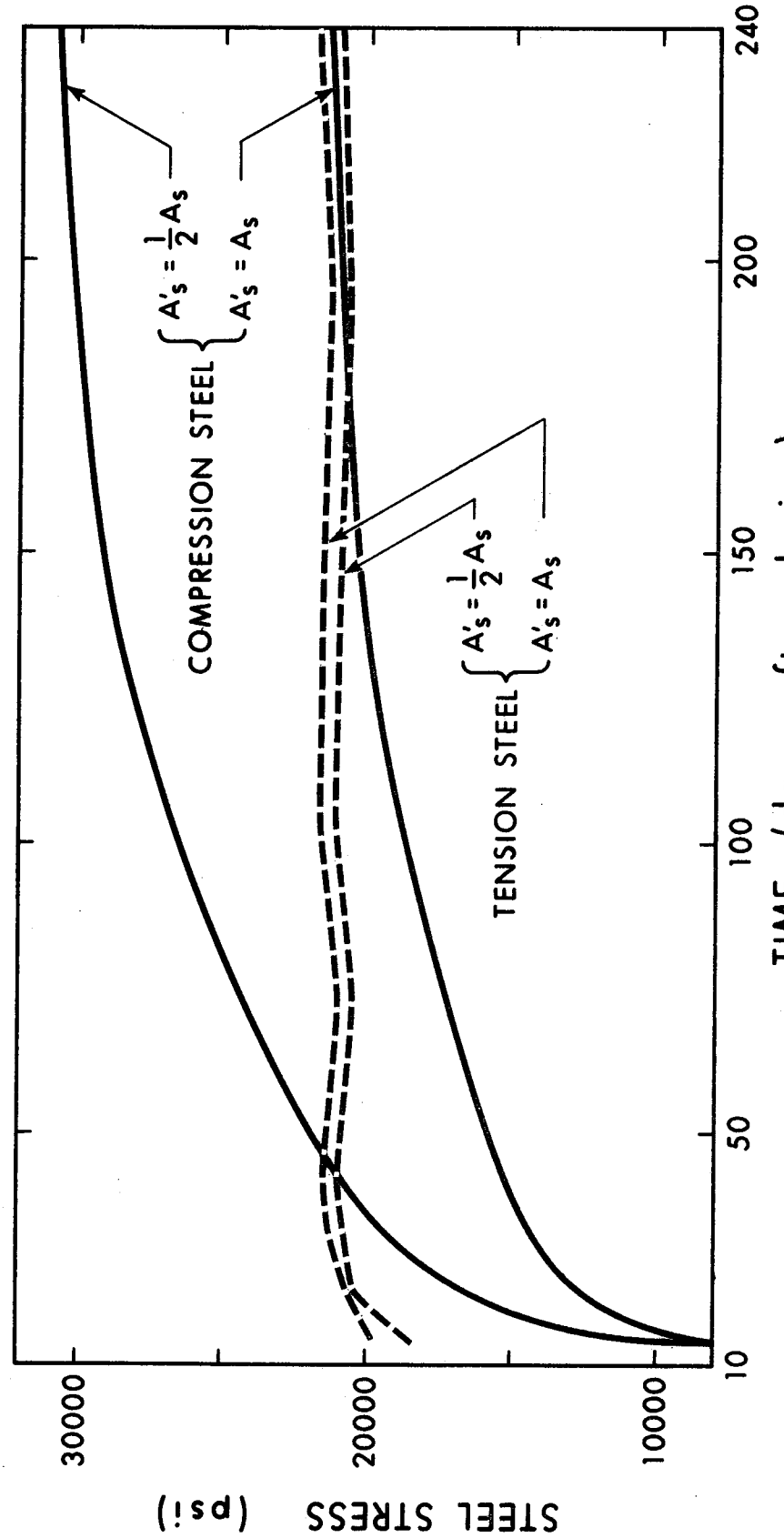

FIGURE 4.14 VARIATION OF STEEL STRESS WITH TIME

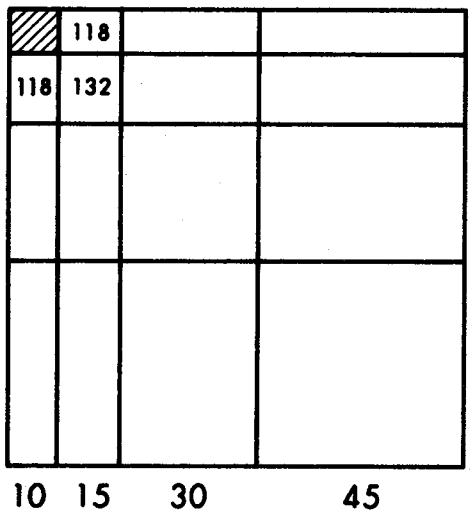

MESH No 1

15 ELEMENTS
24 JOINTS

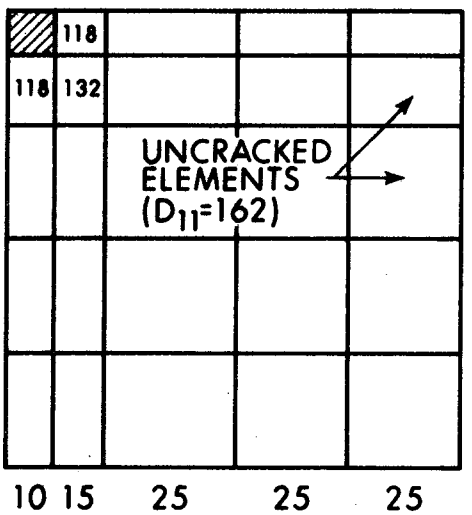

MESH No 2

24 ELEMENTS
35 JOINTS

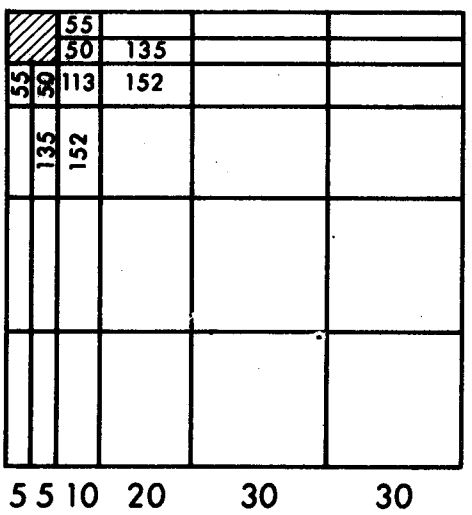

MESH No 3

32 ELEMENTS
45 JOINTS

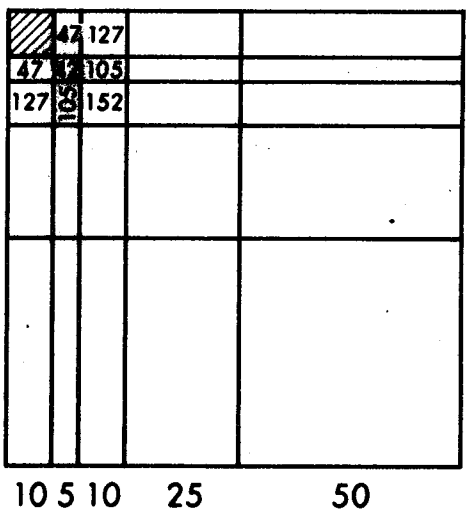

MESH No 4

24 ELEMENTS
35 JOINTS

(NUMBERS SHOWN REPRESENT STIFFNESS (D_{11}) OF CRACKED ELEMENT)

FIGURE 4.15 MESH LAYOUTS 1, 2, 3 AND 4

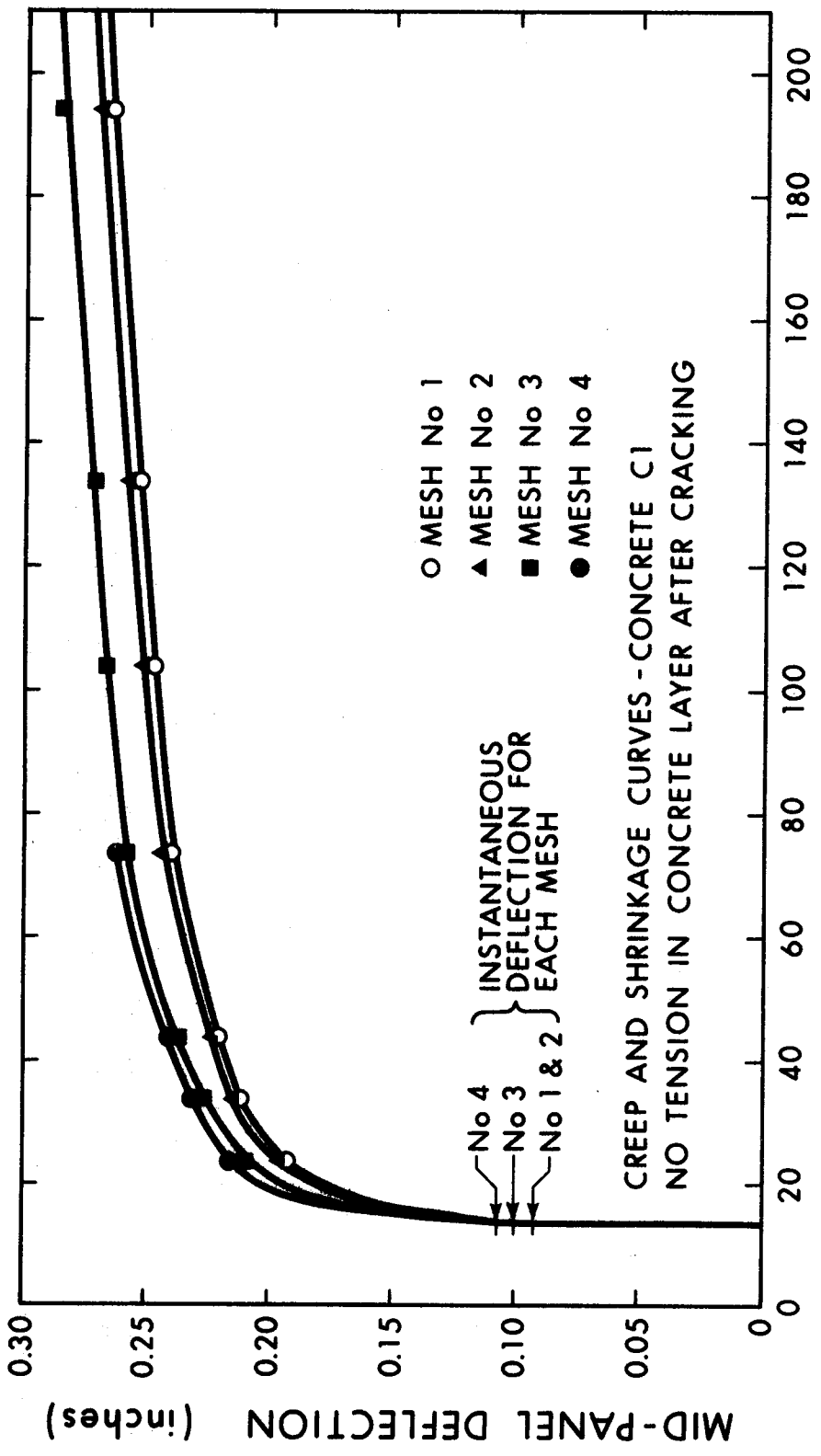

FIGURE 4.16 DEFLECTION-TIME CURVES FOR VARIOUS MESH LAYOUTS

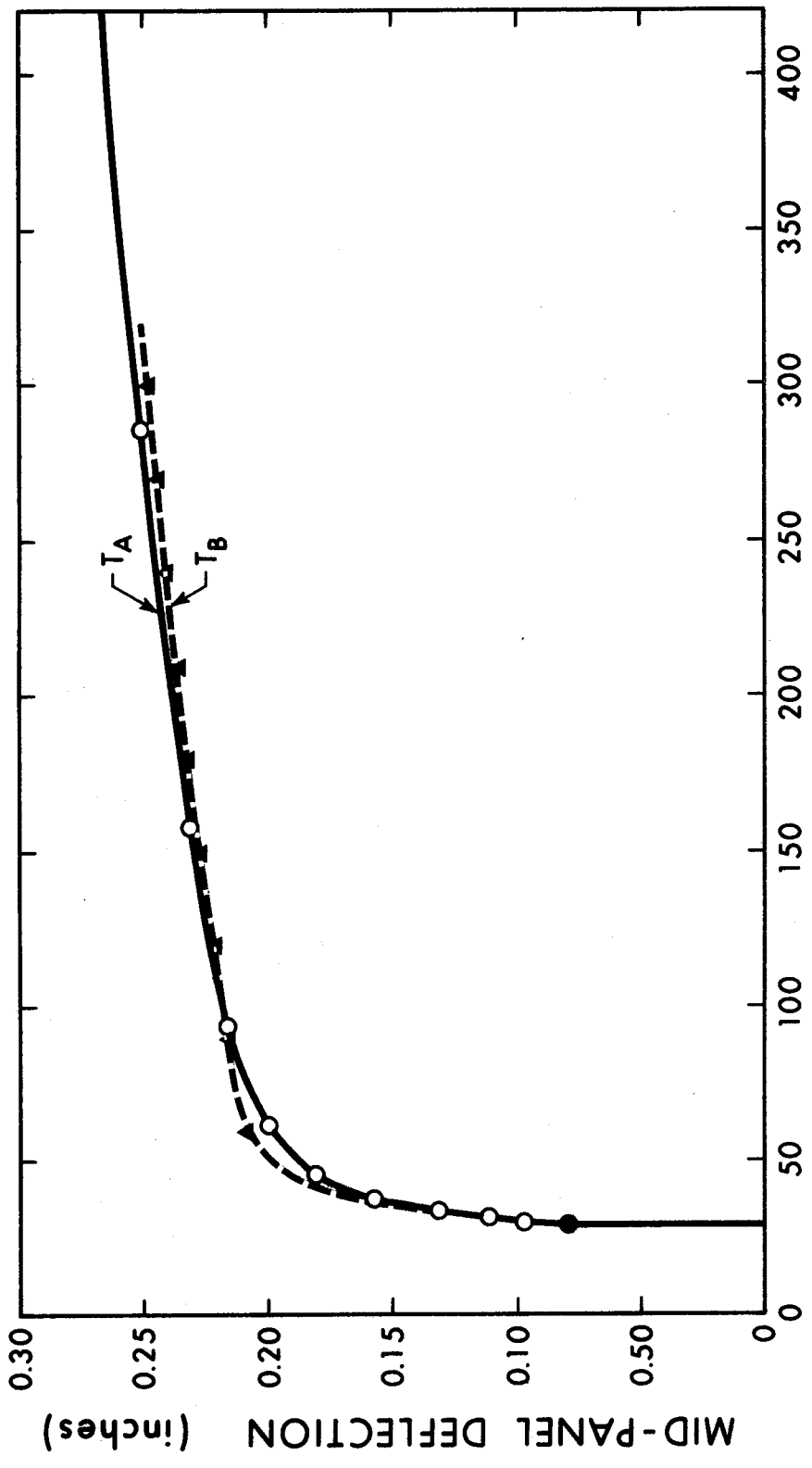

FIGURE 4.17 DEFLECTION-TIME CURVES FOR DIFFERENT TIME STEP LENGTHS

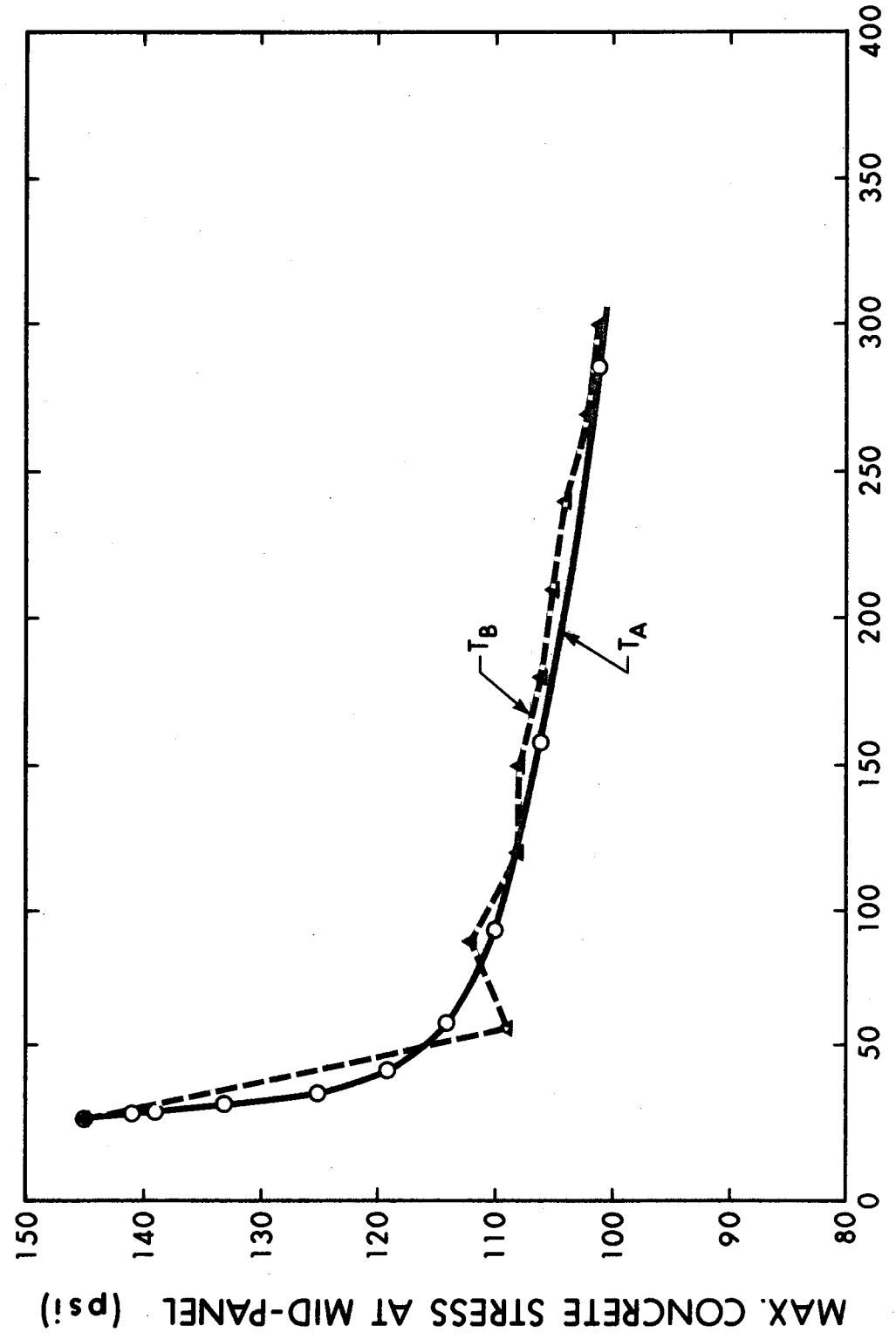

FIGURE 4.18 CONCRETE STRESS-TIME CURVES FOR DIFFERENT TIME STEP LENGTHS

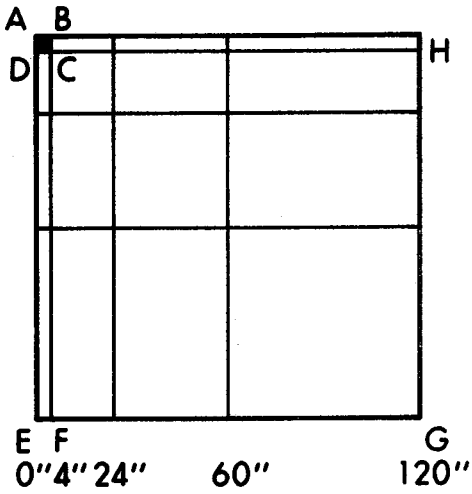

MESH No 5
15 ELEMENTS

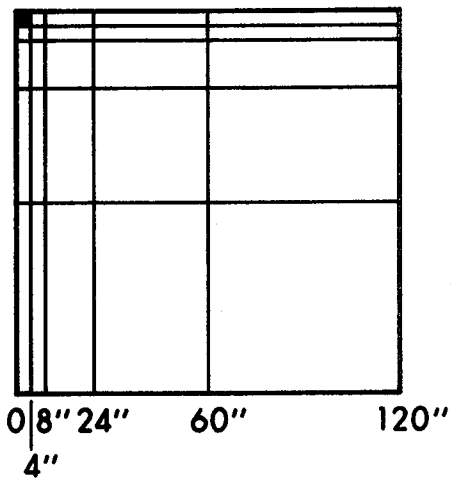

MESH No 6
24 ELEMENTS

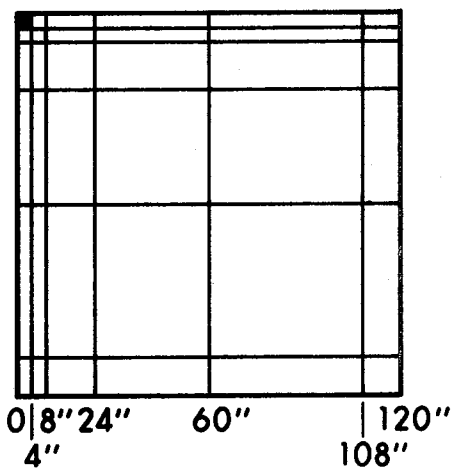

MESH No 7
35 ELEMENTS

FIGURE 4.19 MESH LAYOUTS FOR STUDY OF MOMENTS

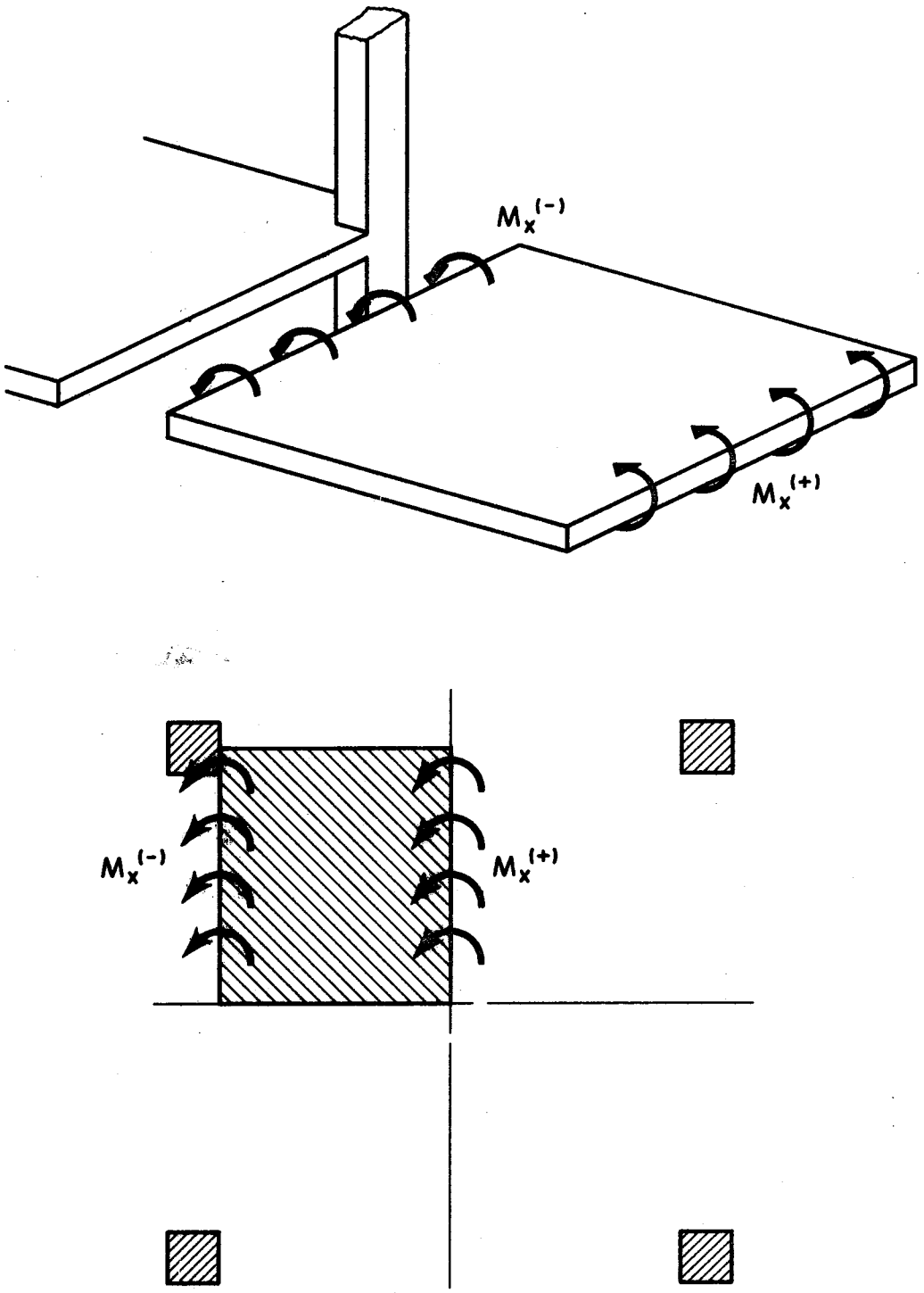

FIGURE 4.20 POSITIVE AND NEGATIVE MOMENT LOCATIONS

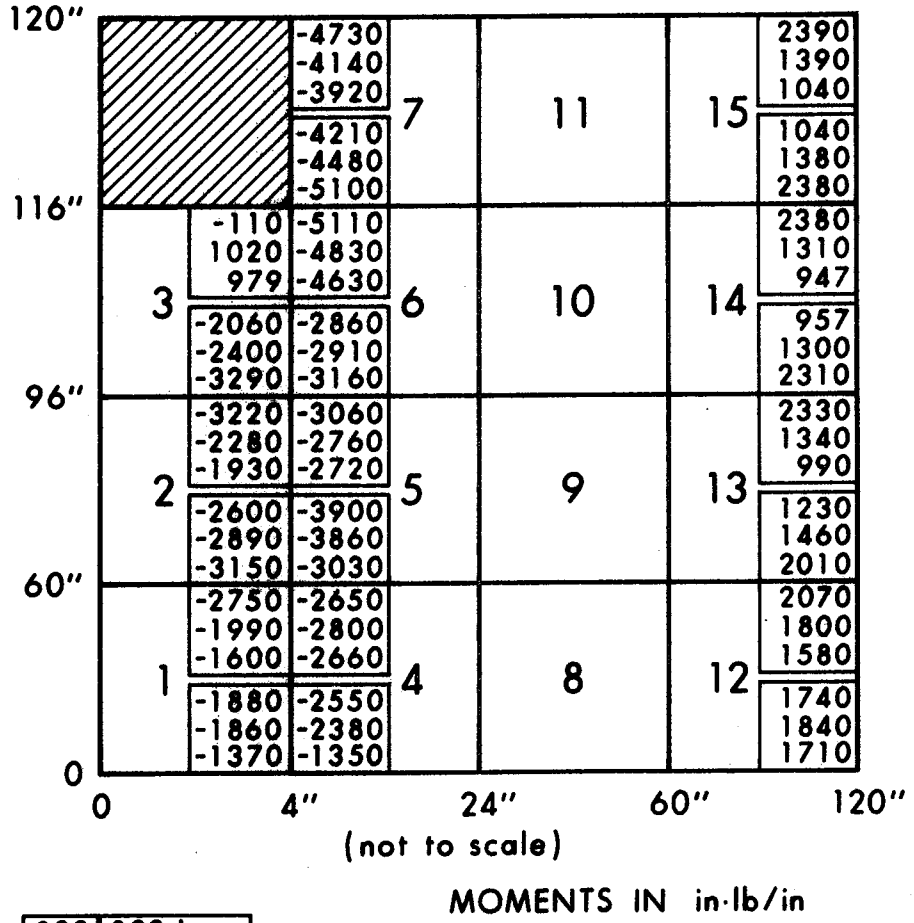

FIGURE 4.21 COMPUTED MOMENTS (M_x) FOR MESH #5

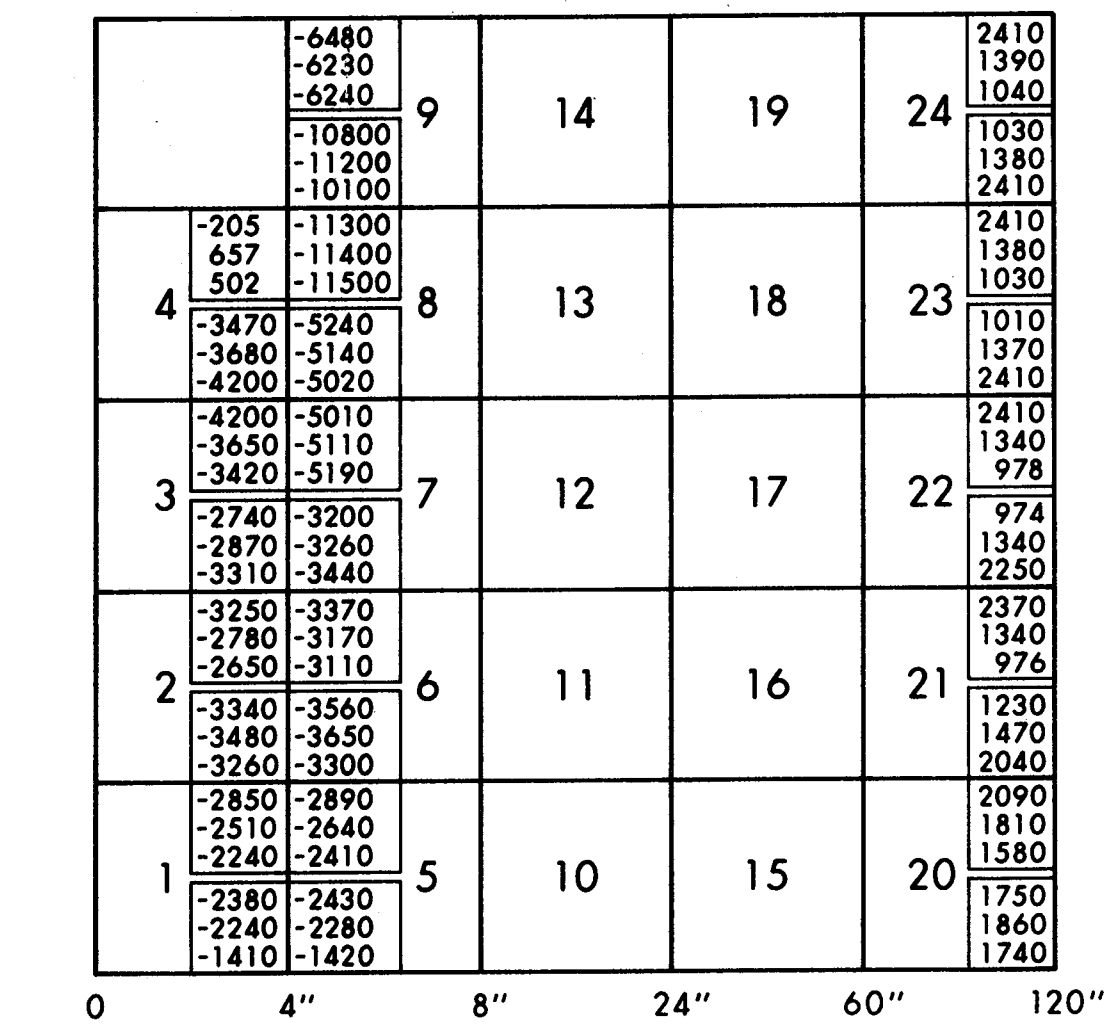

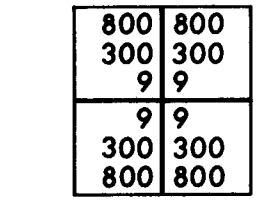

MOMENTS IN in·lb/in

FIGURE 4.22 COMPUTED MOMENTS (M_x) FOR MESH #6

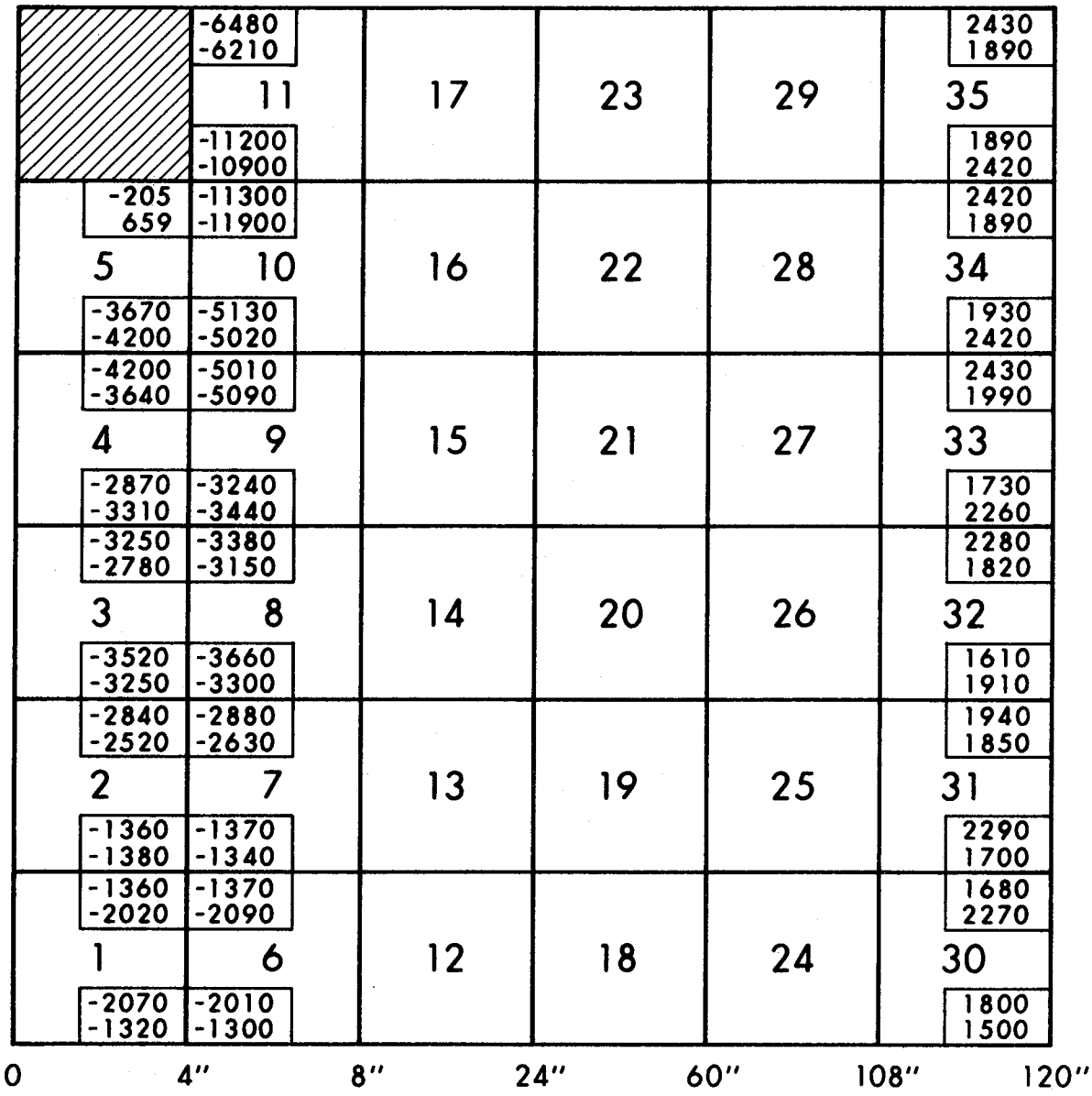

FIGURE 4.23 COMPUTED MOMENTS (M_x) FOR MESH #7

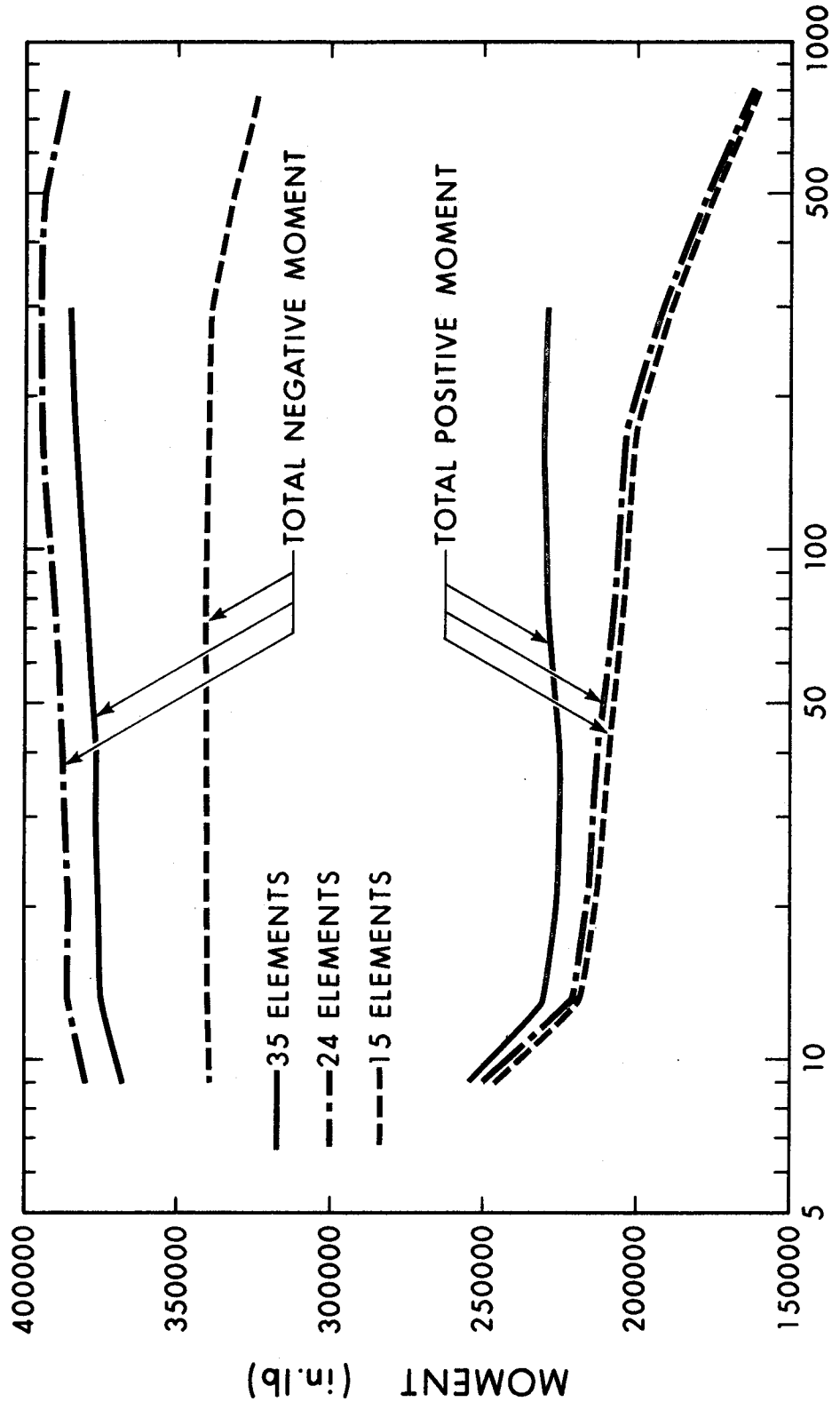

FIGURE 4.24 TOTAL POSITIVE AND NEGATIVE MOMENTS

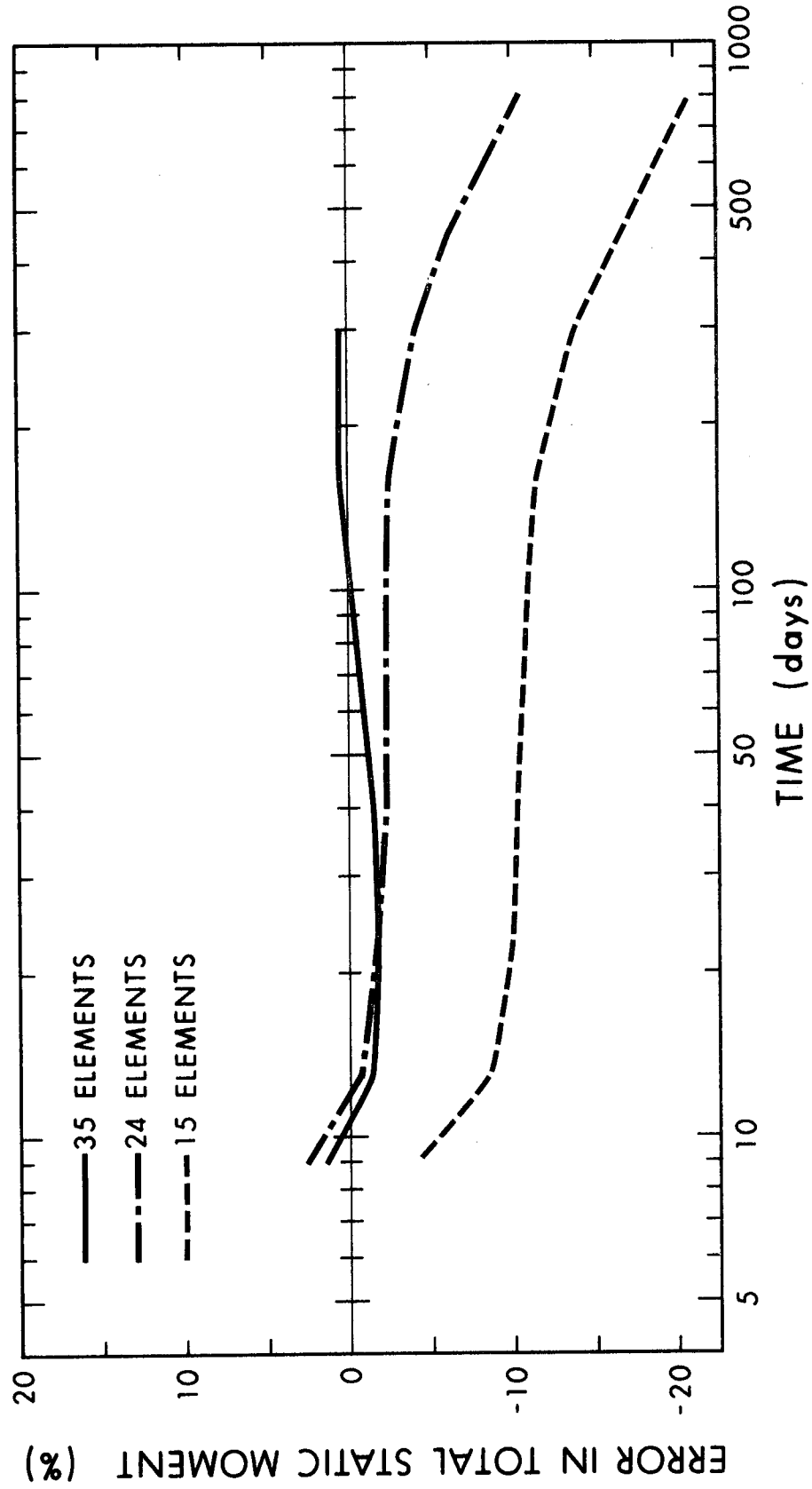

FIGURE 4.25 ERROR IN TOTAL STATIC MOMENT

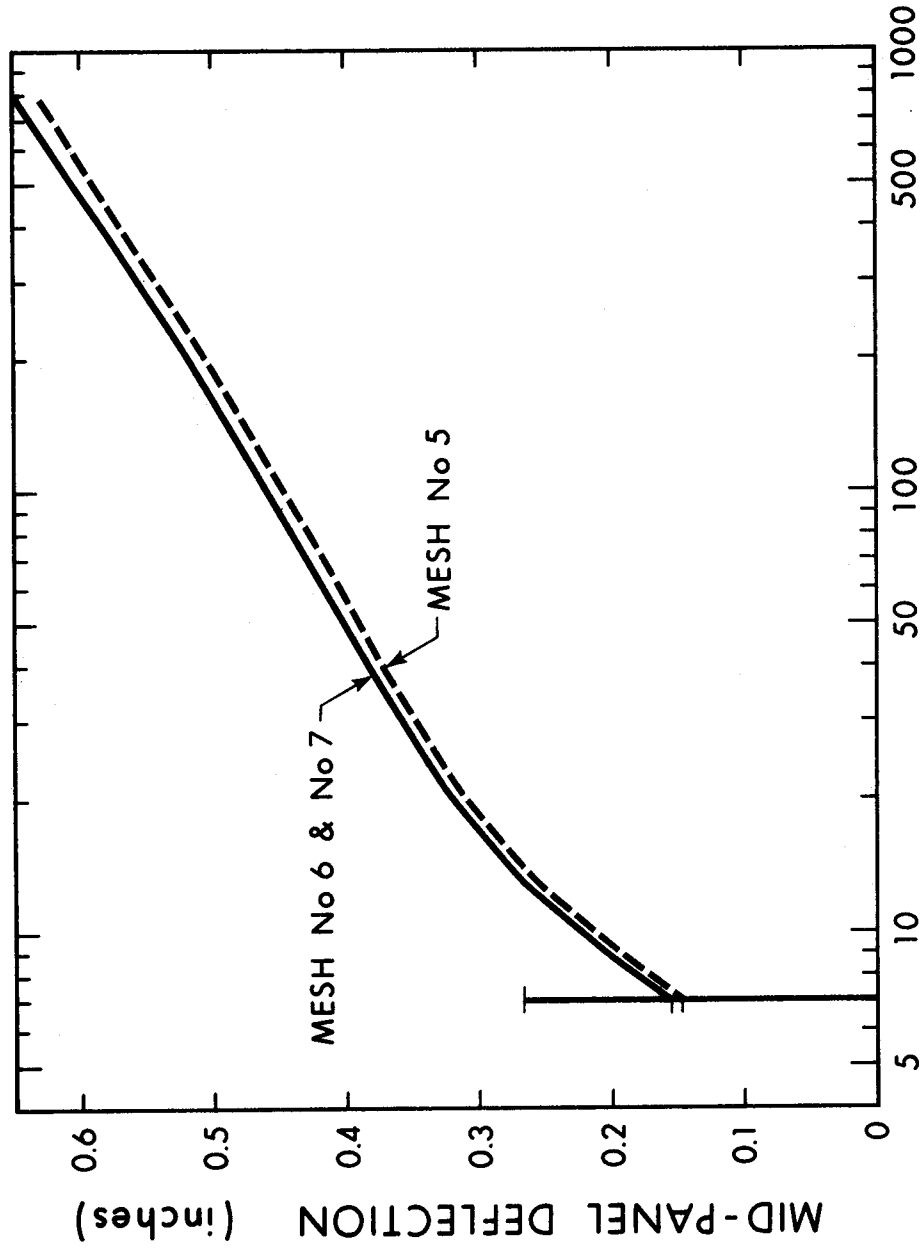

FIGURE 4.26 LOAD DEFLECTION CURVES MESH LAYOUTS 5, 6 AND 7

CHAPTER 5

PARAMETER STUDY OF FACTORS AFFECTING SLAB DEFLECTIONS

5.1 Introduction

The difficulty associated with the computation of deflections of reinforced concrete slabs is due to the large number of factors involved, many of which cannot be specified accurately. Among the parameters which must be considered are the material properties, loading, boundary conditions, the size and shape of panels and the effects of stiffening elements such as beams. The purpose of the parameter study described in this Chapter is to illustrate the application of the present method of analysis in a systematic study of some of these parameters, particularly the effects of geometry, cracking, time-dependent behaviour and non-uniform reinforcement layouts, on slab deflections.

The study was restricted to a square interior panel of a flat plate floor system and the effects of the following parameters were considered,

a) concrete properties

b) loading history

c) span to depth (L/d) ratio

d) column width to span c/L ratio

e) reinforcement layouts

5.2 Slab Design

A typical interior panel may be defined as a panel in an infinite array of identical panels under uniform load as shown in Figure 5.1. From symmetry, only one quadrant of a panel need be considered in the analysis and the boundary conditions are as shown in Figure 5.2.

A constant slab thickness, d = 8 inches, was used throughout the study to determine reinforcing steel requirements, the direct design method of the 1971 A.C.I. Building Code[3] was used, in which the total panel moment M_o is obtained from

$$M_o = \frac{qLL_c^2}{8} \tag{5.1}$$

where q represents the uniform load on the panel, L is the length of the panel in the transverse direction and L_c is the clear span between column faces in the longitudinal direction. The total moment is distributed between column and middle strip and then between positive and negative moment regions as shown in Figure 5.3. From the computed moments, the required reinforcement may be obtained. The reinforcement layout used in this study is shown schematically in Figure 5.4. The area of steel per unit of length in each location is labelled as follows,

Second letter:	C	= column strip
	M	= middle strip
Third letter:	T	= top steel
	B	= bottom steel
Fourth letter:	X	= x-direction
	Y	= y-direction

For example, AMTY represents the area of top steel in the middle strip running in the y-direction. The bottom steel in the negative moment region of the column strip is taken as one half of the steel in the positive moment region. The units are sq. in. per in. All top steel is assumed to be located one inch from the top surface and all bottom

steel seven inches from the top surface.

A total of nine slabs with varying column widths and spans were designed for flexure using a steel yield stress of 40 k.s.i. No attempt was made to fit actual bar sizes and spacing to the computed steel requirements. Instead, the computed area of steel per inch of length was used as input for the computer analysis. From the nine basic slabs designed, nineteen analyses were carried out to study the parameters discussed in Section 5.1. The dimensions and reinforcement details for the nineteen analyses are given in Table 5.1. A summary of the variables considered in the parameter study is presented in Table 5.2.

The design live load on a floor system depends on the type of use, such as apartment, office or warehouse. For the present study a live load of 50 p.s.f. was used. The dead load was the same for all slabs since the thickness was considered to be constant

Live Load	=	50 p.s.f.
Dead load	=	100 p.s.f.
Total load	=	150 p.s.f.

5.3 Parameters Considered in Study

The parameter study is treated in terms of the five factors listed in Section 5.1 and each factor will be discussed in turn. Two mesh layouts were used in the study. These layouts had the general configuration of mesh #5 and #6 in Figure 4.19 with the dimensions adjusted to suit span and column sizes in each case. Table 5.3 specifies the layout for each slab by giving the number of elements used, either 15 for mesh #5 or 24 for mesh #6. In addition, the amount

of machine time required, the number of time increments and the number of cracking iterations for each case are given.

5.3.1 Concrete Properties

The concrete properties which are important in terms of slab deflections are,

a) instantaneous modulus of elasticity and creep characteristics as represented by the creep compliance function for the material

b) variation of shrinkage strains with time

c) modulus of rupture

The material properties used in this study are based on the C.E.B. creep and shrinkage parameters from which creep and shrinkage curves have been obtained. The details of these curves are given in Section 2.5. Two different concretes designated C1 and C2 are used, where C1 represents a concrete exhibiting high creep and shrinkage and C2 represents average or normal creep and shrinkage strains.

The modulus of rupture is a highly variable quantity[50]. For the present study a value of 500 p.s.i. was used throughout. Based on the 1971 A.C.I. Building Code expression,

$$f_r = 7.5 \sqrt{f'_c} \qquad (5.2)$$

This corresponds to a compressive strength of 4450 p.s.i.

An important factor to be considered is the effect of tensile stiffening of the concrete between cracks. This factor was discussed in Chapter 4 in terms of the point supported square slab and has been included in the parameter study analyses of the interior panel. Figure 5.5 shows the stepped stress strain diagram used to

account for tensile stiffening between cracks.

The slabs considered in this section, designated as S1, S2, S3 and S4, have the following properties and assumptions concerning tensile concrete in cracked regions.

S1 - concrete C1 and no tension after cracking

S2 - concrete C2 and no tension after cracking

S3 - concrete C1 and stepped stress strain diagram (tension)

S4 - concrete C2 and stepped stress strain diagram (tension)

The loading history L1 (Figure 5.7) was used in each case. A complete description of this loading history is given in the following section.

Figure 5.6 shows the variation of the mid-panel deflection with time for each case. On first application of load at $t = 7$ days, cracking occurred in the vicinity of the column. Deflections then increased steadily until 21 days at which time an additional load was temporarily applied causing further cracking around the column. The additional load was then removed (also at 21 days) and the slabs continued to deflect with time with no further increase in cracking.

The instantaneous deflection at 7 days is seen to depend on both the compliance curve used and the assumption concerning tensile stiffness in the cracked regions. For each concrete the assumption of no tension after cracking predicted a greater deflection than the stepped stress strain diagram as would be expected. The difference between the deflections for the two different concretes is also evident, concrete C1 producing a greater instantaneous deflection than C2, assuming the same tensile behaviour for the two concretes.

The instantaneous deflections for S2 and S3 are almost equal indicating that the difference in tensile properties for the two

cases is offset by the difference in instantaneous elastic modulus. Between 7 days and 21 days the difference in the response of the two concretes becomes more evident. For each concrete, the difference in deflection at any time between the no tension assumption and stepped stress strain diagram remains more or less constant. The increase in deflection for concrete C1, however, is considerably greater than that for C2. At 21 days the additional deflection due to the increased load is shown. The no tension assumption produces a greater increase in deflection than the stepped stress strain diagram for each concrete.

The deflection values at 21 days just before and just after the instantaneous increase in load indicate a significant difference in the behaviour exhibited by the tensile assumptions. The load after 21 days is less than the load up to 21 days. However, the stiffness after 21 days is also less than the stiffness before 21 days due to the increased cracking. For the no tension case the reduction in stiffness has a greater effect than the reduction in load and a net increase in deflection occurs at 21 days. On the other hand, the reduction in stiffness is less significant for the stepped stress strain diagram and a net decrease in deflection results. After 21 days, deflections continued to increase with time at a greater rate for concrete C1 than for C2. Comparing deflections at 800 days, it is apparent that, as expected, the compliance characteristics of the concrete have a significant effect on long time deflection. The deflection at 800 days for S1 was 2.722 inches compared with 1.510 inches for S4 and 1.698 inches for S2.

Considerable cracking occurred in these four slabs in the

vicinity of the column with much less severe cracking in the positive moment region.

5.3.2 Loading History

The evaluation of long time deflections requires a knowledge of the loading history. While the dead load may be assumed to remain constant with time, the variation of the actual live load with time will not in general be known.

A survey[28] carried out in Sweden indicated the following loads due to persons and furniture in apartment buildings.

Mean load due to persons	= 30 kg/m^2	(6.144 p.s.f.)
Greatest load due to persons	= 128 kb/m^2	(26.214 p.s.f.)
Mean load due to furniture	= 25 kg/m^2	(5.120 p.s.f.)
Greatest load due to furniture	= 105 kg/m^2	(21.504 p.s.f.)

The greatest loads due to persons and furniture did not occur simultaneously. These loads are seen to be considerably smaller than the design live load of 50 p.s.f. and it does not appear reasonable to consider the full live load as sustained load for the purpose or computing long time deflections. In this study a sustained load of 20% of the design live load has been assumed.

In the case of reinforced concrete floor slabs in multi-storey construction where a freshly placed floor slab is supported on previously cast floors, the construction loads on the slabs often exceed the loads under service conditions. Grundy and Kabaila[23] indicate that the total load carried by a slab at the construction stage may exceed twice the dead load of the slab. It is therefore

important to include such construction loads in the analysis for deflections since most of the cracking will take place at the construction stage and this will determine the subsequent overall stiffness of the slab.

Two loading histories, designated L1 and L2 are shown in Figure 5.7. Loading history L1 consisted of a load of 1.5 x D.L. applied at 7 days and held constant to 21 days at which time an additional 0.5 x D.L. was applied instantaneously. The load was then reduced to a value of 1 x D.L. + 0.2 x L.L. and remained constant thereafter. In the case of L2, the maximum load of 2 x D.L. was applied at 7 days and immediately reduced to a sustained load of 1 x D.L. + 0.2 x L.L. Behaviour under the two loading histories is represented by slabs S3 and S14 (Table 5.2) which have identical material properties and dimensions and were analyzed by loading histories L1 and L2 respectively. The stepped stress strain diagram in tension was used.

The variation of mid-panel deflection with time is shown in Figure 5.8 for S3 and S14. The larger instantaneous load applied to S14 at 7 days caused cracking around the columns to a greater extent than experienced by S3, thereby reducing the flexural stiffness of S14 relative to S3. The deflection just after 7 days is approximately the same for each case although the load on S3 is greater than that on S14. The effect of the higher load on S3 however, is to produce a larger increase in creep deflections between 7 and 21 days. At 21 days the load on S3 is increased temporarily and then reduced to the same value as that on S14. At this stage, the deflections for the two cases were almost equal. After 21 days when the loads on the two slabs were equal, the deflections increased with time at approximately the same

rate, with the final deflection of S3 slightly less than that of S14.

These results suggest that the long time deflection under sustained load is not greatly affected by variations in loading history at early age, as long as the maximum load is the same and produces approximately the same degree of cracking.

5.3.3 Span to Depth (L/d) Ratio

From isotropic elastic plate theory[2], the deflection Δ at a point in a plate is given by an expression of the form,

$$\frac{\Delta}{L} = K\, q\left(\frac{L}{d}\right)^3 \qquad (5.3)$$

where K is a constant depending on boundary conditions. The influence of the L/d ratio is explicitly evident in this equation, and minimum thicknesses for control of deflections in slabs have traditionally been based primarily on this quantity.

The extent of cracking in a slab also depends on the L/d ratio. As the span increases the maximum moments increase while as the depth decreases the cracking moment also decreases. In other words for a given loading, the overall flexural stiffness decreases as the L/d ratio increases.

In the study of L/d ratios, the c/L ratio was held constant at 0.1 and loading history L1 was used in each case. Slabs S5, S6, S7, S8 and S1, using concrete C1, were considered with L/d ratios of 15, 22.5, 30, 37.5 and 45 respectively. Concrete was assumed to take no tension after cracking. To illustrate the behaviour using concrete C2, one slab, S2, with a L/d ratio of 45 was considered.

Figure 5.9 shows the variation of mid-panel deflection with

time for each of the slabs analyzed (except S2). Slabs S7, S8 and S1 exhibited cracking at 7 days and further cracking at 21 days when the load was increased. Slabs S5 and S6 produced no cracking at any time. The rapid increase in deflection, both long and short time with increase in the L/d ratio is apparent.

Engineering practice usually considers the deflection to span ratio to be of more significance than the absolute magnitude of the deflection. The relationships between Δ/L and $(L/d)^3$ are therefore plotted in Figure 5.10 where Δ represents the mid-panel deflection. Values are plotted for t = 7 days assuming the concrete to be uncracked, for t = 7 days taking cracking into account and finally for t = 800 days. For each case, the values plotted for concrete C1 are indicated by solid lines. Since only one slab was considered for concrete C2, estimated values for other L/d ratios are shown by the dashed lines. In the following discussion, the values obtained for concrete C1 are considered first.

For the initial application of load at 7 days, the relationship is linear, assuming the slab to be uncracked. The slab thus behaves as an isotropic homogeneous elastic plate and the reinforcement has practically no effect on the behaviour. Allowing for cracking in the slab, it can be seen that cracking has a more pronounced effect as the L/d ratio increases. For the two smallest L/d ratios, no cracking was detected at the load levels considered. However, as the L/d ratio increases, the Δ/L ratio is seen to depart from the uncracked case as the extent of cracking increases.

The relationship shown for t = 800 days illustrates the significant effect which creep and shrinkage have on deflection

behaviour. The increase in deflection due to creep and shrinkage is significantly greater than that due to cracking. A similar trend is indicated for the average creep and shrinkage properties represented by concrete C2, although in this case creep and shrinkage deflections are not as severe as for the high creep concrete. The relationships plotted in Figure 5.10 are based on the assumption of no tension in a concrete layer after cracking, and the deflections obtained are therefore more severe than would be the case where tensile stiffening is accounted for in the cracked regions.

5.3.4 Column Width to Span (c/L) Ratio

The column width affects deflections in two ways. In the first place, a reduction in column width increases the clear span to depth ratio. Secondly, as the column size decreases high concentrations of moment are induced at the columns resulting in increased cracking and a reduction in flexural stiffness.

Slabs S9, S10, S11, S12 and S13 were analyzed with c/L ratios of 0.033, 0.067, 0.1, 0.15 and 0.20 respectively. Loading history L2 and L/d ratio equal to 30 were used in each case. The stepped stress strain diagram in tension was applied to this series.

Figure 5.11 shows the variation of mid-panel deflection with time for each slab. The deflection on application of 2 x D.L. at 7 days is shown in each case, followed by the gradual increase in deflection with time due to the sustained load. The deflection at 800 days for c/L = 0.2 was 0.295 inches compared with 0.65 inches for c/L = 0.033. The results indicate that the c/L ratio has a significant effect on both short and long time deflections.

In Figure 5.12 the relationship between L/Δ and c/L has been plotted at t = 800 days and at t = 7 days (for the deflection due to the reduced load). In each case a curve has been drawn through the points plotted. For the case of t = 800 days the curve fits the points reasonably well whereas at t = 7 days more scatter is evident. This may be due to the fact that a discrepancy in the smaller deflection at t = 7 days will be magnified in the quantity L/Δ. In Section 4.5.1 it was observed that the choice of mesh layout affects the instantaneous deflection to some degree and the long time deflection to a proportionately lesser degree.

Cracking around the columns occurred in all the slabs considered in this series.

5.3.5 Reinforcement Layouts

Reinforcement is required by the 1971 A.C.I. Building Code to resist the design moments allocated to column and middle strips. The amount of reinforcement provided must exceed a specified minimum amount for temperature and shrinkage effects. The slabs of the parameter study described above were based on designs satisfying the A.C.I. code requirements in this regard. The effects of two other layouts were studied. Compression reinforcement equal in amount to the required tension reinforcement was provided in one case and in the other, the negative moment steel was concentrated in the column strip.

It is generally well known that compression reinforcement reduces creep deflections. This was illustrated in Chapter 4 in terms of the Washa and Fluck beam results. An analysis was therefore carried out to determine the effect of providing compression reinforcement in amounts equal to the tension reinforcement for two way construction.

Reinforced concrete floor slabs are generally under-stressed so that large portions of the slab remain uncracked under service conditions. In the uncracked state, the concrete carries most of the tensile stress and relatively little is carried by the steel. Cardenas and Kaar[13] have reported results of a field test of a flat plate floor system in which all negative moment steel was placed in the column strip and none in the middle strip. This layout is more economical than the conventional layout in terms of placing costs but violates the 1970 A.C.I. code requirements. The test indicated that the load carrying capacity was satisfactory and that serviceability requirements (crack widths and deflections) were also satisfactory. This layout of steel was considered in the present study.

To consider the effects of reinforcement layout, slabs S14, S15, S16, S17, S18 and S19,having the same dimensions and loading history L2, were analyzed with the following concrete properties and reinforcement layouts.

S14 - concrete C1, standard reinforcement layout

S15 - concrete C1, standard layout for tension steel and $A_s' = A_s$

S16 - concrete C1, all negative moment steel in column strip

S17 - concrete C1, all negative moment steel in column strip and $A_s' = A_s$

S18 - concrete C2, standard reinforcement layout

S19 - concrete C2, standard layout for tension steel and $A_s' = A_s$

The stepped stress-strain diagram was used for concrete in tension.

Deflections at 7 days and 800 days are presented in Table 5.4

and the mid-panel deflection versus time relationship is plotted in Figure 5.13 for each of the slabs analyzed. Comparing the extreme cases of S14 and S19, it can be seen that concrete properties and reinforcement layout have a significant effect on long time deflections and a much smaller effect on short time deflections. Placing all the negative moment reinforcement in the column strip appears to have little effect on the deflection behaviour of the slab. The deflections for S14 and S16 are approximately equal over the complete loading range with the deflection of S16 at all times slightly less than that of S14. There is however a difference in the behaviour when compression steel equal to the tension steel is added as indicated by comparing S15 and S17. In S17 all of the compression steel in the negative moment region is concentrated in the column strip as is the tension steel. This layout appears to be less effective in restraining creep deflections than the case where the compression steel is distributed between column and middle strips.

The provision of compression reinforcement equal in amount to the tension reinforcement significantly reduces long-time deflections for both layouts. For the standard layout of reinforcement, additional long time deflections due to creep and shrinkage were reduced by 47% for concrete C1 and 32% for concrete C2. For the alternative layout of steel the additional deflections were reduced by 32% for concrete C1.

Cracking occurred in all cases around the columns and to a lesser extent in the positive moment regions of the slab. As an example, the cracked regions produced in slab S19 are shown in Figure 5.14. No attempt is made to show crack spacing or direction.

Extensive cracking is seen to occur in the negative moment region where cracking extended to a distance of more than a quarter of the span for the column. Cracking in the positive moment region occurred to a much lesser extent as illustrated by the comparison between distributions of normal stress at the corner of the column and at the centre of the panel shown in Figure 5.15.

The validity of the linear stress-strain assumption might be questioned for the stress distribution at the column where high compressive stresses are produced. However, this stress distribution corresponds to the high short time load equal to twice the dead load and the load immediately reduces by almost one half to the lower sustained load. In addition the high stresses are localized in the immediate vicinity of the column.

5.4 Summary

This chapter describes a parameter study of several factors which affect deflections of flat plate floor systems. The study was restricted to a square interior panel under a time variable uniformly distributed load. Span and column dimensions were varied to produce L/d and c/L ratios in the range 15 to 45 and 0.033-0.20 respectively. In addition concrete properties, loading history and reinforcement layout were varied. A comparison of some of these results with empirical formulae currently in use is contained in Chapter 6.

SLAB NO.	c(in)	L(ft)	REINFORCEMENT (sq in/in)							
			ACTY	ACTX	AMTY	AMTX	ACBY	ACBX	AMBY	AMBX
S1	36	30	0.0793	0.0793	0.0264	0.0264	0.0427	0.0427	0.0160	0.0160
S2	36	30	0.0793	0.0793	0.0264	0.0264	0.0427	0.0427	0.0160	0.0160
S3	36	30	0.0793	0.0793	0.0264	0.0264	0.0427	0.0427	0.0160	0.0160
S4	36	30	0.0793	0.0793	0.0264	0.0264	0.0427	0.0427	0.0160	0.0160
S5	12	10	0.0160	0.0160	0.0160	0.0160	0.0160	0.0160	0.0160	0.0160
S6	18	15	0.0200	0.0200	0.0160	0.0160	0.0160	0.0160	0.0160	0.0160
S7	24	20	0.0360	0.0360	0.0160	0.0160	0.0190	0.0190	0.0160	0.0160
S8	30	25	0.0550	0.0550	0.0190	0.0190	0.0300	0.0300	0.0160	0.0160
S9	8	20	0.0407	0.0407	0.0160	0.0160	0.0219	0.0219	0.0160	0.0160
S10	16	20	0.0407	0.0407	0.0160	0.0160	0.0219	0.0219	0.0160	0.0160
S11	24	20	0.0350	0.0350	0.0160	0.0160	0.0189	0.0189	0.0160	0.0160
S12	36	20	0.0314	0.0314	0.0160	0.0160	0.0169	0.0169	0.0160	0.0160
S13	48	20	0.0279	0.0279	0.0160	0.0160	0.0160	0.0160	0.0160	0.0160
S14	36	30	0.0793	0.0793	0.0264	0.0264	0.0427	0.0427	0.0160	0.0160
S15	36	30	0.0793	0.0793	0.0264	0.0264	0.0427	0.0427	0.0160	0.0160
S16	36	30	0.1057	0.1057	0.0	0.0	0.0427	0.0427	0.0160	0.0160
S17	36	30	0.1057	0.1057	0.0	0.0	0.0427	0.0427	0.0160	0.0160
S18	36	30	0.0793	0.0793	0.0264	0.0264	0.0427	0.0427	0.0160	0.0160
S19	36	30	0.0793	0.0793	0.0264	0.0264	0.0427	0.0427	0.0160	0.0160

TABLE 5.1 DETAILS OF SLABS USED IN PARAMETER STUDY

Parameter Study	Slab	Variables		Constants
		Conc.	Tension	
Material Properties (5.3.1)	S1	C1	NT	L/d = 45
	S2	C2	NT	c/L = 0.1
	S3	C1	ST	
	S4	C2	ST	Load = L1
		Load		L/d = 45 Conc=C1
Loading History (5.3.2)	S3	L1		c/L = 0.1
	S14	L2		ST
		L/d		
L/d (5.3.3)	S5	15		c/L = 0.1
	S6	22.5		Conc = C1(except for slab S2 which was C2)
	S7	30		
	S8	37.5		
	S1	45		Load = L2
	S2	45		NT
		c/L		
c/L (5.3.4)	S9	0.033		L/d = 30
	S10	0.067		Conc = C1
	S11	0.10		Load = L2
	S12	0.15		ST
	S13	0.20		
		A_s	A'_s	
Reinforcing (5.3.5)	S14	Std.	-	L/d = 45
	S15	Std.	A_s	
	S16	Col.	-	c/L = 0.1
	S17	Col.	A_s	Conc = C1(except that S18 and S19 were C2)
	S18	Std.	-	
	S19	Std.	A_s	Load = L2
				ST

NOTE: NT - no tension in layer after cracking
ST - stepped stress strain diagram
Std. - standard reinforcement layout
Col. - negative moment reinforcement all in column strip

TABLE 5.2 SUMMARY OF SLABS IN EACH PARAMETER STUDY

Slab Nr	Nr of Elements	C.P.U. Time (secs)	Nr of Cracking Iterations	Nr of Time Steps
S1	15	704	23	13
S2	15	711	24	13
S3	15	545	14	13
S4	15	622	19	13
S5	15	312	0	13
S6	15	392	4	13
S7	15	502	12	13
S8	15	559	14	13
S9	24	659	8	11
S10	15	364	6	11
S11	15	328	4	11
S12	15	327	4	11
S13	15	326	4	11
S14	24	617	7	11
S15	24	616	7	11
S16	24	604	7	11
S17	24	630	7	11
S18	24	704	7	11
S19	24	798	12	11

C.P.U. = Central Processing Unit

TABLE 5.3 NUMBER OF ELEMENTS AND MACHINE TIME FOR EACH ANALYSIS

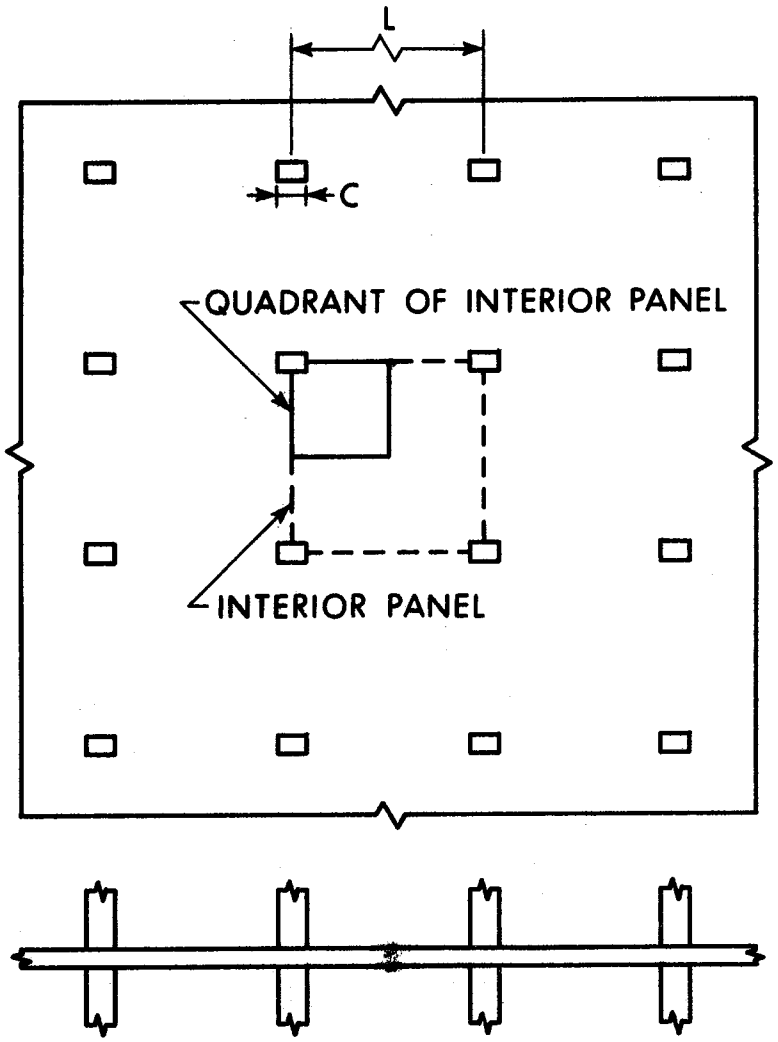

FIGURE 5.1 MULTI PANEL FLOOR SYSTEM CONSISTING OF SQUARE PANELS SUPPORTED ON SQUARE COLUMNS

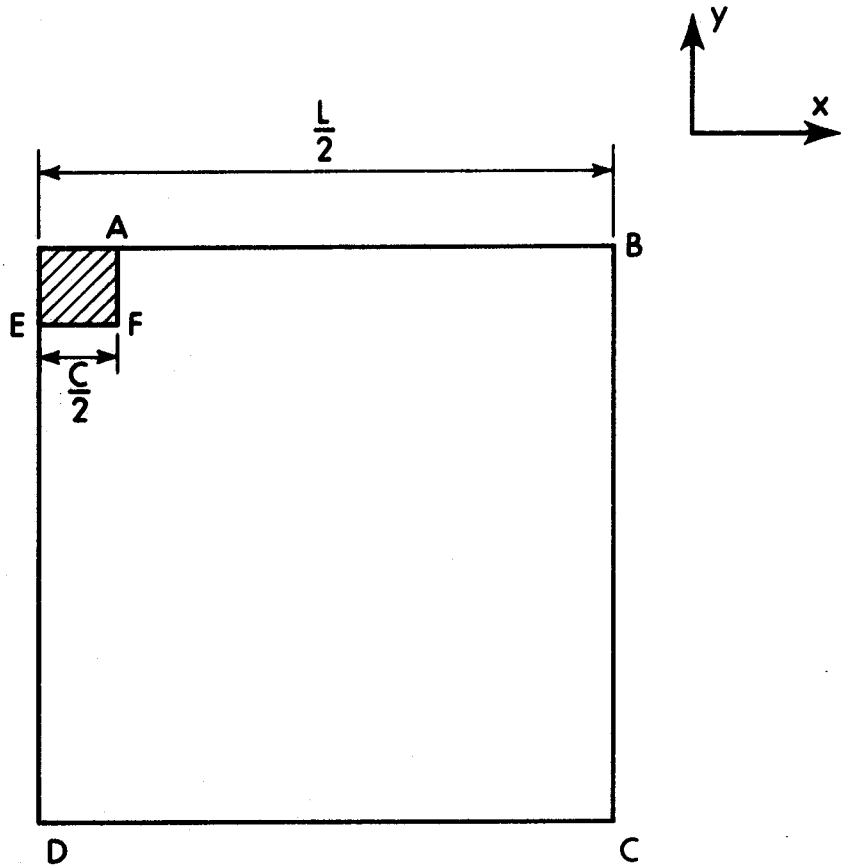

BOUNDARY CONDITIONS:

$$AB,\ DC - \frac{\partial w}{\partial y} = \frac{\partial^2 w}{\partial x\,\partial y} = 0$$

$$ED,\ BC - \frac{\partial w}{\partial x} = \frac{\partial^2 w}{\partial x\,\partial y} = 0$$

$$AF,\ EF - w = \frac{\partial w}{\partial x} = \frac{\partial w}{\partial y} = \frac{\partial^2 w}{\partial x\,\partial y} = 0$$

FIGURE 5.2 BOUNDARY CONDITIONS FOR QUADRANT OF TYPICAL INTERIOR PANEL

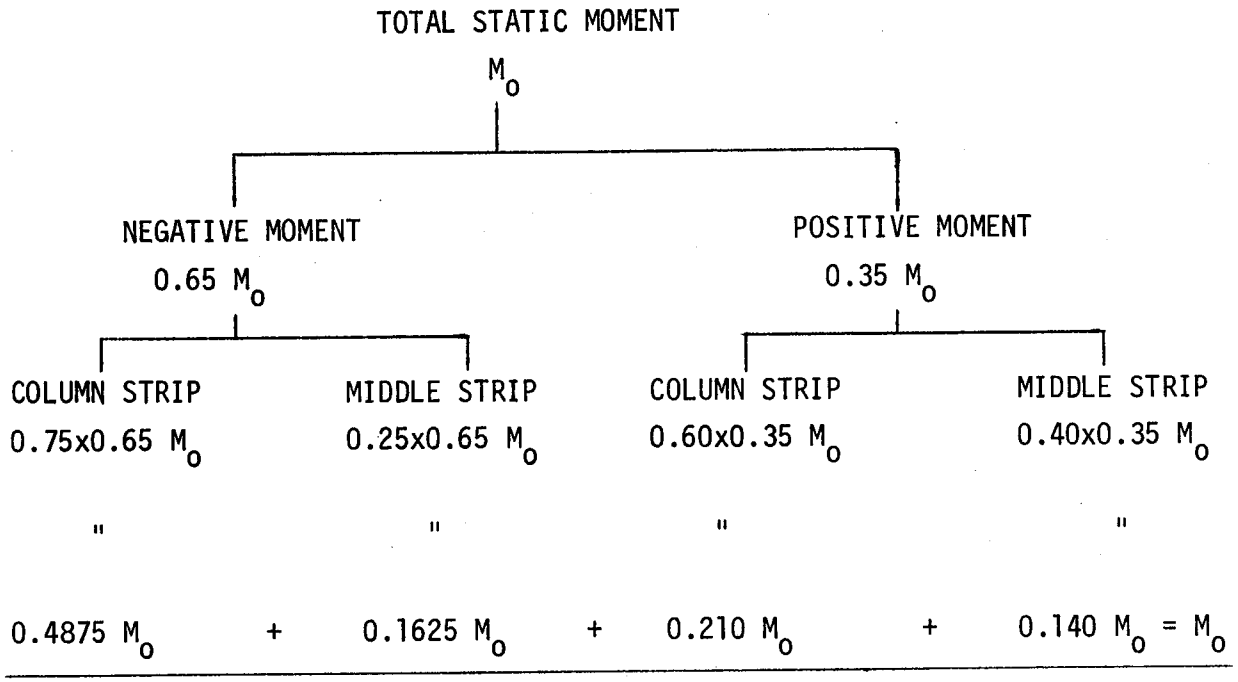

FIGURE 5.3 DISTRIBUTION OF TOTAL STATIC MOMENT IN PANEL

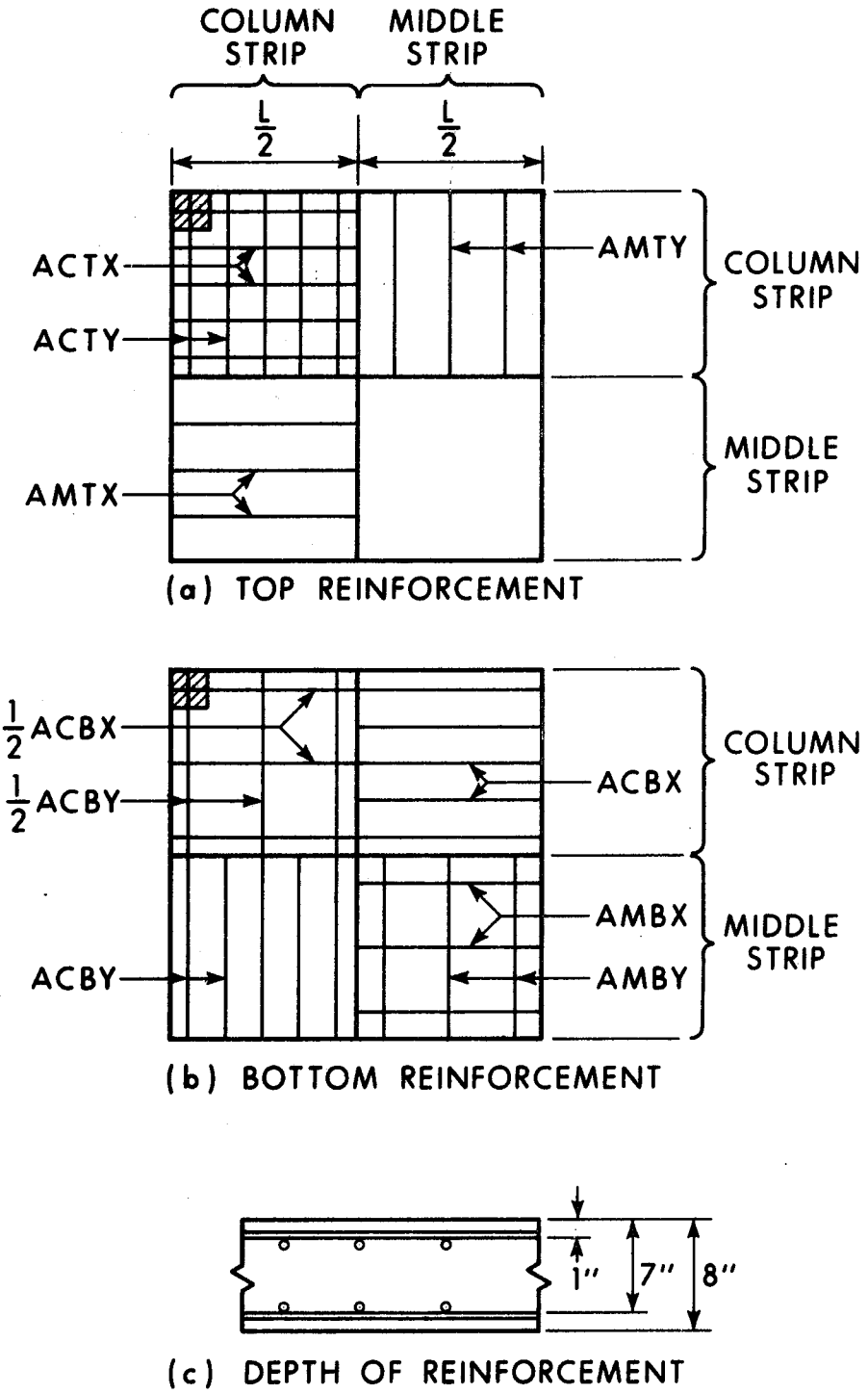

FIGURE 5.4 REINFORCEMENT LAYOUT FOR QUADRANT OF INTERIOR PANEL

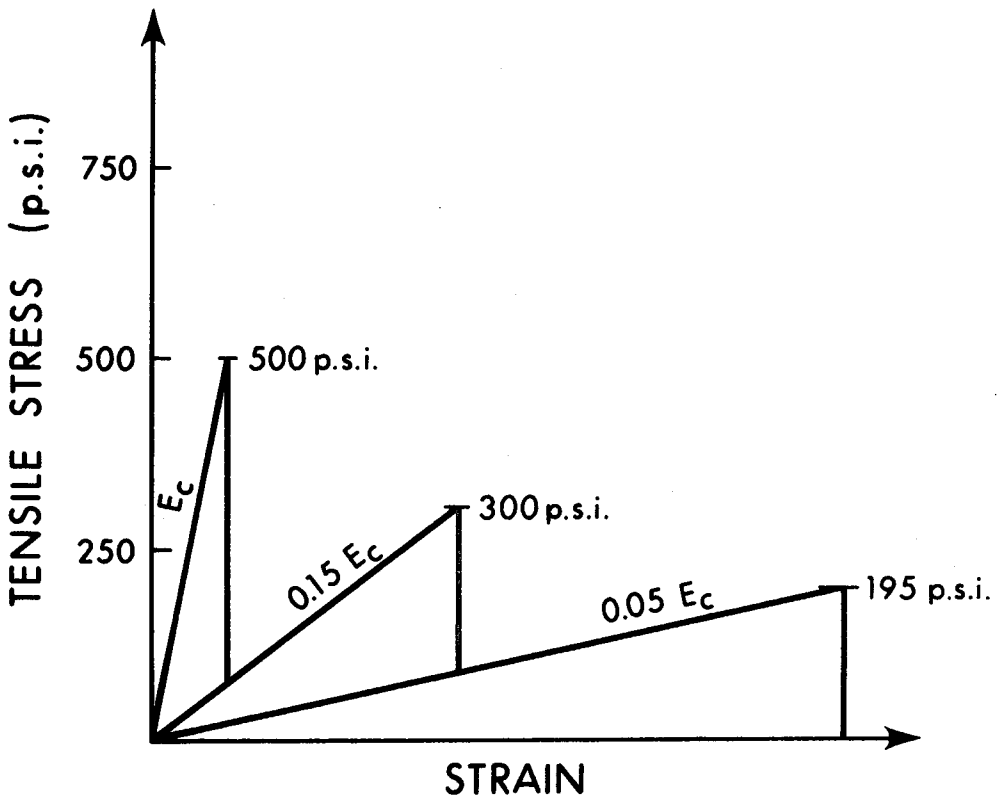

FIGURE 5.5 STEPPED STRESS STRAIN DIAGRAM FOR CONCRETE IN TENSION

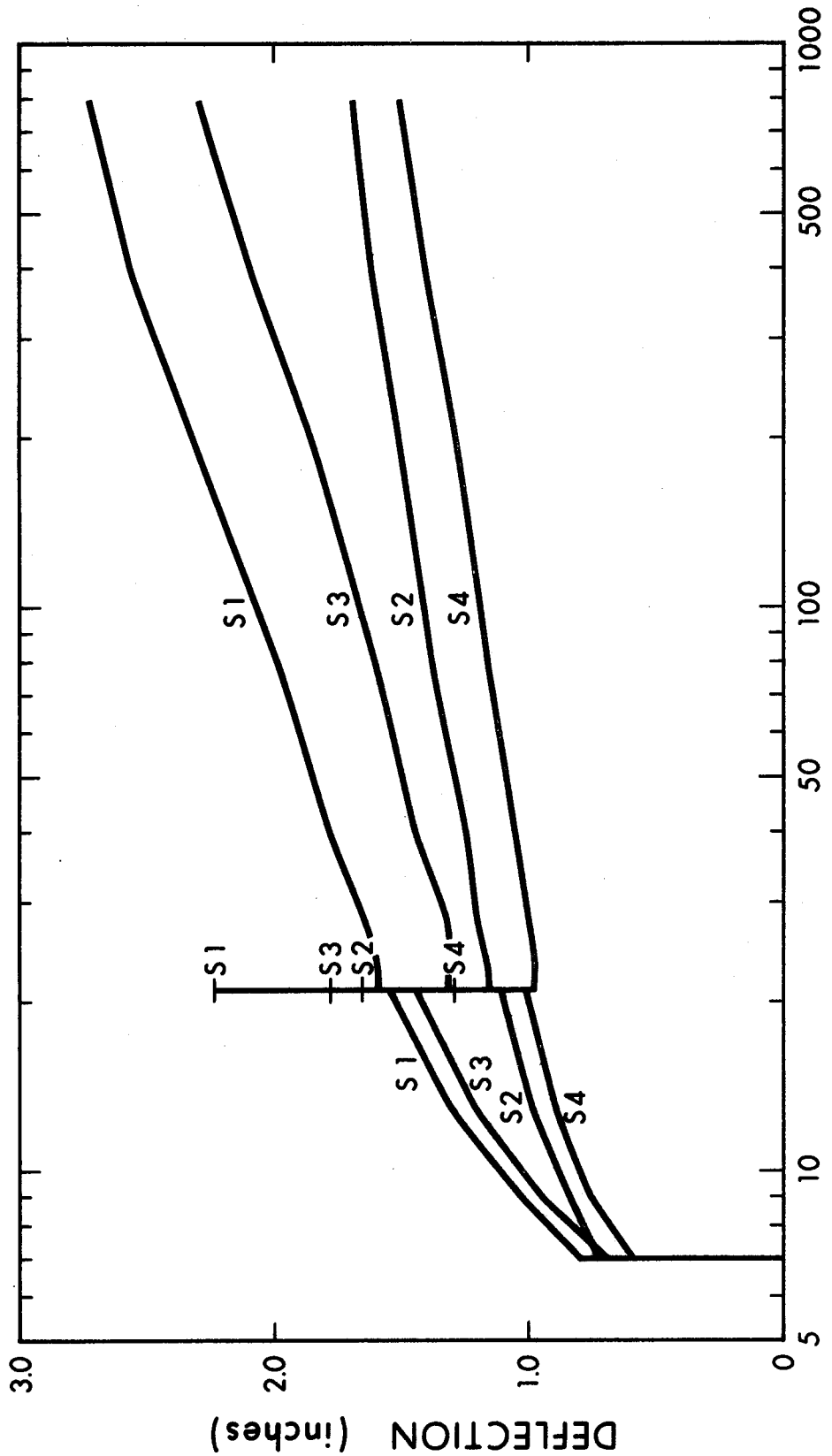

FIGURE 5.6 DEFLECTION TIME CURVES S1, S2, S3, S4

TIME (days)	7	9	13	21	21	21	23	28	40	80	200	400	800
APPLIED LOAD (p.s.f.)	150	150	150	150	200	110	110	110	110	110	110	110	110

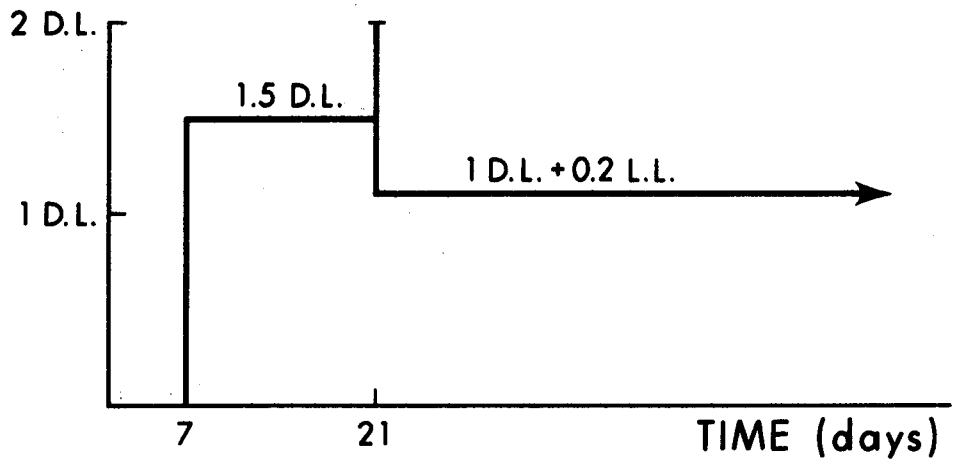

(a) LOADING HISTORY L1

D.L. = 100 p.s.f. L.L. = 50 p.s.f.

TIME (days)	7	7	9	13	21	40	80	160	300	500	800
APPLIED LOAD (p.s.f.)	200	110	110	110	110	110	110	110	110	110	110

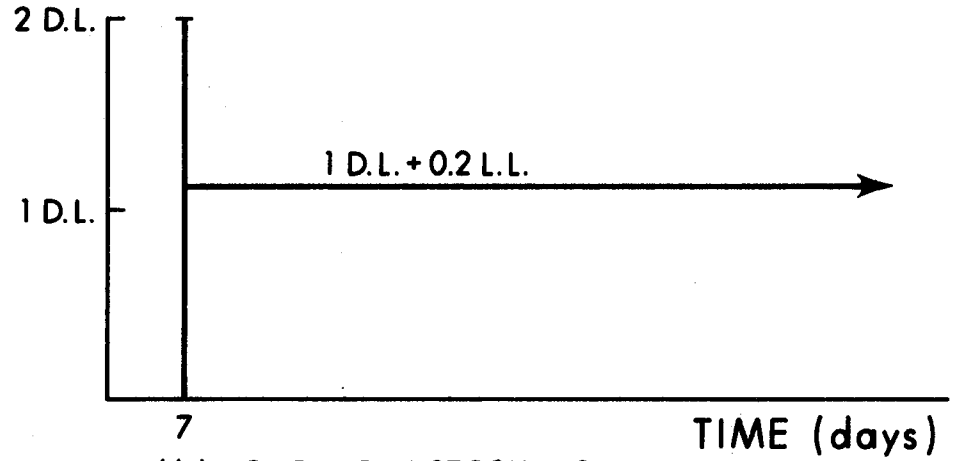

(b) LOADING HISTORY L2

FIGURE 5.7 LOADING HISTORIES L1, L2

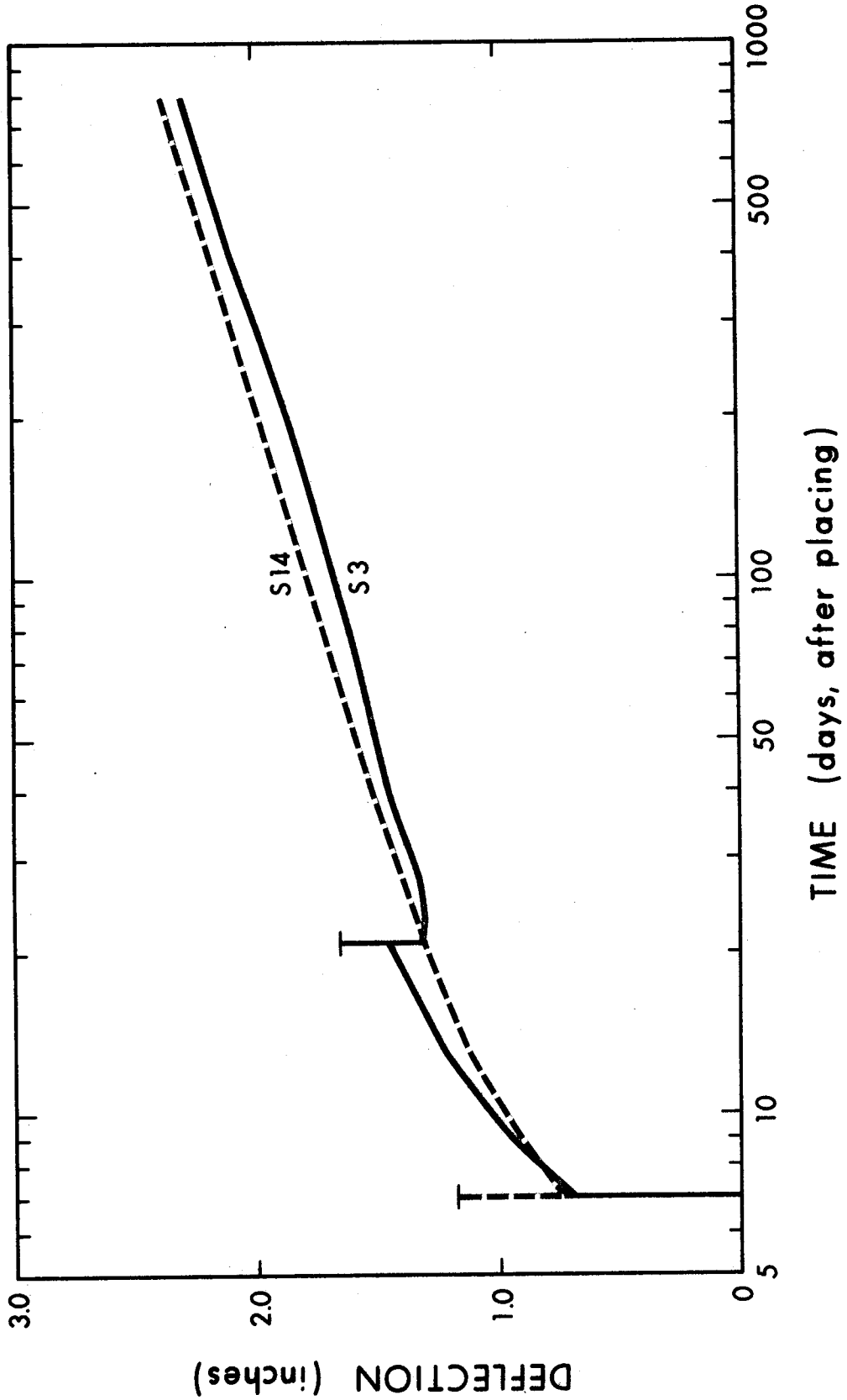

FIGURE 5.8 DEFLECTION-TIME CURVES S3, S14

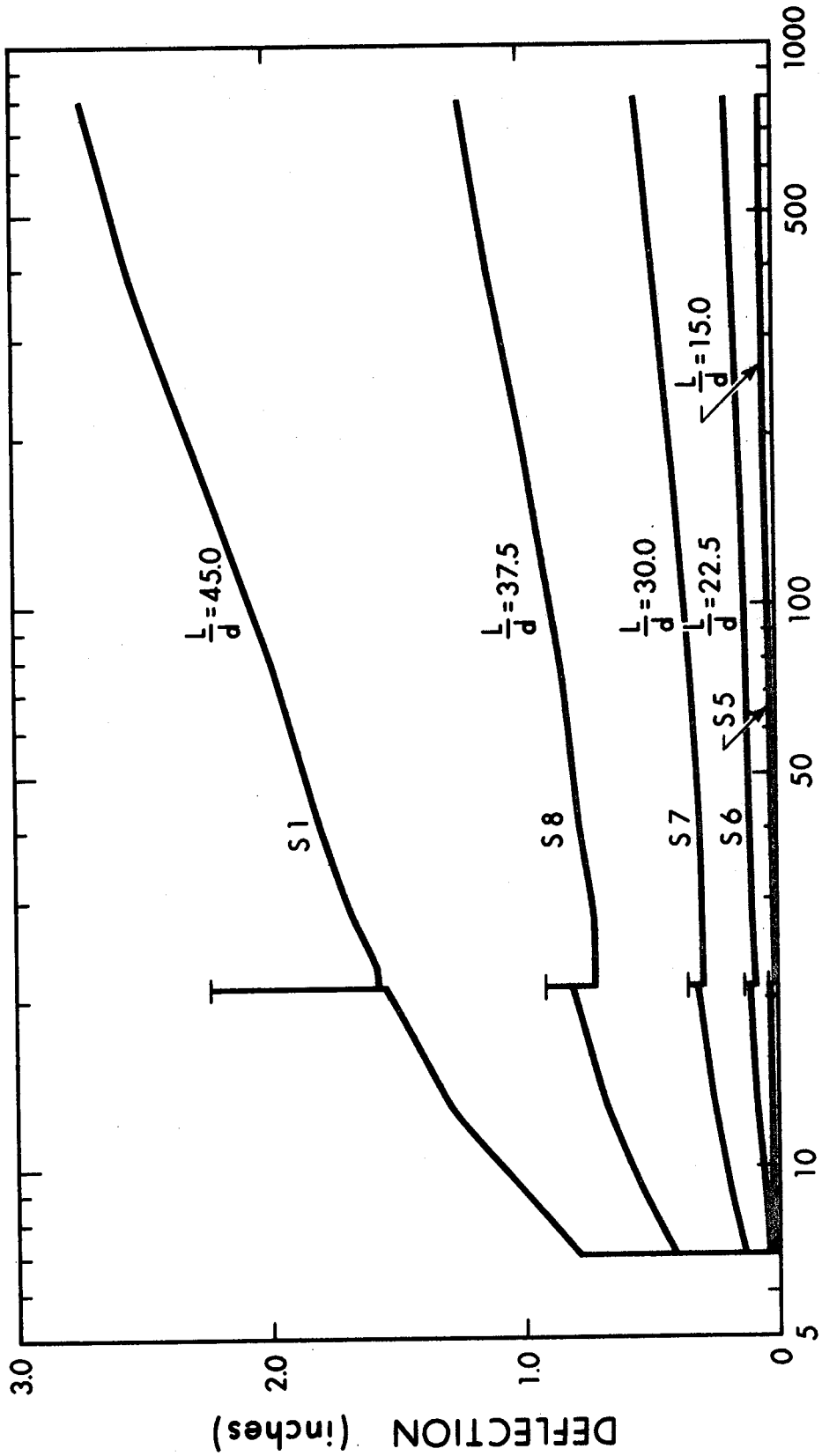

FIGURE 5.9 DEFLECTION-TIME CURVES S5, S6, S7, S8, S1

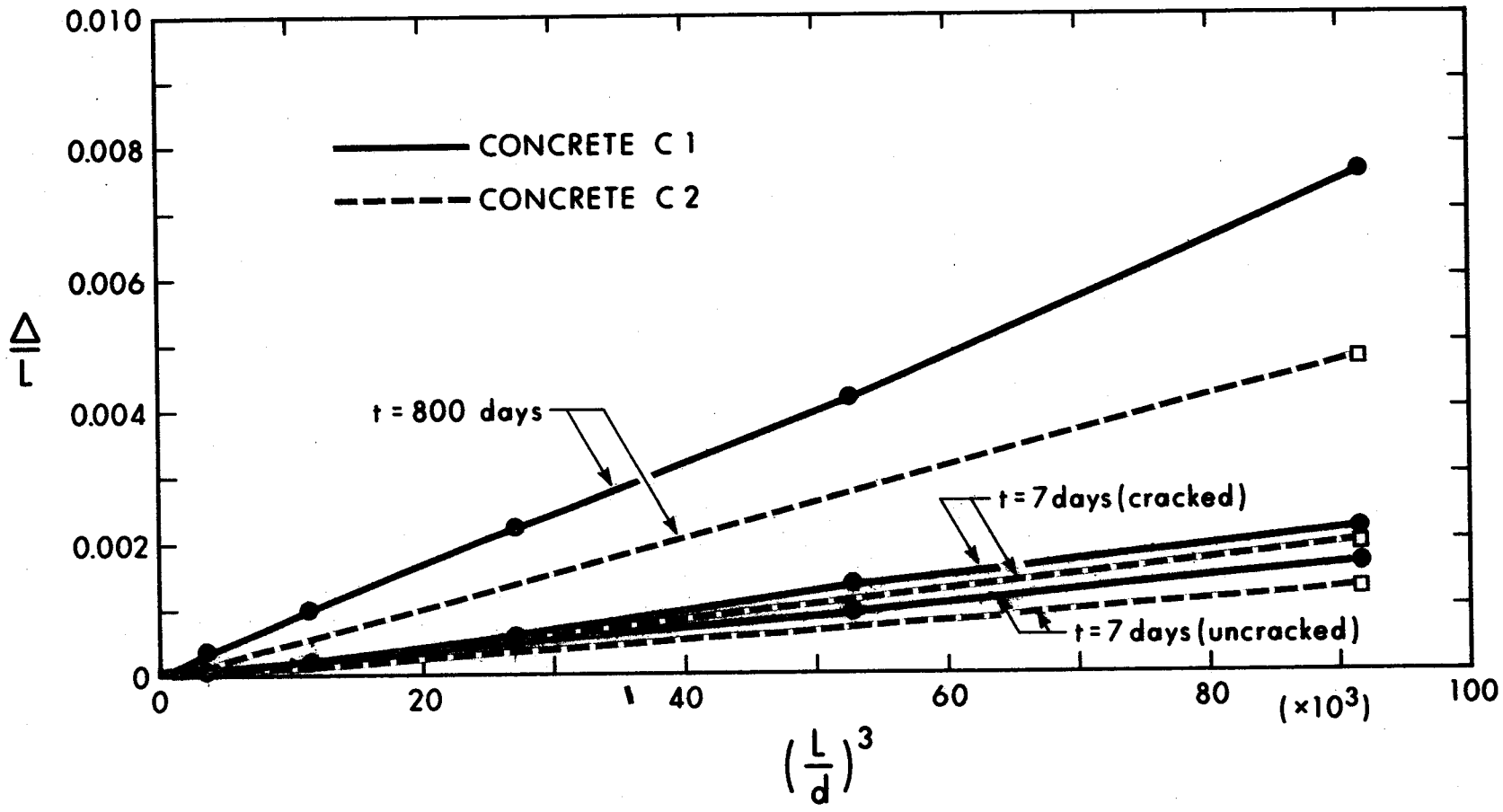

FIGURE 5.10 RELATIONSHIP BETWEEN $\frac{\Delta}{L}$ and $(\frac{L}{d})^3$

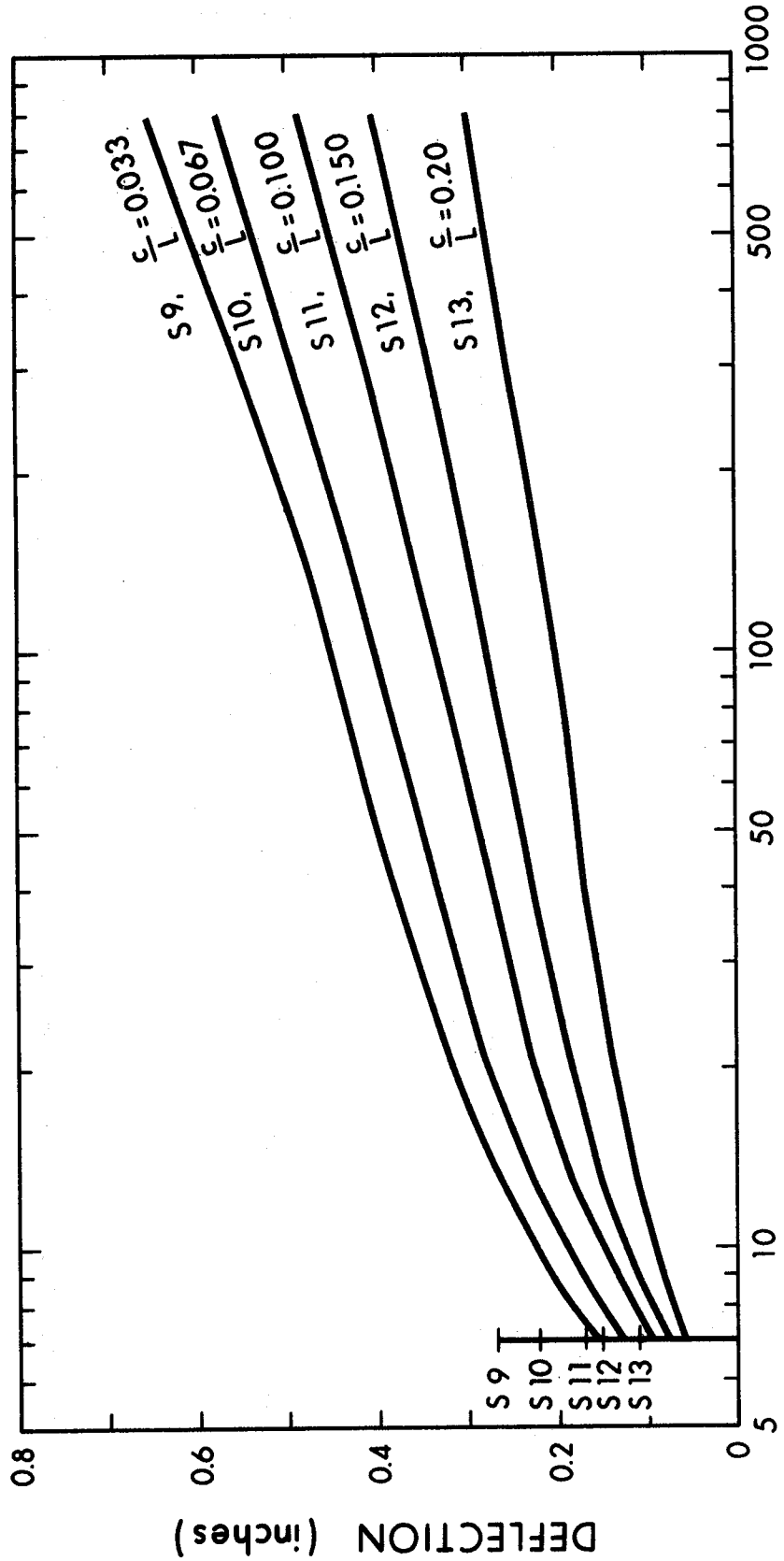

FIGURE 5.11 DEFLECTION-TIME CURVES S9, S10, S11, S12, S13

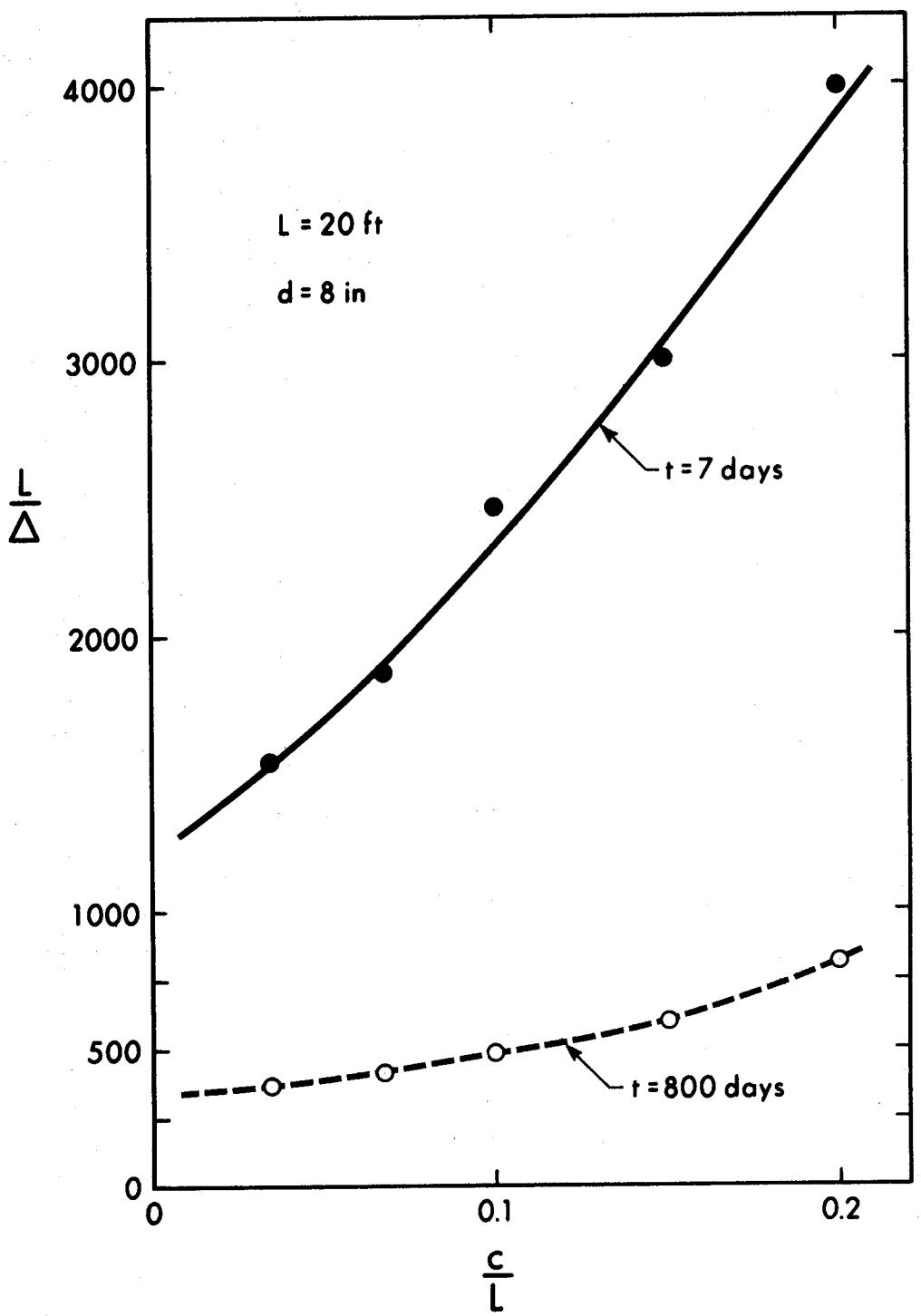

FIGURE 5.12 RELATIONSHIP BETWEEN L/Δ AND c/L

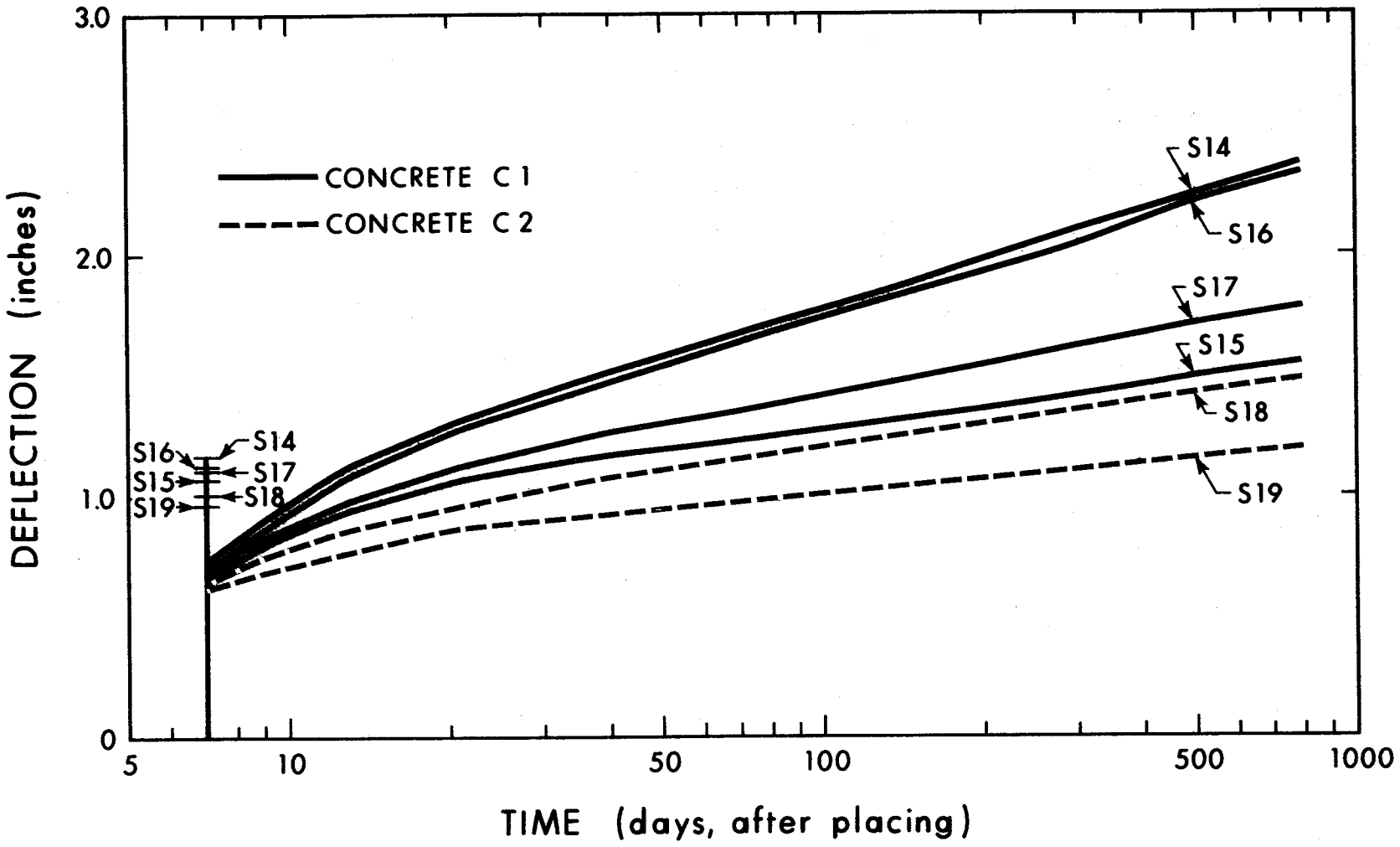

FIGURE 5.13 DEFLECTION-TIME CURVES S14, S15, S16, S17, S18, S19

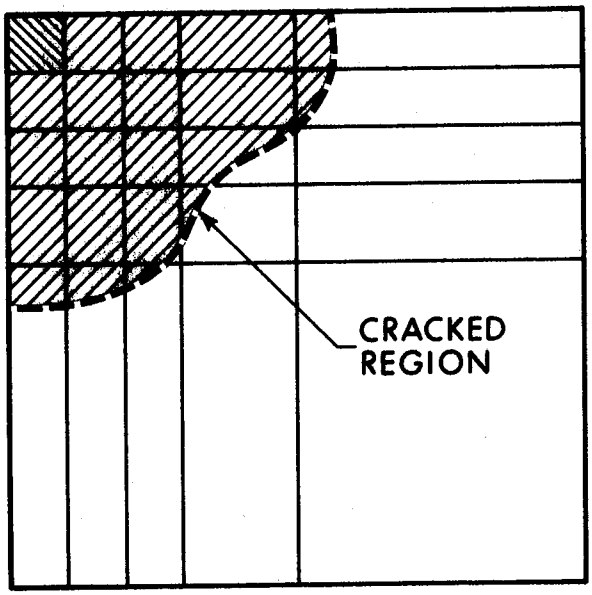

(a) CRACKING ON TOP SURFACE

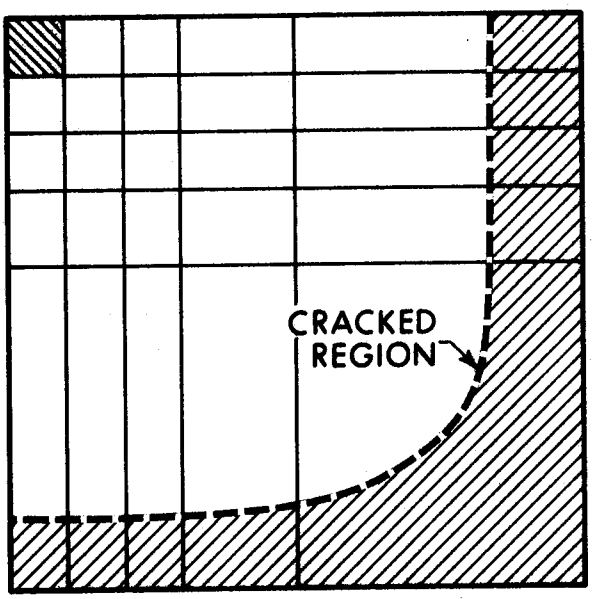

(b) CRACKING ON BOTTOM SURFACE

FIGURE 5.14 CRACKED REGIONS IN SLAB S19

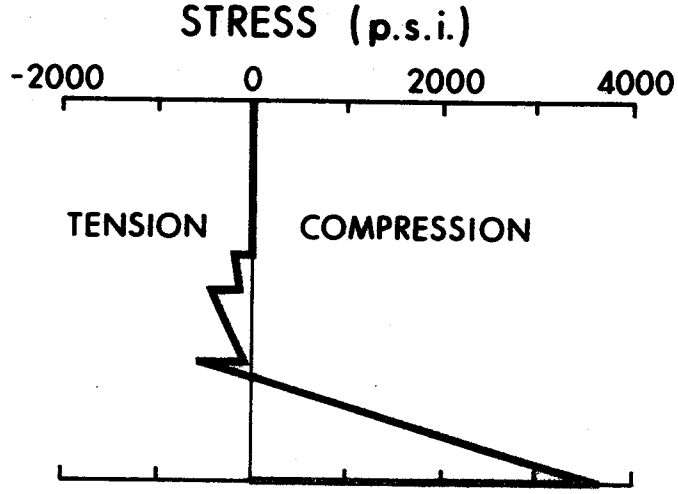

(a) CONCRETE STRESS DISTRIBUTION IN SLAB AT CORNER OF COLUMN

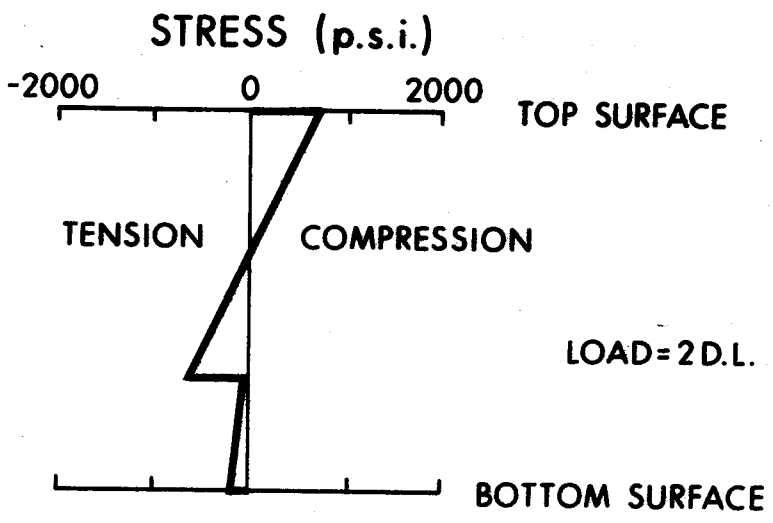

(b) CONCRETE STRESS DISTRIBUTION IN SLAB AT MID-PANEL

FIGURE 5.15 SLAB S19 - STRESS DISTRIBUTIONS

CHAPTER 6

SIMPLIFIED PROCEDURES FOR COMPUTING SLAB DEFLECTIONS

6.1 Introduction

The purpose of this chapter is to examine available simplified procedures for computing deflections of flat plate floor slabs in the light of the results of the brief parameter study described in Chapter 5. The approximate computation of deflections will be considered in three stages,

a) short time deflection of an uncracked slab

b) short time deflection including the effect of cracking

c) long time deflection

6.2 Short Time Deflection of an Uncracked Slab

The deflection of a rectangular, elastic plate under uniform transverse load q may be expressed in the form[47]

$$\Delta = \frac{KqL^4}{D} \qquad (6.1)$$

where $D = \frac{Ed^3}{12(1-\nu^2)}$ represents the plate flexural rigidity and K is a factor which depends on boundary conditions and, in the case of a rectangular plate, on the ratio of long to short span. Poisson's ratio ν, can be seen to have a minor effect on the computation of deflections, since by Equation (6.1) the difference in Δ produced by reducing ν from 0.15 (the value used in the computer analysis), to a value of zero is 2.25%. The plate flexural rigidity D may therefore be replaced, with a small decrease in accuracy by the beam rigidity EI where $I = 1/12\ bd^3$ and b equals unity. Equation (6.1) may then be written as,

$$\Delta = \frac{KqL^4}{EI} \tag{6.2}$$

However, in a reinforced concrete slab the value of I is a function of position since the amount of reinforcement varies throughout the slab.

Elastic plate solutions for a typical interior panel, based on the finite difference approach have been obtained at the University of Illinois and were reported by Vanderbilt, Sozen and Siess[49]. The parameters considered were the c/L ratio, beam to slab stiffness ratio and aspect ratio (short span/long span). The values of K, in Equation (6.1) presented by Vanderbilt for the flat plate (beam stiffness equal to zero), for three c/L ratios, 0.0, 0.1 and 0.2, and four aspect ratios (s/L) 0.4, 0.6, 0.8 and 1.0 are shown in Figure 6.1. An expression for K which fits the plotted points reasonably well is given by Equation (6.3)

$$K = [0.00774(s/L)^2 - 0.00588(s/L) + 0.00395][1-2.5\tfrac{c}{L}] \tag{6.3}$$

which for a square slab (s/L = 1.0) reduces to,

$$K = 0.00581(1-2.5c/L) \tag{6.4}$$

Equation (6.3) is plotted in Figure 6.1 as a set of dashed lines. It should be noted that Equation (6.3) and Equation (6.4) are applicable only for the range of c/L and s/L shown.

In order to illustrate the effect of reinforcement on the deflection of the uncracked slab, values of K were computed by substituting in Equation (6.2),

a) deflections obtained by the present analysis (including reinforcement) on first application of load,

b) the modulus of elasticity used in the analysis in each case, and

c) the gross moment of inertia, $I_g = 1/12 \cdot 1 \cdot d^3$, neglecting steel.

These values of K are tabulated in column 6 of Table 6.1 and are plotted in Figure 6.1. All values are seen to lie below the corresponding line for homogeneous elastic plate deflections indicating the effect of the increased stiffness due to steel. Several slabs were analyzed for a c/L ratio of 0.1 with varying L/d ratios and consequently, varying percentages of reinforcing. The reduction in K obtained, ranged from 7.5% to 22.5% for these slabs. For an 8 inch slab containing 1% tension steel, the increase in moment of inertia due to steel is approximately 15%. If an equal amount of compression steel is included, the increase is approximately 34%.

An effective moment of inertia for each slab, to include the effect of steel was computed by substituting Equation (6.3) for K into Equation (6.2) and using the deflection of the uncracked slab obtained by the present analysis. These values are shown in Table 6.1 as I_{ST}. The average value of I_{ST} computed in this way was 15% greater than the gross moment of inertia $I_g = 42.67$ in^3/in.

While the presence of steel increases the effective moment of inertia of the slab, consideration must be given to cracking which reduces the effective moment of inertia.

6.3 Short-time Deflection Including Cracking

Considerable effort has been directed towards the problem of computing short time deflections of cracked reinforced concrete beams. The problem has generally been considered in two parts,

a) Computation of the stiffness (EI) in a cracked region

and b) Effect of variation of stiffness throughout the member.

Several procedures proposed in the literature have been reviewed in Ref. (4). Of these, a method proposed by Branson has been adopted for use in the 1970 A.C.I. Building Code. Branson's empirical expression for the effective moment of inertia I_{eff} in a cracked region has been discussed in Section 4.3.1. The expression for I_{eff} is given as,

$$I_{eff} = (\frac{M_c}{M})^4 I_g + (1 - (\frac{M_c}{M})^4) I_{cr} \qquad (6.5)$$

To obtain the average value of I_{eff} in a span, Branson recommends that the power 4 be reduced to 3 and M be replaced by M_{max}, the maximum moment in the region. Equation (6.5) is then written as

$$I_{eff} = (\frac{M_c}{M_{max}})^3 I_g + (1 - (\frac{M_c}{M_{max}})^3) I_{cr} \qquad (6.6)$$

which is the expression used in the A.C.I. code.

In Ref. (5) it is suggested that Equation (6.6) also be used in computing deflections for interior panels of slabs using average values of I_{eff} computed in the following manner,

a) flat plates - use the average of the values of I_{eff} computed for the positive and negative moment regions in the long direction column strip,

b) two way slabs - use the average of the values of I_{eff}

computed for the positive and negative moment regions in the short direction middle strip.

Values of I_{eff} computed in this manner for the flat plates considered in the parameter study are shown in Table 6.1. In each case I_{eff} was computed using the design moment from the Direct Design Method of the 1970 A.C.I. code as M_{max}. The ratio $\Delta_{uc}^{(7)}/\Delta_{cr}^{(7)}$ from the present computer analysis is also shown in Table 6.1 for each slab, where $\Delta_{uc}^{(7)}$ represents the deflection at 7 days assuming no cracking and $\Delta_{cr}^{(7)}$ represents the deflection at 7 days allowing for cracking, both deflections obtained at the same load.

Figure 6.2 shows the values of $\frac{\Delta_{uc}^{(7)}}{\Delta_{cr}^{(7)}}$ and $\frac{I_{eff}}{I_g}$ plotted for various c/L ratios. In this series of slabs (S9-S13), cracking occurred only in the vicinity of the columns and it can be seen that computing the average I_{eff} on the basis of the column strip only, underestimates the stiffness of the slab as a whole. Better agreement is obtained with the computer results by using the average I_{eff} computed on the basis of both column and middle strips. As cracking extends into the positive moment region, particularly in the middle strip, the value of I_{eff} computed for the column strip only, tends towards the average value for the slab. This is the case for slabs S14-S19 where the agreement between $\Delta_{uc}^{(7)}/\Delta_{cr}^{(7)}$ and I_{eff}/I_g (where I_{eff} is computed using average values in the column strip only) is better than for the slabs discussed previously.

The correlation between $\Delta_{uc}^{(7)}/\Delta_{cr}^{(7)}$ and I_{eff}/I_g is shown in Figure 6.3 for all the slabs analyzed. In the cases where no tension is assumed in a cracked layer, the computer analysis yields a higher cracked slab deflection than that indicated using Branson's expression

which takes into account the stiffening effect of concrete between cracks. Computing I_{eff} on the basis of both column and middle strips would have the effect of increasing the discrepancy.

The remaining slabs were analyzed on the basis of the stepped stress strain diagram in tension. In cases where no cracking occurred in the positive moment region, the computer analysis produced a smaller deflection than that indicated by I_{eff} based on the column strip only, whereas for those cases in which cracking did occur in the positive moment region, neither procedure consistently produced a higher deflection than the other.

Although the discussion in this section has been based on the gross moment of inertia neglecting steel, the same trend would be shown if I_g were to be replaced by a value of I which included the effect of reinforcing steel, as long as this value was used to compute I_{eff}.

6.4 Long-time Deflection

Simplified procedures have been presented in the literature for the computation of long time deflection of beams. A review of proposed methods is given in Ref. (4). In general these simplified methods involve multiplying the computed short time deflection by a factor to obtain the additional long time deflection. Such an approach has been presented recently in Ref. (5), where the additional long-time deflection Δ_{ti} due to creep and shrinkage effects is given by the following expressions

$$\Delta_{ti} = C_t \Delta_i \tag{6.7}$$

$$\Delta_{ti} = T_t \Delta_i \tag{6.8}$$

where C_t = creep strain/initial strain = creep coefficient and T_t is an empirical factor lumping creep and shrinkage effects together. Equation (6.7) is intended for use when creep and shrinkage effects are considered separately. This expression gives the correct value of creep deflection only when the stress condition in the member remains constant with time, since C_t is defined for constant stress. Due to the interaction between concrete and steel, concrete stresses tend to decrease with time. To account for this, a factor k_r is introduced,

$$k_r = 0.85 - 0.45(A_s'/A_s) \geq 0.40 \qquad (6.9)$$

or

$$k_r = 1.0 - 0.6(A_s'/A_s) \geq 0.40 \qquad (6.10)$$

Equation (6.9) applies to the creep only case while Equation (6.10) applies to the case of creep and shrinkage. Equation (6.7) and Equation (6.8) are then re-written as follows,

$$\Delta_t = k_r C_t \Delta_i \qquad (6.11)$$

$$\Delta_t = k_r T_t \Delta_i \qquad (6.12)$$

The 1970 A.C.I. code recommends Equation (6.12) for computation of long-time deflections with an ultimate value of $T_t = 2.0$, thereby taking no account of variations in material properties.

Ref. (5) recommends that the same method be used for computing long time deflections in two way construction as is used for beams. A limited evaluation of the simplified procedure was made in relation to the results of the computer study.

The creep coefficients (ultimate values) for concretes C1 and C2 used in the parameter study were 3.94 and 2.10 respectively. The

factor k_r was computed from Equation (6.9) for each slab. The quantity $k_r C_u$ (C_u = ultimate value of C_t) is shown in Table 6.1 for each slab. Each of the analyses carried out for the parameter study involved both creep and shrinkage effects. No attempt however has been made to evaluate the additional deflection due to shrinkage curvature by simplified procedures. From the computer results the quantity $\frac{\Delta_t}{\Delta_i} = \frac{\Delta^{(800)} - \Delta^{(7)}}{\Delta^{(7)}}$ has been computed where $\Delta^{(800)}$ represents the deflection at 800 days (taken as ultimate deflection here) and $\Delta^{(7)}$ represents the deflection at 7 days (including the effect of any cracking which takes place). In the case of loading history L2 the deflection considered at 7 days is that due to a load of 1 D.L. + 0.2 L.L.

The correlation between $k_r C_u$ and $\frac{\Delta_t}{\Delta_i}$ is shown in Figure 6.4. The slabs analyzed by loading history L1 are represented by circles in Figure 6.4. For these cases the comparison between computer results and simplified procedure is not strictly valid since the simplified procedure is intended to be used with a constant sustained load whereas the load varies with time for loading history L1. However, these results are included since it was shown in Chapter 5 that the variation in loading between L1 and L2 had a relatively small effect on the deflections. Since shrinkage curvature was not included in the computation by the simplified approach it would be expected that the computer results would yield a greater long time deflection. It can be seen from Figure 6.4 that this is not always the case and no consistent trend appears to be evident. Of the eleven analyses carried out using a constant sustained load, the simplified computation agreed with the computer result within 20% in seven cases, within 25% in ten cases and for the remaining case the discrepancy was slightly over 25%.

For a complete assessment of the simplified approach, further studies are required. However, if the present analysis is considered reliable, it is apparent that further improvements are required to the simplified approach before it may be considered reliable. In particular, the factor k_r should be considered carefully. The primary purpose of k_r is to account for the effect of compression reinforcement in reducing creep deflections and to a lesser extent for the movement of the neutral axis with time at a cracked cross-section. If no cracking occurs at a section, the tension reinforcement has exactly the same effect as compressive reinforcement in restraining creep deflections (assuming tensile and compressive response to be the same for concrete). Stress is gradually transferred from concrete to steel with time whereas when a crack occurs, the stress is immediately transferred to the steel. It would appear therefore that in the computation of long time deflection in terms of initial deflection, some factor should be introduced to account for the degree of cracking.

6.5 Summary

In this chapter the results of the computer analysis have been compared with available simplified procedures for computing slab deflections where cracking, creep and shrinkage take place. In addition, the effect of reinforcing steel on the overall stiffness of the uncracked slab has been examined. Although the evaluation of the simplified procedures was somewhat limited in nature, certain inadequacies of the current state of the art were brought to light. Suggestions are made in the next chapter for further studies directed at a more complete evaluation of the simplified procedures. It should

be noted however that for many practical situations, the agreement obtained between the computer results and simplified procedures would be considered adequate.

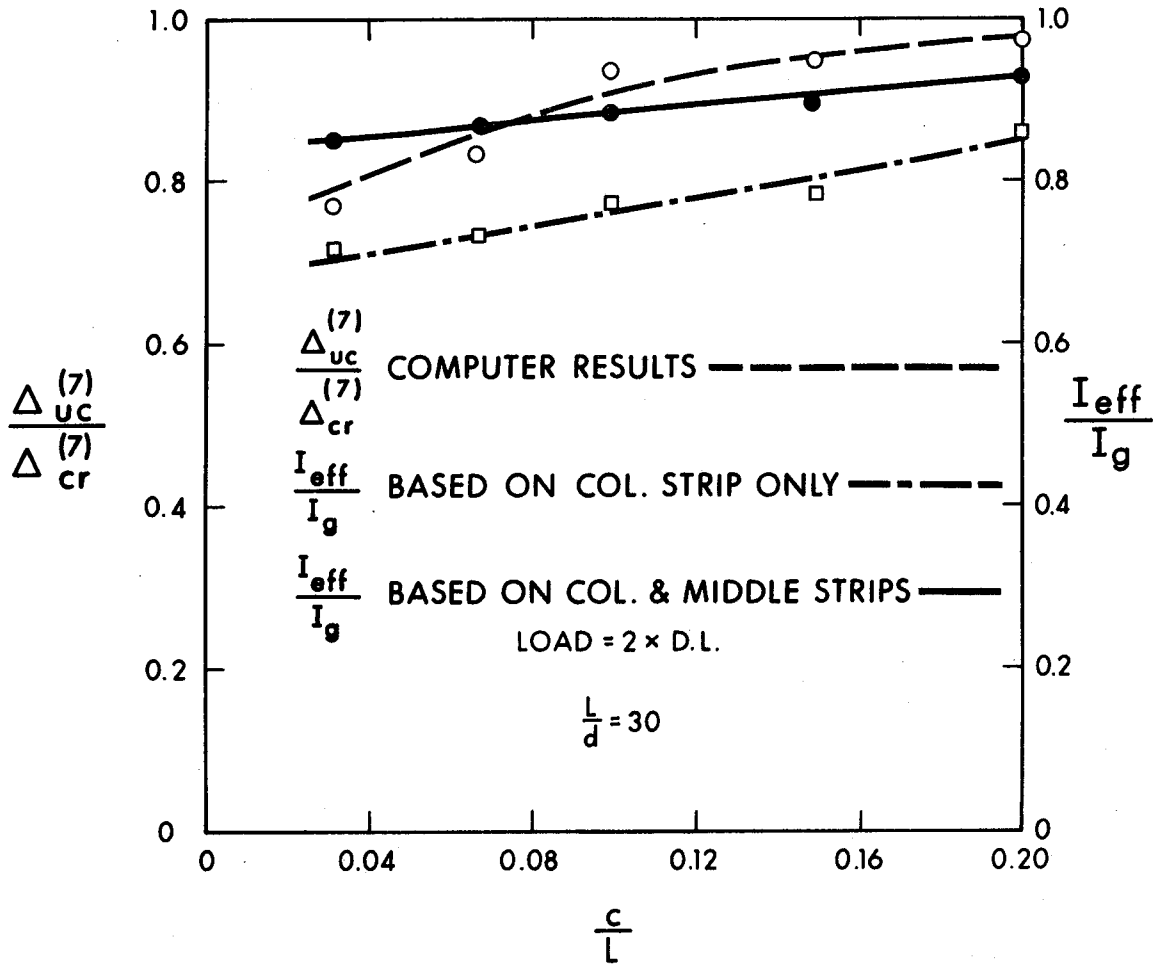

FIGURE 6.2 COMPARISON BETWEEN COMPUTER ANALYSIS AND SIMPLIFIED PROCEDURES FOR CRACKING

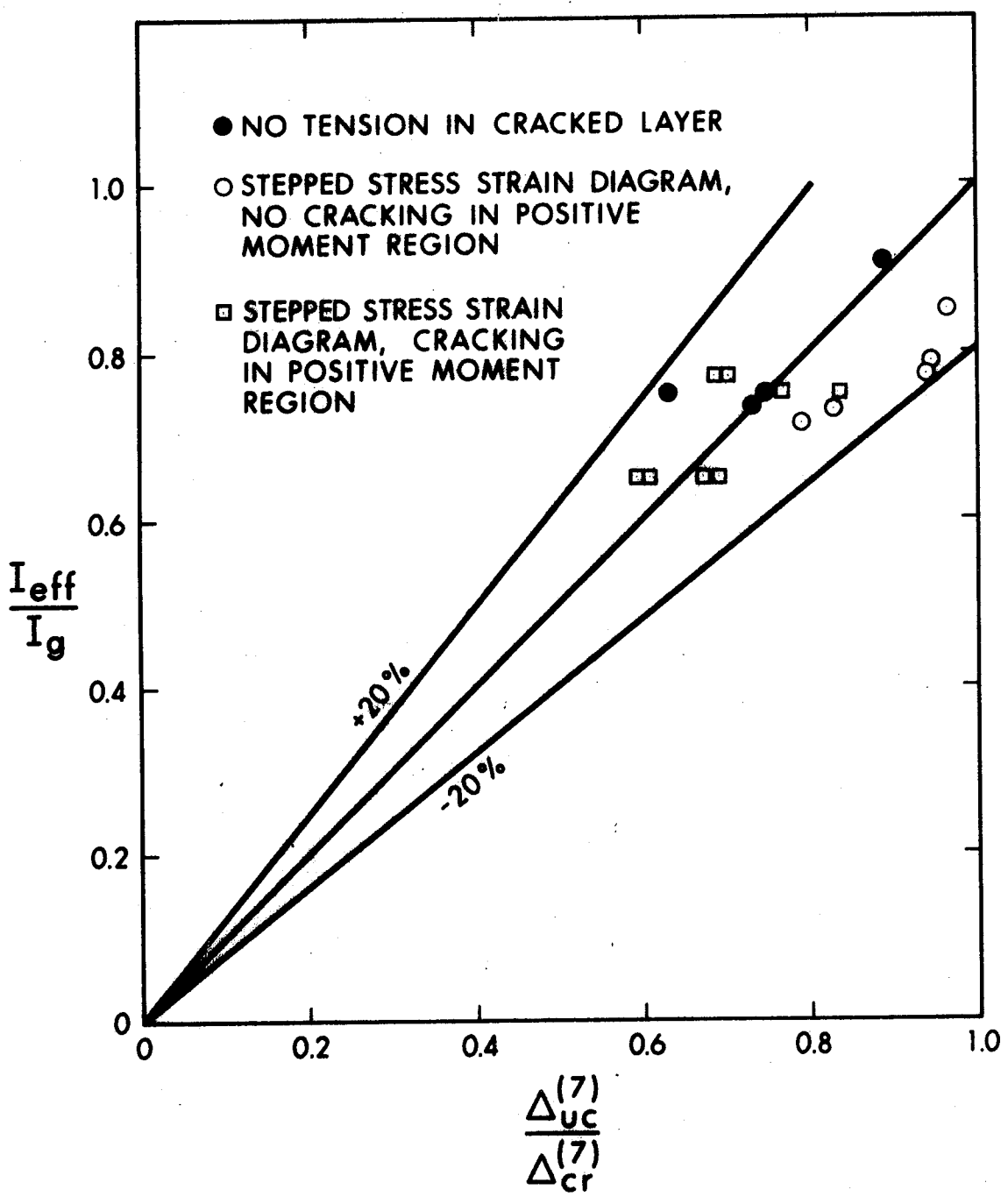

FIGURE 6.3 COMPARISON BETWEEN COMPUTER ANALYSIS AND BRANSON'S METHOD FOR DEFLECTIONS OF CRACKED SLABS

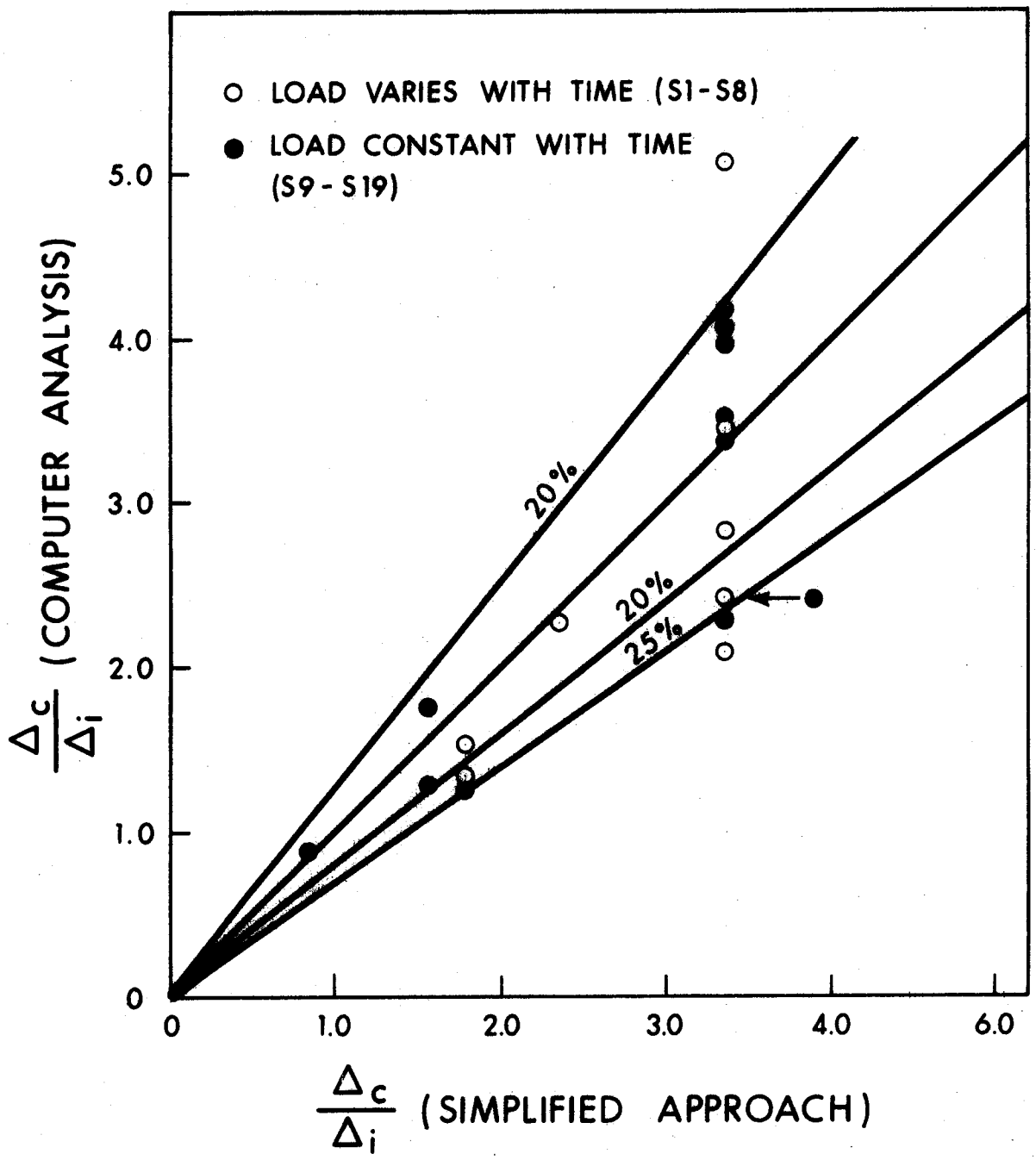

FIGURE 6.4 COMPARISON BETWEEN COMPUTER ANALYSIS AND SIMPLIFIED PROCEDURE FOR LONG TIME DEFLECTIONS

CHAPTER 7

SUMMARY, CONCLUSIONS AND RECOMMENDATIONS

7.1 Summary

A finite element approach to the analysis of reinforced concrete floor slabs has been presented which includes the effects of cracking and time-dependent strains.

The analysis for cracking involves an iterative procedure in which the slab is initially considered to be in an uncracked state. The slab is treated as a layered plate and principal stresses are computed for each layer throughout the slab. Principal tensile stresses are compared with a specified limiting tensile stress and if the limiting stress is exceeded, the constitutive relations for the layer are modified to reflect the reduced stiffness due to cracking. The analysis is repeated until a stage is reached when no further cracking is detected.

In under-reinforced sections, concrete between cracks may have an important effect on the stiffness of the member. To account for this, the concept of a stepped stress-strain diagram for tensile stresses was introduced, in which the modulus of elasticity for concrete in tension is reduced in a step-wise fashion as cracking proceeds. In effect, the tensile stress strain diagram for concrete is assumed to have an unloading portion instead of the brittle type of failure normally attributed to concrete in tension. The moment curvature diagram for a section obtained on this basis was compared with an empirical expression based on experimental data.

An incremental procedure with respect to time is used to

trace the stress and strain history for a given applied load history. Concrete is treated as an ageing linear visco-elastic material and steel as a linear elastic material. At each increment in time a complete analysis is carried out using the initial strain method in which a set of equivalent loads accounts for the effects of inelastic strains.

A limited verification of the mathematical model was obtained in applications to problems for which classical or experimental results were available. The model was then applied in a parameter study of a number of factors which affect deflections of flat plate floor slabs.

A brief comparison with available simplified procedures for the computation of short and long time deflections was carried out, based on the results of the parameter study.

7.2 Conclusions

The mathematical model developed in this dissertation is capable of providing useful information related to the problem of time-dependent deformations of reinforced concrete floor slabs. Although a large number of simplifying assumptions have been introduced, the model has produced reasonable correlation with available experimental data.

From the results of the parameter study on flat plate floor slabs, the following points are worth noting.

1. The primary consideration in terms of short time deflections is the slenderness (L/d) ratio. Not only do deflections increase rapidly with this factor in the uncracked state, but for a given loading, concrete stresses also increase rapidly leading to increased cracking and reduced stiffness (see Figure 5.10).

2. The column width to span (c/L) ratio is also important. An increase in this factor from 0.0 to 0.2 results in a reduction in deflection of approximately 50% for the uncracked slab (Figure 6.1). In addition, as the column width decreases, the clear span increases, leading to increased cracking, particularly around the columns.

3. The results of the parameter study underline the need to consider the creep and shrinkage characteristics of the concrete when evaluating long time deflections.

4. The effect of reinforcement in restraining creep and shrinkage deformation has been evaluated. It is generally well known that compression reinforcement has a beneficial effect in reducing long time deflections. In an uncracked section, the tensile reinforcement has the same effect (assuming creep behaviour to be the same in both tension and compression) leading to a gradual transferral of stress from concrete to steel. The restraint to creep deformation depends on the amount of steel present, in that, for small reinforcement ratios there is less restraint available. This will generally lead to larger creep deflections relative to instantaneous deflections for lightly reinforced sections.

The limited comparison of results obtained by the computer analysis with those from simplified calculation procedures indicates that reasonable results may be obtained using the simplified procedures but that the procedures are not sufficiently developed to reliably predict long term deflections of slabs. Further studies are required for a complete assessment of such procedures.

7.3 Recommendations for Future Studies

In terms of the analytical model it may be desirable to examine the following areas in more detail.

a) The constitutive relations have been specialized for the case of orthotropy in the global coordinate system. The effect of considering cracks oriented perpendicular to the principal tensile stress directions could be studied as well as arbitrary steel layouts.

b) By introducing additional in-plane degrees of freedom in the analysis the effect of restraint to shrinkage deformations at the boundaries, as well as T-beam action could be studied. This will however increase the number of degrees of freedom by fifty percent. The analysis may be extended to include the interaction of beam and column elements which would be useful for further parameter studies. These studies could be carried out with a view to producing design charts suitable for use in engineering practice.

Further parameter studies should also be aimed at assessing the effects of,

a) misplacement of reinforcement.

b) designs based on various ratios of live to dead load.

c) separation of creep and shrinkage effects.

d) development of simplified procedures.

e) deflections in edge and corner spans.

Item (d) is an important consideration since the type of analysis developed in this work requires a large amount of computer time. Particular attention should be paid to the computation of long-time deflection as a multiple of short-time deflection by the procedures discussed in Chapter 6. The present method of analysis may be used to evaluate creep and shrinkage effects separately or together

for this purpose.

The factor k_r of Equation (6.11) and (6.12) may be examined for variations in creep and shrinkage characteristics, tension and compression reinforcement and degree of cracking. Such studies should first be made for beams before considering two-way construction.

LIST OF REFERENCES

1. Ali, I. and Kesler, C.E., "Rheology of Concrete - A Review of Research", University of Illinois, Engineering Exptl. Station Bull. #476, March 1965.

2. American Concrete Institute Committee 318, "Building Code Requirements for Reinforced Concrete (A.C.I. 318-63)", American Concrete Institute, Detroit, Michigan, 1963.

3. American Concrete Institute Committee 318, "Building Code Requirements for Reinforced Concrete (A.C.I. 318-71)", A.C.I. Journal, Proc. V. 67, Nr. 2, Feb., 1970.

4. American Concrete Institute Committee 435, "Deflection of Reinforced Concrete Flexural Members", Proc. A.C.I., V. 63, June 1966.

5. American Concrete Institute Sub-committee II, Committee 209, "Creep, Shrinkage and Temperature Effects in the Design of Concrete Structures", Annual Convention, A.C.I., New York, April, 1970.

6. Argyris, J.H., "Continua and Discontinua", Conf. on Matrix Methods in Structural Mechanics", Wright-Patterson Air Force Base, 1965.

7. Arutyunyan, N.K., "Some Problems in the Theory of Creep", Pergamon Press, 1966.

8. Ashton, J.E., and Whitney, J.M., "Theory of Laminated Plates", Technomic Publishing Co., 1970.

9. Beeby, A.W., "Short-term Deformations of Reinforced Concrete Members", Technical Report #TRA408, Cement and Concrete Association, London, March, 1968.

10. Bogner, F.K., Fox, R.L. and Schmit, L.A. "The Generation of Inter-element Compatible Stiffness and Mass Matrices by the Use of Interpolation Formulas", Conf. on Matrix Methods in Structural Mechanics, Wright-Patterson Air Force Base, 1965.

11. Branson, D.E., "Instantaneous and Time-dependent Deflections of Simple and Continuous Reinforced Concrete Beams", Alabama Highway Research Report #7, Bureau of Public Roads, August, 1963.

12. Bresler, B., Helmich, D. and Ramakrishna, L.V. "Non-uniform Drying Shrinkage in Reinforced Concrete", I.A.B.S.E., Symposium, Madrid, 1970.

13. Cardenas, A.E. and Kaar, P.H., "Field Test of a Flat Plate Structure", Technical Report, Portland Cement Association.

14. Cheung, Y.K., King, I.P. and Zienkiewicz, O.C., "Slab Bridges with Arbitrary Shape and Support Conditions: A General Method of Analysis Based on Finite Elements", Proc., I.C.E., V. 40, May, 1968.

15. Duke, C.M. and Davis, H.E., "Some Properties of Concrete Under Sustained Combined Stress", Proc. A.S.T.M., V. 44, 1944, pp 888-896.

16. Felippa, C.A., "Refined Finite Element Analysis of Linear and Non-Linear Two-Dimensional Structures", Ph.D. Thesis, University of California (Berkeley), 1966.

17. Gallagher, R.H., "Analysis of Plate and Shell Structures", Symposium on Application of Finite Element Methods in Civil Engineering, A.S.C.E., 1969.

18. Gamble, W.L., Sozen, M.A. and Siess, C.P.,"Measured and Theoretical Bending Moments in Reinforced Concrete Floor Slabs", Civil Engineering Studies, Structural Research Series, Nr. 246, Univ. of Illinois, Urbana, June 1962.

19. Ghali, A., Dilger, W. and Neville, A.M., "Time-dependent Forces Induced by Settlement of Supports in Continuous Reinforced Concrete Beams", A.C.I. Journal, Proc., V. 66, No. 11, Nov., 1969.

20. Glucklick, J., "Fracture of Plane Concrete", A.S.C.E. Eng. Mechanics iv., Dec., 1963.

21. Gopalakrishnan, K.S., Neville, A.M. and Ghali, A., "Creep Poisson's Ratio of Concrete under Multi-axial Compression", A.C.I. Journal, Proc., V. 66, No. 12, Dec., 1969.

22. Goto, Y., "Cracks Formed in Concrete Around Deformed Tension Bars", A.C.I. Journal, Proc., V. 68, No. 4, April 1971.

23. Grundy, P. and Kabaila, A., "Construction Loads on Slabs with Shored Formwork in Multi-Storey Buildings", A.C.I. Proc., Dec. 1963.

24. Hamming, R.W., "Numerical Methods for Scientists and Engineers", McGraw-Hill, 1962.

25. Hansen, T.C., "Creep and Stress Relaxation of Concrete", Proc., Swedish Concrete and Research Institute, Stockholm, 1960.

26. Harris, H.G. and Pifko, A.B., "Elastic Plastic Buckling of Stiffened Rectangular Plates", Symposium on Application of Finite Element Methods in Civil Engineering", A.S.C.E., 1969.

27. Jofriet, J.C. and McNeice, G.M., "Finite Element Analysis of Reinforced Concrete Slabs with Progressive Cracking", Struct. Division, A.S.C.E., March, 1971.

28. Johnson, A.I., "The Determination of the Design Factor for Reinforced Concrete Structures", Proc., Symposium on the Strength of Concrete Structures, Cement and Concrete Association, London, 1956.

29. Khojasteh-Bakht, M., "Analysis of Elastic-Plastic Shells of Revolution Under Axi-symmetric Loading by the Finite Element Method", Ph.D. Thesis, University of California (Berkeley), 1967.

30. King, I.P., "Finite Element Analysis of Two-Dimensional Time-Dependent Stress Problems", Ph.D. Thesis, University of California (Berkeley), 1965.

31. Kupfer, H., Hilsdorf, H.K. and Rusch, H., "Behaviour of Concrete Under Biaxial Stresses" , A.C.I. Journal, Proc., V. 66, No. 8, Aug., 1969.

32. Lekhnitskii, S., "Anisotropic Plates", Gordon and Breach, New York, 1968.

33. Lenschow, R. and Sozen, M.Z., "A Yield Criterion for Reinforced Concrete under Biaxial Moments and Forces", Civil Engineering Studies, Structural Research Series, Nr 311, University of Illinois, Urbana, July, 1966.

34. Lin, T.H., "Theory of Inelastic Structures", Wiley, New York, 1968.

35. Manuel, R.F. and MacGregor, J.G., "Analysis of Restrained Reinforced Concrete Columns under Sustained Load", A.C.I. Journal, No. 1, Jan., 1967.

36. Mayer, H. and Rusch, H., "Building Damage Caused by Deflection of Reinforced Concrete Building Components", Technical Translation 1412, National Research Council, Ottawa, from Deutscher Auschussfur Stahlbeton Heft 193, Berlin, 1967.

37. McHenry, D., "A New Aspect of Creep in Concrete and its Application to Design", Proc., A.S.T.M., V. 43, 1943.

38. McIntosh, J.D., "Concrete Mix Design", Cement and Concrete Association, 1966.

39. McNeice, G.M., "Elastic-Plastic Bending of Plates and Slabs by the Finite Element Method", Ph.D. Thesis, University of London, England, Nov., 1967.

40. Morley, C.T., "Experiments on the Distortion of Steel Bars Across Cracks in Reinforced Concrete Slabs", Mag. of Concrete Research 18, March, 1966.

41. Nawy, E.G., "Crack Control in Reinforced Concrete Structures", A.C.I. Journal, Proc., V. 65, No. 10, Oct., 1968.

42. Przemieniecki, J.S., "Theory of Matrix Structural Analysis", McGraw-Hill, 1968.

43. Recommendations pratiques unifiées pour le calcul et l'execution des ouvrages en beton armé, Comité Européen du Béton, Paris, 1964.

44. Ross, A.D., "Creep of Concrete under Variable Stress", Proc. A.C.I., V. 54, 1958.

45. Sandhu, R.S., Wilson, E.L. and Raphael, J.M., "Two Dimensional Stress Analysis with Incremental Construction and Creep", S.E.S.M. Rep. 67-34, University of California, Berkeley, 1967.

46. Selna, L.G., "Time-dependent Behaviour of Reinforced Concrete Structures", S.E.S.M. Rep. 67-19, University of California, (Berkeley), 1967.

47. Timoshenko, S. and Woinowsky-Krieger, S., "Theory of Plates and Shells", McGraw-Hill, 1959.

48. Troxell, G.E., Raphael, J.M. and Davis, R.E., "Long-time Creep and Shrinkage Tests of Plane and Reinforced Concrete", Proc., A.S.T.M., V. 58, 1958.

49. Vanderbilt, M.D., Sozen, M.A. and Siess, C.P.,"Deflections of Multiple-Panel Reinforced Concrete Floor Slabs", Proc. A.S.C.E., Struct. Division, V. 91, Aug., 1965.

50. Walker, S. and Bloem, D.L., "Studies of Flexural Strength of Concrete-Part 3: Effects of Variations in Testing Procedures", A.S.T.M., Proc., V. 57, 1957, p 1122.

51. Washa, G.M. and Fluck, P.G., "The Effect of Compression Reinforcement on the Plastic Flow of Reinforced Concrete Beams", Proc. A.C.I., V. 49, 1952.

52. Woinowsky-Krieger, S., "Bending of a Flat Slab Supported by Square Shaped Columns and Clamped", Journal of Applied Mechanics, A.S.M.E., V. 21, 1954.

53. Zienkiewicz, O.C. and Cheung, Y.K., "The Finite Element Method in Structural and Continuum Mechanics," McGraw-Hill Ltd., London, 1967.

APPENDIX A

FORMULATION OF NUMERICAL INTEGRATION PROCEDURE

A.1 Derivation of Numerical Integration Formulae

The numerical integration technique used to obtain time-dependent strains is based on the formulation by Selna[46] for uni-axial stress conditions. This technique is generalized to the two dimensional case of plane stress. The total strain at time t, including shrinkage, may be expressed in terms of specific compliance, stress history and Poisson's ratio which is assumed to be constant with time.

$$\varepsilon_x^T(t) = \int_{t_o}^{t} C(t,\tau)\frac{\partial \sigma_x(\tau)}{\partial \tau} \cdot d\tau - \nu\int_{t_o}^{t} C(t,\tau)\frac{\partial \sigma_y(\tau)}{\partial \tau} \cdot d\tau + \varepsilon_s(t) \quad (A.1)$$

$$\varepsilon_y^T(t) = -\nu\int_{t_o}^{t} C(t,\tau)\frac{\partial \sigma_x(\tau)}{\partial \tau} \cdot d\tau + \int_{t_o}^{t} C(t,\tau)\frac{\partial \sigma_y(\tau)}{\partial \tau} \cdot d\tau + \varepsilon_s(t) \quad (A.2)$$

$$\gamma_{xy}^T(t) = 2(1+\nu)\int_{t_o}^{t} C(t,\tau)\frac{\partial \tau_{xy}(\tau)}{\partial \tau} \cdot d\tau \quad (A.3)$$

These are Equations (2.18) of Section 2.4.2.

In addition, the assumed form of the creep function results in the expression

$$C(t,\tau) = A_i(\tau)\, B_i(t) + D(\tau) \quad (A.4)$$

which is Equation (2.16b).

Considering only the component ε_x, the strain at time $t + \Delta t$ may be written as,

$$\varepsilon_x^T(t+\Delta t) = \int_{t_o}^{t+\Delta t} C(t+\Delta t,\tau)\frac{\partial \sigma_x(\tau)}{\partial \tau}\, d\tau - \nu\int_{t_o}^{t+\Delta t} C(t+\Delta t,\tau)\frac{\partial \sigma_y(\tau)}{\partial \tau}\, d\tau$$

$$+ \varepsilon_s(t+\Delta t) \qquad (A.5)$$

Subtracting Equation (A.1) from Equation (A.5), and substituting from Equation (A.4), results in

$$\varepsilon_x^T(t+\Delta t)-\varepsilon_x^T(t) = \int_{t_o}^{t} [B_i(t+\Delta t)-B_i(t)]A_i(\tau)\frac{\partial \sigma_x(\tau)}{\partial \tau} + \int_{t}^{t+\Delta t} B_i(t+\Delta t)$$

$$\cdot A_i(\tau)\frac{\partial \sigma_x(\tau)}{\partial \tau}\, d\tau + \int_{t}^{t+\Delta t} D(\tau)\frac{\partial \sigma_x(\tau)}{\partial \tau}\cdot d\tau - \nu\left[\int_{t_o}^{t} [B_i(t+\Delta t)\right.$$

$$-B_i(t)]A_i(\tau)\frac{\partial \sigma_y(\tau)}{\partial \tau} + \int_{t}^{t+\Delta t} B_i(t+\Delta t)A_i(\tau)\frac{\partial \sigma_y(\tau)}{\partial \tau}\cdot d\tau$$

$$\left. + \int_{t}^{t+\Delta t} D(\tau)\frac{\partial \sigma_y(\tau)}{\partial \tau}\, d\tau\right] + \varepsilon_s(t+\Delta t) - \varepsilon_s(t) \qquad (A.6)$$

Writing,

$$V_{xi}(t) = \int_{t_o}^{t} A_i(\tau)\frac{\partial \sigma_x(\tau)}{\partial \tau}\cdot d\tau \qquad (A.7a)$$

$$V_{yi}(t) = \int_{t_o}^{t} A_i(\tau)\frac{\partial \sigma_y(\tau)}{\partial \tau}\cdot d\tau \qquad (A.7b)$$

$$V_{xyi}(t) = \int_{t_o}^{t} A_i(\tau)\frac{\partial \tau_{xy}(\tau)}{\partial \tau}\cdot d\tau \qquad (A.7c)$$

and assuming a linear stress variation and average values for $A_i(\tau)$ in

the time step $t - \Delta t'$ to $t^{(*)}$ we obtain,

$$V_{xi}(t) = V_{xi}(t-\Delta t') + \tfrac{1}{2}[A_i(t-\Delta t')+A_i(t)][\sigma_x(t) - \sigma_x(t-\Delta t')] \qquad (A.8a)$$

$$V_{yi}(t) = V_{yi}(t-\Delta t') + \tfrac{1}{2}[A_i(t-\Delta t')+A_i(t)][\sigma_y(t) - \sigma_y(t-\Delta t')] \qquad (A.8b)$$

$$V_{xyi}(t) = V_{xyi}(t-\Delta t') + \tfrac{1}{2}[A_i(t-\Delta t')+A_i(t)][\tau_{xy}(\tau)-\tau_{xy}(t-\Delta t')] \qquad (A.8c)$$

Equation (A.6) may now be written as,

$$\begin{aligned}\varepsilon_x^T(t+\Delta t)-\varepsilon_x^T(t) = {} & [B_i(t+\Delta t)-B_i(t)]V_{xi}(t) + \int_t^{t+\Delta t} B_i(t+\Delta t)A_i(\tau)\frac{\partial\sigma_x(\tau)}{\partial\tau}\,d\tau \\ & + \int_t^{t+\Delta t} D(\tau)\frac{\partial\sigma_x(\tau)}{\partial\tau}\,d\tau - \nu\Bigg\{[B_i(t+\Delta t)-B_i(t)]V_{yi}(t) \\ & + \int_t^{t+\Delta t} B_i(t+\Delta t)A_i(\tau)\frac{\partial\sigma_y(\tau)}{\partial\tau}\,d\tau + \int_t^{t+\Delta t} D(\tau)\frac{\partial\sigma_y(\tau)}{\partial\tau}\,d\tau\Bigg\} \\ & + \varepsilon_s(t+\Delta t) - \varepsilon_s(t) \qquad (A.9)\end{aligned}$$

If it is now assumed that for the time step $t \to t + \Delta t$ the stress variation is again linear, and using average values for $A_i(\tau)$ and $D(\tau)$ in the interval, we obtain,

$$\begin{aligned}\varepsilon_x^T(t+\Delta t)-\varepsilon_x^T(t) = {} & [B_i(t+\Delta t) - B_i(t)]V_{xi}(t) \\ & + [\sigma_x(t+\Delta t)-\sigma_x(t)]\Bigg\{B_i(t+\Delta t)\frac{[A_i(t+\Delta t)+A_i(t)]}{2} \\ & + \frac{[D(t+\Delta t)+D(t)]}{2}\Bigg\} - \nu\Bigg\{[B_i(t+\Delta t) - B_i(t)]V_{yi}(t)\end{aligned}$$

(* The time intervals $\Delta t'$ and Δt need not be equal)

$$+[\sigma_y(t+\Delta t)-\sigma_y(t)]\left\{B_i(t+\Delta t)\frac{[A_i(t+\Delta t)+A_i(t)]}{2}\right.$$

$$\left.+\frac{[D(t+\Delta t)+D(t)]}{2}\right\}+\varepsilon_s(t+\Delta t)-\varepsilon_s(t) \qquad (A.10)$$

Writing,

$$\frac{1}{\bar{E}(t+\Delta t)} = B_i(t+\Delta t)\frac{[A_i(t+\Delta t)+A_i(t)]}{2}+\frac{[D(t+\Delta t)+D(t)]}{2} \qquad (A.11)$$

where $\bar{E}(t+\Delta t)$ is referred to by Selna as the pseudo-instantaneous modulus of elasticity at time $t+\Delta t$, Equation (A.10) becomes

$$\varepsilon_x^T(t+\Delta t) = \frac{\sigma_x(t+\Delta t)}{\bar{E}(t+\Delta t)}-\frac{\nu\sigma_y(t+\Delta t)}{\bar{E}(t+\Delta t)}+\varepsilon_x^T(t)-\left[\frac{\sigma_x(t)}{\bar{E}(t+\Delta t)}-\frac{\nu\sigma_y(t)}{\bar{E}(t+\Delta t)}\right]$$

$$-\varepsilon_s(t)+[B_i(t+\Delta t)-B_i(t)][V_{xi}(t)-\nu V_{yi}(t)]+\varepsilon_s(t+\Delta t) \qquad (A.12)$$

Equation (A.12) may be written as,

$$\varepsilon_x^T(t+\Delta t) = \varepsilon_x^E(t+\Delta t)+\varepsilon_x^C(t+\Delta t)+\varepsilon_s(t+\Delta t) \qquad (A.13)$$

where

$$\varepsilon_x^E(t+\Delta t) = \frac{\sigma_x(t+\Delta t)}{\bar{E}(t+\Delta t)}-\frac{\nu\sigma_y(t+\Delta t)}{\bar{E}(t+\Delta t)}$$

is the instantaneous elastic strain at time $t+\Delta t$,

$$\varepsilon_x^C(t+\Delta t) = \varepsilon_x^T(t)-\left[\frac{\sigma_x(t)}{\bar{E}(t+\Delta t)}-\frac{\nu\sigma_y(t)}{\bar{E}(t+\Delta t)}\right]-\varepsilon_s(t)$$

$$+[B_i(t+\Delta t)-B_i(t)][V_{xi}(t)-\nu V_{yi}(t)]$$

is the creep strain at time $t+\Delta t$,

and

$\varepsilon_s(t+\Delta t)$ is the shrinkage strain at time $t + \Delta t$.

Similar expressions may be derived for $\varepsilon_y(t+\Delta t)$ and $\gamma_{xy}(t+\Delta t)$ to give,

$$\varepsilon_y^T(t+\Delta t) = \frac{\sigma_y(t+\Delta t)}{\bar{E}(t+\Delta t)} - \frac{\nu\sigma_x(t+\Delta t)}{\bar{E}(t+\Delta t)} + \varepsilon_y^T(t)$$

$$- \left[\frac{\sigma_y(t)}{\bar{E}(t+\Delta t)} - \frac{\nu\sigma_x(t)}{\bar{E}(t+\Delta t)}\right] - \varepsilon_s(t)$$

$$+ [B_i(t+\Delta t)-B_i(t)][V_{yi}(t)-\nu V_{xi}(t)] + \varepsilon_s(t+\Delta t) \qquad (A.14)$$

$$\gamma_{xy}^T(t+\Delta t) = 2(1+\nu)\frac{\tau_{xy}(t+ t)}{\bar{E}(t+\Delta t)} + \gamma_{xy}^T(t) - 2(1+\nu)\frac{\tau_{xy}(t)}{\bar{E}(t+\Delta t)}$$

$$+ 2(1+\nu)[B_i(t+\Delta t)-B_i(t)]V_{xyi}(t) \qquad (A.15)$$

The total strain at time $t + \Delta t$ may thus be expressed as the sum of instantaneous elastic, creep and shrinkage strains.

$$\begin{Bmatrix} \varepsilon_x^T(t+\Delta t) \\ \varepsilon_y^T(t+\Delta t) \\ \gamma_{xy}^T(t+\Delta t) \end{Bmatrix} = \begin{bmatrix} 1/\bar{E}(t+\Delta t) & -\nu/\bar{E}(t+\Delta t) & . \\ -\nu/\bar{E}(t+\Delta t) & 1/\bar{E}(t+\Delta t) & . \\ . & . & \frac{2(1+\nu)}{\bar{E}(t+\Delta t)} \end{bmatrix} \begin{Bmatrix} \sigma_x(t+\Delta t) \\ \sigma_y(t+\Delta t) \\ \tau_{xy}(t+\Delta t) \end{Bmatrix} + \begin{Bmatrix} \varepsilon_x^C(t+\Delta t) \\ \varepsilon_y^C(t+\Delta t) \\ \gamma_{xy}^C(t+\Delta t) \end{Bmatrix} + \begin{Bmatrix} \varepsilon_s(t+\Delta t) \\ \varepsilon_s(t+\Delta t) \\ 0 \end{Bmatrix}$$

(A.16)

Equation (A.16) applies to isotropic materials. For this work, it is extended to the orthotropic case by modifying the pseudo-instantaneous compliance matrix to obtain,

$$\begin{Bmatrix} \varepsilon_x^T(t+\Delta t) \\ \varepsilon_y^T(t+\Delta t) \\ \gamma_{xy}^T(t+\Delta t) \end{Bmatrix} = \begin{bmatrix} 1/\bar{E}_x(t+\Delta t) & -\nu_y/\bar{E}_y(t+\Delta t) & . \\ -\nu_x/\bar{E}_x(t+\Delta t) & 1/\bar{E}_y(t+\Delta t) & . \\ . & . & 2(1+\nu)/\bar{E}(t+\Delta t) \end{bmatrix} \begin{Bmatrix} \sigma_x(t+\Delta t) \\ \sigma_y(t+\Delta t) \\ \tau_{xy}(t+\Delta t) \end{Bmatrix} + \begin{Bmatrix} \varepsilon_x^C(t+\Delta t) \\ \varepsilon_y^C(t+\Delta t) \\ \gamma_{xy}^C(t+\Delta t) \end{Bmatrix} + \begin{Bmatrix} \varepsilon_s(t+\Delta t) \\ \varepsilon_s(t+\Delta t) \\ 0 \end{Bmatrix}$$

(A.17)

From Equation (A.17), stresses at time t + Δt may be expressed as,

$$\begin{Bmatrix} \sigma_x(t+\Delta t) \\ \sigma_y(t+\Delta t) \\ \tau_{xy}(t+\Delta t) \end{Bmatrix} = \begin{bmatrix} \frac{\bar{E}_x(t+\Delta t)}{(1-\nu_x\nu_y)} & \frac{\nu_x\bar{E}_y(t+\Delta t)}{(1-\nu_x\nu_y)} & . \\ \frac{\nu_y\bar{E}_x(t+\Delta t)}{(1-\nu_x\nu_y)} & \frac{\bar{E}_y(t+\Delta t)}{(1-\nu_x\nu_y)} & . \\ . & . & \frac{\bar{E}(t+\Delta t)}{2(1+\nu)} \end{bmatrix} \begin{Bmatrix} \varepsilon_x^T(t+\Delta t) - \varepsilon_x^I(t+\Delta t) \\ \varepsilon_y^T(t+\Delta t) - \varepsilon_y^I(t+\Delta t) \\ \gamma_{xy}^T(t+\Delta t) - \gamma_{xy}^I(t+\Delta t) \end{Bmatrix}$$

or $$\{\sigma(t+\Delta t)\} = [C(t+\Delta t)]\ \{\varepsilon^E(t+\Delta t)\} \qquad (A.18)$$

where $[C(t+\Delta t)]$ represents the pseudo-instantaneous constitutive matrix at time t + Δt.

An examination of Equations (A.8) and (A.13) indicate that the quantity $\varepsilon^I(t+\Delta t)$ may be computed using information obtained from the two previous times, t and t=$\Delta t'$. This numerical integration technique is based on two main approximations,

a) The stress variation in any time increment is linear, and

b) The values $A_i(\tau)$ and $D(\tau)$ are assumed to be constant in the time interval and equal to the average of the values at the beginning and end of the time interval.

Equation (A.11) may be rewritten as

$$\frac{1}{\bar{E}(t+\Delta t)} = \frac{C(t+\Delta t,t+\Delta t) + C(t+\Delta t,t)}{2} \qquad (A.19)$$

Figure A.1 shows the relationship between $1/\bar{E}(t+\Delta t)$ and the length of the time step Δt. It is apparent that $\bar{E}(t+\Delta t)$ decreases for increasing Δt. This effect is more marked for earlier time t in an ageing material such as concrete and it can be seen that the accuracy of the procedure may be improved by decreasing the time step size.

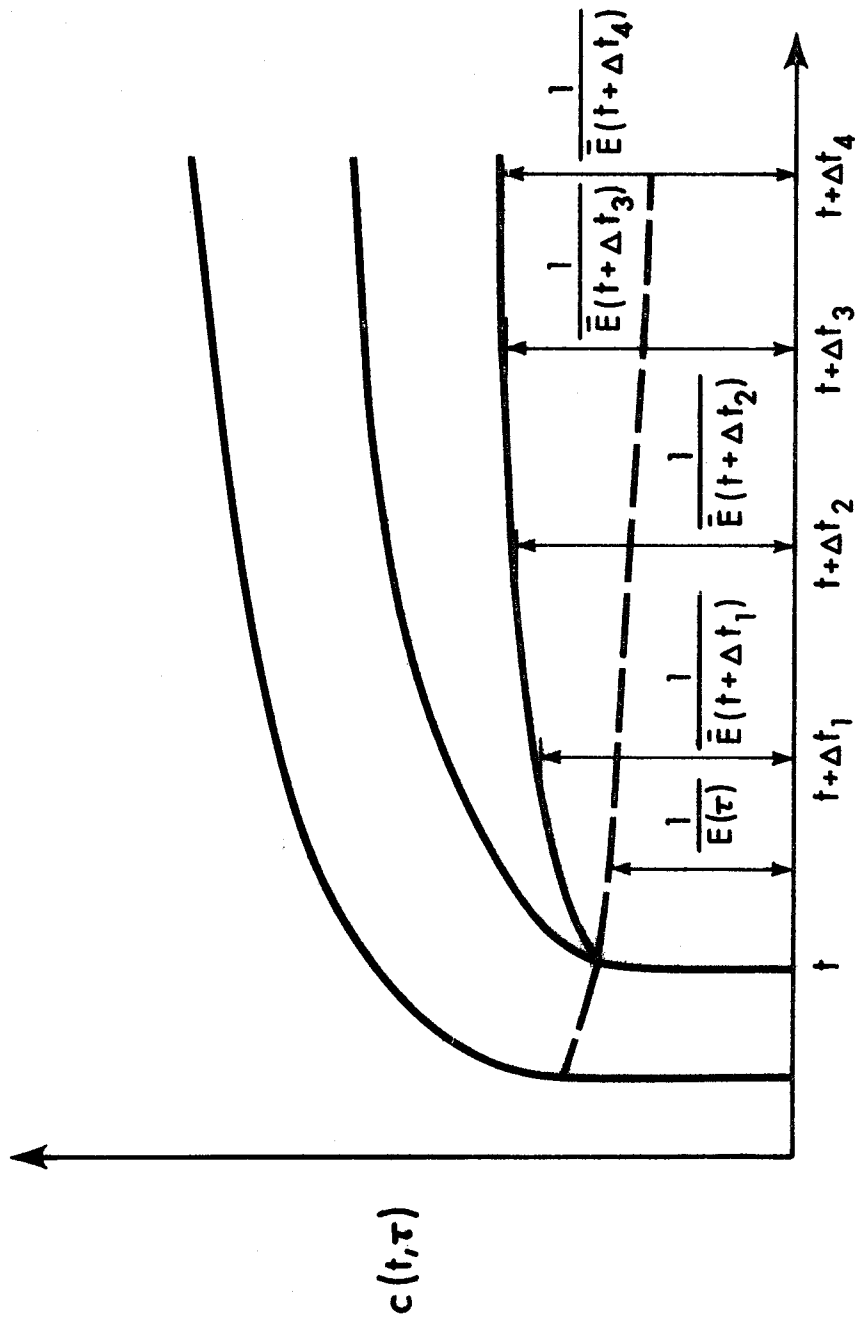

FIGURE A.1 PSEUDO INSTANTANEOUS MODULUS-EFFECT OF INCREASING TIME INCREMENT

necessary a better estimate may be made and the computations repeated.

No attempt has been made to implement this procedure numerically.

APPENDIX B

EVALUATION OF CONSTANTS IN COMPLIANCE FUNCTION BY LEAST SQUARES CURVE FITTING

The compliance function is given in Equation (2.16) by,

$$C(t,\tau) = \frac{1}{E(\tau)} + (a_1+a_2/\tau^{0.1}+a_3/\tau^{0.2}+a_4/\tau^{0.3})\left[\alpha_1(1-e^{-k_1(t-\tau)}) + \alpha_2(1-e^{-k_2(t-\tau)}) + \alpha_3(1-e^{-k_3(t-\tau)})\right] \quad (B.1)$$

where

$$\frac{1}{E(\tau)} = \frac{p}{\tau} + q \quad (B.2)$$

This function can be fit to any set of standard creep test data by the method of least squares.

Let $\bar{C}_j(t,\tau)$ be the observed value of compliance at t for loading at τ and $C_j(t,\tau)$ be the calculated value from Equation (2.16).

Then $e_j = (\bar{C}_j(t,\tau) - C_j(t,\tau))^2$ is the square of the difference.

Summing over N observed values,

$$E = \sum_{j=1}^{N} e_j = \sum_{j=1}^{N} (\bar{C}_j(t,\tau) - C_j(t,\tau))^2 \quad (B.3)$$

The object now is to minimize E and this is accomplished by differentiating E with respect to each of the constants in the compliance function and setting each of the resulting expressions equal to zero.

The first step is to evaluate p and q. This may be done by evaluating the instantaneous modulus for loading at various ages and

APPENDIX B

EVALUATION OF CONSTANTS IN COMPLIANCE FUNCTION BY LEAST SQUARES CURVE FITTING

The compliance function is given in Equation (2.16) by,

$$C(t,\tau) = \frac{1}{E(\tau)} + (a_1+a_2/\tau^{0.1}+a_3/\tau^{0.2}+a_4/\tau^{0.3})\left[\alpha_1(1-e^{-k_1(t-\tau)}) + \alpha_2(1-e^{-k_2(t-\tau)}) + \alpha_3(1-e^{-k_3(t-\tau)})\right] \quad (B.1)$$

where

$$\frac{1}{E(\tau)} = \frac{p}{\tau} + q \quad (B.2)$$

This function can be fit to any set of standard creep test data by the method of least squares.

Let $\bar{C}_j(t,\tau)$ be the observed value of compliance at t for loading at τ and $C_j(t,\tau)$ be the calculated value from Equation (2.16).

Then $e_j = (\bar{C}_j(t,\tau) - C_j(t,\tau))^2$ is the square of the difference.

Summing over N observed values,

$$E = \sum_{j=1}^{N} e_j = \sum_{j=1}^{N} (\bar{C}_j(t,\tau) - C_j(t,\tau))^2 \quad (B.3)$$

The object now is to minimize E and this is accomplished by differentiating E with respect to each of the constants in the compliance function and setting each of the resulting expressions equal to zero.

The first step is to evaluate p and q. This may be done by evaluating the instantaneous modulus for loading at various ages and

obtaining p and q by least squares. However, it was found to be satisfactory to evaluate $E(\tau)$ for two loading times, substitute in Equation (B.2), and solve the resulting simultaneous equations for p and q. This leaves 10 constants still to be evaluated.

Examination of Equation (B.1) indicates that differentiation with respect to each of the constants k_i will result in non-linear equations in k_i which complicates the solution of the equations. Hamming[24] suggests that the least squares procedure be carried out for several chosen sets of k_i and the set which results in a minimum value for E be adopted. This procedure was followed and for each concrete considered, 10 sets of k_i were used. The remaining 7 constants are obtained by least squares in two stages.

In the first stage the relative values of α_i are obtained by least squares over a set of data for one loading time τ_i.

For loading time τ_i, the compliance function may be written in the form,

$$C(t,\tau_i) = 1/E(\tau_i) + K\alpha_1(1-e^{-k_1(t-\tau_i)}) + K\alpha_2(1-e^{-k_2(t-\tau_i)}) + K\alpha_3(1-e^{-k_3(t-\tau_i)})$$

$$= 1/E(\tau_i) + \bar{\alpha}_1(1-e^{-k_1(t-\tau_i)}) + \bar{\alpha}_2(1-e^{-k_2(t-\tau_i)}) + \bar{\alpha}_3(1-e^{-k_3(t-\tau_i)})$$

$$= 1/E(\tau_i) + \bar{\alpha}_1 X_1 + \bar{\alpha}_2 X_2 + \bar{\alpha}_3 X_3$$

where $K = (a_1 + a_2/\tau_i^{0.1} + a_3/\tau_i^{0.2} + a_4/\tau_i^{0.3})$

and $X_j = (1-e^{-k_j(t-\tau_i)})$

Forming E and differentiating with respect to each $\bar{\alpha}_k$,

$$\bar{\alpha}_1 \sum(X_1^2)_\ell + \bar{\alpha}_2 \sum(X_1X_2)_\ell + \bar{\alpha}_3 \sum(X_1X_3)_\ell = \sum(X_1)_\ell(\bar{C}(t_\ell,\tau_j) - 1/E(\tau_j))$$

$$\bar{\alpha}_1 \sum(X_2X_1)_\ell + \bar{\alpha}_2 \sum(X_2^2)_\ell + \bar{\alpha}_3 \sum(X_2X_3)_\ell = \sum(X_2)_\ell(\bar{C}(t_\ell,\tau_j) - 1/E(\tau_j)) \quad (B.4)$$

$$\bar{\alpha}_1 \sum(X_3X_1)_\ell + \bar{\alpha}_2 \sum(X_3X_2)_\ell + \bar{\alpha}_3 \sum(X_3^2)_\ell = \sum(X_3)_\ell(\bar{C}(t_\ell,\tau_j) - 1/E(\tau_j))$$

where $\sum = \sum_{\ell=1}^{M}$

and M is the number of observation times for loading time τ_j.

Solving Equation (B.4) for $\bar{\alpha}_1$, $\bar{\alpha}_2$, and $\bar{\alpha}_3$, relative values of α_i may now be computed from

$$\begin{aligned} \alpha_3 &= 1.0 \\ \alpha_2 &= \bar{\alpha}_2/\bar{\alpha}_3 \\ \alpha_1 &= \bar{\alpha}_1/\bar{\alpha}_3 \end{aligned} \quad (B.5)$$

The second stage involves an application of the least squares procedure over the complete range of data for several loading times.

Equation (B.1) is now expressed in the form,

$$C(t,\tau) = (a_1 p_1 + a_2 p_2 + a_3 p_3 + a_4 p_4)\, Y(t,\tau) + 1/E(\tau) \quad (B.6)$$

where $p_1 = 1.0$

$p_2 = 1/\tau^{0.1}$

$p_3 = 1/\tau^{0.2}$

$p_4 = 1/\tau^{0.3}$

and $Y(t,\tau) = \sum_{i=1}^{3} \alpha_i(1-e^{-k_1(t-\tau)})$

Computing E for $\bar{M}$ points and differentiating with respect to each constant a_1, a_2, a_3 and a_4 results in the 4 simultaneous equations,

$$[D]\{a\} = \{B\} \tag{B.7}$$

where $$D_{ij} = \sum_{\ell=1}^{\bar{M}} p_k\, p_j\, Y_\ell^2(t,\tau)$$

and $$B_i = \sum_{\ell=1}^{\bar{M}} [\bar{C}_\ell(t,\tau) - 1/E_\ell(\tau)]\, p_i \cdot Y_\ell(t,\tau)$$

Equation (B.7) is solved for {a} which completes the solution for the 12 constants in the compliance function.

Ten sets of k_i were considered for the compliance function used in this work and the set which produced a minimum value for the quantity E (Equation B.3) was used in each case. A comparison of the compliance functions obtained by least squares with the data used may be seen in Figures 2.7 and 2.8.

Tables B.1 and B.2 show the results of the least squares analysis for two sets of k_i which were considered for concrete C1. For each known point on the compliance curve, the time of loading and time of observation are noted, followed by the given value of specific compliance and the value computed by the least squares analysis. The difference between the two values is shown as a percentage. On the bottom line the computed values of the constants are given as well as the quantity E defined above. These two sets of data represent the maximum and minimum values of E obtained for the range of k_i considered and it can be seen that the correlation is good in each case.

TIME OF LOADING	TIME OF OBSERVATION	COMPLIANCE (EXPTL.)	COMPLIANCE (CALC.)	DIFFERENCE-%
28.00	29.00	0.39100×10^{-6}	0.37988×10^{-6}	-2.84422
28.00	32.86	0.52200×10^{-6}	0.56740×10^{-6}	8.69715
28.00	38.00	0.65300×10^{-6}	0.64578×10^{-6}	-1.10536
28.00	49.00	0.78500×10^{-6}	0.75026×10^{-6}	-4.42555
28.00	70.00	0.91500×10^{-6}	0.89370×10^{-6}	-2.32831
28.00	128.00	0.10450×10^{-5}	0.10842×10^{-5}	3.75173
28.00	232.00	0.11770×10^{-5}	0.11647×10^{-5}	-1.04827
7.00	8.00	0.50700×10^{-6}	0.54471×10^{-6}	7.43690
7.00	11.86	0.68900×10^{-6}	0.78896×10^{-6}	14.50853
7.00	17.00	0.87400×10^{-6}	0.89106×10^{-6}	1.95224
7.00	28.00	0.10590×10^{-5}	0.10272×10^{-5}	-3.00735
7.00	49.00	0.12410×10^{-5}	0.12140×10^{-5}	-2.17656
7.00	107.00	0.14250×10^{-5}	0.14621×10^{-5}	2.60632
7.00	211.00	0.16110×10^{-5}	0.15669×10^{-5}	-2.73492
90.00	91.00	0.32800×10^{-6}	0.32005×10^{-6}	-2.42337
90.00	94.86	0.42600×10^{-6}	0.46015×10^{-6}	8.01556
90.00	100.00	0.52400×10^{-6}	0.51871×10^{-6}	-1.01040
90.00	111.00	0.62200×10^{-6}	0.59676×10^{-6}	-4.05790
90.00	132.00	0.72100×10^{-6}	0.70392×10^{-6}	-2.36890
90.00	190.00	0.81700×10^{-6}	0.84625×10^{-6}	3.58003
90.00	294.00	0.91600×10^{-6}	0.90636×10^{-6}	-1.05270

K1	K2	K3	ALPH1	ALPH2	ALPH3	A1	A2	A3	A4
0.50000	0.02000	0.00200	7.144211	6.50423	1.00000	-0.49977E-07	0.83100E-07	0.11961E-06	-0.89228E-07

E = 0.254914E-13

TABLE B.1 RESULTS OF LEAST SQUARES ANALYSIS - E MAXIMUM

TIME OF LOADING	TIME OF OBSERVATION	COMPLIANCE (EXPTL.)	COMPLIANCE (CALC.)	DIFFERENCE-%
28.00	29.00	0.39100×10^{-6}	0.33300×10^{-6}	-14.83402
28.00	32.86	0.52200×10^{-6}	0.52578×10^{-6}	0.72433
28.00	38.00	0.65300×10^{-6}	0.66123×10^{-6}	1.25958
28.00	49.00	0.78500×10^{-6}	0.79289×10^{-6}	1.00466
28.00	70.00	0.91500×10^{-6}	0.90737×10^{-6}	-0.83403
28.00	128.00	0.10450×10^{-5}	0.10439×10^{-5}	-0.10566
28.00	232.00	0.11770×10^{-5}	0.11775×10^{-5}	0.04304
7.00	8.00	0.50700×10^{-6}	0.48381×10^{-6}	-4.57444
7.00	11.86	0.68900×10^{-6}	0.73536×10^{-6}	6.72896
7.00	17.00	0.87400×10^{-6}	0.91210×10^{-6}	4.35903
7.00	28.00	0.10590×10^{-5}	0.10839×10^{-5}	2.35112
7.00	49.00	0.12410×10^{-5}	0.12333×10^{-5}	-0.62192
7.00	107.00	0.14250×10^{-5}	0.14114×10^{-5}	-0.95226
7.00	211.00	0.16110×10^{-5}	0.15858×10^{-5}	-1.56584
90.00	91.00	0.32800×10^{-6}	0.28509×10^{-6}	-13.08131
90.00	94.86	0.42600×10^{-6}	0.42929×10^{-6}	0.77299
90.00	100.00	0.52400×10^{-6}	0.53060×10^{-6}	1.26033
90.00	111.00	0.62200×10^{-6}	0.62909×10^{-6}	1.13923
90.00	132.00	0.72100×10^{-6}	0.71472×10^{-6}	-0.87132
90.00	190.00	0.81700×10^{-6}	0.81684×10^{-6}	-0.01966
90.00	294.00	0.91600×10^{-6}	0.91678×10^{-6}	0.08506

K1	K2	K3	ALPH1	ALPH2	ALPH3	A1	A2	A3	A4
0.20000	0.04000	0.00200	0.39105	0.37638	1.00000	-0.17189E-05	0.45416E-05	-0.13153E-06	-0.75942E-07

E = 0.111925E-13

TABLE B.2 RESULTS OF LEAST SQUARES ANALYSIS - E MINIMUM

APPENDIX C

DETAILS OF ELEMENT STIFFNESS MATRIX AND LOAD VECTOR

C.1 Generation of Element Stiffness Matrix

The element stiffness matrix is given by Equation (3.24),

$$[k_e] = \int_0^a \int_0^b [B]^T[D][B]\, dx\, dy \tag{C.1}$$

Expressed in non dimensionalized coordinates, $\xi = \frac{x}{a}$, $\eta = \frac{y}{b}$

$$[k_t] = \int_0^1 \int_0^1 [\bar{B}]^T[D][\bar{B}]\, ab\, d\xi\, d\eta \tag{C.2}$$

The matrix $[\bar{B}]^T$ is given in Table C.1.

Writing

$$[\bar{B}]^T[D][\bar{B}] = \begin{bmatrix} b_{11}\ b_{21}\ b_{31} \\ b_{12}\ b_{22}\ b_{32} \\ \vdots \\ b_{1i}\ b_{2i}\ b_{3i} \\ \vdots \\ b_{1,16}\ b_{2,16}\ b_{3,16} \end{bmatrix} \begin{bmatrix} D_{11}\ D_{12}\ D_{13} \\ D_{21}\ D_{22}\ D_{23} \\ D_{31}\ D_{32}\ D_{33} \end{bmatrix} \begin{bmatrix} b_{11}\ b_{12} \cdots b_{1j} \cdots b_{1,16} \\ b_{21}\ b_{22}\ \ b_{2j}\ \ b_{2,16} \\ b_{31}\ b_{32}\ \ b_{3j}\ \ b_{3,16} \end{bmatrix} \tag{C.3}$$

where b_{mn} is a polynomial of the form

$$b_{mn} = C_0(m,n)\{C_1(m,n)+C_2(m,n)\xi+C_3(m,n)\xi^2+C_4(m,n)\xi^3\}\{p_1(m,n)+p_2(m,n)\eta + p_3(m,n)\eta^2+p_4(m,n)\eta^3\} \tag{C.4}$$

The general term k_{ij} becomes, by matrix multiplication

$$k_{ij} = \int_0^1 \int_0^1 b_{1i}b_{1j}D_{11}+b_{2i}b_{1j}D_{21}+b_{3i}b_{1j}D_{31}+b_{1i}b_{2j}D_{12}+b_{2i}b_{2j}D_{22}$$

$$+b_{3i}b_{2j}D_{32}+b_{1i}b_{3j}D_{13}+b_{2i}b_{3j}D_{23}+b_{3i}b_{3j}D_{33}\}a\cdot b\cdot d\xi d\eta \qquad (C.5)$$

or,

$$k_{ij} = A_{11}(i,j)D_{11}+A_{21}(i,j)D_{21}+A_{31}(i,j)D_{31}+A_{12}(i,j)D_{12}+A_{22}(i,j)D_{22}$$

$$+A_{32}(i,j)D_{32}+A_{13}(i,j)D_{13}+A_{23}(i,j)D_{23}+A_{33}(i,j)D_{33} \qquad (C.6)$$

where the general term $A_{mn}(i,j)$ is derived as follows

$$b_{mi}b_{nj} = c_o(m,i)c_o(n,j)\{c_1(m,i)+c_2(m,i)\xi+c_3(m,i)\xi^2+c_4(m,i)\xi^3\}$$

$$\{c_1(n,j)+c_2(n,j)\xi+c_3(n,j)\xi^2+c_4(n,j)\xi^3\}\{p_1(m,i)+p_2(m,i)\eta$$

$$+p_3(m,i)\eta^2+p_4(m,i)\eta^3\}\{p_1(n,j)+p_2(n,j)\eta+p_3(n,j)\eta^2$$

$$+p_4(n,j)\eta^3\} \qquad (C.7)$$

or,

$$b_{mi}b_{nj} = C_{o_{mn}}(i,j)\{Q_1+Q_2\xi+Q_3\xi^2+Q_4\xi^3+Q_5\xi^4+Q_6\xi^5+Q_7\xi^6\}\{R_1+R_2\eta+R_3\eta^2$$

$$+R_4\eta^3+R_5\eta^4+R_6\eta^5+R_7\eta^6\} \qquad (C.8)$$

where Q_1, Q_2 ... are given by,

$$Q_1 = c_1(m,i)\ c_1(n,j)$$

$$Q_2 = c_1(m,i)\ c_2(n,j) + c_2(m,i)\ c_1(n,j)$$

$$Q_3 = c_1(m,i)\ c_3(n,j) + c_3(m,i)\ c_1(n,j) + c_2(m,i)\ c_2(n,j)$$

$$Q_4 = c_1(m,i)\ c_4(n,j) + c_4(m,i)\ c_1(n,j) + c_2(m,i)\ c_3(n,j) + c_3(m,i)\ c_2(n,j)$$

$$Q_5 = c_2(m,i)\ c_4(n,j) + c_4(m,i)\ c_2(n,j) + c_3(m,i)\ c_3(n,j)$$

$$Q_6 = c_3(m,i)\ c_4(n,j) + c_4(m,i)\ c_3(n,j)$$

$$Q_7 = c_4(m,i)\ c_4(n,j)$$

Expressions for R_1, R_2 ... R_7 are obtained by replacing Q by R and c by p in these expressions.

Integrating,

$$A_{mn}(i,j) = c_{o_{mn}}(i,j)\{Q_1+Q_2/2+Q_3/3+Q_4/4+Q_5/5+Q_6/6+Q_7/7\}$$

$$+ \{R_1+R_2/2+R_3/3+R_4/4+R_5/5+R_6/6+R_7/7\}\cdot a\cdot b \qquad (C.9)$$

Subroutine ELEM was written to generate the terms in the element stiffness matrix for an orthotropic plate in which case the terms D_{13}, D_{23}, D_{31}, D_{32} are zero. The multiplying coefficients for these terms were therefore not included in the program. However, it is apparent that only a slight modification to the subroutine would be required to deal with a full matrix [D] representing a generally anistropic material.

C.2 Applied Load Vector

The applied load vector {R} for an arbitrary transverse load $q(\xi,\eta)$ is given by Equation (3.21) in the form,

$$\{R\} = \int_A q(\xi,\eta)\ \{\phi\}\ dA \tag{C.10}$$

For a uniformly distributed load, $q(\xi,\eta) = q$, on an element, the load vector is given by

$$\begin{aligned}\{R\} = \langle & q\ ab/4,\ q\ a^2b/24,\ q\ ab^2/24,\ q\ a^2b^2/144,\\ & q\ ab/4,\ q\ a^2b/24,\ -q\ ab^2/24,\ -q\ a^2b^2/144,\\ & q\ ab/4,\ -q\ a^2b/24,\ -q\ ab^2/24,\ q\ a^3b^2/144,\\ & q\ ab/4,\ -q\ a^2b/24,\ a\ qb^2/24,\ -q\ a^2b/144\rangle^T\end{aligned} \tag{C.11}$$

This expression and expressions for other loading cases are presented in Ref. (10).

C.3 Equivalent Load Vector

The expression for the equivalent load vector $\{Q\}$ evaluated for an element is given by Equation (3.28) in the form

$$\{Q\} = \int_A [B]^T \{M^I\}\ dA \tag{C.12}$$

As discussed in Section 3.6.3, the vector $\{M^I\}$ is assumed to be a constant for the element. Performing the matrix multiplication and integrating each term in the resulting vector, the following expression is obtained for the equivalent load vector

$$
\begin{aligned}
\{Q\}^T = \langle\ & 2M_{xy}^I, && -\frac{bM_x^I}{2}, && -\frac{aM_y^I}{2}, && -\left(\frac{M_x^I b^2}{12}+\frac{M_y^I a^2}{12}\right), \\
& -2M_{xy}^I, && -\frac{bM_x^I}{2}, && \frac{aM_y^I}{2}, && \left(\frac{M_x^I b^2}{12}+\frac{M_y^I a^2}{12}\right), \\
& 2M_{xy}^I, && \frac{bM_x^I}{2}, && \frac{aM_y^I}{2}, && -\left(\frac{M_x^I b^2}{12}+\frac{M_y^I a^2}{12}\right), \\
& -2M_{xy}^I, && \frac{bM_x^I}{2}, && -\frac{aM_y^I}{2}, && \left(\frac{M_x^I b^2}{12}+\frac{M_y^I a^2}{12}\right) \rangle
\end{aligned}
\qquad (C.13)
$$

	1	2	3
1	$1/a^2(12\xi-6)(2\eta^3-3\eta^2+1)$	$1/b^2(2\xi^3-3\xi^2+1)(12\eta-6)$	$2/ab(6\xi^2-6\xi)(6\eta^2-6\eta)$
2	$1/a(6\xi-4)(2\eta^3-3\eta^2+1)$	$a/b^2(\xi^3-2\xi^2+\xi)(12\eta-6)$	$2/b(3\xi^2-4\xi+1)(6\eta^2-6\eta)$
3	$b/a^2(12\xi-6)(\eta^3-2\eta^3+\eta)$	$1/b(2\xi^3-3\xi^2+1)(6\eta-4)$	$2/a(6\xi^2-6\xi)(3\eta^2-4\eta+1)$
4	$b/a(6\xi-4)(\eta^3-2\eta^2+\eta)$	$a/b(\xi^3-2\xi^2+\xi)(6\eta-4)$	$2(3\xi^2-4\xi+1)(3\eta^2-4\eta+1)$
5	$-1/a^2(12\xi-6)(2\eta^3-3\eta^2+1)$	$-1/b^2(2\xi^3-3\xi^2)(12\eta-6)$	$-2/ab(6\xi^2-6\xi)(6\eta^2-6\eta)$
6	$1/a(6\xi-2)(2\eta^3-3\eta^2+1)$	$a/b^2(\xi^3-\xi^2)(12\eta-6)$	$2/b(3\xi^2-2\xi)(6\eta^2-6\eta)$
7	$-b/a^2(12\xi-6)(\eta^3-2\eta^2+\eta)$	$-1/b(2\xi^3-3\xi^2)(6\eta-4)$	$-2/a(6\xi^2-6\xi)(3\eta^2-4\eta+1)$
8	$b/a(6\xi-2)(\eta^3-2\eta^2+\eta)$	$a/b(\xi^3-\xi^2)(6\eta-4)$	$2(3\xi^2-2\xi)(3\eta^2-4\eta+1)$

TABLE C.1 MATRIX $[\bar{B}]^T$

	1	2	3
9	$-1/a^2(12\xi-6)(2\eta^3-3\eta^2)$	$-1/b^2(2\xi^3-3\xi^2+1)(12\eta-6)$	$-2/ab(6\xi^2-6\xi)(6\eta^2-6\eta)$
10	$-1/a(6\xi-4)(2\eta^3-3\eta^2)$	$-a/b^2(\xi^3-2\xi^2+\xi)(12\eta-6)$	$-2/b(3\xi^2-4\xi+1)(6\eta^2-6\eta)$
11	$b/a^2(12\xi-6)(\eta^3-\eta^2)$	$1/b(2\xi^3-3\xi^2+1)(6\eta-2)$	$2/a(6\xi^2-6\xi)(3\eta^2-2\eta)$
12	$b/a(6\xi-4)(\eta^3-\eta^2)$	$a/b(\xi^3-2\xi^2+\xi)(6\eta-2)$	$2(3\xi^2-4\xi+1)(3\eta^2-2\eta)$
13	$1/a^2(12\xi-6)(2\eta^3-3\eta^2)$	$1/b^2(2\xi^3-3\xi^2)(12\eta-6)$	$2/ab(6\xi^2-6\xi)(6\eta^2-6\eta)$
14	$-1/a(6\xi-2)(2\eta^3-3\eta^2)$	$-a/b^2(\xi^3-\xi^2)(12\eta-6)$	$-2/b(3\xi^2-2\xi)(6\eta^2-6\eta)$
15	$-b/a^2(12\xi-6)(\eta^3-\eta^2)$	$-1/b(2\xi^3-3\xi^2)(6\eta-2)$	$-2/a(6\xi^2-6\xi)(3\eta^2-2\eta)$
16	$b/a(6\xi-2)(\eta^3-\eta^2)$	$a/b(\xi^3-\xi^2)(6\eta-2)$	$2(3\xi^2-2\xi)(3\eta^2-2\eta)$

TABLE C.1(cont'd) MATRIX $[\bar{B}]^T$

APPENDIX D

COMPUTER PROGRAMMING

D.1 Description of Subroutine

The program developed in this investigation was written in FORTRAN IV and computations were carried out on the IBM 360/67 computer of the University of Alberta Computing Centre. The flow chart of Figure D.1 outlines the sequence of computations required for the solution for time-dependent strains and cracking in reinforced concrete floor slabs.

The program consists of a set of subroutines in which the computations in each step of the program are carried out, and a main programme which controls the order in which the subroutine are called. A flow chart by subroutine is given in Figure D.2. In the following, a brief description of each subroutine is given.

COEFF reads in a set of coefficients required for the element stiffness matrix.

INPUT reads and writes input data required for the analysis. Full details of input preparation are given below.

LOAD computes the contribution of each element to the applied load vector (for a uniformly applied load over the slab) and to the equivalent load vector corresponding to the distribution of initial strains. The total load vector is assembled for the structure.

STIFCS computes d_{nx} and d_{ny} (Equation 3.7) and the stiffness coefficient matrix [D] at the corner of each element, from which the average value of [D] for each element is computed.

ELEM generates the terms in the element stiffness matrix as described in Appendix C.

STIFF computes the band width of the structure stiffness matrix and assembles the components of the element stiffness matrix for each element, in the structure stiffness matrix.

DISPL modifies the assembled structure stiffness matrix for the prescribed boundary conditions and calls the equation solver BANSOL which solves for the unknown displacement vector. From the displacements, curvatures and twist are computed at the corner of each element.

MODIFY is called by DISPL and participates in the modification of equations for the boundary conditions.

BANSOL solves the simultaneous equations by a Gauss elimination procedure which utilizes the banded symmetric form of the equations. This subroutine is based on a subroutine developed at the University of California (Berkeley) by Felippa.*

STRESS defines the distribution of strains over the depth at the corner of each element from the computed curvatures by imposing equilibrium of normal stress resultants. Stresses are computed in each layer and checked for cracking. The memory function and cracking coefficients are modified if further cracking is detected. Bending and twisting moments are computed at the corner of each element.

CMOD computes the pseudo instantaneous elastic modulus and shear modulus for each time step.

CREEP computes the new set of initial strains (creep and shrinkage) at every step.

---

* Dr. C.A. Felippa, formerly graduate student at University of California

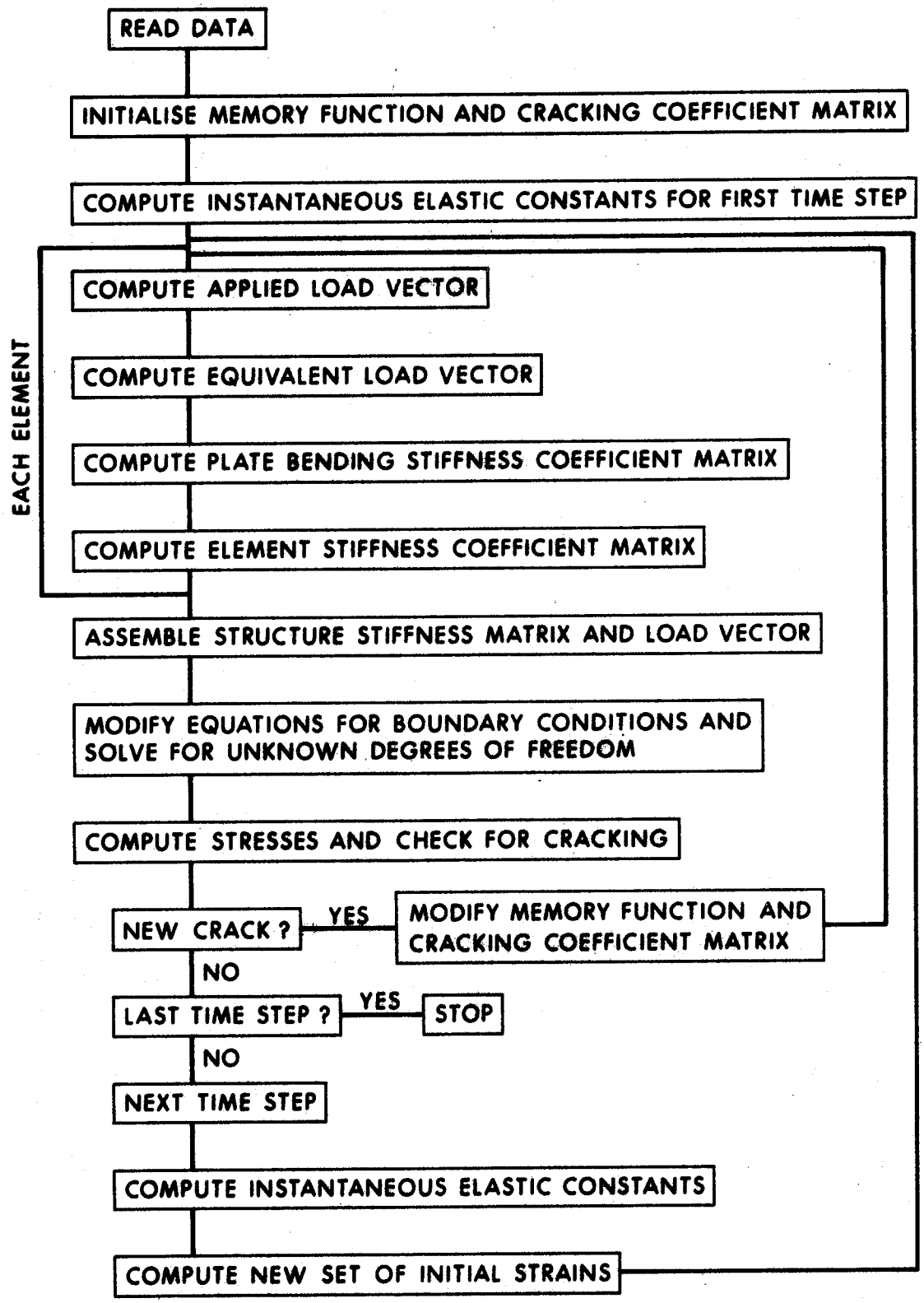

FIGURE D.1 PROGRAM OUTLINE

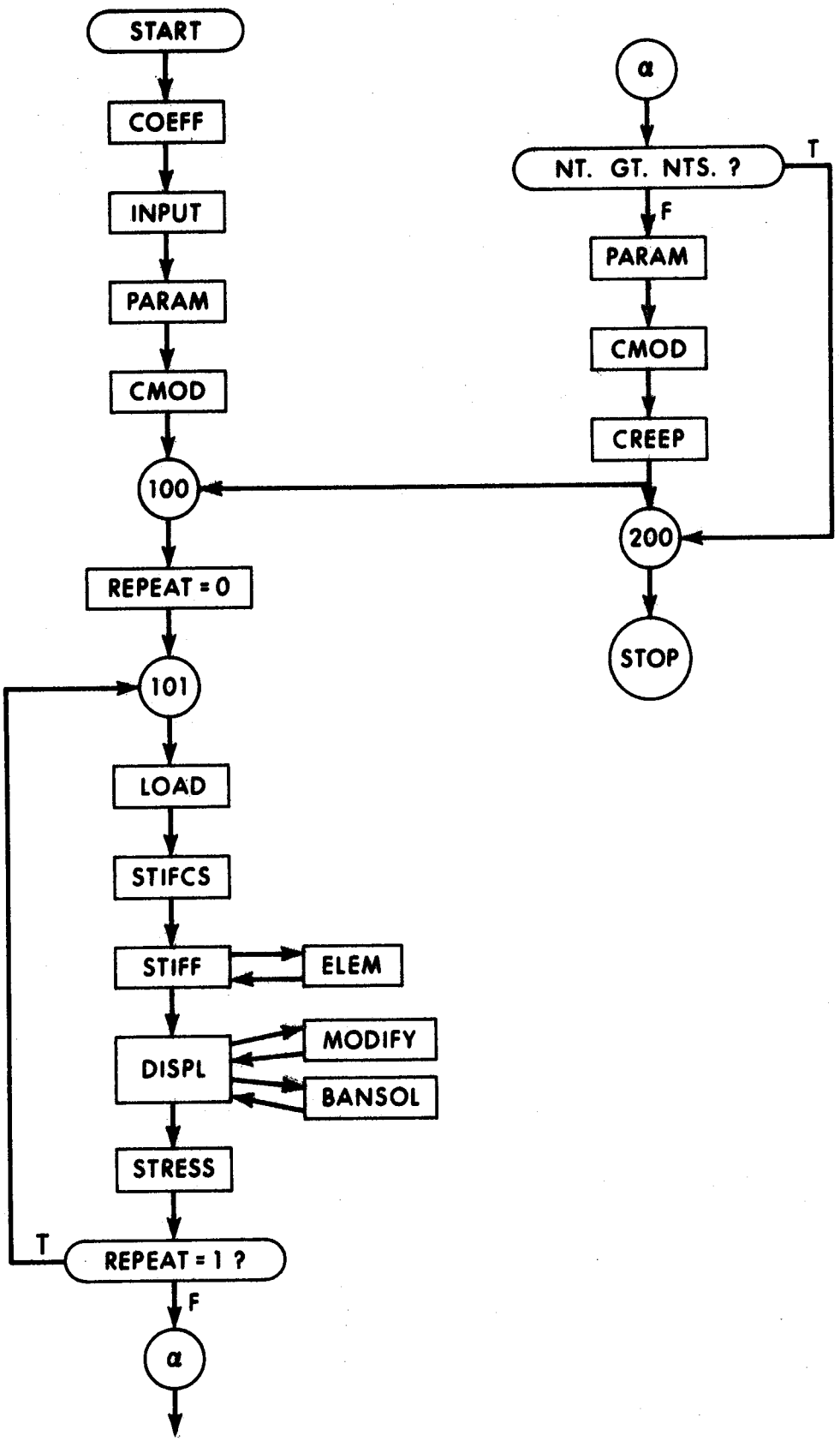

FIGURE D.2 FLOW CHART BY SUBROUTINE

D.2 Program Limitations

The program in its present form is capable of dealing with maximums of

50 Elements

65 Nodal points

10 Layers

25 Time steps

Band width = 40.

The solution of problems exceeding these limits will require an increase in dimension statements and possibly the use of out-of-core storage.

D.3 Preparation of Input Data

The preparation of input data required for use of the computer program is described below.

1. Heading, 20A4, 1 card
2. Control card, 5I5, 1 card

Column 1 - 5	Nr. of nodal points	(NJ)
6 - 10	Nr. of elements	(NE)
11 - 15	Nr. of layers	(NL)
16 - 20	Nr. of time steps	(NTS)

3. Information concerning the stepped stress strain diagram, 2 cards.
   a) 4F10.5

Column 1 - 10	Cracking coefficient "α" for second branch of curve (GAM1)
11 - 20	Cracking coefficient "α" for third branch of curve (GAM2)

21 - 30 Cracking coefficient "α" for fourth branch of curve (GAM3)

31 - 40 Cracking coefficient "α" for fifth branch of curve (GAM4)

b) 4F10.5

Column 1 - 10 Limiting tensile stress for first branch of curve (SCT1)

11 - 20 Limiting tensile stress for second branch of curve (SCT2)

21 - 30 Limiting tensile stress for third branch of curve (SCT3)

31 - 40 Limiting tensile stress for fourth branch of curve (SCT4)

4. Creep function constants (Equation 2.16), 3 cards.

a) 6F10.7

Column 1 - 10 k_1 (K1)

11 - 20 k_2 (K2)

21 - 30 k_3 (K3)

31 - 40 α_1 (ALPH1)

41 - 50 α_2 (ALPH2)

51 - 60 α_3 (ALPH3)

b) 4E15.6

Column 1 - 15 a_1 (A1)

16 - 30 a_2 (A2)

31 - 45 a_3 (A3)

46 - 60 a_4 (A4)

c) 2E15.6

Column 1 - 15 p (AAC)

16 - 30 q (BBC)

5) Element Data: Nodal point numbers at corners of each element, and print code, 9I5, 1 card per element.

Column 1 - 5 Element number (M)

6 - 10 Nodal point number for corner 1 (NODG(M))

11 - 15 Nodal point number for corner 2 (NODH(M))

16 - 20 Nodal point number for corner 3 (NODI(M))

21 - 25 Nodal point number for corner 4 (NODT(M))

26 - 30 Print code for corner 1 (IPRINT(M,1))

31 - 35 Print code for corner 2 (IPRINT(M,2))

36 - 40 Print code for corner 3 (IPRINT(M,3))

41 - 45 Print code for corner 4 (IPRINT(M,4))

The parameter IPRINT determines whether output (stresses, strains, moments) is to be printed at each time step.

If IPRINT = 1, output will be printed.

If IPRINT = 0, output will not be printed.

$$\left.\begin{matrix}\text{NODG(M)}\\ \text{NODH(M)}\\ \text{NODI(M)}\\ \text{NODJ(M)}\end{matrix}\right\} \text{ is nodal point number at corner } \left\{\begin{matrix}1\\2\\3\\4\end{matrix}\right\} \text{ of element M}$$

The element nodal point numbers must be ordered in the sequence shown in Figure D.3.

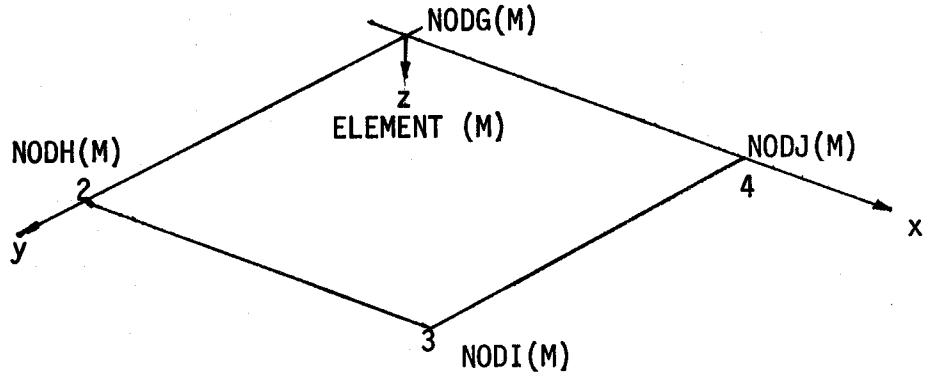

FIGURE D.3 ELEMENT NODAL POINT NUMBERING SYSTEM

6) Nodal point information: Boundary condition code and x,y coordinates defining the location of the nodal point, 2I5, 2F10.3, 1 card per nodal point.

Column 1 - 5 Nodal point number (M)

6 - 10 Boundary condition code (KODE(M))

11 - 20 x-coordinate of nodal point (X(M))

21 - 30 y-coordinate of nodal point (Y(M))

The boundary condition code is as follows,

Column 6 Blank

7 1 = displacement boundary condition for w

0 = force boundary condition for w

8 1 = displacement boundary condition for $w_{,x}$

0 = force boundary condition for $w_{,x}$

9) Details of loading history and shrinkage strains, 2F10.5, E15.6, 1 card per time step

Column 1 - 10 Time (days) T(I)

11 - 20 Uniformly distributed load at time T(I) UUDL(I)

21 - 35 Shrinkage strain at time T(I) ESH(I)

10) Depths of layer boundaries from top surface, F10.5, 1 card per layer boundary (total number = number of layers + 1)

Column 1 - 10 Distance of layer boundary from top surface

D.4 Description of Output

The following is a brief description of the output obtained from the computer program. The subroutines from which the appropriate output FORMAT statements may be obtained are given in each case.

a) All input data is printed for record and checking (see COEFF and INPUT).

b) The time (T days) for which each analysis is carried out is printed followed by the pseudo instantaneous elastic and shear moduli (see PARAM and CMOD).

c) For each cracking iteration, the coefficients in the plate bending stiffness matrix [D] are printed (see STIFCS).

d) If cracking is detected, the message "CRACKING DETECTED THIS ITERATION" is printed and no further output is printed for the iteration (see STRESS).

e) Concrete stresses ($\sigma_x, \sigma_y, \tau_{xy}$), total strains ($\varepsilon_x^T, \varepsilon_y^T, \gamma_{xy}^T$) and inelastic strains ($\varepsilon_x^I, \varepsilon_y^I, \gamma_{xy}^I$) are printed for each layer J at each corner I of each element M if the parameter IPRINT(M,I) equals unity

(see STRESS).

f) Steel stresses are printed at each corner I of each element M if IPRINT(M,I) equals unity (see STRESS).

g) Moments M_x and M_y are printed at each corner I of each element M (see STRESS).

h) The displacement vector for each time T days is printed (see STRESS).

j) For each time step the cracking coefficient matrix is printed (see STRESS).

D.5 PROGRAM LISTING

The author and the University of Alberta disclaim responsibility for the misuse of the following program, nor will they be responsible for errors in the listing.

```
C*************************************
C       MAIN PROGRAMME
C*************************************
      COMMON A(260,40),S(16,16),B(260),V1(3,50,4,10,2),
     1 V2(3,50,4,10,2),
     2 EIX(50,4,10),EIY(50,4,10),FIXY(50,4,10),SCX(50,4,10),
     3 SCY(50,4,10),SCXY(50,4,10),                              DNX(50,4),
     4 DNY(50,4),FIX(50,4),FIY(50,4),FIXY(50,4),EDX(50,4),EDY(50,4),
     5CA(3,3),CB(3,3),X(65),Y(65),W(65),WX(65),WY(65),WXY(65),HED(20),
     6 D(65),DX(65),DY(65),DXY(65),ABX(50),ABY(50),ATX(50),ATY(50),
     7 DTX(50),DTY(50),CBX(50),CBY(50),DPTH(50),T(25),UUDL(50),Z(11),
     8 AJX(10),AJY(10),AMX(10),AMY(10),DC11(10),DC22(10),DC12(10),CO(2),
     1                          DELTA(50,4,10),KODE(65),NODG(50),
     2 NODH(50),NCDI(50),NODJ(50),LM(4),NE,NJ,NL,NEQ,MBAND,NT,
     3 REPEAT,NTS
      DOUBLE PRECISION A,S,B
      INTEGER REPEAT
      INTEGER DELTA
      CALL COEFF
      CALL INPUT
      CALL PARAM
      CALL CMOD
  100 CONTINUE
      REPEAT=0
  101 CONTINUE
      CALL LOAD
      CALL STIFCS
      CALL STIFF
      CALL DISPL
      CALL STRESS
      IF (REPEAT.EQ.1) GO TO 100
      IF (NT.GT.NTS)GO TO 200
      CALL PARAM
      CALL CMOD
      CALL CREEP
      GO TO 100
  200 CONTINUE
      STOP
      END
```

```
      SUBROUTINE COEFF
C************************************
C    INPUTS COEFFICIENTS FOR ELEMENT STIFFNESS MATRIX
C************************************
      COMMON /LYN/C1(3,16),C2(3,16),C3(3,16),C4(3,16),P1(3,16),P2(3,16),
     1P3(3,16),P4(3,16)
      DOUBLE PRECISION C1,C2,C3,C4,P1,P2,P3,P4
C
      DO 20 J=1,16
      DO 20 I=1,3
   20 READ(5,500) I,J,C1(I,J),C2(I,J),C3(I,J),C4(I,J),P1(I,J),P2(I,J),
     1P3(I,J),P4(I,J)
      WRITE (6,450)
      DO 21 J=1,16
      DO 21 I=1,3
   21 WRITE (6,600) I,J,C1(I,J),C2(I,J),C3(I,J),C4(I,J),P1(I,J),P2(I,J),
     1P3(I,J),P4(I,J)
C
  450 FORMAT (' ','    I    J    C1   C2   C3   C4   P1   P2   P3   P4')
  500 FORMAT ( 2I5,F6.0,7E5.0)
  600 FORMAT ( 2I5,F6.0,7E5.0)
C
      RETURN
      END
```

```
      SUBROUTINE INPUT
C ****************************************
C      READS AND WRITES INPUT DATA
C****************************************
C
      COMMON A(260,40),S(16,16),B(260),V1(3,50,4,10,2),
     1 V2(3,50,4,10,2),
     2 EIX(50,4,10),EIY(50,4,10),EIXY(50,4,10),SCX(50,4,10),
     3 SCY(50,4,10),SCXY(50,4,10),                          DNX(50,4),
     4 DNY(50,4),EIX(50,4),EIY(50,4),EIXY(50,4),ECX(50,4),EOY(50,4),
     5CA(3,3),CB(3,3),X(65),Y(65),W(65),WX(65),WY(65),WXY(65),HED(20),
     6 D(65),DX(65),DY(65),DXY(65),ABX(50),ABY(50),ATX(50),ATY(50),
     7 DTX(50),DTY(50),DBX(50),DBY(50),DPTH(50),T(25),UUDL(50),Z(11),
     8 AJX(10),AJY(10),AMX(10),AMY(10),DC11(10),DC22(10),DC12(10),CD(2),
     1                          DELTA(50,4,10),KODE(65),NODG(50),
     2 NODH(50),NODI(50),NODJ(50),LM(4),NE,NJ,NL,NEC,MBAND,NT,
     3 REPEAT,NTS
      COMMON/TRACK/NTT
      COMMON/PARMS/ K1,K2,K3,ALPH1,ALPH2,ALPH3,A1,A2,A3,A4,AAC,BBC
      COMMON/CHEK/QCX(50,4,10),QCY(50,4,10)
      COMMON/CRAK/ SCT1,SCT2,SCT3,SCT4,GAM1,GAM2,GAM3,GAM4
      COMMON/CONC/MUC,ES,EC,SCT,GC
      COMMON/SHRINK/ESH(25)
      COMMON/PLSTC/ D11(50),D22(50),D12(50),D33(50)
      COMMON/PRNT/IPRINT(50,4)
      DOUBLE PRECISION  D11,D12,D22,D33
      DOUBLE PRECISION A,S,B
      INTEGER REPEAT
      INTEGER DELTA
      REAL MUC
      REAL K1,K2,K3
C
      READ(5,1000) HED,NJ,NE,NL,NTS
      WRITE(6,2000) HED,NJ,NE,NL,NTS
C
      READ(5,4001) GAM1,GAM2,GAM3,GAM4
      WRITE(6,5001)GAM1,GAM2,GAM3,GAM4
C
      READ(5,4001)    SCT1,SCT2,SCT3,SCT4
      WRITE(6,5002)   SCT1,SCT2,SCT3,SCT4
C
      READ(5,4020) K1,K2,K3,ALPH1,ALPH2,ALPH3
      READ(5,4030) A1,A2,A3,A4
      READ(5,4040) AAC,BBC
      WRITE(6,4025) K1,K2,K3,ALPH1,ALPH2,ALPH3,A1,A2,A3,A4,AAC,BBC
C
      WRITE (6,2003)
      DO 200 M=1,NE
      READ (5,1002) M,NODG(M),NODH(M),NODI(M),NODJ(M),IPRINT(M,1),
     1 IPRINT(M,2),IPRINT(M,3),IPRINT(M,4)
      WRITE (6,2004) M,NODG(M),NODH(M),NODI(M),NODJ(M),IPRINT(M,1),
     1 IPRINT(M,2),IPRINT(M,3),IPRINT(M,4)
  200 CONTINUE
C
      WRITE (6,2001)
      DO 100 M=1,NJ
      READ (5,1001) M,KODE(M),X(M),Y(M)
  101 WRITE (6,2002) M,KODE(M),X(M),Y(M)
  100 CONTINUE
```

```
C
      READ(5,1020) MUC,ES
      WRITE(6,2020)MUC,ES
C
      WRITE(6,2026)
      DO 150 M=1,NE
      READ(5,1025) ATX(M),ABX(M),ATY(M),ABY(M),DTX(M),DBX(M),DTY(M),
     1DBY(M),DPTH(M)
      WRITE(6,2025)ATX(M),ABX(M),ATY(M),ABY(M),DTX(M),DBX(M),DTY(M),
     1DBY(M),DPTH(M)
  150 CONTINUE
C
      WRITE(6,3000)
      DO 78 I=1,NTS
      READ(5,3001) T(I),UUDL(I),ESH(I)
      WRITE(6,3002) T(I),UUDL(I),ESH(I)
   78 CONTINUE
C
      NNL=NL+1
      WRITE(6,3005)
      DO 39 J=1,NNL
      READ(5,3003) Z(J)
      WRITE(6,3004) J,Z(J)
   39 CONTINUE
C
C    ****** INITIALISE ************
C
      DO 17 M=1,NE
      DO 17 K=1,4
      DO 17 L=1,NL
      QCX(M,K,L)=1.
      QCY(M,K,L)=1.
      DELTA(M,K,L)=1
C
      EIX(M,K,L)=0.0
      EIY(M,K,L)=0.0
      EIXY(M,K,L)=0.0
   17 CONTINUE
C
      CA(1,1)=0.0
      CA(2,1)=0.0
      CA(3,1)=0.0
      NTT=1
      NT=1
C
 1000 FORMAT (20A4/4I5)
 1001 FORMAT (2I5,2F10.3)
 1002 FORMAT (9I5)
 1020 FORMAT(F5.3,E15.6)
 1025 FORMAT(   9F8.5)
 2000 FORMAT ('1',20A4/' NUMBER OF JOINTS---='I4/
     1 ' NUMBER OF ELEMENTS-='I4 / ' NUMBER OF LAYERS---=' I4 /
     2 ' NUMBER OF TIMESTEPS=' I4 )
 2001 FORMAT('0','     JOINT       CODE     X           Y')
 2002 FORMAT (2I10,2F10.5)
 2003 FORMAT('0','   ELEMENT          G           H           I           J
     1 PRINT CODE ')
 2004 FORMAT (' ',5I10,I5,3I2)
 2020 FORMAT('0',' POISSONS RATIO (CONCRETE)=',F5.3,/
     1 ' YOUNGS MODULUS (STEEL)   =',F15.6    )
```

```
2025 FORMAT (' '9F8.5)
2026 FORMAT('0',' ATX      ABX      ATY      ABY      DTX      DBX
    1  DBY      DEPTH ' )
3000 FORMAT('1','       TIME--(DAYS)        U.D.L.(P.S.I.) SHRINKAGE')
3001 FORMAT(2F10.5,E15.6)
3002 FORMAT(' ',2F20.5,F15.6)
3003 FORMAT(F10.5)
3004 FORMAT(' ',' ',I4,'           ',F8.4)
3005 FORMAT('1',' LAYER BOUNDARY NR     DISTANCE FROM REF SURFACE')
4001 FORMAT(4F10.5)
4020 FORMAT(6F10.7)
4025 FORMAT('0',' CREEP FUNCTION PARAMETERS',/' K1=',F10.5,/' K2=',
    1 F10.5,/' K3=',F10.5,/' ALPH1=',F10.7,/' ALPH2=' ,F10.7,/
    2 ' ALPH3=',F10.7,/' A1=',E15.6,/' A2=',F15.6,/' A3=',E15.6,/
    3 ' A4=',F15.6,/' AAC=',E15.6,/' BBC=',F15.6)
4030 FORMAT(4F15.6)
4040 FORMAT(2F15.6)
5001 FORMAT('0',' GAM1=',F10.5,' GAM2=',F10.5,' GAM3=',F10.5,
    1  ' GAM4=',F10.5)
5002 FORMAT('0',' SCT1=',F10.4,' SCT2=',F10.4,'SCT3=',F10.4,
    1   ' SCT4=',F10.4)
     RETURN
C
     END
```

```
      SUBROUTINE LOAD
C************************************
C     COMPUTES APPLIED AND EQUIVALENT LOAD VECTORS
C************************************
      COMMON A(260,40),S(16,16),B(260),V1(3,50,4,10,2),
     1 V2(3,50,4,10,2),
     2 FIX(50,4,10),FIY(50,4,10),FIXY(50,4,10),SCX(50,4,10),
     3 SCY(50,4,10),SCXY(50,4,10),                          DNX(50,4),
     4 DNY(50,4),FIX(50,4),FIY(50,4),FIXY(50,4),FOX(50,4),FOY(50,4),
     5CA(3,3),CB(3,3),X(65),Y(65),W(65),WX(65),WY(65),WXY(65),HED(20),
     6 D(65),DX(65),DY(65),DXY(65),ABX(50),ABY(50),ATX(50),ATY(50),
     7 DTX(50),DTY(50),DBX(50),DBY(50),DPTH(50),T(25),UUDL(50),Z(11),
     8 AJX(10),AJY(10),AMX(10),AMY(10),DC11(10),DC22(10),DC12(10),CD(2),
     1                          DELTA(50,4,10),KODE(65),NODG(50),
     2 NODP(50),NODI(50),NODJ(50),LM(4),NE,NJ,NL,NEQ,MBAND,NT,
     3 REPEAT,NTS
      COMMON/CHEK/QCX(50,4,10),QCY(50,4,10)
      COMMON/CONC/MUC,ES,EC,SCT,GC
      DIMENSION W1(4),W2(4),W3(4),W4(4),Q1(4),Q2(4),Q3(4),Q4(4)
      DIMENSION MXI(50,4),MYI(50,4),MXYI(50,4)
      DOUBLE PRECISION A,S,B
      INTEGER REPEAT
      INTEGER G
      INTEGER DELTA
      REAL MUC
      REAL MXI,MYI,MXYI
C
C  ASSUMING  ALL  PRESCRIBED  DISPLACEMENTS  ARE  ZERO
C
      DO 147 I=1,NJ
      W(I)=0.0
      WX(I)=0.0
      WY(I)=0.0
      WXY(I)=0.0
  147 CONTINUE
C
      DO 200 M=1,NE
      G=NODG(M)
      I=NODI(M)
      AX=X(I)-X(G)
      BY=Y(I)-Y(G)
C
      UDL=UUDL(NT)
C
      W1(1)= UDL*AX*BY/4.
      W1(2)= UDL*AX*BY/4.
      W1(3)= UDL*AX*BY/4.
      W1(4)= UDL*AX*BY/4.
C
      W2(1)= UDL*AX**2*BY/24.
      W2(2)= UDL*AX**2*BY/24.
      W2(3)=-UDL*AX**2*BY/24.
      W2(4)=-UDL*AX**2*BY/24.
C
      W3(1)= UDL*AX*BY**2/24.
      W3(2)=-UDL*AX*BY**2/24.
      W3(3)=-UDL*AX*BY**2/24.
      W3(4)= UDL*AX*BY**2/24.
C
```

```
      W4(1)= UDL*AX**2*BY**2/144.
      W4(2)=-UDL*AX**2*BY**2/144.
      W4(3)= UDL*AX**2*BY**2/144.
      W4(4)=-UDL*AX**2*BY**2/144.
  352 CONTINUE
C
C
C ************   INELASTIC  LOADS   (CREEP) ************************
  132 CONTINUE
C
      DO 100 K=1,4
      MXI(M,K)=0.0
      MYI(M,K)=0.0
      MXYI(M,K)=0.0
      DNXY=DPTH(M)/2.
      DO 100 L=1,NL
      H=Z(L+1)-Z(L)
      CEC1=EC/(1-MUC**2)*H*QCX(M,K,L)*EIX(M,K,L)
      MXI(M,K)=MXI(M,K)+(DNX(M,K)-(Z(L+1)+Z(L))/2.)*CEC1
      CEC2=MUC*EC*H/(1.-MUC**2)*QCX(M,K,L)*QCY(M,K,L)*EIY(M,K,L)
      MXI(M,K)=MXI(M,K)+(DNX(M,K)-(Z(L+1)+Z(L))/2.)*CEC2
      CEC3=MUC*EC/(1.-MUC**2)*H*QCY(M,K,L)*QCX(M,K,L)*EIX(M,K,L)
      MYI(M,K)=MYI(M,K)+(DNY(M,K)-(Z(L+1)+Z(L))/2.)*CEC3
      CEC4=EC/(1-MUC**2)*QCY(M,K,L)*H*EIY(M,K,L)
      MYI(M,K)=MYI(M,K)+(DNY(M,K)-(Z(L+1)+Z(L))/2.)*CEC4
      CEC5=H*GC*EIXY(M,K,L)
      MXYI(M,K)=MXYI(M,K)+(DNXY      -(Z(L+1)+Z(L))/2.)*CEC5
  100 CONTINUE
C
      MXI(M,1)=(MXI(M,1)+MXI(M,2)+MXI(M,3)+MXI(M,4))/4.
      MXI(M,2)=MXI(M,1)
      MXI(M,3)=MXI(M,1)
      MXI(M,4)=MXI(M,1)
C
      MYI(M,1)=(MYI(M,1)+MYI(M,2)+MYI(M,3)+MYI(M,4))/4.
      MYI(M,2)=MYI(M,1)
      MYI(M,3)=MYI(M,1)
      MYI(M,4)=MYI(M,1)
C
      MXYI(M,1)=(MXYI(M,1)+MXYI(M,2)+MXYI(M,3)+MXYI(M,4))/4.
      MXYI(M,2)=MXYI(M,1)
      MXYI(M,3)=MXYI(M,1)
      MXYI(M,4)=MXYI(M,1)
C
C
      Q1(1)=MXYI(M,1)/(AX*BY)*2.
      Q1(2)=-MXYI(M,2)/(AX*BY)*2.
      Q1(3)=MXYI(M,3)/(AX*BY) *2.
      Q1(4)=-MXYI(M,4)/(AX*BY)*2.
      Q2(1)=-MXI(M,1)/(2.*AX)
      Q2(2)=-MXI(M,2)/(2*AX)
      Q2(3)=MXI(M,3)/(2.*AX)
      Q2(4)=MXI(M,4)/(2.*AX)
      Q3(1)=-MYI(M,1)/(2.*BY)
      Q3(2)=MYI(M,2)/(2.*BY)
      Q3(3)=MYI(M,3)/(2.*BY)
      Q3(4)=-MYI(M,4)/(2.*BY)
      Q4(1)=-    (MXI(M,1)*BY/(12.*AX)+MYI(M,1)*AX/(12.*BY))
      Q4(2)=    (MXI(M,2)*BY/(12.*AX)+MYI(M,2)*AX/(12.*BY))
      Q4(3)=-    (MXI(M,3)*BY/(12.*AX)+MYI(M,3)*AX/(12.*BY))
```

```
      SUBROUTINE STIFCS
      COMMON A(260,40),S(16,16),B(260),V1(3,50,4,10,2),
     1 V2(3,50,4,10,2),
     2 FIX(50,4,10),FIY(50,4,10),FIXY(50,4,10),SCX(50,4,10),
     3 SCY(50,4,10),SCXY(50,4,10),                          DNX(50,4),
     4 DNY(50,4),FIX(50,4),FIY(50,4),FIXY(50,4),ECX(50,4),ECY(50,4),
     5CA(3,3),CB(3,3),X(65),Y(65),W(65),WX(65),WY(65),WXY(65),HED(20),
     6 D(65),DX(65),DY(65),DXY(65),ABX(50),ABY(50),ATX(50),ATY(50),
     7 DTX(50),DTY(50),DBX(50),DBY(50),DPTH(50),T(25),UUDL(50),Z(11),
     8 AJX(10),AJY(10),AMX(10),AMY(10),DC11(10),DC22(10),DC12(10),CD(2),
     1                          DELTA(50,4,10),KODE(65),NODG(50),
     2 NCDE(50),NCDI(50),NODJ(50),LM(4),NE,NJ,NL,NEC,MBAND,NT,
     3 REPEAT,NTS
      COMMON/PLSTC/ D11(50),D22(50),D12(50),D33(50)
      COMMON/CHEK/QCX(50,4,10),QCY(50,4,10)
      COMMON/CONC/MUC,ES,EC,SCT,GC
      DIMENSION ACX(4),ACY(4),AMAX(4),AMAY(4),DD11(4),DD22(4),DD12(4)
      DOUBLE PRECISION A,S,B
      DOUBLE PRECISION D11,D12,D22,D33
      INTEGER REPEAT
      INTEGER DELTA
C
C ****  COMPUTE EFFECTIVE TRANSFORMED AREAS ***********
      REAL MR
      REAL MUC
      MR=ES/EC
      DO 100 M=1,NE
      DO 20 I=1,4
      ACX(I)=0.0
      ACY(I)=0.0
      DO 10 J=1,NL
      H=Z(J+1)-Z(J)
      AJX(J)=QCX(M,I,J)*H
      AJY(J)=QCY(M,I,J)*H
      ACX(I)=ACX(I)+AJX(J)
      ACY(I)=ACY(I)+AJY(J)
   10 CONTINUE
      ACX(I)=ACX(I)+MR*(ATX(M)+ABX(M))
      ACY(I)=ACY(I)+MR*(ATY(M)+ABY(M))
   20 CONTINUE
C
C ****  COMPUTE NEUTRAL AXIS DEPTHS *****
C
      DO 40 I=1,4
      AMAX(I)=0.0
      AMAY(I)=0.0
      DO 30 J=1,NL
      H=Z(J+1)-Z(J)
      AMX(J)=QCX(M,I,J)*H*(Z(J+1)+Z(J))/2.
      AMY(J)=QCY(M,I,J)*H*(Z(J+1)+Z(J))/2.
      AMAX(I)=AMAX(I)+AMX(J)
      AMAY(I)=AMAY(I)+AMY(J)
   30 CONTINUE
      AMAX(I)=AMAX(I)+   MR*(ATX(M)*DTX(M)+ABX(M)*DBX(M))
      AMAY(I)=AMAY(I)+MR*(ATY(M)*DTY(M)+ABY(M)*DBY(M))
      DNX(M,I)=AMAX(I)/ACX(I)
      DNY(M,I)=AMAY(I)/ACY(I)
   40 CONTINUE
C
```

```
      SUBROUTINE STIFF
C ************************************************
C      ASSEMBLES STRUCTURE STIFFNESS MATRIX IN BANDED FORM
C ************************************************
C
      COMMON A(260,40),S(16,16),B(260),V1(3,50,4,10,2),
     1 V2(3,50,4,10,2),
     2 EIX(50,4,10),EIY(50,4,10),EIXY(50,4,10),SCX(50,4,10),
     3 SCY(50,4,10),SCXY(50,4,10),                          DNX(50,4),
     4 DNY(50,4),FIX(50,4),FIY(50,4),FIXY(50,4),EOX(50,4),EOY(50,4),
     5CA(3,3),CB(3,3),X(65),Y(65),W(65),WX(65),WY(65),WXY(65),HED(20),
     6 C(65),DX(65),DY(65),DXY(65),ABX(50),ABY(50),ATX(50),ATY(50),
     7 DTX(50),DTY(50),DBX(50),DBY(50),DPTH(50),T(25),UUDL(50),Z(11),
     8 AJX(10),AJY(10),AMX(10),AMY(10),DC11(10),DC22(10),DC12(10),CD(2),
     1                          DELTA(50,4,10),KODE(65),NODG(50),
     2 NODH(50),NODI(50),NODJ(50),LM(4),NE,NJ,NL,NEQ,MBAND,NT,
     3 REPEAT,NTS
C
      COMMON/IDS/ ID
      DIMENSION NOD(4)
      DOUBLE PRECISION A,S,B
      INTEGER REPEAT
      INTEGER DELTA
C
C      DETERMINE BAND WIDTH
C
      ND=0
      DO 50 I=1,NE
      NOD(1)=NODG(I)
      NOD(2)=NODH(I)
      NOD(3)=NODI(I)
      NOD(4)=NODJ(I)
C
      DO 50 J=1,3
      JJ=J+1
C
      DO 50 K=JJ,4
C
      KK=IABS(NOD(J)-NOD(K))
C
      IF((KK-ND).LE.0) GO TO 50
      ND=KK
   50 CONTINUE
      MBAND=(ND+1)*4
      NEQ=4*NJ
      DO 200 I=1,NEQ
      B(I)=0.0
      DO 200 J=1,MBAND
  200 A(I,J)=0.0
C
      DO 500 N=1,NE
C      FORM 16X16 ELEMENT STIFFNESS MATRIX
      ID=N
C
      CALL ELEM
C
C      ADD ELEMENT STIFFNESS TO TOTAL STIFFNESS
C
      LM(1)=4*NODG(N)-4
```

```
      LM(2)=4*NODH(N)-4
      LM(3)=4*NODI(N)-4
      LM(4)=4*NODJ(N)-4
C
      DO 400 I=1,4
      DO 400 J=1,4
C
      DO 400 K=1,4
      II=LM(I)+K
      KK=4*I-4+K
C
      DO 400 L=1,4
      JJ=LM(J)+L-II+1
      IF (JJ.LE.0) GO TO 400
      IF (JJ.GT.MBAND) GO TO 400
      LL=4*J-4+L
      A(II,JJ)=A(II,JJ)+S(KK,LL)
  400 CONTINUE
C
  500 CONTINUE
C
      RETURN
C
      END
```

```
      CC(1,6)=-1/AX
      CC(2,6)=-AX/BY**2
      CC(3,6)=-2/BY
      CC(1,7)=BY/AX**2
      CC(2,7)=1/BY
      CC(3,7)=2/AX
      CC(1,8)=BY/AX
      CC(2,8)=AX/BY
      CC(3,8)=2.
      CC(1,9)=1/AX**2
      CC(2,9)=1/BY**2
      CC(3,9)=2/(AX*BY)
      CC(1,10)=-1/AX
      CC(2,10)=-AX/BY**2
      CC(3,10)=-2/BY
      CC(1,11)=-BY/AX**2
      CC(2,11)=-1/BY
      CC(3,11)=-2/AX
      CC(1,12)=BY/AX
      CC(2,12)=AX/BY
      CC(3,12)=2.
      CC(1,13)=-1/AX**2
      CC(2,13)=-1/BY**2
      CC(3,13)=-2/(AX*BY)
      CC(1,14)=1/AX
      CC(2,14)=AX/BY**2
      CC(3,14)=2/BY
      CC(1,15)=-BY/AX**2
      CC(2,15)=-1/BY
      CC(3,15)=-2/AX
      CC(1,16)=BY/AX
      CC(2,16)=AX/BY
      CC(3,16)=2.
C
      DO 400 I=1,16
      DO 400 J=1,16
      DO 300 M=1,5
C
      IF (M.LE.3) GO TO 200
      IF (M.EQ.4) GO TO 210
      IF (M.EQ.5) GO TO 220
  200 K=M
      L=M
      GO TO 250
  210 K=2
      L=1
      GO TO 250
  220 K=1
      L=2
      GO TO 250
  250 CONTINUE
C
      Q1(M)=C1(K,I)*C1(L,J)
      Q2(M)=C1(K,I)*C2(L,J)+C2(K,I)*C1(L,J)
      Q3(M)=C1(K,I)*C3(L,J)+C2(K,I)*C2(L,J) +C3(K,I)*C1(L,J)
      Q4(M)=C1(K,I)*C4(L,J)+C2(K,I)*C3(L,J)+C3(K,I)*C2(L,J)+C4(K,I)*
     1C1(L,J)
      Q5(M)=C2(K,I)*C4(L,J)+C3(K,I)*C3(L,J)+C4(K,I)*C2(L,J)
      Q6(M)=C3(K,I)*C4(L,J)+C4(K,I)*C3(L,J)
      Q7(M)=C4(K,I)*C4(L,J)
```

```
C
      R1(M)=P1(K,I)*P1(L,J)
      R2(M)=P1(K,I)*P2(L,J)+P2(K,I)*P1(L,J)
      R3(M)=P1(K,I)*P3(L,J)+P2(K,I)*P2(L,J)+P3(K,I)*P1(L,J)
      R4(M)=P1(K,I)*P4(L,J)+P2(K,I)*P3(L,J)+P3(K,I)*P2(L,J)+
     1P4(K,I)*P1(L,J)
      R5(M)=P2(K,I)*P4(L,J)+P3(K,I)*P3(L,J)+P4(K,I)*P2(L,J)
      R6(M)=P3(K,I)*P4(L,J)+P4(K,I)*P3(L,J)
      R7(M)=P4(K,I)*P4(L,J)
      AQ(M)=Q1(M)+Q2(M)/2.+Q3(M)/3.+Q4(M)/4.+Q5(M)/5.+Q6(M)/6.+Q7(M)/7.
      AR(M)=R1(M)+R2(M)/2.+R3(M)/3.+R4(M)/4.+R5(M)/5.+R6(M)/6.+R7(M)/7.
      ZZ(M)=AQ(M)*AR(M)
C
  300 CONTINUE
      A1(I,J)=ZZ(1)
      A2(I,J)=ZZ(2)
      A3(I,J)=ZZ(3)
      A4(I,J)=ZZ(4)
      A5(I,J)=ZZ(5)
C
  400 S(I,J)=AX*BY*(CO(1,I)*CO(1,J)*A1(I,J)*D11(ID)
     1 +CO(2,I)*CO(2,J)*A2(I,J)*D22(ID)  +CO(3,J)*A3(I,J)*CO(3,I)
     2 *D33(ID) +CO(2,I)*CO(1,J)*A4(I,J)*D12(ID)
     3 +CO(1,I)*CO(2,J)*A5(I,J)*D12(ID))
C
C
C
      RETURN
      END
```

```
      SUBROUTINE BANSOL
C ***********************************************
C       IN-CORE LINEAR EQUATION SOLVER FOR SYMMETRIC BAND MATRICES
C
      COMMON A(260,40),S(16,16),B(260),V1(3,50,4,10,2),
     1 V2(3,50,4,10,2),
     2 EIX(50,4,10),EIY(50,4,10),EIXY(50,4,10),SCX(50,4,10),
     3 SCY(50,4,10),SCXY(50,4,10),                          DNX(50,4),
     4 DNY(50,4),FIX(50,4),FIY(50,4),FIXY(50,4),EOX(50,4),EOY(50,4),
     5CA(3,3),CB(3,3),X(65),Y(65),W(65),WX(65),WY(65),WXY(65),HED(20),
     6 D(65),DX(65),DY(65),DXY(65),ABX(50),ABY(50),ATX(50),ATY(50),
     7 DTX(50),DTY(50),DBX(50),DBY(50),DPTH(50),T(25),UUDL(50),Z(11),
     8 AJX(10),AJY(10),AMX(10),AMY(10),DC11(10),DC22(10),DC12(10),CD(2),
     1                          DELTA(50,4,10),KODE(65),NODG(50),
     2 NODH(50),NODI(50),NODJ(50),LM(4),NE,NJ,NL,NEC,MBAND,NT,
     3 REPEAT,NTS
      INTEGER REPEAT
      INTEGER DELTA
      DIMENSION SS(10400)
      EQUIVALENCE (SS,A)
      DOUBLE PRECISION A,S,B
      DOUBLE PRECISION SS,PIVOT,C
C
      NCOL=260
      NN=4*NJ
      NR=NN
      NRS=NR-1
      MMR=MBAND-1
C
  100 DO 120 N=1,NRS
      M=N-1
      MR=MIN0 (MBAND,NR-M)
C
C
      PIVOT=SS(N)
C
C
      J=N
      DO 120 L=2,MR
      J=J+NCOL
  104 C=SS(J)/PIVOT
C
C
      II=M+L
      I2=II+(MR-L)*NCOL
      II=J
      DO 110 I=II,I2,NCOL
      SS(I)=SS(I)-C*SS(II)
  110 II=II+NCOL
  120 SS(J)=C
C
C
      ICHECK=0
      DO 150 I=1,NN
      IF (SS(I).LE.C.0) ICHECK=1
  150 CONTINUE
      IF (ICHECK.EQ.1) CALL EXIT
C
  200 DO 220 N=1,NRS
```

```
      MR=MINO(MMR,NR-N)
      C=B(N)
      B(N)=C/SS(N)
      K=N
      L1=N+1
      L2=N+MR
      DO 220 L=L1,L2
      K=K+NCOL
  220 B(L)=B(L)-SS(K)*C
      B(NR)=B(NR)/SS(NR)
  300 DO 320 I=1,NRS
      N=NR-I
      MR=MINO(MMR,I)
      J=N
      L1=N+1
      L2=N+MR
      DO 320 L=L1,L2
      J=J+NCOL
  320 B(N)=B(N)-SS(J)*B(L)
C
  400 RETURN
      END
```

```
      SUBROUTINE CMOD
C ************************************************
C     COMPUTES PSEUDO-INSTANTANEOUS ELASTIC AND SHEAR MODULI
C ************************************************
      COMMON A(260,40),S(16,16),B(260),V1(3,50,4,10,2),
     1 V2(3,50,4,10,2),
     2 EIX(50,4,10),EIY(50,4,10),EIXY(50,4,10),SCX(50,4,10),
     3 SCY(50,4,10),SCXY(50,4,10),                    DNX(50,4),
     4 DNY(50,4),EIX(50,4),EIY(50,4),EIXY(50,4),ECX(50,4),EOY(50,4),
     5CA(3,3),CB(3,3),X(65),Y(65),W(65),WX(65),WY(65),WXY(65),HED(20),
     6 D(65),DX(65),DY(65),DXY(65),ARX(50),ARY(50),ATX(50),ATY(50),
     7 DTX(50),DTY(50),DBX(50),DBY(50),DPTH(50),T(25),UUDL(50),Z(11),
     8 AJX(10),AJY(10),AMX(10),AMY(10),DC11(10),DC22(10),DC12(10),CD(2),
     1                          DELTA(50,4,10),KODE(65),NODG(50),
     2 NODH(50),NODI(50),NODJ(50),LM(4),NE,NJ,NL,NEC,MBAND,NT,
     3 REPEAT,NTS
      COMMON/CONC/MUC,ES,EC,SCT,GC
      DOUBLE PRECISION A,S,B
      INTEGER REPEAT
      INTEGER DELTA
      REAL MUC
C
      EC=0.0
      DO 20 IJ=1,3
      EC=EC+CB(IJ,2)*(CA(IJ,3)+CA(IJ,2))
   20 CONTINUE
      EC=EC+CD(2)+CD(1)
      EC=2.0/EC
      GC=EC/(2.*(1.+MUC))
      WRITE(6,9035) EC   ,GC
 9035 FORMAT('0',' INST. ELASTIC MODULUS=',F12.5,/
     1 ' SHEAR MODULUS          =',F12.5)
      RETURN
      END
```

```
      SUBROUTINE PARAM
C ********************************************
CC       COMPUTES CREEP PARAMETERS CA,CB,CD.
C ********************************************
      COMMON A(260,40),S(16,16),B(260),V1(3,50,4,10,2),
     1 V2(3,50,4,10,2),
     2 FIX(50,4,10),FIY(50,4,10),FIXY(50,4,10),SCX(50,4,10),
     3 SCY(50,4,10),SCXY(50,4,10),                    DNX(50,4),
     4 DNY(50,4),FIX(50,4),FIY(50,4),FIXY(50,4),FDX(50,4),FDY(50,4),
     5CA(3,3),CB(3,3),X(65),Y(65),W(65),WX(65),WY(65),WXY(65),HED(20),
     6 D(65),DX(65),DY(65),DXY(65),ARX(50),ARY(50),ATX(50),ATY(50),
     7 CTX(50),CTY(50),CRX(50),CRY(50),DPTH(50),T(25),UUDL(50),Z(11),
     8 AJX(10),AJY(10),AMX(10),AMY(10),DC11(10),DC22(10),DC12(10),CD(2),
     1                          DELTA(50,4,10),KODE(65),NODG(50),
     2 NCOH(50),NCOI(50),NODJ(50),LM(4),NE,NJ,NL,NEG,MBAND,NT,
     3 REPEAT,NTS
      COMMON/TRACK/NTT
      COMMON/PARMS/ K1,K2,K3,ALPH1,ALPH2,ALPH3,A1,A2,A3,A4,AAC,BBC
      COMMON/CONC/MUC,ES,EC,SCT,GC
      DOUBLE PRECISION A,S,B
      INTEGER REPEAT
      INTEGER DELTA
      REAL MUC
      REAL K1,K2,K3
C
C *************CREEP PARAMETERS     ************************
      IF(NT.EQ.1) GO TO 72
      J1=1
      GO TO 73
   72 J1=2
   73 DO 101 J=J1,3
      JJ=J-1
      IF(J.EQ.1) TT=T(NT-1)
      IF(J.EQ.2) TT=T(NT)
      IF(J.EQ.3)TT=T(NT+1)
   29 CONTINUE
      IF(NTT.EQ.1) TT=T(NT)
   30 CONTINUE
C
      F1=K1*TT
      F2=K2*TT
      F3=K3*TT
C
      CAA=A1+A2/TT**0.1+A3/TT**0.2+A4/TT**0.3
C
C
      CA(1,J)=-ALPH1*CAA*EXP(F1)
      CA(2,J)=- ALPH2*CAA*EXP(F2)
      CA(3,J)=-ALPH3*CAA*EXP(F3)
C
      IF (JJ.LT.1) GO TO 101
      F4=-F1
      F5=-F2
      F6=-F3
      CB(1,JJ)=EXP(F4)
      CB(2,JJ)=EXP(F5)
      CB(3,JJ)=EXP(F6)
C
      CC(JJ)=(ALPH1+ALPH2+ALPH3)*CAA+AAC/TT+BBC



C
   31 CONTINUE
  101 CONTINUE
C
      WRITE(6,5003) T(NTT)
      NTT=NTT+1
5003 FORMAT('1',' ***************ANALYSIS AT TIME T=',F10.5,
     1 ' DAYS **********************')
C
      RETURN
      END
```

```
      SUBROUTINE CREEP
C ***********************************************
C     COMPUTES INELASTIC STRAINS AT EACH TIMESTEP
C ***********************************************
      COMMON A(260,40),S(16,16),B(260),V1(3,50,4,10,2),
     1 V2(3,50,4,10,2),
     2 EIX(50,4,10),EIY(50,4,10),EIXY(50,4,10),SCX(50,4,10),
     3 SCY(50,4,10),SCXY(50,4,10),                    DNX(50,4),
     4 DNY(50,4),FIX(50,4),FIY(50,4),FIXY(50,4),EOX(50,4),EOY(50,4),
     5CA(3,3),CB(3,3),X(65),Y(65),W(65),WX(65),WY(65),WXY(65),HED(20),
     6 D(65),DX(65),DY(65),DXY(65),ABX(50),ABY(50),ATX(50),ATY(50),
     7 DTX(50),DTY(50),CBX(50),CBY(50),DPTH(50),T(25),UUDL(50),Z(11),
     8 AJX(10),AJY(10),AMX(10),AMY(10),DC11(10),DC22(10),DC12(10),CD(2),
     1                          DELTA(50,4,10),KODE(65),NODG(50),
     2 NOCH(50),NODI(50),NODJ(50),LM(4),NE,NJ,NL,NEQ,MBAND,NT,
     3 REPEAT,NTS
      COMMON/SHRINK/ESH(25)
      COMMON/VIVA/V3(3,50,4,10,2),SOX(50,4,10),SOY(50,4,10),
     1  SOXY(50,4,10)
      COMMON/CHEK/QCX(50,4,10),QCY(50,4,10)
      COMMON/CONC/MUC,ES,EC,SCT,GC
      DIMENSION  ESS(2)
      DOUBLE PRECISION A,S,B
      INTEGER REPEAT
      INTEGER DELTA
      REAL MUC
      ESS(2)=ESH(NT+1)
      ESS(1)=ESH(NT)
C
      DO 750M=1,NE
      DO 750 I=1,4
      DO 740 J=1,NL
C
C
C ********   CREEP STRAINS **********************
      IF(NT.EQ.1) GO TO 28
      GO TO 29
C
C *****  FOR FIRST TIME STEP ONLY  ***************
C
   28 CA(1,1)=CA(1,2)
      CA(2,1)=CA(2,2)
      CA(3,1)=CA(3,2)
      K=I
      L=J
      SCX(M,I,J)=0.0
      SOY(M,I,J)=0.0
      SOXY(M,I,J)=0.0
      DO 32 II=1,3
      V1(II,M,K,L,1)=0.0
      V2(II,M,K,L,1)=0.0
      V3(II,M,K,L,1)=0.0
      V1V=(SCX(M,K,L)-SCX(M,K,L))*(CA(II,1)+CA(II,2))/2.
      V1(II,M,K,L,2)=V1(II,M,K,L,1)+V1V
      V2V=(SCY(M,K,L)-SCY(M,K,L))*(CA(II,1)+CA(II,2))/2.
      V2(II,M,K,L,2)=V2(II,M,K,L,1)+V2V
      V3V=(SCXY(M,K,L)-SCXY(M,K,L))*(CA(II,1)+CA(II,2))/2.
      V3(II,M,K,L,2)=V3(II,M,K,L,1)+V3V
   32 CONTINUE
```

```
      GO TO 153
   29 CONTINUE
C
C *****  FOR SUBSEQUENT TIME STEPS      ******************
C
      K=I
      L=J
      DO 153 II=1,3
      V1V=(SCX(M,K,L)-SOX(M,K,L))*(CA(II,1)+CA(II,2))/2.
      V1(II,M,K,L,2)=V1(II,M,K,L,1)+V1V
      V2V=(SCY(M,K,L)-SCY(M,K,L))*(CA(II,1)+CA(II,2))/2.
      V2(II,M,K,L,2)=V2(II,M,K,L,1)+V2V
      V3V=(SCXY(M,K,L)-SOXY(M,K,L))*(CA(II,1)+CA(II,2))/2.
      V3(II,M,K,L,2)=V3(II,M,K,L,1)+V3V
  153 CONTINUE
      CR1=0.0
      CR2=0.0
      CR3=0.0
C
      DO 100 II=1,3
      CR1=CR1+(CB(II,2)-CB(II,1))*(V1(II,M,K,L,2)-MUC*V2(II,M,K,L,2))
      CR2=CR2+(CB(II,2)-CB(II,1))*(V2(II,M,K,L,2)-MUC*V1(II,M,K,L,2))
      CR3=CR3+(CB(II,2)-CB(II,1))*(V3(II,M,K,L,2) )
  100 CONTINUE
      CR3=2.*(1.-MUC)*CR3
      CR11=(SCX(M,K,L)-MUC*SCY(M,K,L))/EC
      CR22=(SCY(M,K,L)-MUC*SCX(M,K,L))/EC
      CR33=SCXY(M,K,L)*2.*(1.-MUC)/EC
C
C ***    TOTAL STRAINS IN COORD DIRECTIONS  ***************
C
      ETX=ECX(M,I)-(Z(J+1)+Z(J))/2.*FIX(M,I)
      ETY=ECY(M,I)-(Z(J+1)+Z(J))/2.*FIY(M,I)
      ETXY=(DPTH(M)/2.-(Z(J+1)+Z(J))/2.)*FIXY(M,I)
      ETXY=-ETXY
C
C
      EIX(M,K,L)=CR1+ETX-CR11+ESS(2)-ESS(1)
      EIY(M,K,L)=CR2+ETY-CR22+ESS(2)-ESS(1)
      EIXY(M,K,L)=CR3+ETXY-CR33
C
      DO 720 II=1,3
      V1(II,M,K,L,1)=V1(II,M,K,L,2)
      V2(II,M,K,L,1)=V2(II,M,K,L,2)
      V3(II,M,K,L,1)=V3(II,M,K,L,2)
  720 CONTINUE
      SOX(M,K,L)=SCX(M,K,L)
      SOY(M,K,L)=SCY(M,K,L)
      SOXY(M,K,L)=SCXY(M,K,L)
  740 CONTINUE
C
  750 CONTINUE
      NT=NT+1
      RETURN
      END
```

```
      SUBROUTINE STRESS
C ***********************************************
C     COMPUTES REFERENCE SURFACE STRAINS ,STEEL & CONCRETE STRESSES, MOMENTS
C     AND CHECKS FOR CRACKING
C ***********************************************
      COMMON A(260,40),S(16,16),B(260),V1(3,50,4,10,2),
     1 V2(3,50,4,10,2),
     2 FIX(50,4,10),FIY(50,4,10),FIXY(50,4,10),SCX(50,4,10),
     3 SCY(50,4,10),SCXY(50,4,10),                          DNX(50,4),
     4 DNY(50,4),FIX(50,4),FIY(50,4),FIXY(50,4),ECX(50,4),ECY(50,4),
     5CA(3,3),CB(3,3),X(65),Y(65),W(65),WX(65),WY(65),WXY(65),HED(20),
     6 D(65),DX(65),DY(65),DXY(65),ABX(50),ABY(50),ATX(50),ATY(50),
     7 DTX(50),DTY(50),DBX(50),DBY(50),DPTH(50),T(25),UUDL(50),Z(11),
     8 AJX(10),AJY(10),AMX(10),AMY(10),DC11(10),DC22(10),DC12(10),CD(2),
     1                          DELTA(50,4,10),KODE(65),NODG(50),
     2 NODH(50),NODI(50),NODJ(50),LM(4),NE,NJ,NL,NEQ,MBAND,NT,
     3 REPEAT,NTS
      COMMON/CHEK/QCX(50,4,10),QCY(50,4,10)
      COMMON/CRAK/ SCT1,SCT2,SCT3,SCT4,GAM1,GAM2,GAM3,GAM4
      COMMON/CONC/MUC,ES,EC,SCT,GC
      COMMON/PRNT/IPRINT(50,4)
      DIMENSION RMX(50,4),RMY(50,4)
      DIMENSION ETX(10),ETY(10),ETXY(10),EEX(10),EEY(10),EEXY(10)
      DOUBLE PRECISION A,S,B
      INTEGER REPEAT
      INTEGER TQX,TQY
      INTEGER DELTA
      REAL MUC
      REAL NUMTR
C
C   ************      REFERENCE SURFACE STRAINS    ***************
      DO 55 M=1,NE
      DO 55 I=1,4
      A11=0.0
      A12=0.0
      A22=0.0
      C11=0.0
      C22=0.0
      DO 45 J=1,NL
C
      H=Z(J+1)-Z(J)
      A11=EC/(1-MUC**2)*QCX(M,I,J)*H +A11
      A12=MUC*QCX(M,I,J)*QCY(M,I,J)*H*EC/(1-MUC**2) +A12
      A22=EC/(1-MUC**2)*QCY(M,I,J)*H +A22
      C1A=(Z(J+1)+Z(J))/2.*FIX(M,I)+FIX(M,I,J)
      C2A=MUC*(Z(J+1)+Z(J))/2.*FIY(M,I)*QCY(M,I,J)
     1  +MUC*EIY(M,I,J)*QCY(M,I,J)
      C11=C11+QCX(M,I,J)*H*EC/(1-MUC**2)*(C1A+C2A)
      C1B=(Z(J+1)+Z(J))/2.*FIY(M,I)+EIY(M,I,J)
      C2B=MUC*(Z(J+1)+Z(J))/2.*FIX(M,I)*QCX(M,I,J)
     1  +MUC*EIX(M,I,J)*QCX(M,I,J)
      C22=C22+QCY(M,I,J)*H*EC/(1-MUC**2)*(C1B+C2B)
C
   45 CONTINUE
C
      A11=A11+ES*(ATX(M)+ABX(M))
      A22=A22+ES*(ATY(M)+ABY(M))
      C11=C11+ES*(DTX(M)*FIX(M,I)*ATX(M)+DBX(M)*FIX(M,I)*ABX(M))
      C22=C22+ES*(DTY(M)*FIY(M,I)*ATY(M)+DBY(M)*FIY(M,I)*ABY(M))
```

```
      NUMTR=C11*A22-C22*A12
      DMTR=A11*A22-A12*A12
C
      FCX(M,I)=NUMTR/DMTR
C
      NUMTR=C11*A12-C22*A11
      DMTR=A12*A12-A22*A11
C
      FCY(M,I)=NUMTR/DMTR
C
   55 CONTINUE
C
C *********STRESSES AND MOMENTS *********
C
      DO 50 M=1,NF
      DO 50 I=1,4
C
      RMX(M,I)=0.0
      RMY(M,I)=0.0
      IF(REPEAT.EQ.1) GO TO 155
C
C    STEEL STRAINS
C
      ESTY=FCY(M,I)-DTY(M)*FIY(M,I)
      ESTX=FCX(M,I)-DTX(M)*FIX(M,I)
      ESBY=FCY(M,I)-DBY(M)*FIY(M,I)
      ESBX=FCX(M,I)-DBX(M)*FIX(M,I)
C
C ********* FORCE IN STEEL ***********
C
      STY=ATY(M)*ESTY*ES
      STX=ATX(M)*ESTX*ES
      SBY=ABY(M)*ESBY*ES
      SBX=ABX(M)*ESBX*ES
  155 CONTINUE
C
      DO 40 J=1,NL
C
C *********TOTAL STRAINS *************
C
      ETX(J)=FCX(M,I)-(Z(J+1)+Z(J))/2.*FIX(M,I)
      ETY(J)=FCY(M,I)-(Z(J+1)+Z(J))/2.*FIY(M,I)
      ETXY(J)=-(DPTH(M)/2.-(Z(J+1)+Z(J))/2.)*FIXY(M,I)
C
C ********* PLASTIC STRAINS ***********
C
      EPX(J)=ETX(J)-EIX(M,I,J)
      EPY(J)=ETY(J)-EIY(M,I,J)
C
C *********CONCRETE STRESSES *********
C
      XCS=QCX(M,I,J)*EPX(J)+MUC*QCX(M,I,J)*QCY(M,I,J)*EPY(J)
      YCS=MUC*QCX(M,I,J)*QCY(M,I,J)*EPX(J)+QCY(M,I,J)*EPY(J)
      SCX(M,I,J)=EC/(1-MUC**2)*XCS
      SCY(M,I,J)=EC/(1-MUC**2)*YCS
      SCXY(M,I,J)=GC*(ETXY(J)-EIXY(M,I,J))
C
      K=I
      L=J
C
```

```
C ********* PRINCIPAL STRESSES **************
C
      DIFF=SCX(M,I,J)-SCY(M,I,J)
      IF(DIFF.EQ.0.C) GC TO 22
      ANG=2.*SCXY(M,I,J)/(SCX(M,I,J)-SCY(M,I,J))
      THET=ATAN(ANG)/2.0
      THET1=THET+3.1415926/2.
      GO TO 23
   22 CONTINUE
      THET=C.0
      THET1=THET+3.1415926/2.
   23 CONTINUE
      SS1=          SCX(M,I,J)*(CCS(THET))**2+SCY(M,I,J)*(SIN(THET))**2
     1   +2.*SCXY(M,I,J)   *COS(THET)*SIN(THET)
      SS2=          SCX(M,I,J)*(CCS(THET1))**2+SCY(M,I,J)*(SIN(THET1))**2
     1   +2.*SCXY(M,I,J)*SIN(THET1)*COS(THET1)
C
C *********  CHECK CRACKING  MATRIX **********************
C
      IF(((SS1.LT.SCT3).OR.(SS2.LT.SCT3)).AND.(DELTA(M,K,L).EQ.3))
     1  GC TO   333
      GO TO 317
  333 IF(SCX(M,K,L).LT.0.0) QCX(M,K,L)=GAM3
      IF(SCY(M,K,L).LT.0.0) QCY(M,K,L)=GAM3
      DELTA(M,K,L)=4
      REPEAT=1
  317 CONTINUE
      IF(((SS1.LT.SCT2).OR.(SS2.LT.SCT2)).AND.(DELTA(M,K,L).EQ.2))
     1  GC TO   433
      GC TO 417
  433 IF(SCX(M,K,L).LT.0.0) QCX(M,K,L)=GAM2
      IF(SCY(M,K,L).LT.0.0) QCY(M,K,L)=GAM2
      DELTA(M,K,L)=3
      REPEAT=1
  417 CONTINUE
C
      IF(((SS1.LT.SCT1).OR.(SS2.LT.SCT1)).AND.(DELTA(M,K,L).EQ.1))
     1  GC TO   533
      GO TO 517
  533 IF(SCX(M,K,L).LT.0.0) QCX(M,K,L)=GAM1
      IF(SCY(M,K,L).LT.0.0) QCY(M,K,L)=GAM1
      DELTA(M,K,L)=2
      REPEAT=1
  517 CONTINUE
  836 CONTINUE
C
  100 CONTINUE
C
      IF(REPEAT.EQ.1) GO TO 156
C
C    MOMENT (CONCRETE)
C
      RMX(M,I)=SCX(M,I,J)*(Z(L+1)-Z(L))*(Z(L+1)+Z(L))/2.0+RMX(M,I)
      RMY(M,I)=SCY(M,I,J)*(Z(L+1)-Z(L))*(Z(L+1)+Z(L))/2.0 +RMY(M,I)
  156 CONTINUE
   40 CONTINUE
      IF(REPEAT.EQ.1) GC TO 157
      IF(IPRINT(M,I).NE.1) GO TO 701
C
      WRITE (6,7020)
```

```
      WRITE(6,2010)
      DO 520 J=1,NI
      WRITE(6,2020) M,I,J,SCX(M,I,J),SCY(M,I,J),SCXY(M,I,J),FTX(J),
     1 FTY(J),FTXY(J),FIX(M,I,J),FIY(M,I,J),FIXY(M,I,J)
  520 CONTINUE
C
      SSTY=FSTY*FS
      SSTX=FSTX*FS
      SSBY=FSBY*FS
      SSBX=FSBX*FS
C
      WRITE (6,7010)
      WRITE(6,2055) M,SSTY,SSTX,SSBY,SSBX
  701 CONTINUE
C  MOMENT  (ADD STEEL  CONTRIBUTION)
      RMX(M,I)=STX*CTX(M)+SBX*DBX(M)+RMX(M,I)
      RMY(M,I)=STY*CTY(M)+SBY*CBY(M)+ RMY(M,I)
  157 CONTINUE
   50 CONTINUE
C
      IF(REPEAT.EQ.1) GO TO 552
C
      WRITE(6,7030)
      WRITE(6,3428)
      DO 12 M=1,NF
      WRITE(6,3426) M,NODG(M),RMX(M,1),RMY(M,1),NODH(M),RMX(M,2),
     1 RMY(M,2),NODI(M),RMX(M,3),RMY(M,3),NODJ(M),RMX(M,4),RMY(M,4)
   12 CONTINUE
C
      WRITE (6,2008)(N,D(N),DX(N),DY(N),DXY(N),N=1,NJ )
      WRITE(6,2018)  T(NT)
      GO TO 553
  552 CONTINUE
      WRITE(6,2092)
  553 CONTINUE
C
      IF(REPEAT.EQ.1) GO TO 29
      WRITE(6,3095)
      WRITE(6,3094)
      DO 28 II=1,NF
      DO 28 JJ=1,4
      WRITE(6,3093) II,JJ,((QCX(II,JJ,KK),QCY(II,JJ,KK)),KK=1,10)
   28 CONTINUE
   29 CONTINUE
C
2008 FORMAT (70H1       JOINT       W               WX                WY
     1            WXY  /(I10,4E15.6))
2010 FORMAT('0',' ELEM CORNER LAYER   SCX         SCY         SCXY
     1 FTX           FTY          FTXY          FIX         EIY         EIXY')
2018 FORMAT('0',' ****DISPLACEMENTS  FOR  TIME  T=',F8.4,' ******')
2020 FORMAT(' ',I4,I5,I6,9F12.3)
2055 FORMAT(' ',' ELEM',I5,' SSTY=',F15.6,' SSTX=',F15.6,' SSBY=',
     1F15.6,' SSBX=',F15.6)
2092 FORMAT('0','   CRACKING DETECTED THIS ITERATION ')
3426 FORMAT(I4,I5,2E12.3,I5,2F12.3,I5,2E12.3,I5,2F12.3)
3428 FORMAT('0',' ELEM NODG   RMXG           RMYG     NODH  RMXH
     1   RMYH     NODI   RMXI           RMYI     NODJ      RMXJ        RMYJ')
3093 FORMAT(' ',215,20F5.3)
3094 FORMAT('0',' ELEM CORNR    1X    1Y    2X    2Y    3X    3Y    4X    4Y
     15X    5Y    6X    6Y    7X    7Y    8X    8Y    9X    9Y   10X   10Y ')

3095 FORMAT('1',' CRACKING COEFFICIENTS - LAYERS 1 TO 10')
7010 FORMAT('0',' STEEL STRESSES ')
7020 FORMAT('0',' CONCRETE STRESSES AND STRAINS ')
7030 FORMAT ('0',' MOMENTS COMPUTED AT NODAL POINTS ')
C
C
      RETURN
      END
```

```
      SUBROUTINE MODIFY
C ***********************************************
C     CALLED BY  DISPL FOR MODIFICATION  OF EQUNS FOR BOUNDARY CONDITIONS
C ***********************************************
      COMMON A(260,40),S(16,16),B(260),V1(3,50,4,10,2),
     1 V2(3,50,4,10,2),
     2 EIX(50,4,10),EIY(50,4,10),EIXY(50,4,10),SCX(50,4,10),
     3 SCY(50,4,10),SCXY(50,4,10),                          DNX(50,4),
     4 DNY(50,4),FIX(50,4),FIY(50,4),FIXY(50,4),ECX(50,4),ECY(50,4),
     5CA(3,3),CB(3,3),X(65),Y(65),W(65),WX(65),WY(65),WXY(65),HED(20),
     6 D(65),DX(65),DY(65),DXY(65),ABX(50),ABY(50),ATX(50),ATY(50),
     7 CTX(50),CTY(50),CBX(50),CBY(50),DPTH(50),T(25),UUDL(50),Z(11),
     8 AJX(10),AJY(10),AMX(10),AMY(10),DC11(10),DC22(10),DC12(10),CO(2),
     1                          DELTA(50,4,10),KODE(65),NODG(50),
     2 NODH(50),NODI(50),NODJ(50),LM(4),NE,NJ,NL,NEQ,MBAND,NT,
     3 REPEAT,NTS
      COMMON/CONC/MUC,ES,EC,SCT,GC
      COMMON /TEM / TEMP , NI
      DOUBLE PRECISION A,S,B
      INTEGER REPEAT
      INTEGER DELTA
      REAL MUC
C
      DO 20 K=2,MBAND
      I=NI-K+1
      IF(I.LE.0) GO TO 10
      B(I)=B(I)-A(I,K)*TEMP
      A(I,K)=0.0
   10 II=NI+K-1
      IF(II.GT.NEQ) GO TO 20
      B(II)=B(II)-A(NI,K)*TEMP
      A(NI,K)=0.0
   20 CONTINUE
      RETURN
      END
```